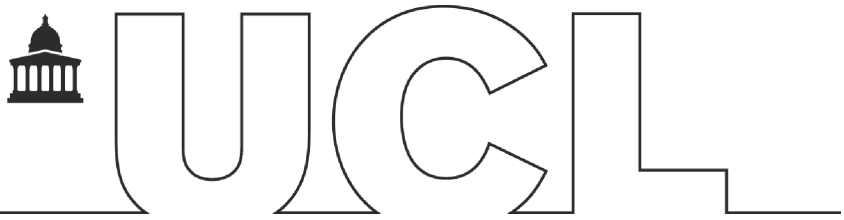

Satellite clock time offset prediction in global navigation satellite systems

Santosh Bhattarai

Department of Civil, Environmental and Geomatic Engineering

University College London

A thesis submitted for the degree of

Doctor of Philosophy

July 2014

I, *Santosh Bhattarai* confirm that the work presented in this thesis is my own. Where information has been derived from other sources, I confirm that this has been indicated in the thesis.

.....

Abstract

In an operational sense, satellite clock time offset prediction (SCTOP) is a fundamental requirement in global navigation satellite systems (GNSS) technology. SCTOP uncertainty is a significant component of the uncertainty budget of the basic GNSS pseudorange measurements used in standard (i.e not high-precision), single-receiver applications. In real-time, this prediction uncertainty contributes directly to GNSS-based positioning, navigation and timing (PNT) uncertainty. In short, GNSS performance in intrinsically linked to satellite clock predictability. Now, satellite clock predictability is affected by two factors: (i) the clock itself (i.e. the oscillator, the frequency standard etc.) and (ii) the prediction algorithm. This research focuses on aspects of the latter.

Using satellite clock data—spanning across several years, corresponding to multiple systems (GPS and GLONASS) and derived from real measurements—this thesis first presents the results of a detailed study into the characteristics of GNSS satellite clocks. This leads onto the development of strategies for modelling and estimating the time-offset of those clocks from system time better, with the final aim of predicting those offsets better. The satellite clock prediction scheme of the International GNSS Service (IGS) is analysed, and the results of this prediction scheme are used to evaluate the performance of new methods developed herein. The research presented in this thesis makes a contribution to knowledge in each of the areas of characterisation, modelling and prediction of GNSS satellite clocks.

Regarding characterisation of GNSS satellite clocks, the space-borne clocks of GPS and GLONASS are studied. In terms of frequency stability—and thus predictability—it is generally the case that the GPS clocks out-perform GLONASS clocks at prediction lengths ranging from several minutes up to one day ahead. There are three features in the GPS clocks—linear frequency drift, periodic signals and and complex underlying noise processes—that are not observable in the GLONASS clocks. The standard clock model does not capture these features. This study shows that better prediction accuracy can be obtained by an extension to the standard clock model.

The results of the characterisation and modelling study are combined in a Kalman filter framework, set up to output satellite clock predictions at a range of prediction intervals. In this part of the study, only GPS satellite clocks are considered. In most, but not all cases, the developed prediction method outperforms the IGS prediction scheme, by between 10% to 30%. The magnitude of the improvement is mainly dependent upon clock type.

Acknowledgements

I would like to thank my supervisors, Professor Marek Ziebart and Dr Paul Groves, for their support and guidance over the course of my research and for their careful review and comments on earlier versions of this thesis. I would also like to thank Dr John Davis of the National Physical Laboratory for working with me on developing the satellite clock prediction algorithm, and for sharing his knowledge and experience of time and frequency analysis methods.

I thank my colleagues in the Space Geodesy and Navigation Laboratory, past and present. I shared my journey with them.

This work was funded through an EPSRC studentship as part of the Insight project, which was a large UK collaboration between industry and academia aiming to address technical challenges relating to multi–constellation GNSS interoperability.

Contents

List of Figures

List of Tables

Nomenclature

List of acronyms and abbreviations

AC	Analysis Centre
ACC	Analysis Centre Coordinator
ACES	Atomic Clock Ensemble in Space
ADev	Allan Deviation
AFS	Atomic Frequency Standard
BDT	Beidou Time
BIPM	Bureau International des Poids et Mesures
BRDC	Broadcast Navigation Message RINEX Data File
BTRF	Beidou Terrestrial Reference Frame
C/A	Coarse Acquisition
CDDIS	Crustal Dynamics Data Information System
CDPE	Clock Difference Prediction Error
Cs	Caesium
COD/CODE	Centre for Orbit Determination in Europe
CPE	Clock Prediction Error
CT	Coordinate Time
ECEF	Earth-Centred Earth-Fixed
ECI	Earth-Centred Inertial
EGM08	Earth Gravity Model 2008
ESA	European Space Agency
ESOC	European Space Operations Centre
ECKF	Extended Clock model Kalman Filter
ECM	Extended Clock Model
EMP method	Extended Model Prediction method
FEI	Frequency Electronics Incorporated
FFM	Flicker Frequency Modulation
FFT	Fast Fourier Transform
FFO	Fractional Frequency Offset
FPM	Flicker Phase Modulation
GESS	Galileo Experimental Sensor Station
GFZ	German Research Centre for Geosciences

GIOVE	Galileo In-Orbit Validation Element
GLONASS	GLObalnaya NAvigatsionnaya Sputnikovaya Sistema
GNSS	Global Navigation Satellite System
GPS	Global Positioning System
GPST	GPS Time
GPSTk	The GPS Toolkit
GR	General Relativity
GRACE	Gravity Recovery and Climate Experiment
GST	Galileo System Time
GTRF	Galileo Terrestrial Reference Frame
HDev	Hadamard Deviation
HL	High Latency
ICD	Interface Control Document
IERS	International Earth Rotation Service
IGR	IGS Rapid
IGS	International GNSS Service
IGST	IGS Time
IGU	IGS Ultra-rapid
IGU-O	Observed part of IGS Ultra-rapid
IGU-P	Predicted part of IGS Ultra-rapid
IMVP	Institute of Metrology for Space and Time, Russia
INRiM	Italian National Institute for Metrological Research
JPL	Jet Propulsion Laboratory
KF	Kalman Filter
LFD	Linear Frequency Drift
LL	Low Latency
MIT	Massachussetts Institute of Technology
MDev	Modified Allan Deviation
MJD	Modified Julian Date
NASA	National Aeronautics and Space Administration (USA)
NFO	Normalised Frequency Offset
NGS	National Geodetic Survey
NLOS	Non-Line-Of-Sight
ODTS	Orbit Determination and Time Synchronisation
PE	Perkin Elmer
PED	Prediction Error Deviation
PHM	Passive Hydrogen Maser
PNT	Position, Navigation and Time
PPP	Precise Point Positioning
PRN	Pseudo-Random Noise
PTFM	Precise Time and Frequency Metrology
PVT	Position, Velocity and Time

PT	Proper Time
PZ–90.02	Parameters of the Earth 1990 (Version 2)
R&D	Research and Development
Rb	Rubidium
RCC	Relativistic Clock Correction
RFFO	Relativistic Factory Frequency Offset
RINEX	Receiver Independent Exchange Format
RMS	Root Mean Square
RRFM	Random Run Frequency Modulation
RTT	Relativistic Time Transformation
RWFM	Random Walk Frequency Modulation
SBAS	Satellite-based Augmentation System
SC	Satellite Clock
SCC	Satellite Clock Correction
SCD	Satellite Clock Difference
SCTE	Satellite Clock Time Error
SCKF	Standard Clock model Kalman Filter
SCM	Standard Clock Model
SCTO	Satellite or Space Clock Time Offset
SCTOP	Satellite Clock Time Offset Prediction
SCP	Satellite Clock Prediction
SCTS	Satellite Clock Time Synchronisation
SP3	Standard Product (Orbits and Clocks) 3
SP3c	Extended Standard Product 3
SVN	Space Vehicle Number
TAI	International Atomic Time
TOF	Time-Of-Flight
TT	Terrestrial Time
TTFF	Time-To-First-Fix
TWSTFT	Two Way Satellite Time and Frequency Transfer
UCL	University College London
UERE	User Equivalent Range Error
USN/USNO	United State Naval Observatory
UTC	Coordinated Universal Time
VCXO	Voltage–Controlled Crystal Oscillator
WGS84	World Geodetic System 1984
WHU	Wuhan University
WFM	White Frequency Modulation
WPM	White Phase Modulation

List of symbols

a_0	Time (or phase) offset parameter
a_1	Frequency offset parameter
a_2	Frequency drift parameter
Δt_{rel}	GNSS relativistic time transformation (general)
$\Delta t_{rel(c)}$	The GPS conventional relativistic time transformation
$\Delta t_{rel(e)}$	The GPS relativistic eccentricity correction
$\Delta t_{rel(eu)}$	The GPS relativistic eccentricity correction (receiver form)
$\Delta t_{rel(eo)}$	The GPS relativistic eccentricity correction (operational control form)
$\Delta t_{rel(k)}$	The GNSS satellite clock frequency offset (constant)
$\Delta t_{rel(p)}$	The GNSS precise relativistic time transformation
δt^s	Satellite Clock Time Offset
$E_{ij,p,n}$	Error in the prediction of difference between clock i and clock j at epoch labelled by n
$E_{Ri,p,n}$	Error in the prediction of the satellite clock time offset of clock i at epoch n with reference timescale denoted here by R
T_b	Beidou Time
T_e	Galileo Time
T_g	GPS Time
T_G	GNSS Time (general)
T_r	GLONASS Time
T_{igr}	IGS Rapid Time
T_{igs}	IGS Time
T_{igu}	IGS Ultra–rapid Time
T_{tai}	International Atomic Time
T_{tcg}	Geocentric Coordinated Time
T_{tt}	Terrestrial Time
T_{utc}	Universal Coordinated Time
T_R	Reference Timescale (general)
$\mathbf{x_k}$	State vector
$V = V(\mathbf{r})$	Earth's gravitational potential at position $\mathbf{r}$

Chapter 1

Introduction

The work presented in this thesis addresses aspects of the satellite clock time offset prediction (SCTOP)—or satellite clock prediction (SCP)—problem in the field of global navigation satellite systems (GNSS) technology. Here, this problem is broken down into four distinct components—characterisation, modelling, estimation and prediction—but there is considerable feedback and overlap between them.

In this chapter, the concept of satellite clock time offset (SCTO)in GNSS is introduced and with it the motivation for this research. The aims of this project along with the methods adopted to fulfil those aims are presented. An outline of the following chapters of the thesis follows.

1.1 Background

This section introduces the satellite clock time offset, and its role in GNSS. The purpose is to provide some of the background required to appreciate the context and motivation of the research that is presented in this thesis. Some of this work could be applied to clock prediction generally, i.e. outside of the GNSS context.

1.1.1 Satellite clock time offset (SCTO) as a problem in GNSS

Precise timing, at the nanoseconds level, is a critical requirement in GNSS. The basic GNSS measurement, the pseudorange, is essentially a time–of–flight (TOF) measurement, of the difference in time between when the wavefront of an electromagnetic (EM) signal is emitted from a navigation spacecraft's antenna to when that same wavefront is received at the user's antenna. In theory, the product of this TOF quantity and the speed of light in vacuum, gives the distance, or geometric range, between the spacecraft's antenna and the user's antenna. In reality however, a number of factors affect the receiver's ability to make accurate geometric range measurements. One of these factors is the satellite clock time offset (SCTO), which limits the receiver's ability to know the time of EM signal transmission.

In GNSS, the SCTO is the offset from system time of the time according to the clocks in orbit and on board GNSS spacecraft. Each GNSS has its own system time, which

is the reference timescale that enables the time–tagging of all time–varying phenomenon associated with that system. Assuming, for now, that system time represents *true* time then because the *perfect* clock does not exist, the SCTO for any satellite clock is always non–zero, at some level. For GPS and GLONASS satellite clocks, the typical value of the SCTO ranges from several nanoseconds to several microseconds, i.e. large enough to be problematic if unaccounted for. As such, the methods associated with knowing, with sufficient accuracy, the SCTO and the time–evolution of the SCTO, for all active satellite clocks in a constellation are fundamental to GNSS operation. Fundamental in the sense that satellite clock time prediction error is intrinsically linked to error in the modelling of the basic GNSS pseudorange measurement. There is an oft-quoted relationship between timing error and pseudorange modelling error—1 ns of timing uncertainty maps directly onto 30 cm error in modelled pseudorange. And depending on the number of measurements available and the geometry, pseudorange errors impact directly upon GNSS-based position, velocity and timing (PVT) solutions. The entire purpose for determining the SCTO, is to correct the satellite clock time measurements to make them agree with system time, i.e. to synchronise the satellite clock with the reference timescale. Thus, the problem of determining SCTO, for all clocks in a constellation, with sufficient accuracy, is sometimes referred to as the satellite clock time synchronisation (SCTS) problem, and this term is used here also. For this reason, the SCTO is also commonly referred to as the satellite clock correction (SCC).

There are several core components to the SCTS problem, which include:

- **The performance of precise timing technologies that operate in space.** This relates to the physical devices that generate the timing signal onboard the GNSS spacecraft. Usually, these are quartz oscillators with their frequency controlled by an atomic frequency standard (AFS) [Prestage & Weaver, 2007]. The ability to fly such *ultra-stable atomic clocks* in the space environment is one of the basic enabling factors of GNSS technology as it exists today. Here, a precise timing technology, or an ultra-stable atomic clock, is defined as a clock that is capable of keeping time with accuracy at the level of a few nanoseconds, or better, at a period of up to one day since its time was compared and synchronised to a reference timescale or another clock. Alongside the agencies that are responsible for providing the time–keeping systems for current and future GNSS satellites, there are several fundamental science missions that are driving the development of newer, better-performing (in terms of frequency stability, power, weight etc.), space–ready precise timing technologies [Cacciapuoti & Salomon, 2009; Prestage & Weaver, 2007].

- **The characterisation of SCTO,** which describes the process of studying and reporting on observations of actual satellite clock behaviour[1]—in essence a data analysis and statistical inference exercise. This can be conducted on the ground, e.g. at the test bed phase, to aid in the design and development of the clocks that eventually will form a component of the satellite flight hardware [Rawicz *et al.*, 1993].

[1] Here, satellite clock behaviour refers to the time–evolution of SCTO, for a single clock.

Or, there is in–orbit characterisation [Senior *et al.*, 2008; Waller *et al.*, 2010], which is the study of satellite clock behaviour when the satellite is in orbit. Of course, it is the in–orbit characteristics of the satellite clocks that affect GNSS performance, and therefore these are the focus in this study. Characterisation can be short–term (several seconds) [Griggs *et al.*, 2013; Hauschild *et al.*, 2013; Hesselbarth & Wanniger, 2008], medium–term (several minutes up to one day ahead) [Senior *et al.*, 2008; Waller *et al.*, 2010] or long–term (several days up to one month ahead) [Zhang *et al.*, 2007]. The scope of this project is limited to the study of the medium–term characteristics of GNSS satellite clock behaviours.

- **The modelling of SCTO,** which is the process of developing a suitable mathematical description of satellite clock behaviour. Models of SCTO are usually referred to simply as clock models. Typically, in the precise time and frequency metrology (PTFM) community, clock models are first–order linear stochastic differential equations [Galleani & Tavella, 2010], where the model parameters for a single clock are determined from a characterisation based on observations of the past behaviour of that same clock. In GNSS, in the case of the satellite clocks, there is an additional element to the modelling problem, which arises from the need to compare the in–orbit satellite clocks with ground–based terrestrial clocks or timescales[1]. This is the relativistic component of the SCTO modelling problem, which consists primarily of the phenomena of velocity time dilation and gravitational time dilation, due to the relative motion and the differences in gravitational potential, respectively, between the satellites and ground observers [Ashby, 2008]. The consequence of these relativistic phenomena for ground users is an apparent frequency shift of the satellite clocks that is dependent on the relative satellite–user position and velocity, which must be accounted for. An in–depth study of the impact of these relativistic effects in GNSS, presented in Chapter 7, forms a core component of this research.

- **The estimation of SCTO,** which is the problem of estimating SCTO from GNSS observational data. From the ground, the signal generated by a GNSS satellite clock can not be observed directly. Instead, the SCTO is usually inferred from satellite–receiver range measurements (e.g. GNSS pseudoranges). These measurements are collected at a distributed network of satellite tracking stations, and then sent to a central facility, where the data is processed and estimated values of the SCTO quantity, for all satellites in the system, are produced. As a result of inevitable delays arising from the data collection and data processing stages, SCTO estimates can not be disseminated to GNSS users in real-time. However, systems capable of disseminating SCTO estimates in near real-time (i.e. with latency at the order of tens of seconds or less) have begun to emerge in recent years. Most are set up as commercial services [Leandro *et al.*, 2011; Rocken *et al.*, 2011], but the International GNSS Service Real-Time (IGS-RT) Service, which is free, is also now available[Caissy *et al.*, 2011]. In this study, in relation to the topic of SCTO estimation in GNSS,

[1] In the case of all GNSS, system time is a real–time realisation of terrestrial time (TT), see Chapter 2 for details relating to the timescales in GNSS.

the developed prediction method centres around the use of the IGS precise satellite clock combination as input data for a Kalman filter estimator. The concept of SCTO estimation is developed further in Chapters 2, 3 and 4 and 8.

- **The prediction of SCTO,** which is the problem of obtaining a value of SCTO quantity in the future, based on past estimates of SCTO. For real-time users of (single-receiver i.e. non-differential) GNSS, predictions of the SCTO quantity are crucial, as for such users there is a direct link between SCTOP error and position, velocity and time (PVT) estimation error. Satellite clock time prediction algorithms can be simple or sophisticated. Usually, the performance of a satellite clock prediction algorithm is highly dependent upon prediction length. Prediction algorithms rely upon the characterisation of satellite clock behaviour based on historical data. Mathematical models and estimation algorithms are also important components of a satellite clock time predictor.

1.1.2 Satellite clock time offset predictions

It requires careful consideration of each of the components listed in Subsection 1.1.1 to fully appreciate the intrinsic link between satellite clock behaviour and GNSS performance, in terms of accuracy and reliability both, and some of these aspects are developed further in the following chapters. But clearly, this is a vast jigsaw puzzle, for which this research has focussed on only some of the pieces. If there is an overarching theme however, which holds together all of the findings reported herein, then this is topic of satellite clock prediction (SCP) in GNSS, and so this is covered in more detail in this section.

SCTOP and GNSS performance

The impact of uncertainty in the determination of the SCTO quantity is strongest in applications that rely upon measurements collected with a single receiver only. This is in contrast to differential GNSS, where there are two or more receivers, with the location of at least one of those receivers known exactly, and the effects of SCTO uncertainty on PVT estimation in the *roving* receiver is cancelled to a large extent (details in Chapter 2). Further, in single–receiver scenarios where a real–time PVT estimate is required, users *must* rely upon a predicted value of the SCTO quantity. In such scenarios, the performance of a satellite clock predictor directly affects overall GNSS performance,

- in **accuracy** terms, because of the direct link between SCTO prediction error and GNSS measurement modelling error.
- in **reliability** terms, i.e. integrity, continuity and availability through the reduction of failure detection thresholds.

The dissemination of SCTO predictions in real–time

SCTO predictions or estimates are disseminated to users in various forms (e.g. via information modulated onto an EM signal, via an ascii data file, etc). This can be in real–time

(predictions) or with a certain latency (estimates). Collectively, these SCTO predictions or estimates, which are packaged (in some way) for dissemination to the user community are referred to as satellite clock products.

As far as satellite clock prediction products are concerned, there are two broad categories available to users today:

- **The near real-time, low latency (LL) predictions,** which are satellite clock predictions based on satellite clock estimates determined using data from several seconds up to several tens of seconds in the past. These are a relatively new class of predicted clock product that has become available to real-time users in recent times, motivated largely by advances in the real-time precise point positioning (RT-PPP) data processing strategy, see Rizos *et al.* [2012]. In essence, the LL prediction products exist to enable real-time sub-decimetre level positioning using the PPP data processing method. But as LL–type prediction products are not built into the basic receiver interface specification of the current GNSS, additional hardware and software capabilities are required to use them.

- **The navigation message type, high latency (HL) predictions,** are satellite clock predictions that are computed using SCTO estimates based on data from several minutes (usually at least 15 minutes) up to twenty-four hours in the past. These are the prediction products which are computed by the GNSS operation control segments, and delivered to users via a modulation scheme on the TOF ranging signals. These HL predictions are written in the GNSS receiver–signal interface specification Department of Defense, United States of America [2008]; Galileo ICD [2006]; GLONASS ICD [1998], which means the positioning algorithms of most GNSS–enabled receivers rely upon this type of prediction. The research in this thesis focuses on this category of prediction.

1.2 Objectives and methodology

A statement of the general objective of this research, which is the project's overarching goal is presented in Subsection 1.2.1. Subsection 1.2.2 outlines the key components of the prediction method that is developed to address the general objective. Subsection 1.2.3 gives a statement of the detailed objectives of this study. These are research tasks to be conducted with the general objective in mind. Subsection 1.2.4 details the motivating factors that underpin the detailed objectives.

1.2.1 Statement of general objective

The general objective of this work is to develop an enhanced satellite clock time offset prediction method, based on a modelling strategy that is led by a detailed study of real clock behaviour data. To validate this approach, a GNSS satellite clock time offset prediction scheme is tested in software, and this simulates an anticipated real–time process. This simulation enables the comparison of this newly developed prediction method with the

prediction method of the International GNSS Service (IGS)—a well-respected and highly influential scientific GNSS organisation—in a variety of scenarios.

1.2.2 Prediction method

Broadly speaking, satellite clock time offset prediction (SCTOP) methods in GNSS can be separated into two categories, based on the input data that the method demands. The first type of SCTOP method uses GNSS measurements (e.g. code or carrier phase pseudoranges) as input data. The second type works with SCTO estimates as input. The first type of method is a simple one–stage process: GNSS measurements in, SCTO predictions out. The second type of method is the second–stage of a two–stage process, this is the method adopted in this study. In theory, as far as SCTOP performance is concerned, there should be no difference between the two methods, as the underlying GNSS measurement information is the same.

In practice however, there are several advantages to the second approach with regards to data quality and tractability of method, which are described in detail in later chapters. Briefly, the second method allows for using the IGS clock combination products, a high–quality, well–documented and widely–used satellite clock data set. In turn, this enables the research to focus on the study of satellite clock behaviours, rather than getting involved in accounting for the other error sources that affect the GNSS measurements[1].

In this method, each satellite clock is considered on a case-by-case basis. The method starts with clock characterisation using one month of satellite clock estimate data. Here, characterisation is done using a combination of time–domain (e.g. Allan variance) and frequency domain (e.g. FFT–based power spectral density diagrams) stability analysis techniques. The results of characterisation are used to initialise the parameters of the *standard* clock model, for that clock. This is essentially a first–order linear stochastic differential equation, with three parameters in the deterministic component that correspond to the clock time offset, frequency offset and linear frequency drift. Based on the results of this analysis, an appropriate model is chosen for that satellite clock. This model is implemented in a Kalman filter, which is set up to output SCTO predictions over a range of desired prediction intervals.

1.2.3 Statement of detailed objectives

In this section, the detailed objectives of this project are outlined. These are research tasks, designed with the general objective in mind, and these include:

- A systematic study of GPS and GLONASS clock behaviour using several years of *precise* satellite clock data, and considering the full constellation of satellites, to gain an understanding of the characteristics of current in–orbit clocks. Precise satellite

[1] At some level, the IGS clock products are affected by mismodelling or estimation inaccuracy in the parameters partially correlated to the clock models, e.g. satellite orbit related errors. However, given the extent of the IGS tracking network and the maturity of the estimation schemes used by the IGS, these correlations are likely to be at worst a second order effect.

clock data is the name given to the post–processed estimates of satellite clock time offsets that are generated by the leading GNSS data analysis centres.

- An analysis of existing, operational prediction schemes to quantify current performance over a range of prediction lengths, in order to determine the key factors that are likely to be limiting their performance.
- An investigation into the general implications of using a more rigorous model for the relativistic component of the satellite clock time offset model, based on the use of precise satellite–receiver relative velocity data along with a detailed description of gravitational potential differences using the Earth Gravity Model 2008 (EGM08) to degree and order 20.
- The performance testing and analysis of the developed SCTO prediction method.
- The development and testing of a set of software tools (C++/MATLAB) that will enable experiments to be conducted in order to test and validate a new prediction method.

1.2.4 Motivation

In this section, the line of reasoning that led to the formulation of the research tasks as they are outlined in Subsection 1.2.3 is given.

A study of GPS and GLONASS in–orbit satellite clock characteristics

A satellite clock prediction algorithm can not be built without an intuitive understanding of the in–orbit behaviour of GNSS clocks, which can only be achieved by looking at real data. There is literature reporting on the characteristics of the in–orbit behaviour of GNSS clocks[Senior *et al.*, 2008; Waller *et al.*, 2010], but these were published over three years ago, using data from over five years ago, and cover only the GPS and Galileo satellite clocks[1], respectively. A detailed report on the characteristics of GLONASS in–orbit clocks, based on the analysis of real data, does not exist in the literature, but there are a variety of GLONASS SCTO data products which are now publicly available. Also, since 2010, newer satellites equipped with updated precise timing technologies have been launched (four GPS satellites, four Galileo In–Orbit Validation (IOV) satellites, eleven GLONASS satellites). With all of this is mind, it makes sense that this project should start with a report on the analysis of the best data sets that can be obtained for the two fully operational GNSS (in 2013), which are GPS and GLONASS. The result of such an analysis is presented in Chapter 5, and certainly in the GLONASS case this fills a clear gap in the existing literature.

[1] In the form of a detailed in–orbit assessment of the clocks on the GIOVE-A and GIOVE-B satellites[Waller *et al.*, 2010].

A study of an operational GNSS SCTO prediction scheme

As mentioned before, SCTO predictions are fundamental for GNSS operation, and as such, every GNSS must operate its own SCTO prediction scheme of some kind. However, in the existing literature, the SCTO prediction strategies of GPS and GLONASS—the two fully operational GNSS (2013)—are barely mentioned in any real depth; perhaps because they are both military systems. The performance of the GPS SCTO prediction scheme is monitored and regularly reported by the IGS [Dow *et al.*, 2009] at `http://acc.igs.org/media/Gmt_sum_ultcmp_all_clk_smooth_ALL.gif`, where the (Root Mean Square) RMS prediction error of the GPS broadcast clock product is shown to be ≈ 4 ns (when comparing against the IGS rapid timescale, see Chapter 2)[1], which is ~ 1.2 m of ranging error. While this analysis is useful because it gives a sense of the typical value of the uncertainty in the GPS broadcast SCTO prediction, it does not provide any meaningful insight into the underlying prediction strategy. Crucially, the relationship between SCTO prediction error and prediction length is not emphasised in this reporting. This is a critical point. It makes intuitive sense that prediction error should increase as the prediction interval increases. Therefore, without an idea of the prediction intervals associated with these published SCTO prediction error values, it is difficult to make a meaningful inference of the actual performance of these prediction schemes.

A more rigorous model of the relativistic time transformation

As far back as 2000, Ray [2000] reported that periodic signals could be observed in GPS satellite clock behaviour. Then in 2002, Kouba [2002] presented the results of an investigation into the GPS conventional relativistic time transformation (RTT), which is used by GPS receivers to compute the relativistic component of the GPS SCTO on the recommendation of the GPS Directorate in its GPS Interface Control Document (ICD) [IS-GPS-200E, 2010][2]. Kouba [2002] and the follow–up paper[Kouba, 2004], showed that this conventional method for implementing the relativistic time transformation was in error at a rate of up to 0.2 ns per day, with cyclic variations of up to 0.2 ns and 0.07 ns of period 14 days and 6 hours, respectively, and the cause was attributed to numerical approximation (or truncation) error.

The GPS conventional RTT is an simplified version of the analytical model for the GPS RTT. A first–principles derivation of the analytical GPS RTT is found in Ashby [2008]. This analytical model captures the effects of velocity time dilation and gravitational time dilation on the SCTO. In the analytical model, the relativistic time transformation is a function of the relative satellite–receiver gravitational potential (and thus, relative position) and relative satellite–receiver velocity. The approximation errors in the conventional RTT that [Kouba, 2004] found in the satellite clock data arose from the use of a first–order model of Earth gravity field (which treats the Earth as a point mass) to calculate the satellite–receiver gravitational potential difference. Kouba [2004] used

[1] In the GLONASS case, such a performance report does not exist.

[2] The SCTO model in the GPS ICD is often referred to as the GPS broadcast clock model, and the relativistic component is the GPS relativity correction or (in the terminology of Kouba [2002]) the GPS conventional relativistic time transformation.

a second–order model, which considers the effects of modelling the Earth as an oblate spheroid on the GPS satellite orbits and on the GPS RTT directly. Kouba [2004] noticed RTT approximation errors with 14 days and 6 hours period when comparing satellite clock models using this improved RTT were compared with models using the GPS conventional RTT.

The idea for this component of the project is to take this line of inquiry one step further, by using the highest–quality (precise) GPS orbit solutions and a more complete description of the gravitational potential variations using the Earth Gravity Model 2008 (EGM08) (up to degree and order 20). The objective is to assess the impact of an even more rigorous RTT in the modelling of GNSS SCTO's, and to determine whether such an approach could contribute to an improved prediction method.

The development and testing of an SCTO prediction system

There are features in the SCTO signals of many GPS satellite clocks that are not accounted for by the standard clock model, which is presented in Chapter 3. But, there are alternative models that can be explored, and as there are many applications (e.g. prediction of the satellite clock parameters in the GNSS navigation messages, precise point positioning (PPP)—a single–receiver technique, low–latency (or real–time) GNSS time–transfer etc.) that would benefit from interpolated or extrapolated clock values of the highest quality, it is worthwhile to do so.

In this work, extension to the standard clock model (SCM) is presented. Here, this will be referred to as the extended clock model (ECM). The ECM accounts for periodic signals, present in many of the GPS satellite clocks, and deals with flicker noise processes (FPM and FFM), as seen in GPS and GLONASS satellite clocks, which are difficult to model analytically. The ECM also includes a component, known here as the reference timescale offset term, which allows for clock information of different types, or from different sources, to be combined. The KF implementation of the extended clock model forms the core component of a new GPS satellite clock prediction strategy, which uses IGS GPS satellite clock data as input. This prediction system was designed in such a way that it is compatible with current IGS products—to slot into the existing framework. The prediction method that is tested here is a partial implementation of a potentially more complete prediction scheme.

1.3 Thesis outline

This section provides a brief description of the following chapters of this thesis. Chapter 2 further establishes the motivation for this research in the GNSS context by introducing the aspects of GNSS that are relevant to satellite clock time offset prediction. Chapter 3 contains all of the key concepts, definitions and methods that are fundamental in the field of time and frequency metrology, but are also relied upon heavily in this research. Chapter 4 provides an in–depth review of the key works that ultimately influenced the direction and scope of this research project. Also, the data sources used for this research

are described here, along with some details of the software tools used to carry out the research. Chapter 5 presents a study of the characteristic of GPS and GLONASS satellite clocks, based around the analysis of the full set of GPS and GLONASS satellite clock data over a period of several years. Chapter 6 centres around a performance analysis of the IGS prediction scheme for the GPS satellite clocks. The product of the IGS prediction are archived and publicly available, and for this reason the IGS predictions provides a rich source of data for studying existing GNSS satellite clock prediction methods. Chapter 7 presents a study of relativistic time transformation (RTT) modelling and considers how RTT modelling fits into the broader context of SCTO prediction in GNSS. Chapter 8 presents a new, data–driven method for GPS satellite clock time offset prediction that is compared in performance terms against the outputs of the IGS GPS satellite clock prediction algorithm. Chapter 9 is the final chapter of this thesis. Here, the conclusions of this project are given along with a discussion of implications of the results in a broader context.

Chapter 2

Aspects of GNSS that are relevant to satellite clock prediction

Chapter outline

The purpose of this chapter is to introduce global navigation satellite systems, describing briefly the science and engineering underlying the technology as it exists today, setting the scene for the in-depth study of GNSS satellite clocks presented in later chapters. There are several excellent texts on the topic of GNSS, but Hofmann-Wellenhof *et al.* [2008], Groves [2013] and Misra & Enge [2011], together, provide a fairly comprehensive overview of the field, and were used often in preparing this chapter.

The problem of satellite clock estimation and prediction in GNSS is complicated. Often, the connection between a physical on-board timekeeping device in a navigation spacecraft, and the performance of a GNSS receiver on the ground, is difficult to imagine. Thus, a particular emphasis is given here to describing the hardware, software and mathematical models associated with satellite clocks in GNSS, and the interplay between them. From this, a clearer picture should emerge of what it means to characterise, model, and predict GNSS space clocks—in the sense of how these terms are defined in Chapter 1—and why these are important in the GNSS context. The characterisation, modelling and prediction of GNSS satellite clock time offsets is the primary focus of the following chapters of this thesis.

2.1 An overview of the relevant aspects of GNSS theory

This section presents a basic introduction to the theory of GNSS, which was written for a specific purpose. Here, the aim is not to give a full description of how an operational GNSS works, but rather to establish the key ideas that are necessary to start a meaningful discussion on the topic of satellite clocks in GNSS. The treatment of all other aspects are kept to a minimum, or avoided entirely. As such, the section focuses specifically on the following topics: spatial reference frames and timescales, the satellite clock time and satellite orbit determination problem and also, the mathematical model of the basic GNSS pseudorange measurement and the contribution of the satellite clock time offset in

it. These components of GNSS theory are critical for understanding—and defining—the satellite clock problem in GNSS. Other important aspects of GNSS theory—the signals, the measurement combinations[1], the position, velocity and time (PVT) estimation algorithms, and so on—are not directly relevant and so they are not covered here.

2.1.1 Spatial reference frames and timescales

Two basic foundations for any GNSS are the spatial reference system and the time reference system or reference timescale. These are the sets of rules for assigning co-ordinates to each point in space and for labelling instances in time, respectively.

Earth-centred Inertial and Earth-centred Earth-fixed reference frames

For dealing with space, there are two classes of reference system that are relevant, which are labelled inertial, i.e. non-accelerating, or non-inertial. In GNSS, both are necessary. This is mainly because the theory of spacecraft motion (astrodynamics), which is more or less based upon classical Newtonian mechanics, is expressed in its most natural form with equations describing motion in inertial space. But for users, most who are fixed on the surface of the Earth, a non-inertial rotating reference frame with rotation rate equal to the Earth's rotation rate is required. As these are Earth-based positioning systems, the natural choice for the origin is the Earth's centre of mass. So, Earth-centred inertial (ECI) reference systems and Earth-centred Earth-fixed (ECEF) reference systems are two basic requirements for GNSS.

Proper time, co-ordinate time and satellite clock time

In dealing with time, the concepts of proper time (PT) and coordinate time (CT) are helpful. Proper time is time according to a single perfect clock where the time measurements are observed in the body frame of that clock. By contrast, co-ordinate time is time according to a perfect clock at rest in a specific and fully defined inertial coordinate system. For GNSS users, as mentioned previously such a coordinate system is naturally an ECI system. Proper time and co-ordinate time are concepts that originate from the theory of space and time based on General Relativity (GR), but at this stage it is not necessary to go into the ideas behind in any more detail.

Although similar in several ways to the concept of proper time, it is useful to introduce the notion of satellite clock time (SCT), or simply satellite time (ST). SCT is time according to the active clock onboard an orbiting satellite, in the body frame of the satellite, and as such it is an approximation of a proper time. The essential difference between a proper time and satellite clock time is that the latter is time according to a real clock.

[1]The so–called ionosphere–free observable does crop up at several point later on in the thesis, although the underlying principles behind it are not covered. Without going into more detail than is required, the ionosphere–free observable is a mathematical quantity used in various GNSS PNT algorithms that is formed by combining measurements across two or more frequencies. The most common example of this is the GPS L1/L2 combination. To first order, the GNSS ionosphere–free observable is free from errors associated with GNSS signal transit delay due to the paths of the signals through the ionosphere.

The international standards

The science and engineering behind the realisation of usable reference frames and timescales is quite complex, and the topic continues to evolve, but a good source for the latest developments in the field of reference frame and timescale realisation is the latest version of the International Earth Orientation Service (IERS) Conventions document [Petit, G. & Luzum, B. (eds), 2010]. In essence, the IERS Conventions are a set of methods for producing reference frames and timescales that are accepted as standard by the international scientific community. These include:

- the **International Terrestrial Reference System (ITRS),** which provides the rules for realising an **International Terrestrial Reference Frame (ITRF),** using measurements based on the four geodetic techniques of GNSS, Very Long Baseline Interferometry (VLBI), Satellite Laser Ranging (SLR) and Doppler Orbitography and Radio-positioning Integrated by Satellite (DORIS). ITRF2008 [Altimimi *et al.*, 2011] is the latest realisation of the ITRS that is officially available, but there are plans to release a newer version, ITRF2013, in 2014 [Altimimi *et al.*, 2013]. An ITRF provides its users with an ECEF reference frame suitable for the most demanding applications that require measurements on or near the Earth's surface.

- the **International Celestial Reference System (ICRS),** which gives the rules for realising an **International Celestial Reference Frame (ICRF)**, which is the standard international ECI reference for applications on or near the Earth.

- **Geocentric Coordinated Time (TCG)**, which is a timescale that is defined so as to be consistent to GR theory, in the neighbourhood of a non-rotating Earth i.e. this is defined in ECI terms. Because of this, TCG is not directly observable, and is of limited use in GNSS, besides in providing a standard, underlying relativistic co–ordinate timescale. In one sense, it can be thought of as a theoretical abstraction that enables aspects of GNSS theory, especially in terms of the timescales, to be expressed within the framework of GR theory.

- **Terrestrial Time (TT),** a theoretical but physically realisable proper time system. The TT rate (time–interval), dTT is related to TCG rate, $dTCG$ by a scale factor, by convention [Petit & Wolf, 1997]

$$\frac{dTT}{dTCG} = 1 - \frac{W_0}{c^2} \tag{2.1}$$

  where $W_0 = 62636857\ \mathrm{m^2 s^{-2}}$, a fundamental constant, is the Earth's gravitational potential at mean sea level (i.e. on the geoid.) TT provides the theoretical framework for realising **International Atomic Time (TAI),** an atomic timescale based on time according to an ensemble of primary frequency standards located at various sites across the globe, with the Systemé International (SI) second as its fundamental time interval. The SI second is formally defined as [BIPM, 1969]:

the duration of 9,192,631,770 periods of the radiation corresponding to the transition between two hyperfine levels of the ground state of the caesium 133 atom, with the caesium atom at rest, on the rotating geoid, at a temperature of 0 K.

TAI is closely related to **Coordinated Universal Time (UTC),** the time used today for civil timekeeping purposes. They are related in the sense that TAI is the frequency standard for UTC. The only difference between them is the intermittent introduction of leap seconds to UTC so that UTC differs from TAI by an integer number of seconds. Without this the link between UTC and the Earth's rotation rate would gradually disappear as the continuous and uniform TAI timescale diverges indefinitely from **Universal Time (UT1)**, a timescale defined by the Earth's rotation [Audoin & Guinot, 2001]. The origin of TAI was set to satisfy $T_{ut1} - T_{tai} = 0$ on 0000 of 1 January 1958. TAI is computed at the BIPM using clock measurements from about 400 atomic clocks running in timing laboratories across the globe. Due to the procedures and algorithms related to the collecting and combining of these measurements, TAI is only available to users with a latency of about thirty days, although efforts are ongoing to reduce this to seven days, see Petit *et al.* [2012] and Whibberley *et al.* [2011].

The relationship between UTC and TAI is defined by the following expression:

$$T_{utc} - T_{tai} = l \tag{2.2}$$

which reads time according to UTC minus time according to TAI, where l is an integer that represents leap seconds introduced to UTC. On 1 January 1972, l was ten. As of 6 August 2013, l is thirty-five, and will remain so until 30 June 2014. The IERS is the organisation responsible for the introduction of leap seconds when it is necessary. An up-to-date record of the date and time when leap seconds were introduced to UTC is maintained by the BIPM at `http://hpiers.obspm.fr/iers/bul/bulc/Leap_Second_History.dat`. [Arias *et al.*, 2011] provides greater detail on the method involved in generation of UTC and TAI at the BIPM, along with an analysis of the performance of these timescales in a frequency stability sense.

GNSS reference frames and timescales

For GNSS purposes, a key issue is that the standard reference frame and timescale, ITRF and TAI (or UTC), respectively, are not accessible in real-time. Thus, it is necessary that each GNSS generate its own realisation of ITRS and TAI to enable day-to-day operation. As a result, there are several different reference frames and timescales in GNSS.

For GPS, the **World Geodetic System 1984 (WGS84)** is adopted as the system reference frame. The relevant timescales are **GPS System Time (GPST)** and the realisation of **UTC at the United States Naval Observatory (UTC(USNO))**. GPST is the internal reference timescale for all GPS clocks, both in space and on the ground. However, unlike UTC and thus UTC(USNO), which are affected by the introduction of leap seconds, GPST is a continuous timescale. The relationship between GPST and TAI

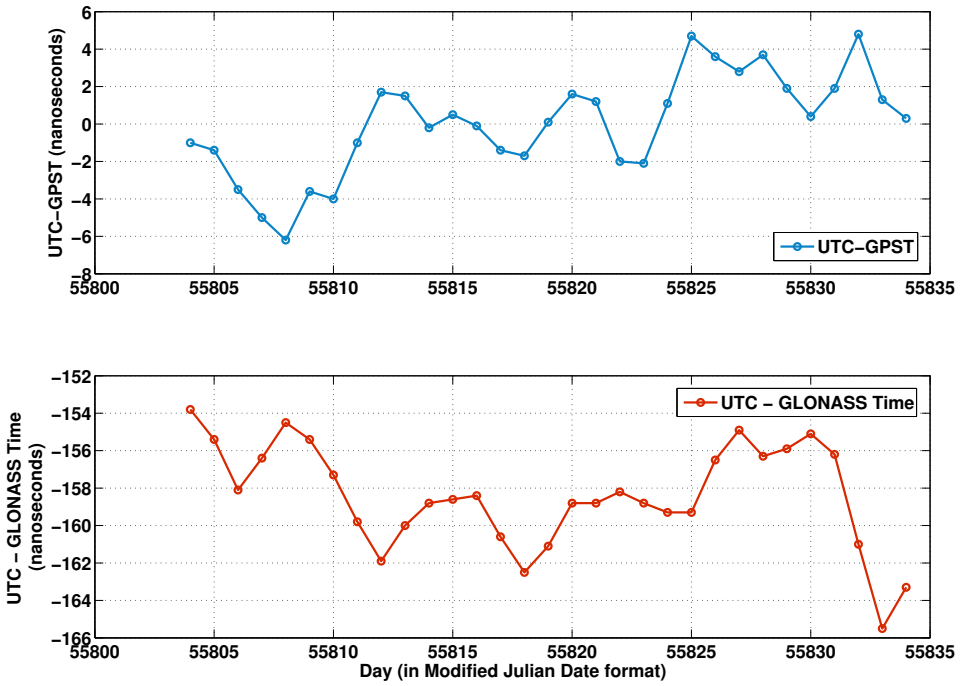

Figure 2.1: Time–series for September 2011 of $T_{utc} - T_g$(above), the difference between time according to UTC and time according to GPS Time, and of $T_{utc} - T_r$(bottom), the difference between UTC and GLONASS Time. The data used to generate these plots can be acquired from the BIPM Circular T Bulletin at ftp://ftp2.bipm.org/pub/tai/publication/cirt.285.

is expressed as

$$T_{tai} - T_g = 19 + C_0 \tag{2.3}$$

because at the origin (i.e. the zero epoch) of GPST on 0000 hrs of 6 January 1980, UTC was ahead of TAI by nineteen seconds. Here, $C_0 <= 1\ \mu s$ represents the specified level of consistency between GPST and UTC(USNO), which is also a good approximation of the level of agreement between GPST and TAI. In practice the agreement is much better, at the level of tens of nanoseconds [McCarthy & Seidelmann, 2009]. The top axes in figure 2.1 also supports this. Here, in September 2011, the offset between UTC and GPST (neglecting the leap seconds), which is the C_0 quantity, agrees with UTC as the few nanoseconds level, with a maximum absolute value of the 6 ns throughout the whole month.

In the GLONASS case, **Parametry-Zemli**[1] **1990 (PZ-90.02)** is the reference frame and **GLONASS Time** is the reference timescale. GLONASS time is kept within one microsecond of the realisation of **UTC at the Institute of Metrology for Space and Time (IMVP), Russia, often denoted UTC(SU)**. Unlike GPST, which is continuous, GLONASS Time is aligned to UTC(SU) and therefore is affected by the introduction of

[1]Paremetry-Zemli = "the parameters of the Earth"

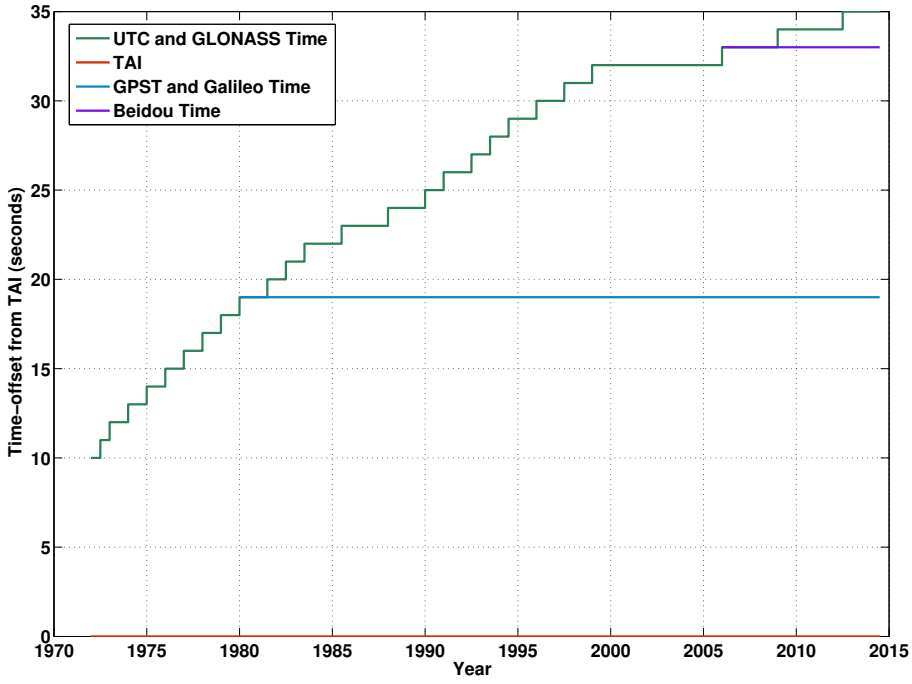

Figure 2.2: The GNSS system timescales: GPS Time, GLONASS Time, Galileo Time and Beidou Time, and their relationship with UTC and TAI. Here, TAI (red line), being continuous, provides a sort of *fundamental* reference timescale.

leap seconds to UTC. The relationship between GLONASS Time and UTC is expressed as

$$T_{utc(su)} - T_r = C_1 \tag{2.4}$$

where $C_1 <= 1\ \mu s$. Similar to the GPS case, the bottom axes in figure 2.1 supports this assertion, the variability in the $T_{utc(su)} - T_r$ quantity is about 10 ns across the January 2011, i.e. well within the $1\ \mu s$.

The other two main GNSS, Galileo and Beidou, each have their own independent realisations of ITRS, which are the Galileo Terrestrial Reference Frame (GTRF) and the Beidou Terrestrial Reference Frame (BTRF), respectively. Also, they have their own reference timescales, Galileo System Time (GST) and Beidou System Time (BDT), respectively.

IGS Reference Frame and IGS Time

The reference frames and timescales of the International GNSS Service (IGS) are also important in this work. The IGS Reference Frame is a realisation of the ITRS and IGS System Time is a realisation of UTC. The IGS reference frames and the IGS timescale are evaluated using data collected by the IGS global GNSS data tracking network. The IGS is introduced in more detail in Chapter 4.

Practical implications for this research

There are some practical implications that arise due to the variety of reference frame and timescales that are widely used in GNSS. The main issue is that given a set of data—e.g. time or position data of a satellite or a receiver—the reference timescale and spatial reference frame to which the data corresponds is not always immediately apparent. This information must be available, as some form of metadata, for that data set to be physically meaningful to the user. There are several independent sources of GNSS satellite clock time data, and some of the results of this research are based on the analysis and comparison of data sets where the underlying reference timescales are different. The difference in timescales must be addressed in the analysis, and this issue is explored in some depth in Chapter 6. A key aspect of this project is the development of a method to account for timescale differences in a satellite clock prediction algorithm. The development of this method enables the prediction algorithm to use all the available satellite clock data and is presented in Chapter 8.

2.1.2 Satellite orbit and satellite clock time determination

The estimation of a user's position and time from GNSS measurements requires that the satellite position and satellite clock time are quantities known to the user. To meet this requirement there are two processes involved. The first process is orbit determination and time synchronisation (ODTS). This is an estimation procedure, which means that parameters associated with the satellite orbits and clocks are determined using actual observations of satellite–receiver ranges from a distributed network of GNSS satellite tracking stations. The second process is satellite orbit and clock prediction. In this process, parameters associated with the satellite orbit and satellite clock, which are outputs from an ODTS process, are extrapolated using mathematical models that describe the time–evolution of those parameters. In many real–time applications, users rely upon the outputs of this second process to estimate their current position and time using GNSS. Thus, it is a basic feature of GNSS technology that the satellite position and satellite clock time are predictable. Here, predictable means that the satellite position and satellite clock time can be determined accurately—where the accuracy requirement is determined by the positioning and timing accuracy specifications of the system, or the end–user.

The predictability of satellite orbits and satellite clock time

For satellite orbits, predictability is closely related to the fidelity of the mathematical modelling of the conservative and non-conservative forces acting on the satellite and by the observability of the initial conditions of position and velocity. It is a similar story for the satellite clocks, where predictability is determined by the fidelity of the mathematical model for SCTO and the the observability of the initial conditions of those clock model parameters. Here, the key difference between the two cases is that the clock model represents the performance of a physical on–board timekeeping device, and this physical device experiences significant random frequency fluctuations. Ultimately, it is these stochastic

variations, i.e. the inherent clock noise, that limit satellite clock time predictability. An in–depth look at the deterministic and stochastic characteristics of the GPS and GLONASS satellite clocks is presented in Chapter 5.

The ODTS process

A broad description of the satellite orbit and satellite clock time determination process, in the case of GPS, is given in Zumberge & Bertiger [1996]. Satellite orbit and clock time determination for GLONASS, Galileo and Beidou also follow similar methods, see Hofmann-Wellenhof *et al.* [2008].

Briefly, this is how the ODTS process works. The GNSS ground control segment—the component of a GNSS that maintains and operates the system's ground-based infrastructure—has a distributed network of satellite monitor stations. At these monitoring stations, code and phase pseudo-range data are collected, across multiple frequencies. The multiple frequencies allow for the effects of the ionosphere to be accounted for. The transit time of a GNSS signal is delayed in its path through the ionosphere, but the magnitude of the delay depends upon the signal's frequency and this frequency dependency enables the formation of the so-called ionosphere-free observables wherein the ionospheric delay is substantially modelled out. The monitor station receivers are equipped with atomic clocks for timing purposes. In principle, with the monitoring station position known exactly, and known to be stationary in an ECEF reference frame, and with station clock time known with good accuracy, then the satellite orbit and clock parameters, for a single satellite, might be determined either by combining observations of satellite–receiver ranges over multiple epochs, or, where observations to the same satellite are made from multiple tracking stations, the geometry of the tracking network, which is known and fixed, might be used to constrain the estimated orbit and clock parameters.

So, in a nutshell this describes the ODTS process. A lot of details have been left out here. However, as far as this research is concerned, the key point is that in GNSS the satellite clock parameter estimates are determined directly from GNSS measurements. The number of tracking stations may vary, the exact data processing methods and software may vary, the way in which the outputs of the ODTS process are distributed to users may vary, but fundamentally, all ODTS processes based on GNSS measurements are carried out in the way that is described in this section. The significance of this is that satellite clock behaviour is not observed directly, rather it is inferred from pseudorange data. Due to various errors sources associated with the pseudorange measurement process and the ODTS clock parameter estimation process, satellite clock data that is obtained in the way is sometimes referred to as apparent clock data, see Section 2.2.

2.1.3 The pseudorange measurement

Once the spatial reference frame and the reference timescale are established, and the satellite position and satellite clock time are known, it is possible to start building a mathematical model of the basic GNSS pseudorange measurement. It is possible also to

discuss the impact of the SCTO on measurement modelling uncertainty here, by studying a very basic, and general, version of the GNSS pseudorange equation

$$P_r^s(t) = \rho(t) + c(\delta t_r(t) - \delta t^s(t-\tau)) + \varepsilon(t) \tag{2.5}$$

where $P_r^s(t)$ is the pseudorange from user receiver antenna labelled with subscript r to navigation spacecraft antenna labelled with superscript s, $\rho(t) = c(t_r(t) - t^s(t-\tau)) = |\mathbf{x}_r(t) - \mathbf{X}^s(t-\tau)|$ is the geometric range—$X^s(t-\tau)$ is satellite position at time $t-\tau$ and $\mathbf{x}_r$ is ground receiver position at time t—τ is the time-of-flight of the ranging signal, $t_r(t)$ is time of signal reception according to the receiver clock, $t^s(t-\tau)$ is the time of signal transmission according to the satellite clock, $\delta t^s(t-\tau)$ is satellite clock time-offset from system time at time $t-\tau$ and $\delta t_r(t)$ is receiver clock time-offset. In this expression, the term $\varepsilon(t)$ is a catch-all error term which captures the contributions of all other factors that contribute to the bias, noise or uncertainty in the measured pseudorange. Among these, the main factors are commonly broken down into three components—satellite–side factors, signal propagation related factors and the receiver-side factors. The satellite–side factors comprise bias or uncertainties in the modelled values of the $\mathbf{X}^s(t-\tau)$ and $\delta t^s(t-\tau)$ quantities. The signal propagation related factors are separated into ionospheric and tropospheric delay components. The receiver-side factors comprise multipath, non–line–of–sight (NLOS) reception, receiver hardware delay, receiver clock offset and more. Although these are labelled as receiver–side error factors, not all of these errors (e.g. multipath and NLOS reception) are errors caused by the receiver equipment, rather they are caused by the local environment of the receiver. The combination of the receiver clock offset and the receiver hardware delay are estimated in the receiver software.

In table 2.1, the typical contribution of several of these error sources to the pseudorange measurement error, often called the user equivalent range error (UERE), using values published in Conley *et al.* [2006], that correspond to GPS-based measurements using the GPS standard positioning service—i.e. the C/A code only. For now, if we make an assumption that all error sources are independent, then the sum of the variances of each individual error source is equal to the variance of the UERE. These typical error values and their contribution the UERE error budget are designed to be used as simple tools for analysing the impact of individual error sources on the total accuracy of the range measurement. As mentioned in Groves [2013], all such published error budgets make varying assumptions about system performance, user equipment, number of satellites and so on. As such, this approach for analysing the impact of individual error sources should be used carefully. In short, UERE error budget analyses can be used to aid in analysis, but should not be used to make scenario-specific claims about GNSS pseudorange measurement performance.

The ionosphere errors tend to be highly correlated (spatially and temporally), so the ionosphere delay error won't necessarily contribute to the position error with quite the impact that it would appear–that is, the resulting position may be biased but not noisy, with the bias-like effect changing slowly (e.g. circa 1 dm over a few tens of seconds). But, after this, in the case where measurements are available from a single–receiver only, the satellite clock time offset estimation/prediction error provides the most significant

Error source	1σ error (m)
Satellite clock offset	1.1
L1 P(Y) - L1 C/A group delay	0.3
Satellite orbit	0.8
Ionospheric delay	7.0
Tropospheric delay	0.2
Receiver tracking noise	0.1
Multipath	0.2
UERE	7.1

Table 2.1: Pseudorange measurement error budget for a GPS standard positioning service (SPS) scenario. This table is mostly adapted from Conley *et al.* [2006].

contribution to the pseudorange uncertainty budget. However, those users that require high accuracy positioning with GNSS can use some form of differential data processing technique where estimates of the satellite clock time offset at another receiver at a known location (the reference station) are used to correct for the satellite clock time offset at the user's (roving) receiver, but, the need for additional data processing capabilities and a communication link with the reference station creates additional software and hardware requirements for user's receiver. Therefore, user equipment with differential capabilities tends to be more expensive, bulkier due to additional hardware components and require a greater level of expertise to operate.

2.2 Satellite clock time offset in GNSS

With the relevant GNSS background established, it is now possible to focus more specifically on the processes of SCTO estimation and prediction in GNSS. First, it is useful to clarify further about the actual physical quantity being estimated here, which is the time offset of the *apparent* clock from system time. In this section, some of the terms frequently used in the GNSS community, such as satellite clock correction (SCC) and satellite clock error (SCE) that relate to the apparent clock are also introduced.

2.2.1 The apparent clock

Usually, in a timing standards laboratory for example, the outputs of a physical clock in the form of time or frequency measurements are directly observable. This is not the case with GNSS in-orbit clocks, which can not be observed directly. Instead, it is the apparent clock which is observed by the GNSS user. This term, the apparent clock, first appears in the literature in Waller *et al.* [2010], and it is nicely described in Senior *et al.* [2008] as *"encompassing not only onboard atomic frequency standards, but also the integrated non-dispersive [and un-modelled] effects of all satellite components as observed from the ground"*, although the exact term itself is not used in that paper.

In this sense, the apparent clock can only observed be as a virtual estimated clock. The extent to which this estimated clock represents the true behaviour of the on-board clock is limited by the performance of the mathematical models and the estimation algorithms

that perform the estimation.

2.2.2 The satellite clock time offset parameter, the $\delta t^s(t-\tau)$ term.

In the context of GNSS algorithms and data processing for PNT determination, the apparent clock is represented by the satellite clock time offset parameter, δt^s, in the mathematical model of the pseudorange (see equation 2.5).

Sometimes, the SCTO parameter is referred to as satellite clock error (SCE). It is called the satellite clock error because, mathematically at least, it represents the extent of the mis-synchronisation between the satellite clock and the reference timescale. Specifically, what this means is that the reference timescale is assumed to represent correct time, and the satellite clock error term in the pseudorange captures the difference in time according to the satellite clock and correct time according to the reference timescale. In many cases, δt^s, is simply called the satellite clock term, and the same meaning is understood.

Also, the SCTO is often known as the satellite clock correction (SCC). This is because when the value of the product of the SCTO and the speed of light is subtracted from the value of the measured pseudorange, the result is a corrected pseudorange. In theory, the SCTO is fully accounted for in this corrected pseudorange.

2.2.3 Satellite clock models in GNSS

In GNSS, as far as the modelling of satellite clock behaviour is concerned, there are two classes of model that are relevant: the broadcast models and the high–performance models. In this project, the main focus in on the high–performance class of models. But, in terms of GNSS operations, both classes of model are inherently linked. As such, both classes of model are considered in this section. The relativistic time transformation (RTT) is a key component in SCTO models, and a major focus of this project. Thus, this is covered in more depth in its own Section (2.2.4).

The broadcast models

The most widely used satellite clock models in GNSS are models that are based upon values broadcast in the navigation messages, usually known as the broadcast models. These models are purely deterministic. They are applied at the user end (i.e. by the receiver) to compute values for the SCTO. In the case of GPS and Galileo, the SCTO is parametrised in the form of a second-order polynomial (plus a relativistic component), see IS-GPS-200E [2010] and Galileo ICD [2006]. For GLONASS, a first-order polynomial (with no relativistic component) is used, see GLONASS ICD [1998].

Generally, the family of broadcast satellite clock models can be expressed

$$\Delta x(t) = a_0(t_{oc}) + a_1(t - t_{oc}) + a_2(t - t_{oc})^2 + \Delta t_{rel}(t) \tag{2.6}$$

where $\Delta x(t)$ is the value of the SCTO at time t; and a_0, a_1 and a_2 are the parameters that represent the time offset, frequency offset and linear frequency drift, respectively, at time

t_{oc} (often called the time–of–clock). In all cases, the underlying reference timescale is the system time of the relevant GNSS (i.e. GPST for GPS, GLONASS Time for GLONASS etc). In the case of GLONASS, the a_2 coefficient does not exist in the navigation message, and the Δt_{rel} correction, which is discussed in more detail in section 2.2.4, is probably[1] accounted for by the GLONASS operational control segment.

The performance of these broadcast models are limited by two factors: approximation (or truncation) errors (e.g. no higher–order components, no periodic components) and quantisation errors (due to the maximum precision of the clock parameters in the navigation messages). The origin of both factors is the same, which is that the number of bits allocated to the satellite clock parameters in the navigation message are limited. In GPS, 46 bits [IS-GPS-200E, 2010] are allocated to the three parameters (a_0, a_1 and a_2) of the GPS broadcast SCTO model, with only 8 bits for the a_2 parameter; in the GLONASS case, 33 bits [GLONASS ICD, 1998] are allocated to the two parameters (a_0 and a_1) of the GLONASS broadcast SCTO model. For GPS, the signal–in–space (SIS) error, which is a measure of uncertainty in computed range due to orbit and clock uncertainty combined (but it dominated by satellite clock uncertainty [Heng *et al.*, 2011]), was 3 ns (0.9 m) in 2011 [Groves, 2013] ; for GLONASS it was just over 5 ns (1.6 m) in 2011 [Revnivykh, 2011].

High–performance models

Besides the broadcast SCTO models, there are another class of SCTO models in GNSS, let's call them the high–performance models. High–performance because, unlike the broadcast models, which are subject to precision constraints due to operational limitations, the key purpose of these models is to accurately describe observed clock behaviour. As such, here there is scope for increased complexity in the model creation process, where it is justified. In essence then, the distinction between broadcast models and high–performance models lies in their complexity: broadcast models (simple, low–complexity) and high–performance models (detailed, high–complexity).

Periodic signals in the GPS satellite clocks. At least in the GPS case, the requirement for high–performance models is driven by the presence of deterministic features (periodic signals) Senior *et al.* [2008] in the GPS satellite clocks, which were first reported in [Ray, 2000], where Captain Steven Hutsell of the United State Naval Observatory (USNO), Colorado Springs is accredited with their discovery. Following the discovery of these periodic signals, for GPS applications demanding the highest levels of accuracy the following modelling approach was recommended for the GPS satellite clocks in [Ray, 2000].

For GPS satellite clocks with their active clock controlled by a Caesium (Cs) atomic frequency standard (AFS), they suggested

$$\Delta x(t) = a_0(t_0) + a_1(t - t_0) + \text{sinusoid} \tag{2.7}$$

where $\Delta x(t)$, a_0 and a_1 are as defined in Equation 2.6, and sinusoid indicates the periodic

[1] *Probably,* because the documentation/verification of the approach has not been found.

component of the model for describing the observed cyclic variations. And, for GPS satellite clocks with a Rubidium (Rb) AFS controlling their active clocks, they suggested

$$\Delta x(t) = a_0(t_0) + a_1(t - t_0) + a_2(t - t_0)^2 + \text{sinusoid} \tag{2.8}$$

where all terms are as defined in Equations 2.6 and 2.7. As far as these periodic features in the GPS satellite clocks are concerned, they have been confirmed and studied by several groups [Heo *et al.*, 2010; Huang *et al.*, 2013; Montenbruck *et al.*, 2011], and in the high–accuracy applications of GNSS it is accepted that they must be accounted for in SCTO modelling [Senior *et al.*, 2008]. What is lacking however, is a set of standards, or conventions, guiding GNSS developers (algorithms, software) on how to best capture these periodic signals in their models.

The stochastic model. If the broadcast models are purely deterministic, then the high–performance models comprise both a deterministic component and a stochastic component. So, the output from an SCTO computation using a high–performance model are value for each of the deterministic model parameters, but also values for the uncertainty in each of the computed parameters, which is described by the stochastic model.

2.2.4 Modelling the relativistic time transformation (RTT)

In the context of SCTO modelling in GNSS there is an additional element in the modelling problem, which is of particular importance in applications that rely upon the comparison of space–based clocks with ground–based clocks. This is the relativistic component of the SCTO modelling problem, denoted in Equation 2.6 by the symbol Δt_{rel}, and often referred to as the relativistic clock correction (RCC) within the GNSS community. The relativistic clock correction is derived from the relativistic time transformation (RTT), and the modelling the RTT is a core focus of this research. In this section, the topic of RTT modelling, along with its application in GNSS SCTO modelling is introduced. A review of the relevant literature on the topic of RTT modelling for in–orbit clocks is given in Section 4.1.3. The work within the project in exploring alternative methods for accounting for the RTT, in the GNSS SCTO modelling context, is presented in Chapter 7.

The relativistic time transformation (RTT) is a mathematical operation that must be performed on a measurement of satellite clock time—i.e proper time as defined in Subsection 2.1.1—to enable that time measurement to be expressed with respect to a terrestrial (ground–based) timescale as reference. Basically, the RTT enables comparisons between in–orbit clocks and ground clocks, in a way that is consistent with the theory of General Relativity (GR).

The analytical relativistic time transformation.

Now, the theoretical foundation of RTT modelling in GNSS today is the Schwarzschild metric, a solution of the Einstein field equations that describes (to a good enough approximation), the properties of space and time—or spacetime—in the vicinity of a slowly rotating mass (e.g. the Earth, the Sun etc.). Specifically, an approximation of the Schwarzschild

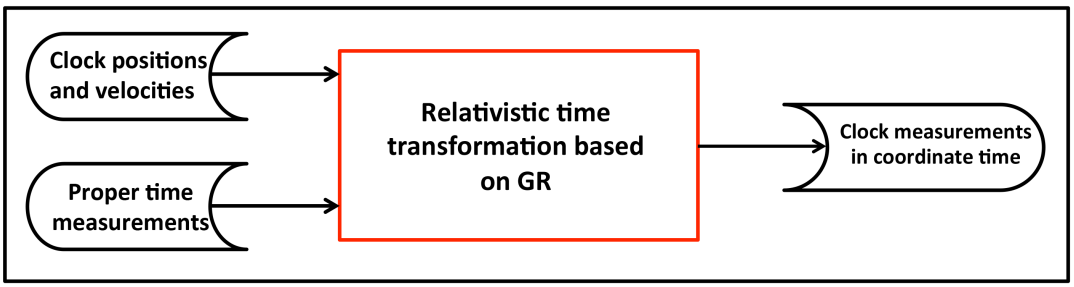

Figure 2.3: The GNSS relativistic time transformation process.

metric is used, where terms below order -2 with respect to the the quantity c are neglected; call this the analytical relativistic time transformation. The properties of such an analytical relativistic time transformation are described in Petit & Wolf [1997]. According to this analytical RTT, which is precise at the 10^{-18} seconds level, the relationship between satellite time and terrestrial time (TT)—all GNSS timescales (e.g. GPST, GLONASS Time etc.) are real–time realisations (and approximations) of TT—is expressed in Kouba [2004] as

$$\frac{dt^s}{dt_{GNSS}} = 1 - \frac{V(x,y,z) - W_0 + \Delta V(x,y,z) + \frac{\mathbf{v}^2}{2}}{c^2} \tag{2.9}$$

where V is the Earth's gravitational potential, ΔV is the sum of the *tidal* potentials i.e. the resultant gravitational potential due to the moon, sun and planets, at the clock position (x, y, z) and $\mathbf{v}$ is the clock's velocity. W_0 is the Earth's gravitational potential at mean sea level as defined in Chapter 2. The relativistic component of the GNSS broadcast clock model (Equation 2.6), call them the conventional GNSS RTT's, are simplified versions of the analytical RTT (Equation 2.9).

From this line of thinking, there is a question that arises, which this research aims to address. If the analytical RTT [Petit & Wolf, 1997] is precise at the 10^{-18} level, what then are the precision level of the conventional GNSS RTT models? To answer this requires a closer study of the link between the analytical GNSS RTT and the conventional GNSS RTT. Here, this is done by focussing on the assumptions and approximations that are made in the case of the GPS conventional RTT models.

The precision of the GPS conventional RTT.

GPS broadcast SCTO models are designed to be accurate (and precise) at or below the nanoseconds level; any less accurate and the contribution of SCTO uncertainty to the total pseudorange uncertainty budget—i.e. the UERE budget—would be unacceptably large, as discussed in Chapter 2. And, as far as precise SCTO (post–processed) estimates are concerned, the best GPS SCTO solutions are accurate at the 0.1 ns level. With these numbers in mind, in GPS (and GNSS more generally), the accuracy/precision that is required in the RTT ranges from the tens of picoseconds (10^{-11}) level, for the post–processed high–accuracy application scenarios, to the nanosecond (10^{-9}) level, in the real–time cases where SCTO is computed using navigation message data. Thus, in the established GPS

data processing algorithms, the factors that contribute to the GPS RTT below the picosecond level are considered negligible, and are omitted from the RTT computation.

In both the conventional GPS RTT and the high–performance GPS RTT, the direct effects of the tidal potential, $\Delta V(x, y, z)$, can be safely neglected [Kouba, 2004]. But, the effects of the Earth's gravity field has a more significant effect: indirectly through the effect that it has on the satellite's orbit [Kouba, 2004] and directly, through the contribution of $V(x, y, z)$ in the full, analytical RTT. In this study, the objective is to investigate the direct effects of Earth gravity field modelling on the performance of GPS RTT models.

The satellite clock constant relativistic frequency adjustment.

It turns out that the bulk of the GNSS RTT can be accounted for by a constant frequency adjustment of the in–orbit clock, which to first–order with respect to the model for Earth gravity, approximates the contribution of time dilation due to relative velocity and gravitational potential difference, both. In this case, a point mass model of the Earth that assumes perfectly circular orbits is used to compute the values of the frequency adjustment according to [Ashby, 2008],

$$\Delta t_{rel(c)} = \frac{3GM_E}{2ac^2} + \frac{W_0}{c^2} \tag{2.10}$$

where $a = 26561400\,\text{m}$ is the mean satellite orbit radius, $M_E = 5.9742 \times 10^{24}\,\text{kg}$ is the Earth's mass, $G = 6.673 \times 10^{-11}\,\text{m}^3\text{kg}^{-1}\text{s}^{-2}$ is the gravitational constant, W_0 is the geoidal potential as defined in Chapter 2. The symbol $\Delta t_{rel(k)}$ is used here to denote this constant relativistic frequency adjustment; the (k) signifies that this value is a constant, although its value is system–specific.

In the case of GPS and GLONASS, this constant frequency adjustment occurs on the ground, prior to satellite launch. For this reason, this frequency adjustment is often referred to as the satellite clock relativistic factory frequency offset (RFFO). However, in the case of the GALILEO satellite clocks, no such on–ground factory frequency offset is planned [Galileo ICD, 2006].
In figure 2.4, the values of $\Delta t_{rel(c)}$ are plotted for a range of mean orbital radii, a, values, and in table 2.2 the values of the RFFO for each system along with values for Geostationary Earth Orbit (GEO) and Low Earth Orbit (LEO).

The eccentricity correction.

The model used to derive the satellite clock constant relativistic frequency adjustment assumes a perfectly circular orbit. GPS orbits are not circular, and for this reason there is an additional term, the satellite clock relativistic eccentricity correction, $\Delta t_{rel(e)}$, which is is added to the constant term (Equation 2.10), to provide a more complete physical description of the GPS RTT. In the GPS Interface Control Document [IS-GPS-200E, 2010], this satellite clock relativistic eccentricity correction is given in two forms,

$$\Delta t_{rel(eu)} = -\frac{2}{c^2}\sqrt{aGM_E}e\sin E \tag{2.11}$$

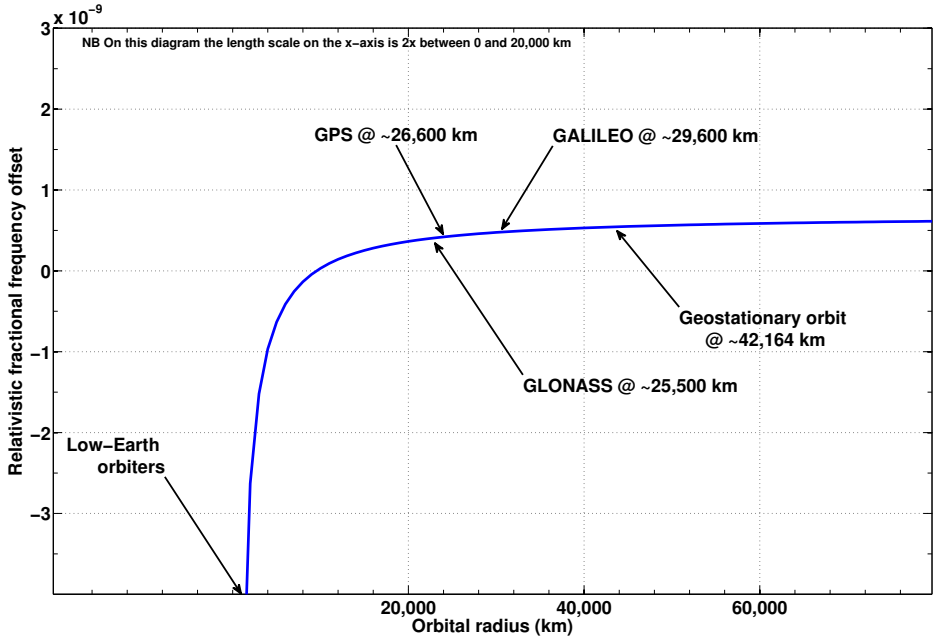

Figure 2.4: The GNSS factory clock frequency offset.

$$\Delta t_{rel(eo)} = -2\frac{\mathbf{r}.\mathbf{v}}{c^2} \tag{2.12}$$

where from Equation 2.11, a is the orbit semi-major axis, e is the orbit eccentricity and E is the eccentric anomaly. This is a representation of the GPS orbits based on Keplerian elements, the specific details of this are laid out in IS-GPS-200E [2010][1]. From Equation 2.12, $\mathbf{r}$ and $\mathbf{v}$ are the spacecraft's position and velocity, respectively, in and Earth-centred inertial (ECI) reference frame. Mathematically, both of these forms of the eccentricity correction are equivalent. But, the parameters required to compute the $t_{rel(eu)}$ quantity of Equation 2.11 are broadcast to GPS users in the navigation message. And so, the $t_{rel(eu)}$ quantity should be read as *"the GPS relativistic eccentricity correction applied in the user equipment"*. Thus, this is the form used within GPS receivers for computing the eccentricity correction in real–time. The second form, the $t_{rel(eo)}$ quantity of Equation 2.12, is used by the GPS operational control segment in its data processing software. This, in this form, the $t_{rel(eo)}$ quantity should be read as *"the GPS relativistic eccentricity correction applied by the operational control segment"*.

In GPS, the additive effects of the combination of the frequency offset correction and the eccentricity correction forms what the so-called conventional GPS relativistic satellite clock correction. The development of this approach to dealing with the relativistic effects on the satellite clocks, is described in Ashby & Spilker Jr. [1996]. The research in this thesis explores the impact of using an alternative, high–fidelity relativistic satellite clock correction which uses a more detailed model of Earth gravity, and the results of that work are presented in Chapter 7.

[1]For a comprehensive overview of the models and methods underlying this description of spacecraft motion in GNSS, Montenbruck & Gill [2000] is highly recommended.

System	Orbital radius (km)	RFFO ($\times 10^{-10}$)	Rate ($\frac{\mu s}{\text{day}}$)
GPS	26,600	−4.46	−38.6
GLONASS	25,500	−4.36	−37.7
GALILEO	29,600	−4.72	−40.8
GEO	42,200	−5.39	−46.6
LEO	< 8000	$> +1.35$	$> +11.6$

Table 2.2: Values for the satellite clock relativistic fractional frequency offset based on a first–order approximation w.r.t. Earth gravity modelling. The values in the RFFO (second) column are obtained by using Equation 2.10. Computed in this way, this value represents the number of seconds lost or gained per second as a result of the frequency shift due to the combined effects of relative velocity time dilation and relative gravitational potential time dilation, to first order. The values in the Rate (third) column are computed by multiplying the values in the RFFO column by 86400 s. Thus, these values represent the time offset between two clocks (one on the Earth's surface and the other in orbit with radius value of the first column), after a single day due to the first–order relativistic time dilation, if these clocks were perfectly synchronised at the start of the day. The values given here are precise to 3 significant figures.

2.2.5 Satellite clock time offset predictions

The satellite clock time offset (SCTO) is satellite–specific, and for this reason for users that require real-time GNSS based positioning, satellite clock predictions are essential. Predictions are the means by which the real–time users account for SCTO. As far as the delivery of satellite clock predictions to users is concerned, there are two basic approaches, which we discuss in this section; both use predictions based on past clock behaviour. The fundamental difference is latency[1]. This particular concept of latency is closely related—almost interchangeable—with the concept of prediction length. That is to say, if a user requires a satellite clock correction now, but the latency to the last available observation-based correction is one hour, then the user must use a predicted value of the satellite correction, and that prediction length is one hour. Ultimately, the performance of any satellite clock prediction scheme is a function of prediction length. Due to the stochastic nature of the satellite clock variation, in general it is true that, as prediction length grows, the expected prediction error grows also.

The navigation message type, high latency (HL) predictions

Approach one, the method adopted by GPS operational control, uses clock predictions up to a prediction length of around 24 hours, but typically around 2–4 hours, see IS-GPS-200E [2010]. These predictions are extrapolated values based on clock parameter estimates obtained using observations from the previous twenty-four hours. The parameters corresponding to time-offset, frequency offset and linear frequency drift are broadcast in the navigation message, and from these the satellite clock correction is calculated in real-time at the user-end. Although there are minor differences, the other GNSS—GLONASS,

[1]Here, the intended meaning of *latency* is best described with an example. Say the current time is 0100 hrs, but the time of the last available satellite clock estimates based on real observations is 0000 hrs. In this case, the latency is one hour. What this means is that we must predict the satellite clock correction for the current time based on an extrapolation of the clock behaviour we observed at 0000 hrs, and that the prediction length is one hour.

Galileo and Beidou—also use the same approach in generating the predicted satellite clock corrections that are broadcast in their navigation messages. As an example, GLONASS operational control estimate and upload satellite clock correction values to the satellite, for broadcasting to the users, twice a day according to GLONASS ICD [1998]. This implies a maximum predictions length of around twelve hours. This approach is illustrated, to some extent, by figure 2.5.

Another relevant factor here is the format of the navigation message, specifically the bit allocation to the broadcast clock parameters. For example, one instance of the GPS navigation message is made up of 1500 bits, and of this 46 bits are allocated to the broadcast clock parameters: 22 bits, 16 bits and 8 bits associated with the time-offset, frequency offset and linear frequency drift parameters, respectively IS-GPS-200E [2010]. The consequence of this is quantisation error where the broadcast SCTO is concerned—that is, the control segment may be able to compute SCTO very precisely, but the bit allocation fails to capture the precision of that prediction. This is particularly relevant where the linear frequency drift parameter is concerned.

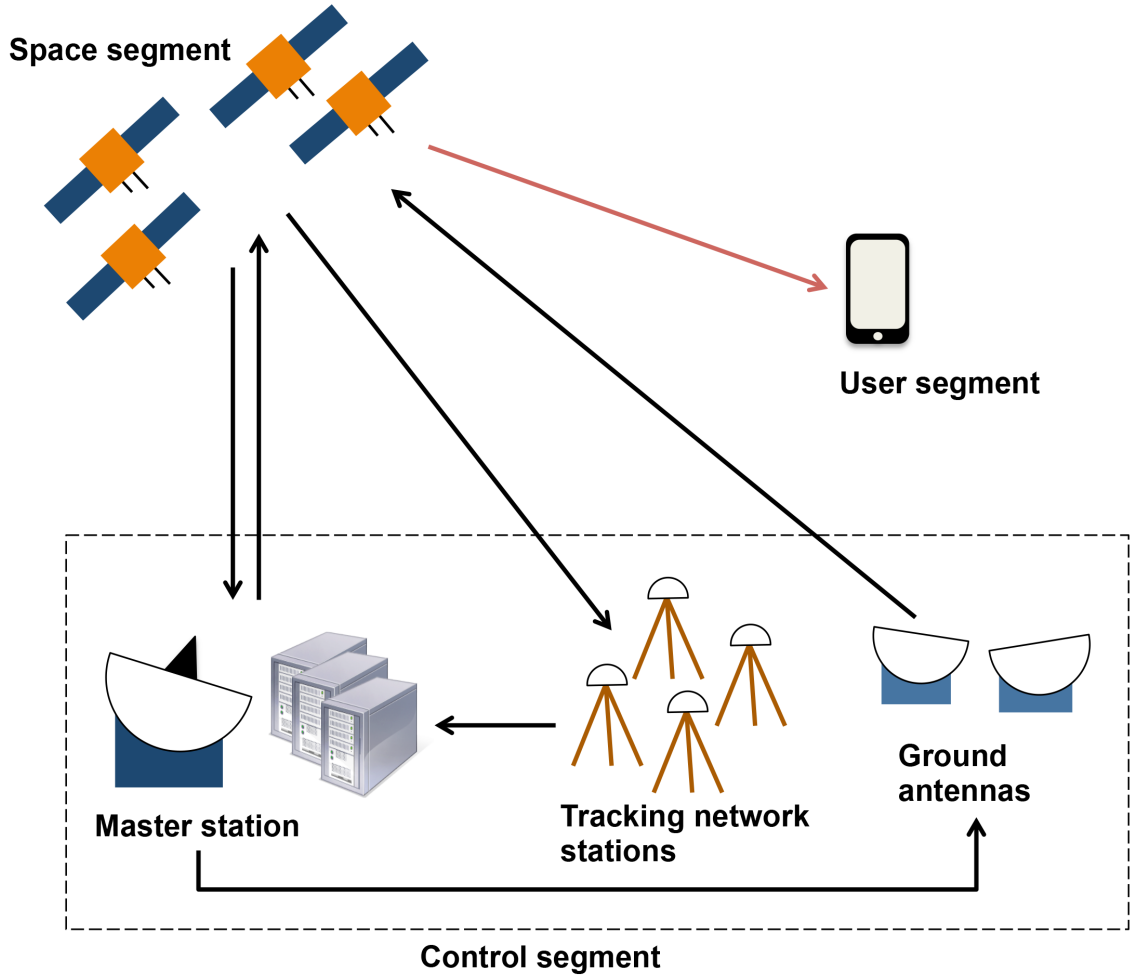

Figure 2.5: The standard method for delivering the predicted satellite clock correction to the user is via the broadcast navigation message. The parameters to compute the satellite clock correction are directly available via signal-in-space—the red line—to any user that has decoded the navigation message.

The near real-time, low latency (LL) predictions

The second approach is to use near real-time estimates, based on a real-time tracking infrastructure that is able to monitor actual clock behaviour, to generate low-latency clock predictions. Here, low-latency typically means several seconds, or tens of seconds. The salient features of this method are presented in figure 2.6.

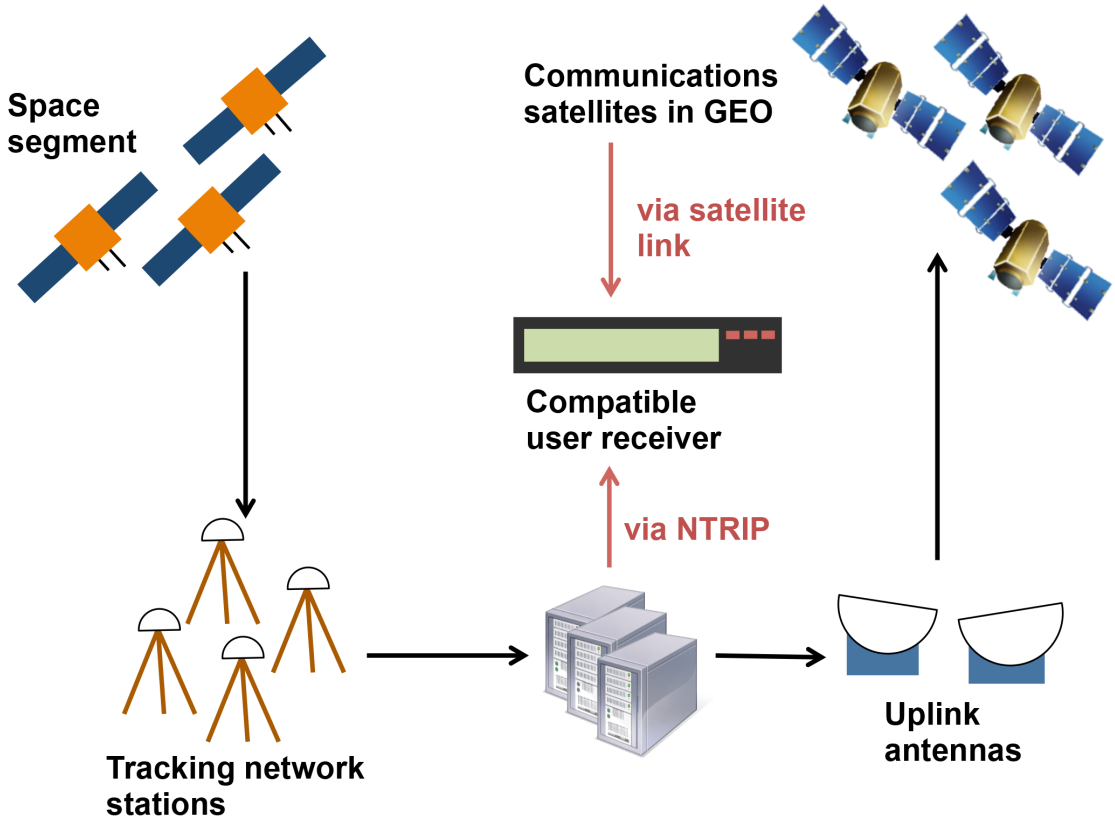

Figure 2.6: The so-called real-time service providers deliver low-latency satellite clock predictions to users.

The essential difference between the two approaches is latency. With approach one, the latency can range for tens of minutes up to around twenty-four hours, but with approach two latency is limited at tens of seconds. For this reason, in terms of positioning performance, the low-latency class of clock product, the second type, is always going to be the winner. This, along with recent advances in the precise point positioning technique, see Zumberge *et al.* [1997], Bisnath & Gao [2009] , has meant that in recent years, the GNSS community has largely focused on the real-time satellite clock estimation—the performance of real-time estimates and low-latency corrections would be comparable. On the topics of real-time estimated clocks specifically, Hauschild & Montenbruck [2009], Zhang *et al.* [2010], Huang & Zhang [2012] and Ge *et al.* [2012] have made advances. The satellite clock prediction problem, of the first type, figure 2.5, has to a large extent, been ignored.

However, there are disadvantages to the real-time, low-latency approach. At the systems side, the main challenges are related to the extra demands of real-time data processing. At the user side, there are limitations in terms of hardware, software and

algorithms capable of providing high-performance[1], real-time solutions based on these near-real time clock products.

As far as positioning applications are concerned, the research presented in Chapter 6 addresses the systems (operations) side of scenarios of the first type, where the prediction lengths are typically at the order of several hours up to a maximum of around twenty-four hours. Further, analyses based on the properties of clock prediction error, are a powerful method of characterising clock performance, we discuss this is more detail also.

2.3 The status of the GNSS's (GPS and GLONASS)—2013

In this section, some details are given on the status of the global navigation satellite systems during the period 2011 through to June 2013. This information is important in this research, mainly because the characteristics of satellite clocks can be categorised according to system (GPS or GLONASS), or clock-type (rubidium or caesium or hydrogen maser), or clock-age as identified by satellite block (IIA or IIR or IIF for GPS, M or K for GLONASS). This is explored in greater depth in chapter 5.

Of the four GNSS—GPS (US), GLONASS (Russia), Galileo (EU) and Beidou(China)—only two are fully operational today (June 2013). The approach developed for this research is dependent upon the availability of high-quality, precise satellite clock estimates over a period of several months. These data sets are available for GPS, and to a lesser extent GLONASS, but not for Galileo and Beidou. For this reason, this study looks at GPS and GLONASS satellite clocks only, with a greater emphasis of GPS satellite clocks; Galileo and Beidou are not included.

2.3.1 NAVSTAR Global Positioning System

The NAVSTAR Global Positioning System (GPS) is a global navigation satellite system managed by the 2nd Space Operations Squadron (2 SOPS)—a division of the United States Air Force. Originally, the system was designed to provide military users with position, velocity and time in a common reference system, anywhere on or near the Earth on a continuous basis. Today, GPS remains a military technology, but it is without doubt that civilian applications of GPS far outnumber military applications—and GPS has become an integral part of modern society—socially and economically. Table 2.3 gives information relating to the components of the GPS space segment and operational control segment, as of January 2013, that are relevant, in that they are referred to in later chapters. This is a reference table summarising the status of GPS during the time period of our analysis. For an up-to-date summary table of the GPS system status, the GPS constellation status file, a component of JPL's GIPSY–OASIS data processing software, which can be accessed from `ftp://sideshow.jpl.nasa.gov/pub/gipsy_files/gipsy_params/PRN_GPS.gz`, is recommended. This was the main source for GPS satellite constellation status information in this study. It is particularly useful because it holds the full GPS constellation status

[1] High-performance in terms of the standard performance criteria of accuracy, integrity, availability and integrity.

dating back to 1978.

Feature	Status (2011-2013)
No. satellites	30
In-orbit satellite types	Blocks IIA, IIR(IIR-M) and IIF
Satellite identifier	Satellite Vehicle Number (SVN)
Age range of satellites	Oldest—SVN 39 launched 1993
	Newest—SVN 65 launched 2012
Satellite clock types	Rubidium or Caesium
System reference frame	WGS-84
System timescale	GPS System Time

Table 2.3: Relevant aspects of the NAVSTAR GPS space and operational control segments (2011–2013). In this period, the nominal size of the GPS constellation was 24 satellites, but about 30 spacecraft were active (or mostly active) and broadcasting a navigation signal during that time.

2.3.2 The GPS satellite clocks (2012)

There are two main features of GPS satellite clocks that can provide a first indication of satellite clock performance: (i) age, (ii) clock type. Satellite clock age is closely linked to the GPS satellite development programme (i.e. block) that the satellite belongs to. There have been five GPS satellite blocks: Block I, Block II, Block IIA (first satellite launched in 1990), Block IIR (first successful launch in 1997), Block IIR–M (first launch 2005) and Block IIF (first launch 2010). Satellite clock type refers to the element used by the onboard atomic frequency (i.e. Rubidium or Caesium). In table 2.4, these features of GPS satellite clocks are listed. In total, during the year 2012, the data relating to 30 satellites, is considered. In PRN slots, 24 and 27, there are satellite changes as well as long periods of missing data. For this reason, those PRN slots are ignored. Also, there are only four caesium in–orbit clocks, and all of these clocks belong to the older Block IIA generation. Most of the GPS satellite clock data used in this research is from 2012, which is why this information is presented here.

PRN (SVN)	IIA	IIR/IIR–M	IIF	Rb	Cs
1 (63)			✓	✓	
2 (61)		✓		✓	
3 (33)	✓				✓
4 (34)	✓			✓	
5 (50)		✓		✓	
6 (36)	✓			✓	
7 (48)		✓		✓	
8 (38)	✓				✓
9 (39)	✓				✓
10 (40)	✓				✓
11 (46)		✓		✓	
12 (58)		✓		✓	
13 (43)		✓		✓	
14 (41)		✓		✓	
15 (55)		✓		✓	
16 (56)		✓		✓	
17 (53)		✓		✓	
18 (54)		✓		✓	
19 (59)		✓		✓	
20 (51)		✓		✓	
21 (45)		✓		✓	
22 (47)		✓		✓	
23 (60)		✓		✓	
24 (—)					
25 (65)			✓	✓	
26 (26)	✓			✓	
27 (—)					
28 (44)		✓		✓	
29 (57)		✓		✓	
30 (35)	✓			✓	
31 (52)		✓		✓	
32 (23)	✓			✓	
Total	9	19 (7)	2	26	4

Table 2.4: Features of GPS satellites relevant to the study of the in–orbit clocks (2012 only). The ✓ symbol to indicates IIR-M satellite.

2.3.3 GLONASS

GLONASS (Global'naya Navigatsionnaya Sputnikovaya Sistema) is a global navigation satellite system developed and operated by Russia. Like GPS, GLONASS is a military technology, which was initially designed to provide military users with continuous PNT

services across the globe. In table 2.5, the details relating to the key elements of the GLONASS space segment and operational control segment are given.

2.3.4 The GLONASS space segment

Feature	Status (2011-2013)
No. satellites	24
In-orbit satellite types	Blocks M and K
Satellite identifier	GLONASS Number (GN)
Age range of satellites	Oldest—GN 715 launched 2006
	Newest—GN 801 launched 2012
Satellite clock types	Caesium
System reference frame	PZ-90.02
System timescale	GLONASS System Time

Table 2.5: Relevant aspects of the GLONASS space and operational control segments (2011-2013)

As with the GPS case, it is expected that GLONASS satellite clock performance should be determined in part by clock age and clock type. But unlike GPS, there is no immediate difference in the overall specification of the satellites that constitute the GLONASS constellation. In 2012, all of the (active) GLONASS satellite clocks belong to the GLONASS–M (first launch 2003) development block. The first of the newer generation GLONASS–K satellites was launched in 2011, but for most of 2012 this satellite was not actively broadcasting a ranging signal to users. In terms of clock type, all GLONASS satellite clocks are based upon Caesium atomic frequency standards.

Summary

In this chapter, the satellite clock prediction problem in GNSS is introduced, in some detail. In short, this is the problem of characterising, modelling, estimating and predicting the apparent clock—this is the $\delta t^s(t - \tau)$ quantity in the mathematical model of the basic GNSS pseudorange measurement.

Chapter 3

Methods from precise time and frequency metrology

Chapter outline

In this chapter, the concept of clock modelling is introduced. Then, methods for characterising and estimating the behaviour of clocks driven by precision oscillators are presented. This is followed by a description of how the results of characterisation and estimation inform the development of the so–called precise clock models. It is the key set of ideas and results supporting these techniques that this research is built around. In GNSS, a key concern is the application of precise clock models for clock prediction. Thus, the implementation of clock models in prediction algorithms is also discussed.

Typically, a precise clock is modelled as a first-order linear stochastic differential equation, and where clock measurements are available the Kalman filter technique is sometimes used for optimal estimation of these model parameters. One such model, which is referred to herein as the standard precise clock model, is introduced in this chapter, and the implementation of this model in a Kalman filter is demonstrated.

The methods of precise clock theory are well-established in the time and frequency community, but somewhat less well-known in the GNSS community. Therefore, although the ideas presented in this chapter are not new, the intention has been to adopt a deliberate, didactic approach. The aim with this is to keep this research thesis self-contained, in as much as it is possible, but also to set the scene for later discussions on the strengths and the limitations of these better established methods that have been used in the study.

For a much broader overview of clock models and the Kalman filter technique Galleani & Tavella [2010] is recommended. The behaviour of a clock must be characterised before any attempt is made to model it. In the literature, precise clock characterisation methods are also known as frequency stability analysis techniques. Sullivan *et al.* [1990] is a good, comprehensive reference on the topic of frequency stability analysis, while Riley [2008] was found to be a useful resource in terms of the application of frequency stability analysis to a given set of precise clock data. A tutorial-type discussion on the topic of clock modelling in a GNSS context is given in Percival [2004], and is highly recommended.

3.1 What is a clock model?

A clock model is a mathematical description of the time-evolution of the time offset of a sequence of clock measurements from a reference timescale, T_R. Although less descriptive, this is often referred to simply as a mathematical model of clock behaviour. The reference timescale, T_R, might simply be another clock or a weighted ensemble of a collection of other clocks. Usually however, the performance of the reference timsecale, in time-keeping terms, far exceeds the performance the clock being modelled. Thus, in so far as we are concerned only about the clock that we wish to model, the reference timescale can be assumed to provide a good approximation to *true* time. With a suitable reference timescale in place then, clock models provide not only a means for assessing the time-keeping ability of individual clocks, but also a mathematical tool for using a single clock to access the underlying reference timescale, at some level.

Mathematically, this can be expressed in one of two ways. For a clock labelled i, the clock behaviour as a function of time might be formulated as either

$$x_{Ri}(t) = T_R(t) - c_i(t) \tag{3.1}$$

or

$$x_{Ri}(t) = x_{Ri0} + \int_{t_0}^{t} y_{Ri}(\tau)d\tau \tag{3.2}$$

where $x_{Ri}(t)$ is the difference between time according to the reference timescale T_R and c_i, which is time according to reading on clock i at time t where the independent time-argument t is based upon T_R; $x_{Ri0} = x_{Ri}(t = t_0)$ is the time-offset of clock i at some initial time t_0, again according to T_R, and y_{Ri} is the is the normalised frequency offset of clock i, which is a quantity that is introduced in greater depth in Section 3.1.2.

3.1.1 Two ways of thinking about clock models

Equations 3.1—call this the time-series representation of a clock model—and 3.2—call this the frequency stability description of a clock model—are two alternative but equivalent ways of thinking about the clock modelling problem. According to equation 3.1, a clock model is essentially a time-series of the difference between a pair of clock measurements, where one clock is the reference timescale and the other is the clock whose behaviour is modelled. This is subtly different to equation 3.2, where the influence of T_R is not explicitly apparent. Rather, in this form, the emphasis is on the frequency stability of clock i, as represented by $y(\tau)d\tau$, which in this case is clearly the underlying dynamical phenomenon driving the clock behaviour.

Figure 3.1 is a conceptual diagram that that aims to capture several of the key feature of clock models, in general, and to show how the two alternative interpretations of clock models, as described by equations 3.1 and 3.2, are actually the same. In figure 3.1, the independent variable is time and is represented by the x-axis. This is time according to

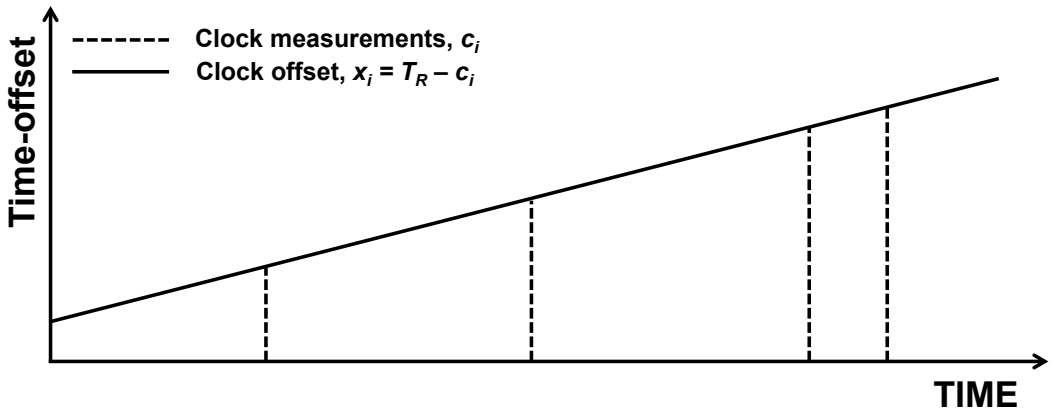

Figure 3.1: Conceptual diagram of a clock model

T_R, and true time for the purposes of the clock model. The y-axis represents the time-offset of clock i, the clock for which the model is built. The straight line drawn across the set of axes is a representation of the behaviour of clock i, that is the evolution in time of the offset between T_R and clock i. The vertical dashed lines represent instances in time when measurements from clock i are recorded. The height of the lines represents the offset $T_R - c_i$, the value that is logged. The intercept represents the initial offset between T_R and c_i, which for the purpose of clock modelling must be assigned some value by some form of calibration. The value of the slope of the line, represents the frequency stability of clock i, and is determined by the clock behaviour. In figure 3.1, the clock behaviour has been represented by a straight line. Of course, this is a simplification. Real clock behaviour is not so easily modelled. Typically, clock models are built up as a linear combination of several deterministic and stochastic components, and such models are introduced in later part of this chapter. The purpose of this section is to establish what is meant by clock behaviour and frequency stability, and how they are more or less equivalent concepts. In other words, the physical, dynamical phenomenon that determines clock performance is frequency stability, and the purpose of a clock model is to describe this.

3.1.2 Introducing the normalised (or fractional) frequency offset

For a given clock, neither the choice of reference timescale nor the nominal frequency of the oscillator that is driving the clock directly influence the timekeeping performance of that clock. Rather, it is the normalised (or fractional) frequency offset, and it's evolution in time that represents the fundamental process that determines the timekeeping performance of that clock[1]. Here, the concept of the fractional frequency offset is formally introduced, although it is re–introduced in the context of the oscillator noise model in Section 3.3.2.

Let $x(t)$ be the instantaneous time offset (or time error) of the clock driven by a

[1]Fractional frequency offset and normalised frequency offset are equivalent terms, and these terms are used interchangeably in this thesis. Sometimes, just fractional frequency or normalised frequency is used. The meaning is the same.

precision oscillator. The instantaneous frequency of this oscillator, usually denoted $\nu(t)$ is given by

$$\nu(t) = \nu_0 + \Delta\nu(t) \tag{3.3}$$

where ν_0 is the nominal frequency of the oscillator and $\Delta\nu(t)$ is the the offset of the instantaneous frequency of the oscillator at time t from the nominal frequency. In the ideal clock, the instantaneous frequency and the nominal frequency are always equal, i.e. $\Delta\nu(t) = 0 \; \forall \, t$, and in such a case the time error of the clock is always 0. In reality, this is never the case, and the evolution of the time error for any clock is driven by the fractional (or normalised) frequency offset, usually denoted with the symbol $y(t)$, which is formally defined as

$$y(t) = \frac{dx(t)}{dt} = \frac{\nu(t) - \nu_0}{\nu_0} \tag{3.4}$$

where $\nu(t)$ is the instantaneous frequency of the clock's oscillator at time t, and ν_0 is the nominal (or fundamental) frequency of the oscillator. For precision oscillators that are sold commercially, the nominal frequency is usually provided by the manufacturer. Note, that fractional frequency offset is a dimensionless quantity.

3.1.3 Clock modelling in practice

The development of any clock model is based upon time series analyses in both time and frequency domains, where the raw data are typically measurements of time-offset (or fractional frequency offset) made sequentially at fixed time intervals. The success of a clock model is determined retrospectively and based upon statistics describing the level of agreement between model estimates or predictions and measured clock data. The performance of any given clock is therefore not determined by the magnitude of its time-offset from T_R but rather by the predictability of the time-offset values at various prediction lengths.

3.2 Clock modelling in the GNSS context

Regarding clock modelling in the GNSS context, the underlying phenomenon being modelled is the same phenomenon described in section 3.1, i.e. the time evolution of clock behaviour. But there are some differences in notation and terminology, but also in the set of methods associated with the modelling task, which are worth clarifying. This section aims to address these.

3.2.1 Revisiting the matter of reference timescales

The first point relates to the reference timescale, T_R. As far as most users are concerned this is defined by the system time of the the system that is used. So, for GPS users this is GPS system time (GPST), for GLONASS users this is GLONASS System Time (RST), and so on. In positioning and navigation applications, where only one GNSS is

involved, the reference timescale has no appreciable effect on the end result, the position or navigation solution. As such, users of GNSS for positioning and navigation only, have little interest in considering the reference timescale issue any further. For users interested in timing applications of GNSS, for example, time and frequency comparisons of distant clocks via the common-view method, see Allan & Weiss [1980], the reference timescale is important. For such methods, the stability of the reference timescale limits the precision and accuracy of time transfer measurements. Also, for users interested in combining measurements from two or more GNSS in one solution, the behaviour of the inter-system timescale difference might be important, and should be carefully considered.

3.2.2 Terminology and notation

Now, let's deal with terminology and notation. In the mathematical model of the basic GNSS pseudorange measurement, there are two clocks—the satellite clock and the receiver clock—and one reference timescale involved. The dynamics of all time-variable parameters of the GNSS pseudorange measurement model are described with time according to T_R providing the independent time-argument. The tacit assumption here is that *true* time is defined by the reference timescale, and that the receiver clock and satellite clock are in error, to the extent that they are in disagreement with T_R. As such, the parameters assigned to describe the satellite and receiver clock are referred to in the GNSS literature as satellite clock corrections, denoted δt^s, and receiver clock corrections, denoted δt_r, respectively.

Here, the point is that although clock modelling in the time and frequency community and clock modelling in the GNSS community refer to the same underlying phenomenon there are important methodological difference in the way that clock modelling task is conducted within the two communities. In GNSS, the data from which the clock model parameters are obtained are the pseudorange and carrier phase measurements. In time and frequency metrology, time offset and fractional frequency data are used.

Also, in the context of the methods developed within this project, the distinction between these two mathematical descriptions of satellite clock behaviour, which we present here, is important. Satellite clock data are typically disseminated to users as time-offsets relative to some reference timescale, as in the form of equation 3.1. But from equation 3.2, it is clear that satellite clock behaviour is determined only by frequency stability and not by the choice of reference timescale. This distinction is not always well understood, and also not immediately apparent, and therefore has been emphasised here. The point being made here is that, the performance of any single clock, can only be established when it is compared against another clock of significantly better performance, in a frequency stability sense.

3.3 The standard clock model

In Section 3.1, the general concept of a clock model is introduced. In this section, one specific clock model, denoted here as the standard clock model (SCM), is introduced. The

standard clock model is a linear stochastic differential equation that is able to model the deterministic and random elements of observed precise clock behaviour with an elegant mathematical formulation. The standard clock model, although it is not explicitly referred to as such in the literature, is a very popular representation of clock behaviour within the precise time and frequency metrology (PTFM) community. But first, it is also worth introducing the a simpler model of clock behaviour, referred to herein as the basic clock model, as the shortcomings of the basic clock model motivates the need for the standard clock model. In GNSS, it is this basic clock model that is used within the receivers to compute satellite clock time offset values from the broadcast navigation message parameters.

3.3.1 The basic clock model

The basic clock model is a purely deterministic representation of the general clock model (Equation 3.2) as a second–order, linear differential equation

$$\ddot{x}(t) = z(t) \tag{3.5}$$

with initial values

$$\dot{x}(t_0) = y(t_0) = y_0 \text{ and } x(t_0) = x_0 \tag{3.6}$$

such that the solution over the time interval $\tau = t - t_0$ is given by

$$x(t) = x_0 + y_0\tau + \frac{1}{2}z_0\tau^2 \tag{3.7}$$

where x_0, y_0 and z_0 represent the initial values associated with the time–offset, fractional frequency offset and drift in the fractional frequency offset. In general, the parameters $x(t)$, $y(t)$ and $z(t)$) are time–dependent.

In much of the older literature, the (fractional) frequency drift parameter, $z(t)$, is referred to as the clock ageing parameter [Riley, 2008]. This is because the frequency stability of precise clocks degrade over time as a result of the ageing of the clock's components. Here, the $z(t)$ parameter is referred to as the linear frequency drift parameter. This is because, in the satellite clocks that are encountered in this study, where the precise clock is driven by a Rubidium frequency standard, there is a deterministic first–order (i.e. linear) frequency drift behaviour that is observable in the data; see Chapter 5. However, there is no immediately justifiable connection between this linear frequency drift (LFD) behaviour and the age of the clocks. Therefore, the terminology relating the $z(t)$ parameter to clock ageing is not used in this thesis.

Thus far, as it has been presented in this section, the standard clock model is a purely deterministic of clock behaviour. To develop the SCM further, it is necessary to consider the random variations in the frequency of the clock's oscillator.

3.3.2 The oscillator noise model

In section 3.1, we established that although there are different ways to describe what it means to model clock behaviour, ultimately clock behaviour is determined by frequency

stability. Intuitively this makes sense. All forms of physical clock are driven by oscillators in periodic motion, as close as possible to some nominal frequency, f_0. Atomic clocks are no different, and as such, there is a way of describing the behaviour of atomic clocks that has established itself as standard, see IEEE [2009], and is often referred to as the oscillator noise model.

The oscillator model for a precise clock relates the physical oscillator driving the timing signal to the observed electronic output. Not only this, but it also provides a nice description of how clock frequency, and clock phase (or time) measurements are derived from what is actually observed, the voltage signal. In the time and frequency literature, this model is almost always the starting point, in the development of further theory in the time and frequency stability analysis domain. Thus, it is presented here also.

As output, an atomic clock produces an electronic signal. The voltage of this signal is typically represented as:

$$V(t) = [V_0 + \epsilon(t)] \sin(2\pi\nu_0 t + \phi(t)) \tag{3.8}$$

where V_0 is its nominal peak voltage amplitude, ν_0 is its nominal frequency, $\phi(t)$ represents random deviations in phase, and $\epsilon(t)$ represents random deviation in amplitude. Generally, variations in voltage amplitude have no appreciable influence on the frequency stability—i.e. the timing performance—of clock oscillators, so it is acceptable to treat amplitude as constant here.

Now, the instantaneous clock frequency can be defined as the time derivative of the phase divided by 2π; the total, accumulated phase giving a measure of time elapsed:

$$\nu(t) = \nu_0 + \frac{1}{2\pi}\frac{d\phi}{dt} \tag{3.9}$$

Here, $\frac{d\phi}{dt}$ represents instantaneous frequency offset. Now, the timing performance of the clock oscillator is determined by frequency stability—the extent of the frequency offset from nominal frequency and how this frequency offset varies—and not total frequency in any absolute sense. Also, the magnitude of the frequency offset tends to be small. Thus, in general, the normalised, or fractional frequency, is more meaningful in describing the frequency stability of a clock:

$$y(t) = \frac{\nu(t) - \nu_0}{\nu_0} = \frac{1}{2\pi\nu_0}\frac{d\phi}{dt} = \frac{dx}{dt} \tag{3.10}$$

where

$$x(t) = \frac{\phi(t)}{2\pi\nu_0} \tag{3.11}$$

is phase expressed in units of time.

It is the variations of the phase and frequency of precise clocks, as described in this section, which clock models aim to capture. Typically, these variations are described as a combination of systematic and random components. The systematic part may comprise parameters that account for time-offset, normalised frequency offset and linear frequency

drift, as in the standard clock model which is introduced in section 3.3. In time and frequency theory, the stochastic part is usually modelled as a linear combination of power law noise processes. These are described in detail in the Appendix A. Before that, it is necessary to introduce a class of statistical methods—for now lets call it the Allan variance class of methods—originating from time and frequency community, which are heavily used in this research.

3.3.3 The standard clock model as a stochastic differential equation

The standard clock model (SCM) is the conventional theoretical description of the behaviour of precise clocks within the precise time and frequency metrology community, which describes how precise clocks are driven by oscillators in periodic motion about a nominal frequency—accepting that the frequency source is subject to both systematic (or deterministic) bias and random frequency fluctuations. Mathematically, the standard clock model is represented as a first–order linear stochastic differential equation (SDE). The development of a two–state (with states representing time–offset and fractional frequency offset) model of clock behaviour in the form of an first–order linear SDE is given in Galleani [2008]; Galleani *et al.* [2003]. Here, a three–state model (with states corresponding to time–offset, fractional frequency offset and frequency drift) is presented, and the presentation of the model here closely follows Chaffee [1987].

As a first–order linear stochastic differential equation, the standard clock model is expressed as

$$\begin{bmatrix} dx(t) \\ dy(t) \\ dz(t) \end{bmatrix} = \begin{bmatrix} 0 & 1 & 0 \\ 0 & 0 & 1 \\ 0 & 0 & 0 \end{bmatrix} \begin{bmatrix} x(t) \\ y(t) \\ z(t) \end{bmatrix} dt + \begin{bmatrix} d\epsilon(t) \\ d\zeta(t) \\ d\eta(t) \end{bmatrix} \tag{3.12}$$

but can also be given in a compact notation as

$$d\mathbf{X}(\mathbf{t}) = \mathbf{A}\mathbf{X}(\mathbf{t}) + \mathbf{dB}(\mathbf{t}) \tag{3.13}$$

where $x(t)$, $y(t)$ and $z(t)$ are the time–offset, fractional frequency offset and frequency drift quantities at time t, and $d\epsilon(t)$, $d\zeta(t)$ and $d\eta(t)$, are modelled as zero–mean Gaussian white noise processes. In the time and frequency literature, the noise processes $\epsilon(t)$, $\zeta(t)$ and $\eta(t)$ are known as white frequency modulation (WFM) noise, random walk frequency modulation (RWFM) noise and random run frequency (RRFM) modulation noise, respectively. These noise processes are described in greater depth Appendix A.

For those interested in the step–by–step methods through which the solution to this SDE (Equation 3.12) is obtained, the best place to start is with Chaffee [1987] accompanied with an introductory textbook on the topic of stochastic differential equations such as Øksendal [2013]. Here, the solution to Equation 3.12 is given as it presented in Chaffee [1987] as

$$\mathbf{X}(\mathbf{t}) = \mathbf{\Phi}(t, t_0)\mathbf{X}(t_0) + \int_{t_0}^{t} \mathbf{\Phi}(t, \tau)\mathbf{dB}(\tau) \tag{3.14}$$

where $\mathbf{\Phi}(t, t_0) = \mathrm{e}^{\mathbf{A}(t-t_0)} = \sum_0^\infty \frac{(A(t-t_0))^2}{n!}$ with $\mathbf{X}(t_0)$ as the initial condition. If the initial

condition, $\mathbf{X}(t_0)$ is assumed to be a non–random constant, then $\mathbf{X}(t)$ is a Gaussian process with stationary increments and the time error, $x(t)$ at time t can be evaluated as being given by

$$x(t) = x(t_0) + y(t-t_0) + z(t_0)\frac{(t-t_0)^2}{2} + \int_{t_0}^{t} d\epsilon(\lambda) + \int_{t_0}^{t}(t-\lambda)d\zeta(\lambda) + \int_{t_0}^{t}\frac{(t-\lambda)^2}{2}d\eta(\lambda) \tag{3.15}$$

where the integrals are of white noise processes and terms above $n = 2$ in the expansion for $\mathbf{\Phi}(t, t_0)$ are excluded. In the Kalman filter implementation of the standard clock model, which is introduced in Section 3.5.2, Equation 3.14 defines the Kalman filter process model (see Appendix B), and the matrix $\mathbf{\Phi}(t, t_0)$ is the state–transition matrix with $\mathbf{B}(t, t_0)$ (which is denoted as $\mathbf{Q}(t, t_0)$ in conventional Kalman filter notation) as the process noise covariance matrix.

3.4 Stability analysis

The stability of a frequency source determines how good that source might potentially be for timing purposes. Both phase and frequency are relevant for timing, so stability in this sense applies to both. Stability analysis is the study of the phase and frequency fluctuations of a frequency source. In this section, the key quantities and methods in precise clock stability analysis are introduced. These methods are fundamental to the research in this thesis. Today, the field of stability analysis in the time and frequency domain is dominated by several time-domain statistical measures that characterise frequency and phase variations. Perhaps the most important—certainly the most prolific—of these stability measures is the Allan variance.

3.4.1 Allan variance

By definition, the Allan variance is an infinite time average of the the square of the difference of two consecutive (fractional) frequency measurements,

$$\sigma_y^2(\tau) = \frac{1}{2}\langle(\hat{y}_{k+1} - \hat{y}_k)^2\rangle \tag{3.16}$$

where $\langle\bullet\rangle$ is the infinite time average operator, and $\hat{y}_k$ is frequency at time t_k. The $\hat{\bullet}$ symbol indicates that frequency is estimated from phase measurements,

$$\hat{y}_k = \frac{1}{\tau}\int_{t_k}^{t_{k+1}} y(t)dt = \frac{x(t_{k+1}) - x(t_k)}{\tau} = \frac{x_{k+1} - x_k}{\tau} \tag{3.17}$$

The Allan deviation, $\sigma_y(\tau)$, is the square-root of the Allan variance. The Allan variance, also known as the two-sample variance, is the default descriptive statistic for time and frequency measurement data sets. It is in fact formally adopted as a standard, see IEEE [2009], for characterising and reporting instabilities in measurements of phase, frequency

or amplitude, in the time domain. In general, the standard variance is not suitable for these purposes, mostly because of the inherent properties of the random variations that affect all frequency sources—mainly that these random variations are non-stationary.

The merits of the Allan variance over the standard variance

The Allan variance is closely related to the standard variance(i.e. of the standard deviation); both quantities are measures of data scatter. To compute the standard variance, the variations from the sample mean, of N data samples, are squared, summed, and divided by N-1. Calculated in this way, the standard variance is an unbiased estimator of the expected value of the squared difference from the mean value. This is why, for added clarity, the standard variance is sometimes labelled the N-sample variance. This terminology is especially prominent in the time and frequency community. In this way, the two-sample in two-sample variance refers to two measurements of frequency. The differences between each set of two consecutive frequency measurements are squared, summed, and divided by 2(M-1), Here, M is equal to N-1, the total number of differences. Thus, much like the standard variance, the two-sample Allan variance gives a unbiased estimator for the expected value of the differences squared.

The standard deviation, evaluated on a set of frequency measurements, is not a useful descriptor of the stochastic properties of the physical process generating those measurements, because in general, this process is non-stationary. The expected value—of frequency and thus phase also—is not constant. Rather, it is time-dependent and sample-dependent. In such cases, where the mean value is non-convergent, the standard deviation is also non-convergent and it should not be used. For this reason, the two-sample deviation, the Allan deviation, is recommended. The Allan deviation converges and gives a meaningful and sample-independent description of the random variability in data-sets generated by the type of non-stationary stochastic processes observed in many precise clock measurements.

The Allan variance of a finite data set

In practice, the infinite time average of equation 3.16 can only be estimated from the available measurements, which is always a finite set. In this form, the Allan deviation is expressed,

$$\sigma_y^2(\tau) = \frac{1}{2(M-1)} \sum_{k=1}^{M-1} (\hat{y}_{k+1} - \hat{y}_k)^2 \tag{3.18}$$

where M is the number of frequency measurements. The Allan deviation of a finite data set can also be expressed in terms of phase, or time-offset, obtained by substituting equation 3.17 in equation 3.18.

$$\sigma_y^2(\tau) = \frac{1}{2(M-1)\tau^2} \sum_{k=1}^{M-1} (x_{k+2} - 2x_{k+1} + x_k)^2 \tag{3.19}$$

The overlapping Allan variance gives an even better estimate of Allan variance by forming all possible overlapping combinations, using all of the available data.

$$\sigma_y^2(\tau) = \frac{1}{2(N-2m)\tau^2} \sum_{k=1}^{N-2m} (x_{k+2m} - 2x_{k+m} + x_k)^2 \tag{3.20}$$

In most cases, unless stated otherwise, the conventional practise is to present the overlapping Allan deviation statistic. In other words, in reporting stability analysis results, what is referred to as Allan variance, unless stated otherwise, is usually the overlapping Allan variance.

3.4.2 Hadamard variance

The Hadamard variance is a measure of dispersion derived from the Hadamard transform, adapted for used in frequency stability analysis by Baugh [1971]. The best way to describe the Hadamard variance in relation to how it used in practise for stability analysis is in direct comparison with the Allan variance. In the same way that the Allan variance is a statistic that describes the variability of second-difference phase variations or first-difference frequency variations, the Hadamard variance is a statistic that summarises the scatter in the third-difference phase variations or second-difference frequency variations.Unlike the Allan variance, the Hadamard variance statistic is insensitive to linear frequency drift, a feature that is particularly in clocks with rubidium-based atomic frequency standard. This is important in the GNSS-specific context because, linear frequency drift is a prominent feature in the GPS satellite clocks, see chapter 5.

As with the Allan variance, the overlapping version of the Hadamard variance is usually implemented in practice.

In terms of phase, the (overlapping) Hadamard variance is expressed as

$$\sigma_H(\tau)^2 = \frac{1}{6(N-3m)\tau^2} \sum_{k=1}^{N-3m} (x_{k+3m} - 3x_{k+2m} + 3x_{k+m} - x_k)^2 \tag{3.21}$$

where $\sigma_H(\tau)^2$ is the Hadamard variance at averaging interval τ, x_k is phase value at time corresponding to the index k and N is equal to the number of phase measurements in the data set.

3.4.3 Modified Allan variance

The modified Allan deviation, see Allan & Barnes [1981], can be used to distinguish between WPM noise and FPM noise. The Allan deviation can not. This is the main reason for which modified variances are used in time and frequency stability analyses.

In terms of phase, the Modified Allan variance is expressed as

$$mod\sigma_y(\tau) = \frac{1}{2m^2\tau^2(N-3m+1)\tau^2} \sum_{k=1}^{N-3m+1} \{ \sum_{k=j}^{j+m-1} (x_{k+2m} - 3x_{k+m} + x_k) \}^2 \tag{3.22}$$

where $mod\sigma_y(\tau)^2$ is the modified Allan variance at averaging interval τ, x_k is phase value

at time corresponding to the index k and N is equal to the number of phase measurements in the data set.

3.4.4 Time–domain stability analysis based on sigma-tau curves

In frequency stability analysis, an Allan (or similar, i.e. Hadamard) variance based analysis of a set of phase or frequency data is almost always associated with a sigma–tau curve. This is a curve that is usually plotted on a log–log scale for which the data points are the computed values of the stability measure (e.g. Allan deviation) at a range of analysis (time) intervals. So, using the Allan deviation as an example, the x–axis of a sigma–tau curve is (log) analysis (time) interval for which the Allan deviation statistic is calculated and the y–axis is (log) Allan deviation corresponding each of the analysis intervals considered. These analysis time intervals are often referred to simply as analysis intervals, but they also as known as averaging intervals. The smallest averaging interval is the time interval at which the phase or frequency data from the frequency source being analysed is recorded, i.e. the basic measurement sampling rate. The main purpose of stability analysis based on sigma–tau is to determine the nature of the relationship between average interval and the variance of the clock measurements, and this relationship reveals the properties of the underlying random processes driving clock behaviour.

Given a set of frequency data, the longest averaging interval is the time span of the entire data set. Given a set of phase data, the largest interval is half the time span of the entire data set. But, at this longest averaging interval, the computed Allan deviation statistic is not reliable, as only one sample of its value is available. Thus, the rule–of–thumb applied in this research, where the data sets are phase quantities rather than frequency, limits the length of the longest averaging interval to one tenth of the time span of the entire data set. This means that in the case of an (ordinary) Allan deviation computation, at least eight samples of the Allan deviation can be computed.

Error bars on sigma–tau curves

There are various methods for computing error bars for computed Allan deviation (and similar) statistics [Greenhall & Riley, 2003; Riley, 2008], but such error bars are not considered in this research, as the error bars even at the longer averaging intervals considered are relatively small. For example, the simplest method for approximating the confidence intervals on computed values of an Allan deviation (or similar) sets the $\pm 1\,\sigma$ error bars at $\pm\frac{\sigma_y(\tau)}{\sqrt{N}}$, where N is the numbers of samples used to compute the value of that statistic [Riley, 2008]. In this research, because of the rule–of–thumb applied, which limits the length of the longest averaging interval to one tenth of the total time span, then even in the worst–case (i.e. with only 8 samples available) the error bars on the computed Allan deviation–type statistics will not exceed $\pm 1.5\%$ of the value of the statistic itself, and in most cases will be much less.

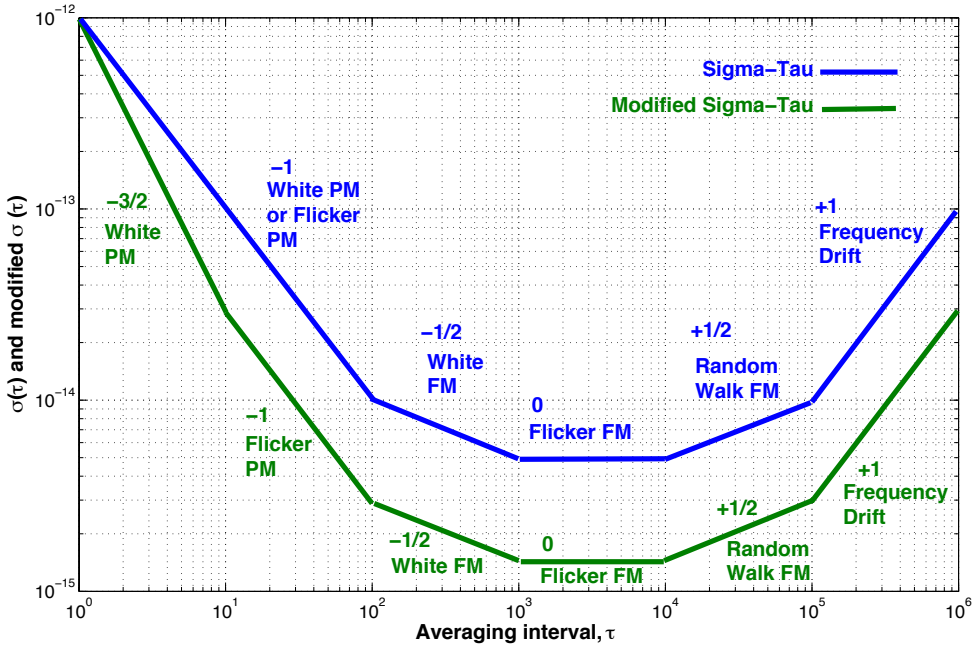

Figure 3.2: Sigma-tau and modified sigma-tau diagrams. This is a conceptual diagram and as such the values on the axes are not intended to be physically meaningful here. They merely serve an instructional purpose. The slopes on the curves of Allan deviation and modified Allan deviation curves against averaging interval, τ, can be used to identify the presence of, and distinguish between different power law noise processes that are commonly observed in time and frequency measurements.

Interpretation of a sigma–tau curve

The power–law noise processes (Appendix A), which are a common features in precise clock data sets can be identified using sigma–tau curves. Figure 3.2 indicates how a sigma–tau diagram based on the Allan–deviation statistic or the Modified Allan deviation statistic can be used to determine the properties of the noise processes that are influencing the clock measurements. As an example, for a given set of clock measurements, at the averaging intervals where sigma–tau curve based on the Allan–deviation statistic has a slope of -1 on a log–log scale, then the dominant noise process influencing the clock's frequency stability at those range of averaging intervals are either white phase noise of flicker phase noise processes. In this case, if a sigma–tau curve based on the Modified Allan deviation statistic is used, then it will be possible to distinguish between those two noise types.

3.4.5 Dynamic (time–domain) frequency stability analysis

Time–domain stability analysis using a single sigma–tau curve, as described in the previous section (3.4.4), provides a good means of characterising the behaviour of a clock at a snapshot in time. To determine the evolution of the characteristics of a clock's behaviour over time, i.e. variations in the clock's frequency stability, then dynamic frequency stability analysis methods are recommended. The Allan variance based dynamic frequency stability

analysis, introduced in Galleani & Tavella [2009], is one popular dynamic stability analysis technique.

In essence, the results of a dynamic stability analysis comprises a sliding sequence of sigma–tau curves, which are plotted alongside each other on a 3-d plot. But, for a full appreciation of the dynamic frequency stability analysis technique, careful consideration of a specific example is recommended. In this work, dynamic frequency stability analysis based on the Hadamard deviation statistic is used to determine the time–evolution of the properties of periodic signals and random variations that are observed in the GPS satellite clocks. A full description of the analysis method and the results of are presented in Chapter 5, Section 5.3.

3.5 The Kalman filter for clock estimation and prediction

The discrete form of the Kalman filter technique is adopted for the clock estimation and prediction work presented in this thesis. In this section, it is explained why the Kalman filter is applicable, and well-suited, to the clock estimation problem, in general.

The standard Kalman filter equations, and algorithms for the implementation of the Kalman filter in estimation and prediction mode, separately, are given in detail in Appendix B. In this section, it is demonstrated how the standard clock model might be expressed in Kalman filter form. Here, this is labelled the standard clock Kalman filter (SCKF). The fundamental components—the basic building blocks—of the standard clock KF are given.

3.5.1 The Kalman filter as estimator of choice

The basic Kalman filter, as first described in Kalman [1960] (although Brown Jr. [1991], Groves [2013] and several other texts are much more accessible on the topic), is a step-by-step recursive method for the optimal estimation of state-vector parameters. Optimal is used here in the sense that the mean-square estimation error is minimised. The appeal of the Kalman filter technique, particularly in applications in the precise time/frequency domain, comes from the following features.

- The method is recursive. The recursive nature of the Kalman filter makes it practical in a computational sense—only results from the previous step are required to compute parameter estimates for the current step—and thus, naturally suitable in real-time applications.
- The technique is stable and robust (to outliers, large measurement errors etc) in a statistical sense, because it combines measurements with predicted state–vector projection in compute the state–vector estimates.
- The method assumes that the errors of the modelled process are systematic, white noise, or Gauss–Markov processes. Or, a linear combination or integral of such processes. Here, this is important as this means that the Kalman filter method can

accommodate non–stationary processes of the type that are typically observed in clock offset data.

In previous work, Davis *et al.* [2005a] and Stein [1988], among others, have adopted the Kalman filter successfully for the purposes of precise clock prediction.

3.5.2 A Kalman filter implementation of the standard clock model

The basic components of all estimation problems expressed in KF form are: the state propagation matrix ($\mathbf{\Phi}_k$), the process noise covariance matrix ($\mathbf{Q}_k$), the measurement matrix ($\mathbf{H}_k$) and the measurement noise covariance matrix ($\mathbf{R}_k$). The components of the process model, $\mathbf{\Phi}_k$ and $\mathbf{Q}_k$, use knowledge of the underlying dynamics of the process to estimate the state, $\mathbf{x}_{k+1}$, of the system at time t_{k+1}, based on an estimate of the state of the process, $\mathbf{x}_k$, at time t_k. The components of measurement model, $\mathbf{H}_k$ and $\mathbf{R}_k$ relates $\mathbf{x}_k$ to the measurements at time t_k. So in theory, the process model and measurement model components are time-varying. In a practical implementation, this is usually not the case. The standard clock model can be expressed in KF form by determining each of these components. Here, these components are given in the following sections, for the specific case of the standard clock model.

The state-vector and the state error covariance matrix

The state vector, $\mathbf{x_k}$, of a Kalman filter is the component that holds the unknown coefficients of a deterministic model of the system. In the standard clock model this would include parameters associated with the time-offset (phase), normalised frequency offset and linear frequency drift quantities. This would then have the form:

$$\mathbf{x}_k = \begin{bmatrix} x_k \\ y_k \\ z_k \end{bmatrix} \tag{3.23}$$

where:

x_k	Time-offset at time t_k
y_k	Normalised frequency offset quantity at time t_k
z_k	Linear frequency drift quantity at time t_k

The state transition matrix

In the SCKF the state transition matrix,$\mathbf{\Phi_k}$, is defined as:

$$\mathbf{\Phi}_k(\tau) = \begin{bmatrix} 1 & \tau & \frac{\tau^2}{2} \\ 0 & 1 & \tau \\ 0 & 0 & 1 \end{bmatrix} \tag{3.24}$$

where:

τ	Time-interval in seconds between t_k and t_{k+1}

The process noise covariance matrix

The process noise covariance matrix describes the intrinsic stochastic variations of the state-vector components. For the SCKF, the process noise covariance, which is derived in Hutsell [1995], is given by

$$\mathbf{Q}_k(\tau) = \begin{bmatrix} \sigma^2_{WFM}\tau + \frac{1}{3}\sigma^2_{RWFM}\tau^3 + \frac{1}{20}\sigma^2_{RRFM}\tau^5 & \frac{1}{2}\sigma^2_{RWFM}\tau^2 + \frac{1}{8}\sigma^2_{RRFM}\tau^4 & \frac{1}{6}\sigma^2_{RRFM}\tau^3 \\ \frac{1}{2}\sigma^2_{RWFM}\tau^2 + \frac{1}{8}\sigma^2_{RRFM}\tau^4 & \sigma^2_{RWFM}\tau + \frac{1}{3}\sigma^2_{RRFM}\tau^3 & \frac{1}{2}\sigma^2_{RRFM}\tau^2 \\ \frac{1}{2}\sigma^2_{RRFM}\tau^3 & \frac{1}{2}\sigma^2_{RRFM}\tau^2 & \sigma^2_{RRFM}\tau \end{bmatrix} \tag{3.25}$$

where:

σ^2_{WFM}	Variance of WFM noise at t_k
σ^2_{RWFM}	Variance of RWFM noise at t_k
σ^2_{RRFM}	Variance of RRFM noise at t_k
τ	Time-interval in seconds between t_k and t_{k+1}

The measurement matrix and the measurement noise covariance matrix

In precise time and frequency metrology, the measurements data sets that are analysed are time–series of either clock time offsets or frequency offsets. The measurement data sets used in this research project are of the former type. So, in this case the measurement matrix, $\mathbf{H}_k$, for the SCKF, takes the following from:

$$\mathbf{H}_k = \begin{bmatrix} 1 & 0 & 0 \end{bmatrix} \tag{3.26}$$

The measurement noise covariance matrix, $\mathbf{R}$, in the SCKF case is a single scalar quantity that represents noise in the measurements of clock time offset.

Kalman filter initialisation

To initialise the Kalman filter the physical state vector components should be set to realistic estimates, and the leading diagonal elements of the associated state error covariance matrix should be set to values that represent the variance of these estimates. Non-diagonal elements of the state error covariance matrix should be set to 0. An algorithm for initialising the state vector and state error covariance matrix in the case where a minimum of three time-offset measurements are available is given in Stein [1988].

Estimating the process noise parameters

Estimating the process noise covariance matrix is more of a challenge, and the process is difficult to automate. In the simplest Kalman filter implementation of the standard clock model, the noise parameters of the process noise covariance are held constant. The values of these parameters are usually estimated using a sufficient set of past data and the combination of several techniques. Here, the techniques used include:

- Incrementally adjusting the parameters until prediction error deviation, σ_p, matches closely with RMS prediction errors obtained from the Kalman filter predictions.

- Simulating sets of measurement data using the same noise parameters as used in the Kalman filter. The noise parameters are incrementally adjusted until the Allan deviation and Hadamard deviation estimates obtained from the simulated data match closely those obtained from the real data. In practice, this is process is done by eye, comparing the Allan deviation based sigma-tau curves of the simulated data set with the Allan deviation based sigma-tau curve for the real data set, and the same for Hadamard deviation.

- FFT–based spectral analysis of the Kalman filter residuals. The noise parameters are then adjusted until the amplitude of the Fourier Transform remains approximately uniform across the frequency spectrum under examination.

Simulation of clock noise to determine the process noise covariance

The process of generating a simulated data set with properties matching those of the noise parameters used in the Kalman filter is described in Davis [2011]. A simulation state vector $\mathbf{x}_{s,k}$ will then evolve according to the following equation between epochs $k-1$ and k:

$$\mathbf{x}_{s,k} = \mathbf{\Phi}(\tau)\mathbf{x}_{s,k-1} + \mathbf{L}_Q(\tau)\mathbf{e}(\tau) \tag{3.27}$$

where $\mathbf{L}_Q$ is a lower triangular matrix obtained by the following Cholesky factorisation:

$$\mathbf{Q} = \mathbf{L}_Q(\tau)\mathbf{L}_Q^T(\tau) \tag{3.28}$$

and $\mathbf{e}(\tau)$ is a vector of uncorrelated noise with a normal distribution and variance unity. The corresponding simulation parameter covariance matrix $\mathbf{P}_{s,k}$ evolves as:

$$\mathbf{P}_{s,k} = \mathbf{\Phi}(\tau)\mathbf{P}_{s,k-1}\mathbf{\Phi}(\tau)^T + \mathbf{Q}(\tau) \tag{3.29}$$

The elements of this $\mathbf{P}_{s,k}$ matrix describe the scatter and correlations within the simulated data sets.

3.6 Clock predictability analysis

One of the key ideas that this work aims to advance is the idea of clock predictability—as opposed to frequency stability—as a measure of clock performance. Stability analysis techniques study the clock measurements, whereas clock predictability analysis studies the accuracy of the process by which predictions of clock offsets enable access to a timescale in real–time.

3.6.1 Prediction error deviation

Clock predictability is ultimately limited by the underlying stochastic noise processes. If the sources of uncertainty are purely stochastic then it is expected that clock prediction error should increase, monotonically, with prediction length. However, in the case where White Frequency Modulation (WFM) noise and Random Walk Frequency Modulation

(RWFM) noise are the dominant noise processes in a clock's timing signal, there is a useful relationship between the Allan Deviation (ADev) and the expected error of a predicted clock reading at some future point. Such an error quantity that represents the accumulated time error of a clock is referred to as the time prediction error deviation (PED) and is expressed in terms of the Allan deviation, σ_y, at prediction length τ_p as [Allan, 1987],

$$\sigma_p(\tau_p) = \sigma_y(\tau_p)\tau_p \tag{3.30}$$

where σ_p denotes prediction error deviation, τ_p is the the length of the prediction and $\sigma_y(\tau_p)$ is the Allan deviation where τ_p is the averaging time. In the GNSS context, this is a useful result because the dominant noise processes observed in the GNSS satellite clocks tends to be WFM noise; see Chapter 5.

3.6.2 Clock difference prediction error

In many applications, specifically in PNT applications, it is the difference between pairs of clocks rather than the performance of a single clock against some reference timescale that is important. This concept is developed further in Section 6.1.3.

Summary

A major theme of this research project is the introduction and integration of methods originating from the field of precise time and frequency analysis, or precise clock theory, into the GNSS satellite clock modelling problem, where it is appropriate. Therefore, it was the aim of this chapter to capture the key methods from precise time and frequency metrology that called upon in the later parts of this thesis, specifically in Chapters 5, 6 and 8. The following chapter includes a review of the research on the topics of SCTO characterisation, modelling, estimation and prediction, which strongly influenced the research work presented in this thesis.

Chapter 4

Review and data sources

Chapter outline

In the previous chapters, satellite clock time offset (SCTO) as well as the differences between satellite clocks, or satellite clock differences (SCD), were identified as critical quantities in the broader context of GNSS. It was argued that the predictability of these quantities is a key factor that ultimately limits the performance of GNSS. The conventional theoretical description of precise clocks—as oscillators in periodic motion about a nominal frequency, but subject to random frequency fluctuations—was introduced. Also, standard methods for processing clock measurement data to infer clock characteristics and to aid in the initialisation of clock prediction strategies were explained.

This chapter is composed of three parts. In the first part, the published literature relating to the topics of precise clock characterisation, modelling and prediction in the context of GNSS, and applications of GNSS are introduced. The aim of this is to set the scene for the contribution that is made by the research presented in this thesis. The second part of this chapter describes the data sets used in this study. The final part details the software tools that were developed and used for the purposes of this study, discussing briefly some aspects of implementation and validation.

4.1 Review

This section provides an overview of the key literature that influenced this research. An objective here is to provide context, in a historical sense, of work that has been done before. This is followed by a discussion of recent developments in the field; with this, the objective is to highlight the challenges or questions that remain today. As emphasised in previous chapters, it is helpful to break down the satellite clock time synchronisation (SCTS) problem in GNSS into its components—characterisation, modelling, estimation and prediction. As it turns out, most of the relevant literature can, with some justification, be assigned to one of these categories.

4.1.1 The in–orbit characteristics of GNSS satellite clocks

As far as characterisation of the in–orbit performance of GNSS space clocks is concerned, there are two bodies of work, published in Senior *et al.* [2008] (for GPS satellite clocks) and Waller *et al.* [2010] (GIOVE(Galileo)), that strongly influenced the work presented in this chapter. Others [Griggs *et al.*, 2013; Hauschild *et al.*, 2013; Hesselbarth & Wanniger, 2008] have studied the short–term characteristics of GNSS satellite clocks (i.e. at the order of several seconds), which are important for those involved in design of prediction schemes that deliver the near real–time, low latency predictions to GNSS users. However, the focus of this work is on the characteristics of GNSS satellite clocks at the order of several minutes up to several hours, which are directly relevant to the design of prediction methods for delivering navigation message type, higher latency predictions.

GPS satellite clocks

In Senior *et al.* [2008], the clock products of the IGS from late 2000 to mid 2007, are used to characterise the in–orbit behaviour of GPS satellite clocks in the sub-daily regime. In this paper, MDev statistics, for the constellation of GPS satellite clocks are computed for a range of averaging times from 30 seconds to about 1.5 days, and plotted on a log-log scale; an application of well–established stability analysis techniques, which are described in Chapter 3. From this, the existence of periodic signals in the GPS satellite clock estimates is suggested, and the paper follows up with standard FFT–based spectral analysis methods to build a quantitative picture of the exact nature of these periodic signals. Based on an analysis of about 6.5 years of data, Senior *et al.* [2008] conclude the presence of periodic signals in all GPS clock types at harmonic frequencies of $\approx 2n$ cycles per day, for $n = 1, 2, 3, 4$, i.e. periods that equal 12 hours, 6 hours, 4 hours and 3 hours. Further, a detailed analysis of the stochastic noise processes up to averaging times of 2000s for each for different category of GPS satellite clocks—IIA Cs, IIA Rb and IIR/IIR–M Rb—is given and used to estimate the prediction and interpolation properties at time intervals in the range 0–2000 s. Thus, Senior *et al.* [2008] provides useful insight into features of GPS satellite clocks, periodic signals in particular, that are useful in the construction of GPS satellite clock models for the purposes of GPS space clock prediction and interpolation.

However, this paper does not provide all of the essential background information required to build a GPS satellite clock predictor. In particular, the linear frequency drift properties of the clocks, which this work focuses on, are not studied. In Senior *et al.* [2008], by removing a second–order polynomial from the clock data prior to computation of the MDev statistic, any linear frequency drift trends are excluded from the analysis. Also, Senior *et al.* [2008] is a study of GPS satellite clock properties focussed on the sub-daily regime: thus, longer term stochastic properties of the clocks are not considered, but are nevertheless important in prediction work focussing on prediction lengths up to and beyond 24 hours. Prediction length 24 hours is significant for GPS users: the satellite clock values broadcast in the GPS broadcast navigation message are predictions—typically at lengths of a few hours ahead[1]—parametrised by a second order polynomial, as described

[1] Although the specification IS-GPS-200E [2010] suggests up to a maximum of one day ahead is possible.

in Section 2.2.3 of Chapter 2.

GIOVE (Galileo) satellite clocks

In Waller *et al.* [2010], the characteristics of the Rb clocks, as well as one passive hydrogen maser (PHM) clock on-board the two satellites of the Galileo In-Orbit Validation Element (GIOVE) experiment: GIOVE-A and GIOVE-B, are characterised, using data from the period late 2006 to early 2009. The most intriguing component of this paper is the demonstration and validation of a PHM on-board a navigation satellite, with prediction error of 1.2 ns at 1 day (1 σ) relative to an active hydrogen maser connected to a Galileo Experimental Sensor Station (GESS) located at the ground station GIEN, which was located at the Institutio Nazionale di Ricerca Metrologica (INRiM)—the Italian National Institute for Metrological Research—in Turin, Italy. This level of clock performance, in terms of prediction error, compares favourably to GPS satellite clock prediction errors at 1 day of $\approx$ 2 ns.

GLONASS satellite clocks

Senior *et al.* [2008] and Waller *et al.* [2010] are comprehensive in their analysis, and provide a valuable and informative account of the in–orbit behaviour of GPS and GIOVE/Galileo satellite clocks. In the literature, no such analysis exists for GLONASS. For this reason, in Chapter 5 we present the results of a detailed analysis of the available GLONASS satellite clock products. In as much as it is possible, we use these data sets to characterise the in-orbit behaviour of GLONASS satellite clocks.

4.1.2 The state–of–the–art in SCTO estimation in GNSS

As it is used in this thesis, the term SCTO estimation refers to the combination of mathematical models and estimation algorithms that are involved in determining SCTO from GNSS observational data. The topic of SCTO estimation is an active area of research, particularly for those interested in precise applications of GNSS (e.g. surveying, precise time and frequency transfer, etc.). Although the key focus of this project is SCTO prediction, the methods associated with SCTO estimation along with the latest developments in the area are also important to this research—mainly because the data sets that this project is built around are based upon the outputs from the SCTO estimation processes of various GNSS analysis centres. The details of these data sets that describe how they are stored (i.e. file formats, archive details etc.), distributed, and how they are used within this project are provided in Section 4.2. In this section, a general description is given, of how SCTO estimation is performed in the state–of–the–art GNSS data processing software packages. The purpose of this is to introduce some of the key issues associated with precise GNSS SCTO estimation, and through provide some indication of the overall level of accuracy/precision of the SCTO data that is used in study.

Walk–through of a typical GNSS analysis centre SCTO estimation process

From the ground, the signal generated by a GNSS satellite clock can not be observed directly. Instead, the SCTO is usually inferred from satellite–receiver range measurements (e.g. GNSS pseudorange, carrier phase). These measurements are collected at a distributed network of satellite tracking stations (which are equipped with high–performance, dual–frequency GNSS receivers), and then sent to a central facility, where the data is processed and estimated values of the SCTO quantity, for all satellites in the system, are produced. In fact, within the chain of processes that produces an analysis center's SCTO estimates, the positions of the satellite tracking stations, as well as the positions (orbits) of the satellites are also determined. Collectively, this is known as the process of precise orbit determination and time synchronisation (ODTS). Many of the major scientific GNSS data processing facilities belong to the International GNSS Service (IGS), and the SCTO estimates that these facilities generate, using independent data processing strategies, are then optimally combined by the IGS analysis center coordinator (ACC). The product of this IGS SCTO combination is the data set that is used in this project for studying the behaviour of GPS satellite clocks in Chapters 5 and 6, and for initialisation of the GNSS satellite clock predictor presented in Chapter 8. The so-called IGS combination product is described in more detail in Section 4.2. Here, the techniques used by the IGS analysis centres in producing their SCTO estimates are reviewed, and from this the accuracy and precision of the SCTO estimates are inferred. Each IGS analysis center has its own independent data processing strategy which is implemented within a precise ODTS software package. These overall strategies are published online and can be found at `http://www.igs.org/igscb/center/analysis/`. The following list outlines the ODTS processes that are carried out by the *typical* IGS analysis center, followed by a description of how the resulting SCTO estimates are combined by the IGS analysis center coordinator. Notable exceptions to this, as well as ongoing research challenges associated with ODTS estimation within the context of the IGS are emphasised. Here, GPS is used as representative case. ODTS within the other systems follow a broadly similar process, although there are minor, but important differences.

- SCTO estimation at an IGS analysis center begins with the **data pre–processing**, where the data in this case are pseudorange and carrier phase measurements on two frequencies, GPS L1 and GPS L2, which are logged in the **RINEX** format [Gurtner & Estey, 2007; 2009]. In all IGS analysis centres, the L1 and L2 pseudorange and carrier–phase measurements are combined, to form the so–called pseudorange ionosphere–free observable, L_c, and the carrier–phase ionosphere–free observable, Φ_c, respectively. The ionosphere–free observable is unaffected by the first–order effects of the GNSS signal transit delay caused by the ionosphere.[1]

- **Modelling of the ionosphere–free linear combination**. One component of the mathematical model of the ionosphere–free linear combination is the SCTO, but

[1] A third GPS frequency, GPS L5, will be broadcast from the GPS IIF generation onwards. The availability of a third-frequency permits the formation of two different *ionosphere–free* linear combinations, the L1/L5 combination and the L2/L5 combination, as well as the formation of a triple combination.

there are several other factors that must also be accounted for. These include: the satellite antenna phase center offset and antenna phase center variations of both satellite and ground station receivers [Schmid *et al.*, 2007; June 2010], signal phase variations caused by yaw motion of the spacecraft—especially during eclipse periods [Bar-Sever, 1996], the higher–order ionospheric errors that aren't accounted for in the iono–free combination [Hernández-Pajares *et al.*, 2007], orbit modelling errors also contribute [Urschl *et al.*, 2007].

- In general, the modelling and estimation strategies used by the each of the IGS analysis centres for computing the SCTO estimates from the ionosphere–free combinations are independent of each other. The IGS combined SCTO estimate is evaluated as a weighted ensemble average of each AC estimate at each epoch. This combination process consists of a timescale alignment step where all of the analysis centre clock products are transformed by a linear model to the same reference timescale. Then, all clock estimates for a single epoch are iteratively combined to get a mean SCTO estimate, with the effects of outliers (or gross errors) accounted for in this process.

- Finally, the IGS timescale is formed as a weighted ensemble combination using station clock and satellite clock solutions from the entire IGS network. Then, the combined SCTO estimates are aligned to the IGS timescale to produce the so–called IGS combined SCTO product.

Taking all of these error sources in the modelling (as well as those inherent within the estimation processes) into account, Senior *et al.* [2008] determine that the precision, i.e. the internal consistency, of the IGS SCTO estimates is around 1 cm (33 ps) most of the time, but that the true accuracy is probably around 3cm (100 ps). In this project, these values are assumed to represent the quality of the SCTO data sets that forms the basis of all the research work presented in this thesis.

4.1.3 Relativistic time transformation modelling in GNSS

In this project, the key motivating factor for studying GNSS RTT modelling methods was to investigate RTT mis–modelling as a potential source of the periodic signals observed in the GPS satellite clock data. As far back as 2000, Ray [2000] reported that periodic signals could be observed in GPS satellite clock behaviour. Then in 2002, Kouba [2002] presented the results of an investigation into the GPS conventional relativistic time transformation (RTT), which is used by GPS receivers to compute the relativistic component of the GPS SCTO on the recommendation of the GPS Directorate in its GPS Interface Control Document (ICD) [IS-GPS-200E, 2010][1]. Kouba [2002] and the follow–up paper[Kouba, 2004], showed that this conventional method for implementing the relativistic time transformation was in error at a rate of up to 0.2 ns per day, with cyclic variations of up to 0.2 ns

[1]The SCTO model in the GPS ICD is often referred to as the GPS broadcast clock model, and the relativistic component is the GPS relativity correction or (in the terminology of Kouba [2002]) the GPS conventional relativistic time transformation.

and 0.07 ns of period 14 days and 6 hours, respectively, and the cause was attributed to numerical approximation (or truncation) error.

The GPS conventional RTT is an simplified version of the analytical model for the GPS RTT. A first–principles derivation of the analytical GPS RTT is found in Ashby [2008]. This analytical model captures the effects of velocity time dilation and gravitational time dilation on the SCTO. In the analytical model, the relativistic time transformation is a function of the relative satellite–receiver gravitational potential (and thus, relative position) and relative satellite–receiver velocity. The approximation errors in the conventional RTT that [Kouba, 2004] found in the satellite clock data arose from the use of a first–order model of Earth gravity field (which treats the Earth as a point mass) to calculate the satellite–receiver gravitational potential difference. Kouba [2004] used a second–order model, which considers the effects of modelling the Earth as an oblate spheroid on the GPS satellite orbits and on the GPS RTT directly. Kouba [2004] noticed RTT approximation errors with 14 days and 6 hours period when comparing satellite clock models using this improved RTT were compared with models using the GPS conventional RTT.

The idea for this component of the project is to take this line of inquiry one step further, by using the highest–quality (precise) GPS orbit solutions and a more complete description of the gravitational potential variations using the Earth Gravity Model 2008 (EGM08) (up to degree and order 20). The objective is to assess the impact of an even more rigorous RTT in the modelling of GNSS SCTO's, and to determine whether such an approach could contribute to an improved prediction method.

Others have worked on RTT modelling in GNSS since. Pascual-Sanchéz [2007] looked into the possibilities for developing a GNSS based upon a "fully relativistic" framework for dealing with space and time, as opposed to the current "Newtonian + corrections" approach adopted in GNSS to account for relativistic effects. Also, Larson *et al.* [2007] studied relativistic effects on Low–Earth orbiter satellites and found that the effects of J2 on the Gravity Recovery and Climate Experiment (GRACE) satellite clock solutions—GRACE satellites carry ultra-stable oscillators on-board—are significant and should be accounted for. Further, these relativistic effects were found to be linked closely to orbital period.

4.1.4 Navigation message style, high latency satellite clock predictions

On the topic of GNSS satellite clock prediction at prediction lengths beyond several minutes and up to twenty-four hours, there are two prior studies, presented in Heo *et al.* [2010] and Huang *et al.* [2013], that looked closely at the problem. Some aspects of the methods developed for these two studies are similar to each other, and similar with the methods developed for this research. In all cases, the focus is on the GPS satellite clocks, with the predictions of the IGS—found in the second half of the IGS ultra-rapid SP3 files—used as the benchmark prediction scheme against which the performance of a new and improved prediction method is judged. In all cases the IGS rapid timescale, T_{igs}, is adopted as the reference timescale. These choices make sense for several reasons. One, the IGS prediction

scheme is better performing than the GPS operational scheme according to the analysis as presented by the IGS analysis co-ordinator in figure 6.1, at least at prediction lenghths up to six hours, and at least in terms of precision if not accuracy—compare the purple curve to the brown curve. Secondly, it is not possible, at least in a straight-forward way, to do a similar prediction algorithm performance study with the GPS operational scheme, or the GLONASS operational scheme. The data for such studies are either not publicly available, or are not amenable to analysis in this way. With regards to GPS satellite clocks then, the IGS ultra-rapid predictions provide a well-formatted, well-documented set of predicted satellite clock correction values, and the IGS rapid and final products provide a suitable truth model. A similar study can't be performed on the GLONASS clocks. The reason is that IGS-like precise clocks do not exist for GLONASS[1].

In both Heo *et al.* [2010] and Huang *et al.* [2013], new satellite clock prediction schemes are proposed, and the results presented. Both extend the classical clock model, incorporating cyclic terms to address the periodic variations, and both claim an improvement in performance at a variety of prediction lengths, with respect to the IGS. The essential difference between the two prediction algorithms are the adopted parameter estimation frameworks—Heo *et al.* [2010] use a *"delay co-ordinate embedding approach"* and Huang *et al.* [2013] use an adaptively weighted least-squares estimation approach. Beyond this, Huang *et al.* [2013], present a positioning domain analysis, comparing PPP-based position time-series computed using the IGS predictions against position time-series based on their own predictions.

The basic goal of both of these papers is to improve upon the performance of the IGS predictions, but neither papers describes the properties of the current, operational IGS prediction scheme in any depth. As a result, there is no satisfactory physical explanation as to why their prediction schemes perform better. On this basis, it is clear that a detailed performance analysis of the IGS predictions of the satellite clocks would be useful, in that it might reveal critical details about the fundamental limiting factors of the IGS approach, and any similar prediction algorithm in turn. One of the research aims of this project is to present such an analysis along with a critical discussion of the implications. That work is presented in Chapter 6.

A further issue is that the results presented in Heo *et al.* [2010] appear to assess the performance of the developed prediction algorithm using a single day of data only—by no means enough to make any general claims relating to the relative performance of their predictions to those of the IGS. In this regard, Huang *et al.* [2013] do better as their analysis uses a month of data. But, Huang *et al.* [2013] exclude the GPS Cs clocks from their analysis, which is certainly a significant factor that contributes to the reported improvement in their prediction method. While the exclusion of the GPS IIA Cs clocks is justifiable on the basis of the future outlook of the GPS constellation, excluding the IIA Cs clocks from their analysis in this way does not enable a like-with-like comparison with

[1]The GNSS community is seeking to address this problem. The limiting factor for the production of IGS-like precise clock correction products for GLONASS is that there there is no agreed-upon standard method for addressing the GLONASS inter-frequency biases, which in turn is preventing the production of a GLONASS combination that is similar to the IGS GPS combinations [Dach *et al.*, 2012].

the IGS. In this work all categories of currently operation GPS clocks, including the IIA Cs clocks are considered.

Outside of the GNSS context, previous developments in precise clock prediction methods are reported in Lepek [1997], Bernier [2005] and Panfilo *et al.* [2012].

4.2 The data

In this section, relevant aspects relating to the data sets used in this research are described. The main source of data is the International GNSS Service (IGS), which is a voluntary organisation that provides it users with observational data from a global network of GNSS tracking stations along with data products that are derived from these observations [Dow *et al.*, 2009].

4.2.1 The CDDIS archive

The International GNSS Service (IGS) maintains an archive of GPS and GLONASS individual satellite clock estimates and predictions dating back to 1992 [Dow *et al.*, 2009]. This archive is stored at a number of data centres, located across North America, in France and in Korea. For the purposes of this study, the Crustal Dynamics Data Information System (CDDIS) archive was used. This is NASA's archive of space geodesy data, and is maintained by Goddard Space Flight Center (GSFC). The contents of this archive are publicly accessible and can be obtained by ftp at `ftp://cddis.gsfc.nasa.gov`.

4.2.2 Key properties of the IGS satellite clock data

There are several properties of the IGS GNSS satellite clock data sets that are relevant to this study. These include:

- whether the data set consists of clock parameters that are **estimated** (i.e. GNSS measurements are used to determine the clock parameters), or whether those clock parameters are **predicted** quantities (i.e. an extrapolation of an estimate based on a dynamic model). The IGS and the various GNSS analysis centres that contribute clock data to the IGS produce and disseminate both estimated and predicted clock parameters to the IGS user–base.

- the property of **data latency**, and related to this, data quality, in terms of precision and accuracy both. In this regard, the IGS clock data sets are classified into three types: **Finals**, **Rapids** and **Ultra-rapids**, which are described in Table 4.1. The Finals are the premier IGS clock products, with satellite clock estimates of the highest quality, in terms of precision, if not accuracy. What this means is that the consistency among the various individual orbit and clock solutions generated by participating GNSS analysis centres is greatest in the Final data products. The Final data products are published with about two weeks delay—these are therefore only suitable for applications that are not time–critical, such as mapping or geophysics.

On the other hand, the Ultra-rapid data products, which comprise of both clock estimates and clock predictions are designed for real–time users, and have been used in applications such as meteorology [Kruse *et al.*, 1999] and rapid orbit determination of Low–Earth orbiter spacecraft [Montenbruck *et al.*, 2005]. The original development and objectives of the IGS ultra–rapid products, to support real–time precise applications of GNSS (real–time atmospheric monitoring mainly for weather prediction), are outlined in Springer & Hugentobler [2001] and Ray & Griffiths [2008]. The current status of the IGS ultra-rapid products are described in Griffiths [2013], where it is stated that the IGS ultra–rapid files are downloaded millions of times per month. Thus, the IGS ultra–rapid data set is a data set that is worth improving upon.

Product type	Latency	Max. data rate
Final (IGS)	12-18 days	30 seconds
Rapid (IGR)	17-41 hours	5 minutes
Ultra-rapid (IGU)	3 hours (start of prediction)	15 minutes

Table 4.1: The IGS satellite clock combination products for GPS.

- the **agency** that is responsible for producing the data set. As far as satellite clock data sets are concerned there are over ten different GNSS agencies involved in the IGS satellite clock data product. These include the Centre for Orbit Determination in Europe (COD), Geodetic Survey of Canada (EMR), the European Space Operations Centre (ESA), the German Research Centre for Geosciences (GFZ), Wuhan University (WHU), United States Naval Observatory (USN), Jet Propulsion Laboratory (JPL), the National Geodetic Survey (NGS) and MIT among others[1]. The GPS satellite clock data set that is produced by the IGS is an ensemble combination of the satellite clock solutions provided by the contributing analysis centres, as described in Beutler *et al.* [1995] and Kouba & Springer [2001]. In table 4.2, the analysis centres that contribute to the data that in used in producing the IGS ultra, rapid and Final GPS satellite clock combinations are listed. There is no such IGS combination for the GLONASS satellite clocks. As mentioned before, this is because there is agreed–upon standard method for addressing the issue of inter–frequency biases in the GLONASS data processing method for producing SCTO estimates [Dach *et al.*, 2012]. And so, because the standard doesn't exist, there are no analysis centres that provide precise GLONASS satellite clock solutions to would enable an IGS GLONASS combination to be computed.

- the underlying **reference timescale**, which is IGS Time for the IGS Final and Rapid products, but some approximation of GPS Time for the IGS Ultra-Rapid clock products. IGS Time is loosely steered to GPS Time in terms of frequency, but otherwise it is produced quite independently of GPS Time as an integrated frequency

[1]The IGS often use three–letter abbreviation to refer to the GNSS analysis centres, as well as the data products that are produced by these analysis centres. The abbreviations listed in table 4.2 are the same abbreviations that are used by the IGS.

Product type	No. of ACs	ACs
Final (IGS)	9	COD, EMR, ESA, GFZ, GRG, JPL, MIT, NGS, SIO
Rapid (IGR)	9	COD, EMR, ESA, GFZ, JPL,NGS, SIO, USN, WHU
Ultra-rapid (IGU)	7	COD, EMR, ESA, USN, GFZ, GOP, BRDC

Table 4.2: The GNSS analysis centres that provide GPS satellite clock solutions that contribute to the IGS GPS satellite clock combination. The IGS does not produce satellite clock combinations for GLONASS.

scale based on a weighted ensemble of selected frequency standards that belong to the IGS network [Ray & Senior, 2003; Senior *et al.*, 2003]. As the underlying reference

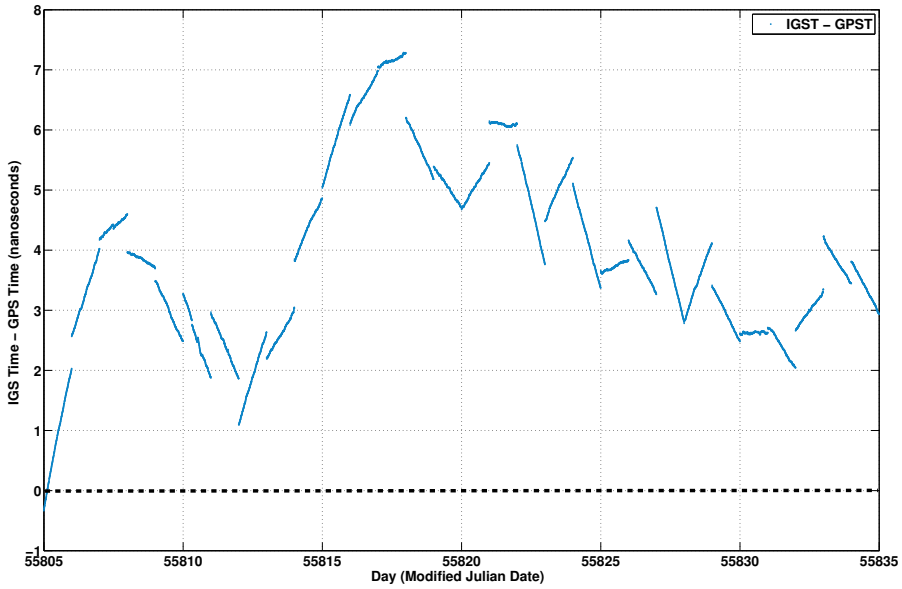

Figure 4.1: IGS Time minus GPS Time during the month of September 2011. The behaviour of the IGS Time minus GPS Time offset must be accounted for if comparisons between IGS Final/Rapid products (which use IGT Time as reference timescale) are to be made with IGS Ultra products or clock solutions generated by any individual GNSS analysis centre (which use GPS Time as the reference timescale).

timescale for the IGS Ultra products are different to the reference timescale for the Rapid and Final Products, any comparison of the Ultra clock solution with the Rapid or Final solutions must take this into account. In figure 4.1, the difference between IGS Time, T_{igs}, and GPS Time, T_{gps}, is plotted during the time period September 2011, using data published in the IGS clock RINEX files, which are described in Subsection 4.2.3, and during this period the level of the difference between IGS Time and GPS Time is significant, at several nanoseconds. Also, during the time period the $T_{igs} - T_{gps}$ timescale offset quantity appears biased in that the time offset is mostly positive. This difference in the underlying reference timescales is one of

the major issues that is dealt with in this research, and the results of a detailed investigation into the implications of this problem are presented in Chapter 6.

4.2.3 The clock data formats

The satellite clock estimates or predictions in the CDDIS archive are presented in text files in a variety of formats: SP3,CLK and NAV/BRDC.

The SP3 format

SP3, or SP3c, is the extended standard product 3 orbit format [Hilla, 2010]. SP3 files are named according to the convention *aaawwwwd.sp3*, where *aaa* is three letter code identifying the agency producing the data, *wwww* is GPS week, *d* is day of week, *.sp3* is the extension for SP3 files provide satellite clock values at a 15 minute rate, alongside the Earth-centred Earth-fixed Cartesian XYZ co-ordinate estimates of the satellite orbit.

The NAV/BRDC format

NAV/BRDC [Gurtner & Estey, 2007], [Gurtner & Estey, 2009] are data files that contains all the information broadcast via signal in space, by the GNSS satellites, which includes the broadcast satellite clock parameters. NAV files are named according to the convention *ssssddd0.yyn*, where *ssss* is four letter code identifying the station or receiver where the data was recorded, *ddd* is day of year, *yy* is the year, and *.n* is the extension for NAV files. The BRDC file is a specific NAV file, with prefix *brdc*, where the other files hold the station identifier. In effect, the BRDC is an amalgamation of the navigation message data recorded at a number of globally distributed tracking stations into a single file, which represents a complete record of the navigation message as it is broadcast via signal in space. BRDC data can be used to study the properties of the GNSS broadcast navigation message parameters. In terms of studying GNSS SCTO, this archive of historical data allows for the study of the predicted SCTO products that the GNSS operational control segments provide to users in real–time.

The CLK format

CLK denotes clock data presented in receiver independent exchange (RINEX) format [Ray & Gurtner, 2010]. CLK files are named according to a convention similar to that of the SP3 files—*aaawwwwd.clk*, *aaawwwwd.clk_30s* or *aaawwwwd.clk_05s*—where *aaa* is a three letter agency identifier, *wwww* is GPS week, *d* is day of week, *.clk* is the extension for CLK files provide satellite clock values for every 5 minutes, *.clk_30s'* is the extension for CLK files that give satellite clock values at 30 seconds and so *.clk_05s* gives clock values at a rate. Ultimately, CLK data was not used in our research, as the 15 minutes data rate given in the SP3 files was sufficient for the need of our study. But, in the early stages of our research, we did investigate the CLK data products, and developed the tools to handle this format. Where an agency gives clock solutions in SP3 format and CLK

format, for clock products of the same type—i.e. final, rapid or ultra—where the epochs match, every 15 minutes, the solutions are identical.

The main data formats used in this study

In this research, the clock products of the IGS for the years 2010–2012 were used. Within that, for the most part SP3–formatted data was used, and data for the year 2012 was the most heavily used.

4.3 Software tools

This section describes the software tools that were used in this research, giving some details of implementation, as well as the methods used to test and validate the code.

The developing and testing of new research software was a major component of the work, as the requirements of the algorithms developed were not catered for by an existing software package. From a pedagogical point-of-view this software development exercise was useful in that the act of implementing algorithms in software—whether these algorithms were newly-developed or well-established—was often far more insightful in getting a sense of the technical gaps and problems that exist in the domain of SCTO prediction in GNSS. This research software comprised a combination of scripts and modules written in C++, MATLAB and in the form of Unix shell scripts.

4.3.1 Data management

One of the core functions of the developed software is data management, which involves the processes of data–fetching, data–extracting and data–storing for access by any application that requires them. In this section, this data management software is described.

The main sources of the satellite clock data used in this research are the IGS satellite clock combination data products, archived in SP3 format. As far as data pre–processing requirements are concerned, there are two components to consider. The first involves retrieving the required data sets from the CDDIS data archive, which is on the Internet. The second part is extracting the relevant information from these data files, and storing this information in a database, such that this information is readily available to the applications developed to study these data sets. For retrieving the SP3 data from the CDDIS archive, a Unix shell script that takes start date and end date as arguments, and is based around the GNU wget utility was used to download the required data files and to store them locally. For storing the satellite clock data in a local (i.e. in computer memory) database, a C++ command line application was written to store all of the SP3, BRDC and CLK data into an associative STL <map> container. Storing the data in this way enables the extraction of clock data over a period of many days for single satellite into a single time–series, which is the form in which this study requires the data.

4.3.2 Code for the clock characterisation, RTT modelling and SCTO prediction algorithm studies

The code to perform the computations and visualisations relating to the clock characterisation study, the RTT modelling study and the clock prediction algorithm performance analysis study was written in MATLAB. The interface between the C++ data processing application and the MATLAB code was done through satellite–specific ascii formatted text files. There were two main reasons for the choice of MATLAB for this stage of the research: i) in terms of code–development, fast progress in MATLAB due to large number of numerical and scientific functions that are built in to the standard MATLAB distribution, ii) MATLAB offers a convenient set of tools for visualisation in terms of the plotting of numerical data, which was necessary in order to present the results of the research.

4.3.3 Code verification

There was some overlap in functionality between the code developed for this project and various applications that form a part of the GPS Toolkit (GPSTk), which is an open–source GPS data processing software [Harris & Mach, 2007]. For this reason, the GPSTk was used for validation of some parts of the developed research software, by comparing the results of the two.

Summary

This chapter comprises three parts: a review of published literature relevant to the topic of SCTO prediction in GNSS that was encountered during this project; a detailed description of the data sources and data sets (outlining their purpose) that are used to produce the results presented in this thesis; and finally, a description of the software tools that were developed and used to perform the study. The following chapter is based around an in–depth characterisation study of the GPS and GLONASS satellite clocks.

Chapter 5

The characteristics of GNSS satellite clocks

Chapter outline

The abundance of high-quality satellite clock data—spanning across many years, corresponding to multiple satellite navigation constellations and derived from real measurements—is the key enabling resource upon which this study is built. For over twenty years, several GNSS data processing agencies, have been independently deriving estimates of GPS and GLONASS satellite clock parameters using data collected from a globally distributed network of geodetic receivers. In attempting to better understand the behaviour of atomic clocks in a space environment, this research aims to exploit this resource to the fullest.

In this chapter, the characteristics of GNSS satellite clocks are inferred, from the analysis of a variety of clock data products published by major GNSS data processing agencies. Naturally, those features that are most relevant for satellite clock time offset (SCTO) estimation and prediction are emphasised. The scope of the characterisation study, the methods involved and the results of the analysis are presented in this chapter. This is followed by a discussion around the main findings.

5.1 The scope of the characterisation study

Parameters of study	Values
Systems	GPS and GLONASS
Characterised quantity	SCTO
Reference timescale	IGS Time and GPS Time
Timeframe of analysis	2012 (01 Jan – 31 Dec)
Time–resolution of characterisation†	15–1440 minutes (24 hours)
Data format	SP3 (15–minute sampling rate)
Data sources	IGS (for GPS) and ESA (for GLONASS)

Table 5.1: Scope of the GNSS SCTO characterisation study. †The time-resolution of a characterisation study can be high (seconds), medium (several minutes up to twenty four hours) or low (days). This study falls into the medium category, and the focus is on the behaviour of in–orbit clocks in the 15 minutes—24 hours range.

In table 5.1, the key parameters of the characterisation study, which is the topic of this chapter, are listed. During this project, data spanning across many years, were considered initially. However, one year of data provides enough evidence to support the key finding presented here. Satellite clock information in the SP3c[1] format, described in Section 1.2.3, was available for the GIOVE (Galileo) satellites. But, the results of the investigation of this data are not presented here. This is mainly because of data quality issues (lots of data gaps) but also the amount of data (3 days) was insufficient for this type of analysis.

5.2 Method

The work presented in this chapter is based entirely upon the ideas and analysis tools that are introduced in Chapter 3. Overall, the method comprises of the following steps:

1. **Data pre–processing,** which involves the processes of fetching (from the Internet), and extracting satellite clock information from SP3 files. Typically, an SP3 file will hold satellite clock information for all satellite clocks in a system, for one day only. Thus, it is necessary to separate the SP3 clock information, satellite by satellite. After separation, all the clock information for a single satellite clock is concatenated to form a time–series of satellite clock data that spans across two (or more) days. In this way, a database of satellite clock information is put together. This database then provides the input data for the satellite clock characterisation work.
2. Basic **time–series analysis** methods are applied to the pre–processed input data. These include the removal of a linear trend—a process known as detrending—from the SCTO data, as well as visualisation (plotting of the pre–processed input data and the detrended data). These are simple, but (very) effective, analysis tools for enabling a quick feel for overall satellite clock behaviour. Also, data quality issues (e.g. data gaps, outliers) are identified by this step.

[1] In this chapter, the terms SP3 and SP3c are used interchangeably.

3. **Stability analysis** based on the ADev, HDev and MDev statistics, over a range of analysis intervals (900–86400 s). Sigma–tau curves and dynamic sigma–tau curves based on these statistics are plotted. The results of these are useful in determining, qualitatively and quantitatively, the nature of the underlying noise processes that are observable in the clock data. The presence of cyclic patterns in the clock data is also picked up by the sigma–tau curves.
4. Running the clock data through the **standard clock Kalman filter (SCKF)**, which provides a means of investigating the time–evolution of the frequency offset and linear frequency drift of the clocks. Initialising the SCKF and determining coefficients for the noise parameters are non–trivial exercises, and difficult to automate[1]. Thus, these are performed manually on a clock–by–clock basis.
5. **FFT–based spectral analysis** of the residuals of the standard clock Kalman filter estimates of clock behaviour, used to determine the exact period of cyclic patterns in the clock data that is not accounted by the clock model of the SCKF.

5.2.1 GPS

In this characterisation study, in the GPS case, all of steps 1–5 of the method detailed in Section 5.2 were performed, on the complete set of IGS SP3 final GPS satellite clock data for the year 2012. To better represent the results, it is helpful to categorise the GPS satellite clocks. The current operational constellation is non–uniform, in the sense that there are important differences in the specifications of the in–orbit spacecraft. As far as SCTO characterisation is concerned, the underlying satellite clock technology as well as the age of those clocks are pertinent. Based on this, a GPS satellite clock classification scheme is proposed.

Classification of GPS satellite clocks

GPS satellite clocks in orbit today can be put into two distinct categories based on the element used by the active onboard atomic frequency standard(AFS): rubidium (Rb) and caesium (Cs). Also, older GPS satellite clocks carry an older generation of onboard atomic clock technology, and the performance of atomic clocks are known to degrade as they get older. It makes sense therefore, to categorise GPS atomic clocks in terms of age also. A natural way to do this is to separate clocks according to GPS satellite block type: I, II/IIA, IIR/IIR-M and IIF. All GPS satellite clocks carry multiple onboard AFSs, see table 5.2. However at any one time, only one of these clocks is designated the active AFS—The others are redundant and serve as back-ups. Some GPS satellites—Block II/IIA and Block IIF—have a combination of Cs and Rb clocks

With this method of classification, GPS satellite clocks can be put into seven categories: (Block) I Rb, I Cs, II/IIA Rb, II/IIA Cs, IIR/IIR-M Rb, IIF Rb IIF Cs. Of these,

[1]There are many published works demonstrating the use of adaptive Kalman filters (where the parameters associated with the noise models are estimated in the Kalman filter, and these parameters evolve as the Kalman filter is operated), of which Davis *et al.* [2005b] and Huang & Zhang [2012] are particularly relevant in the context of GNSS satellite clock estimation and prediction. In this work, adaptive Kalman filter techniques were not used, but this could be an interesting topic for future work.

four: II/IIA Rb, II/IIA Cs, IIR/IIR-M Rb, IIF Rb remain of interest today. Currently, there are no GPS IIF satellite with Cs as the active AFS. The other two categories are interesting in a historical sense only. The IIR/IIR-M Rb is the most common category of active GPS atomic clock in orbit today. Of 32 GPS satellites in orbit in 2012, 19 belonged in this group.

GPS Block	SVN	Onboard clocks	Notes
I	1–3, 4–11	3 Rb, 1 VCXO†	VCXO by Frequency Electronics Inc. (FEI)
		3 Rb, 1 Cs	Rb by Efratom
II/IIA	13–40	2 Rb, 2 Cs	Rb by Efratom, Cs by FTS
IIR/IIR-M	41–61	3 Rb	Rb by Perkin Elmer (PE)
IIF	62–65	2 Rb, 1 Cs	Rb by PE, Cs by Symmetricom

Table 5.2: Satellite clock information for GPS. The information in this table is mainly extracted from Mallette *et al.* [2008]. From this, GPS space clocks have been categorised into seven groups, of which four types are of interest with respect to the current GPS constellation.†Voltage–controlled crystal oscillator (VCXO).

5.2.2 GLONASS

In this characterisation study, in the GLONASS case, only steps 1–3 of the method detailed in Section 5.2 were performed, on the ESA SP3 final clock data spanning the entire year of 2012. In terms of characterisation, steps 4 and 5 are used in the GPS case to probe further into the nature of the periodic signals and seen in the GPS satellite clocks. It turns out that in the GLONASS case, these features are not observable in the data, and therefore, there is nothing to be gained in further analysis beyond step 3. Also, there were data quality issues (the presence of regular discontinuities) with the GLONASS data, which create problems for applying the SCKF–based analysis method on the data. There are methods for handling these within the Kalman filter framework, but these methods were not explored in this work.

Unlike GPS, there is no immediately apparent argument to justify the classification of GLONASS satellite clocks into distinct categories. All of the active GLONASS satellites carry Cs onboard atomic frequency standards, and all belong to the same GLONASS-M family of satellites. The payload specifications of all active GLONASS are identical, so in theory we expect similar performance from all satellites, and all satellite clocks. Therefore, in Section 5.3.2, one satellite clock is chosen—the Cs onboard GLONASS satellite 746 (Kosmos 2478)—and for now, the properties of this clock are used to discuss the characteristics of a typical GLONASS clock, in general. This GLONASS satellite occupies slot 17 in the GLONASS constellation, and was broadcasting on frequency channel 4 in 2012.

5.3 Results

A representative set of results from the characterisation study are presented in this Section. GPS–related results are given in Subsection 5.3.1 and GLONASS–related results are in Subsection 5.3.2.

5.3.1 GPS

Time–series: IGS SP3 Final satellite clock data

In figure 5.1, the pre-processed satellite clock data for a representative selection of GPS satellite clocks are plotted against time, for the period January 2012. The slopes on each of these curves, in so much as the eye can tell, are (almost) straight. This is visual confirmation that the frequency of GPS satellite clocks are stable, and to a large extent deterministic—at least at order 10^{-12}, explained below[1].

In all four clocks presented in figure 5.1, over the course of one month, the time-offset quantity varies typically at the several microseconds level—more in some than in others. In the SVN 62 IIF Rb case the time-offset quantity varies by just over a half microsecond, whereas in the SVN 34 IIA Rb case we see a difference of $\approx$ 30 microseconds. The former belongs to the newest GPS Block IIF generation and the latter belongs to the second-oldest spacecraft in the GPS constellation. Such a difference might suggest that clocks in the older generation of GPS satellites are prone to more variation in the time-offset quantity. In any case, in the context of user's requiring a PNT solution, such first-order, linear variations are highly predictable, and generally will not affect performance. From the point–of–view of the GPS operator, it is problematic if this time–offset becomes too large, because in that case the time–offset information will not be delivered, to the user in the navigation message, at the required precision level. The ultimate metric of the performance of a clock is its predictability. In this regard, the only inference we can make from the straight slopes in all cases in figure 5.1, is that at the micro-seconds level, the time-offsets of GPS satellite clocks from T_{igs}, are highly predictable. In other words, the slopes of the curves in figure 5.1 are, in a sense, a visual representation of the frequency offset of each clock with respect the reference timescale, T_{igs}, and the frequency offset of GPS satellite clocks are deterministic, to a large extent. This is unsurprising, but microseconds level precision is not sufficient for PNT applications based on GPS. This requires examination of the features of the GPS clocks at the several nanoseconds level.

[1] 1 month $\approx 3 \times 10^6$ seconds, which is $\mathcal{O}(10^6)$. Time-offset variation over one month of several microseconds,$\mathcal{O}(10^{-6})$. Normalised frequency offset is $\frac{dx}{dt} \approx \frac{\mathcal{O}(10^{-6})}{\mathcal{O}(10^6)}$, thus 10^{-12}.

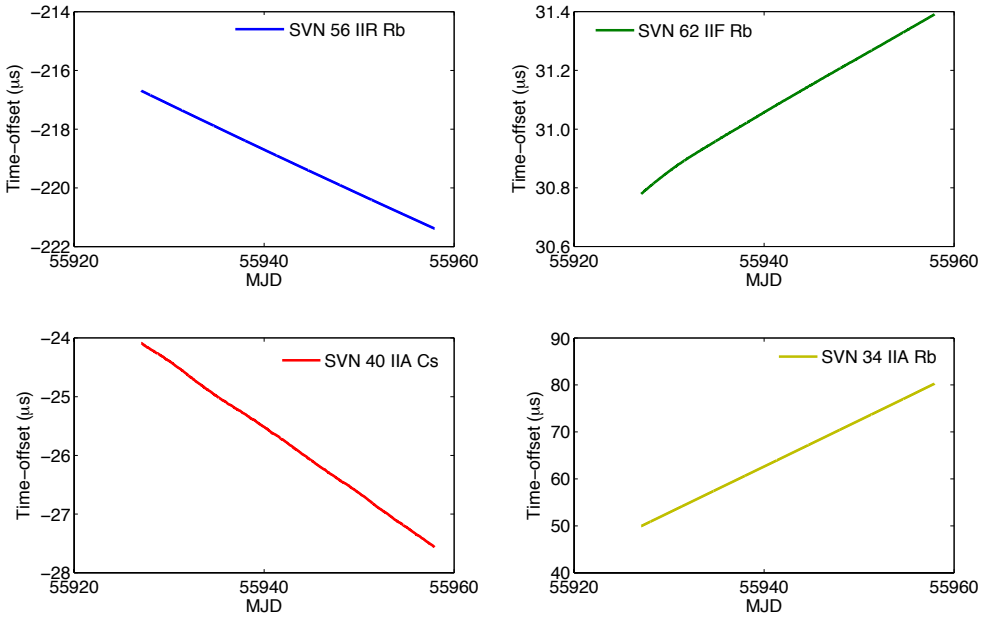

Figure 5.1: Time-series plot of the time-offset with respect to IGS system time, T_{igs}, during January 2012 for a chosen representative selection of GPS satellite clocks.

Time–series: Satellite clock data (detrended)

A largely deterministic time–offset (from IGS Time) in the order of microseconds over several days is a feature common in all GPS satellite clocks. Looking beyond this, clear differences between GPS satellite clocks emerge, dependent on category, see figure 5.2. It is possible to visualise the underlying, higher-order, features of the time-offset quantity by subtracting the corresponding values from a line of best fit to the raw (unprocessed) SCTO time-series, in a process known as detrending. The outputs from this detrending process, for the four satellite clocks already considered in the previous section are shown in figure 5.2. A largely deterministic time–offset in the order of microseconds over several days is a feature common in all GPS satellite clocks.

The parabolic shape of the curves representing time-offset (detrended) of the Rb clocks is a good visual indication of significant linear frequency drift in Rb clocks. In the newer GPS Rb satellite clocks—SVN 56(top-left) and SVN 62(top-right)—the parabolas are smooth, to a large extent. But in the old SVN 34 Rb(bottom-right), the effect of underlying stochastic variations has a significant impact on the parabolic shape. The inference here is that linear frequency drift is significant, and to a large extent deterministic in all GPS Rb clocks—but more so in newer clocks belonging to IIR/IIR-M and IIF, than in older ones belonging to IIA. There is no evidence of linear frequency drift in GPS Cs clocks, SVN 40(bottom-left) showing a typical example of this.

The stochastic variations, or clock noise, in the GPS satellite clocks is evident in each of the examples in figure 5.2—we see this in the high-frequency variations which appears super-imposed onto low-frequency, largely deterministic variations. Here, the exception

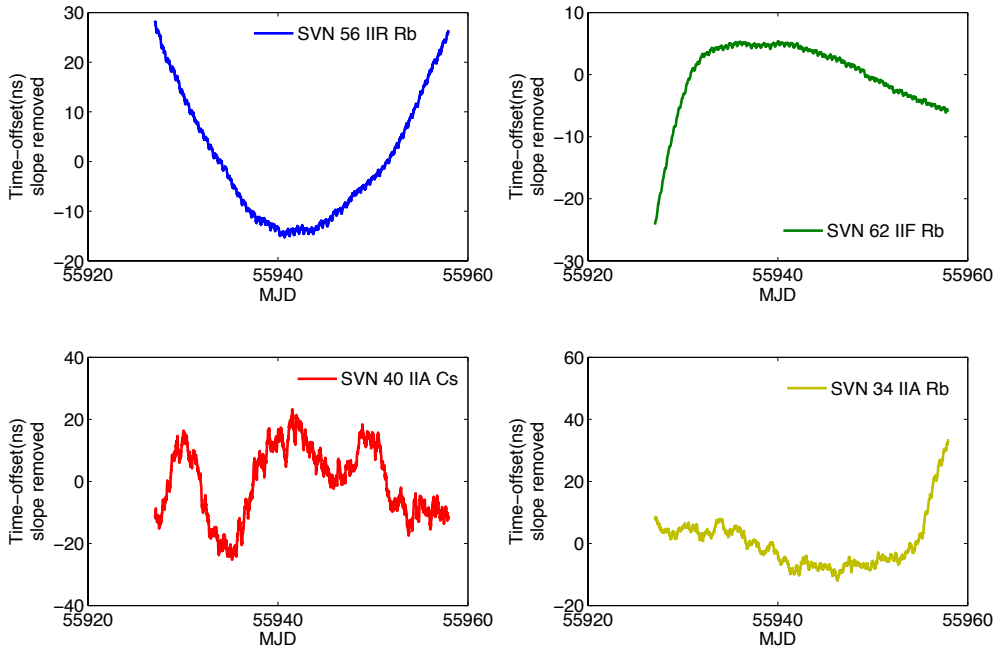

Figure 5.2: Time-series plot of the time-offset (detrended) with respect to IGS system time, T_{igs}, during January 2012 for a chosen representative selection of GPS satellite clocks.

is the SVN 40 IIA Cs, where the clock signal appears to be dominated by the stochastic variations at high frequencies and low frequencies. Another observation from figure 5.2 relates to the magnitude of the random variations—clearly, this is significantly greater in the older IIA satellite clocks, than in the newer generation IIR and IIF clocks. This may be due to clock ageing, but might also be due to the design of the clock itself.

Frequency stability analysis: HDev–based sigma–tau curves

To this stage, the discussion of the characteristics of the GPS satellite clocks has been largely qualitative. For a more rigorous, and quantitative characterisation of the stochastic properties of the GPS satellite clocks, time-domain stability analysis methods, as described in Chapter 3, are very useful.

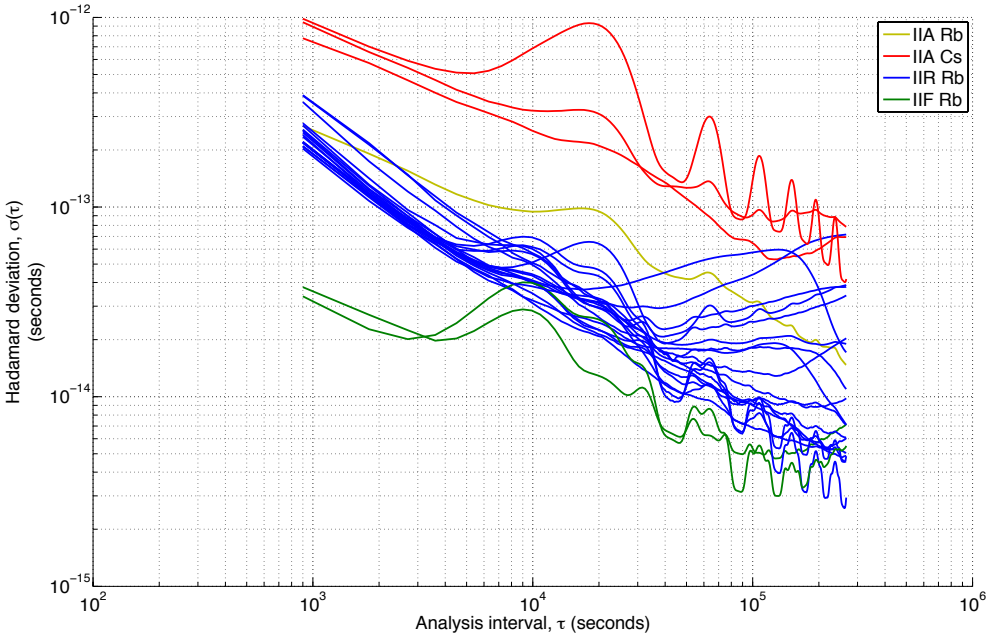

Figure 5.3: Sigma-tau curves based on IGS precise clock data for twenty-four GPS satellite clocks during January 2012. Each curve represents Hadamard deviation of a single GPS satellite clock over a range of averaging intervals from 900 s to ≈ 270,000 s.

In figure 5.3, sigma-tau curves—based on Hadamard deviation calculations over a range of averaging intervals, using data for twenty-four satellite clocks from January 2012—are plotted on the same set of axes, to allow for easy and direct comparison. During this time period, January 2012, data is available for thirty-two GPS satellites, but eight satellites are excluded here for poor data quality reasons; mainly the presence of data gaps, that complicate the computation of all Allan deviation type statistics, including the Hadamard deviation. There are methods for performing Allan variance type analyses even in the presence of a significantly large number of data gaps and outliers, see Sesia & Tavella [2008], but for the purposes of the discussion here twenty-four satellites are sufficient.

Immediately, figure 5.3 reveals two things. One, there is are clear distinction between clocks belonging to the different categories, on the basis of the position of where their corresponding sigma-tau curves occupy the axes. The inference here is that in terms of overall noise level, irrespective of noise type, the IIF Rb clocks are better, in that they are less affected by clock noise, by almost one order of magnitude compared to the IIR Rb and IIA Rb clocks at all averaging intervals, and better still than the IIA Cs clocks. Another way to put this—in a frequency stability sense, there is no contest: the performance of the IIR Rb and IIA Rb clocks are comparable, and they outperform the IIA Cs clocks, but the IIF Rb clocks are the winners. A justifiable, albeit unsurprising, conclusion to make then is this: the GPS satellite clocks in the newer generations are better, in the sense that they are more predictable.

The second feature that jumps out from figure 5.3 is the presence of the periodic

variations. On a sigma-tau curve, a peak followed by a dip indicates the presence of periodic variations, with period equal to the tau-value associated with the dip in the curve. In figure 5.3, looking at the top-most sigma-tau curve, the first dip in the curve following a peak occurs at a tau-value somewhere between forty thousand and fifty thousand seconds, indicating a cyclic variation of about half a day. In this way, sigma-tau curves are effective at identifying the presence of periodic variations, however their use in quantifying a precise value for the period is limited—for such purposes FFT-based spectral analysis techniques are more suited to the task.

These periodic variations are seen in all categories of GPS satellite clock, and further it appears that the magnitude of the variations are satellite-specific, rather than say category-specific. This suggests that in order to establish the root cause of the periodic variations, a good strategy might be to investigate features that are unique to each satellite, or satellite clock.

At this stage, these periodic features, dominating the sigma-tau curves at longer averaging intervals in this way, cause problems for the analyst. Such un-modelled, and largely deterministic, characteristics obscure any underlying structure in the sigma-tau curves—and it is the underlying structure that reveals useful insight into the stochastic properties of the satellite clock data.

At averaging intervals below four thousand seconds, the influence of the cyclic variations on the shape of the sigma-tau curves in figure 5.3 is minimal. Thus, at such averaging intervals (i.e. $< 4000\ s$), making inferences from the sigma-tau curves, regarding the stochastic properties of the IGS GPS satellite clock data is completely justified. So let us proceed in doing so.

On a sigma-tau curve based on Hadamard deviation values calculated over a range of tau-values, and drawn on a log-log scale as in figure 5.3, a slope of -1 indicates a data set showing the influence either of White Phase Modulation (WPM) noise, or Flicker Phase Modulation (FPM) noise. A slope of $-\frac{1}{2}$ suggests the presence of White Frequency Modulation noise. In the case of GPS IIR Rb clocks then, the dominant stochastic process, at averaging intervals below four thousand seconds is WFM noise; for the IIA Cs, IIA Rb and IIF Rb clocks either WPM noise, FPM noise, or some combination of both is dominant. Sigma-tau curves can also be used to distinguish between WPM noise and FPM noise, but for this, the curves should be based upon the Modified Allan deviation statistic.

In figure 5.3, the Hadamard deviation statistic is used in place of the Allan deviation—the accepted standard—because of the linear frequency drift in the Rb clocks, especially those on the IIR and IIF satellites. At short averaging intervals—relative to the magnitude, or influence, of the linear frequency drift—the slopes of sigma-tau curves based on either Hadamard deviation or Allan deviation are indistinguishable. As far as the eye can tell, the slopes are equivalent, but, at longer averaging intervals, where linear frequency drift is present, a sigma-tau curve based on Allan deviation calculated over a range of averaging intervals, will turn and curve upwards with slope +1, on a log-log scale. The Hadamard deviation statistic is not sensitive to linear frequency drift and is therefore not affected in this way.

Summary statistics

In table 5.3, the (ensemble) average value of the Hadamard deviation statistic, at a variety of analysis intervals i.e. 15 minutes, 3 hours, 6 hours, 12 hours and 24 hours are recorded. Here, the various average values are computed using all GPS satellite clocks that belong to the same set, and there are six sets: IIR/IIR-M(19), IIF(2), IIA(9), Cs(4), Rb(4) and All(31)[1]. Again, this analysis used all IGS GPS SCTO data from the period January 2012. The individual satellite clock statistics that were used to compute these values are given in Table C.1 of Appendix C.1. This information is included here because it is useful in providing specific numerical values for quantifying the frequency stability of a typical GPS satellite clock, which is based on the analysis that was conducted on the full GPS constellation. E.g. The typical stability of an in–orbit GPS Rb clock at an analysis interval of 6 hours is 7.03×10^{-14}, suggesting (roughly) a prediction error deviation of $7.03 \times 10^{-14} \times 6 \times 3600 = 1.51\,\text{ns}$ at six hours prediction length, under the assumption that WFM or RWFM noise are the only noise processes influencing that clock's behaviour, as explained in Section 3.6.

PRN(SVN)	HDev ($\times 10^{-14}$) at different averaging intervals (hours)				
	0.25	3	6	12	24
Averages					
IIR/IIR–M	29.6	8.07	7.47	2.46	2.13
IIF	7.17	6.57	3.65	1.23	0.817
IIA	66.2	28.3	24.9	12.7	0.791
Cs	86.0	22.0	19.6	9.92	0.641
Rb	27.1	7.69	7.03	2.37	2.04
All	32.0	9.42	8.52	3.24	2.53

Table 5.3: Summary statistics arising from the frequency stability analysis (HDev) of the GPS satellite clocks.

Additional statistics on the frequency stability characteristics of the typical GPS clock, at a variety of analysis intervals, are given in table 5.4. In this table, a GPS IIR/IIR–M Rb satellite clock is chosen as the representative for a typical GPS clock. This is a reasonable position to take because in 2012, of the 32 GPS satellite that flew in orbit, 19 belonged to the IIR/IIR–M Rb category.

[1]The numbers within the parentheses denote the number of GPS satellite clocks that were included in the computation of the average for that set.

Summary statistics ($\times 10^{-14}$ seconds)	For GPS IIR/IIR–M Rb based on HDev values at different averaging intervals (hours)				
	0.25	3	6	12	24
Mean	32.0	8.88	8.11	2.96	2.37
Median	24.4	4.46	3.01	1.62	1.54
Maximum	98.4	72.2	86.3	14.4	8.63
Minimum	20.3	2.92	1.98	0.953	0.649
Std. Deviation	20.2	15.6	18.8	3.71	2.23

Table 5.4: Summary statistics of HDev–based frequency analysis on the typical GPS satellite clocks belonging to the IIR/IIR–M Rb category.

HDev, ADev and MDev sigma–tau curve comparisons

Sigma-tau curves based on Allan deviation and Hadamard deviation, plotted together on the same set of axes, as in figure 5.4, indicate the presence of significant and deterministic linear frequency drift, if the two types of curve diverge at long averaging intervals, with the Allan deviation curve turning to slope upwards. In figure 5.4, this is seen in the cases of the SVN 56 IIR Rb and the SVN 62 IIF Rb clocks, but not in the other two. It can be very useful to plot a sigma-tau curve based on Modified Allan deviation, on the same set of axes, as Allan deviation or Hadamard deviation sigma-tau curves. On a modified sigma-tau curve, a slope of -1 indicates FPM noise, whereas a slope of $-\frac{3}{2}$ indicates WPM noise. On a sigma-tau curve, a slope of -1 indicates either WPM noise or FPM noise, not distinguishing between the two. Thus, if the slope of the modified sigma-tau (MDev) curve is differs from the slope of the sigma-tau curve (ADev, HDev), particularly at low averaging intervals, this indicates the strong presence of WPM noise. In figure 5.4, the slope of the ADev/HDev sigma-tau curve differs from the slope of the MDev modified sigma-tau curves, in all cases except the case of the SVN 34 IIA Rb. Here, the slope is roughly -1, a good indication of FPM noise. One more observation worth making at this stage—look at the slope of the sigma-tau curves in figure 5.4, all of them, for the SVN 40 II Cs clock. At averaging intervals between 10,000 and 20,000 seconds the slope of the sigma-tau curves are flat, an indication of the influence of FFM noise. Looking closely at figure 5.3, it is clear that this is not the only clock in the GPS constellation to be affected by the FFM noise type.

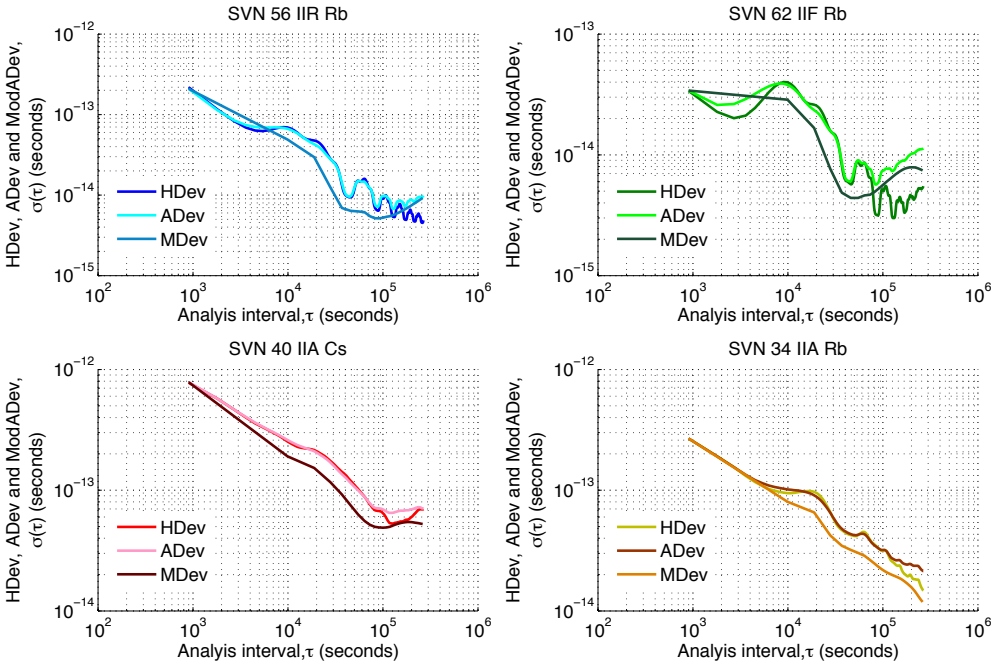

Figure 5.4: Sigma-tau curves for a selection of GPS satellite clocks, January 2012.

Dynamic frequency stability analysis with dynamic HDev sigma-tau curve

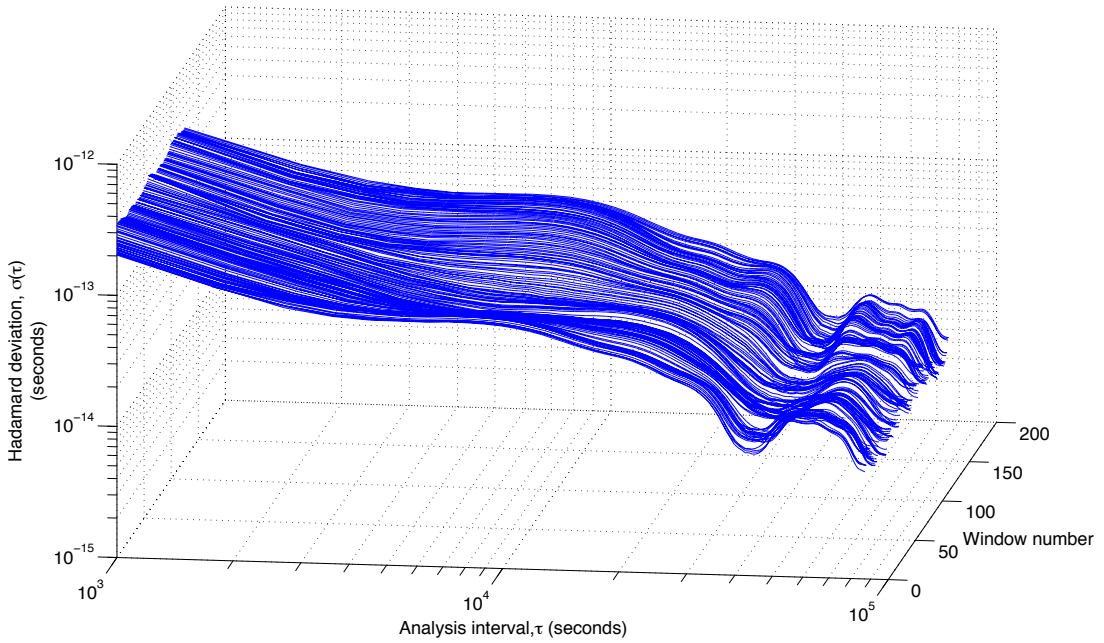

Figure 5.5: The results of a dynamic Hadamard–deviation based stability analysis conducted on IGS GPS SCTO data from GPS SVN 56 IIR Rb, which indicate that the periodic and stochastic variations observed in the data are relatively constant over a period of several months. Here, a total of 166 days of data is used: the first 166 days of 2012. A basic analysis window–length of 10 days is used, with the analysis sliding by one day. First, an HDev–based sigma–tau curve is generated using data from the first ten days of 2012. Then, the analysis data set slides by one day, which means that an HDev–based sigma–tau curve is generated using data spanning day 2 to day 11 of 2012. Then, the analysis data set slides by one day again, and this process is repeated until 166 days of data in total have been used in the overall analysis. Each sigma–tau curve generated in this way are drawn alongside each other on a 3d–plot(above), with the third axis corresponding to analysis window number.

So far, the analysis has focussed on a fixed time–period of data, i.e. the month January 2012. But, what about the stability of these characteristics (e.g. the observed periodic and stochastic variations) over a period of time? One method for investigating this is to perform a dynamic stability analysis, using a dynamic version of the ADev, HDev of MDev, as it is described in Chapter 3. In figure 5.5, the results of a dynamic stability analysis, using sigma-tau curves based on the Hadamard deviation statistic, for the clock on the SVN 56 IIR Rb, are presented. The sigma-tau curves show good consistency over all averaging intervals, in terms of magnitude and shape. The inference here is that the characteristics of the periodic and stochastic variations are more or less constant, at least over a period of several months. The result applies to this clock only, but has important implications for mathematical modelling of the GPS clocks. It means that it may be possible to adequately describe these periodic signals and stochastic variations using parameters that are either (almost) constant or slowly–varying.

SCKF–based estimates: Normalised frequency offset

The standard clock model Kalman filter (SCKF), as described in Section 3.3, was set up to operate on the GPS satellite clock data, providing estimates of SCTO, normalised frequency offset (NFO), and linear frequency drift (LFD), as output. In figure 5.6, the SCKF estimates of NFO during January 2012 are plotted. In this case, the SCKF outputs an NFO estimate every 15 minutes. Note, the first five days of estimates are excluded, during this period, in order to allow the SCKF parameters to converge. Overall, in the newer clocks, the NFO appears deterministic at the order 10^{-12} (IIR) and 10^{-13} (IIF). The older clocks take longer to converge in the NFO parameters, regardless the frequency instabilities are clearly greater in these older clocks, confirming observations from analysis shown in previous sections.

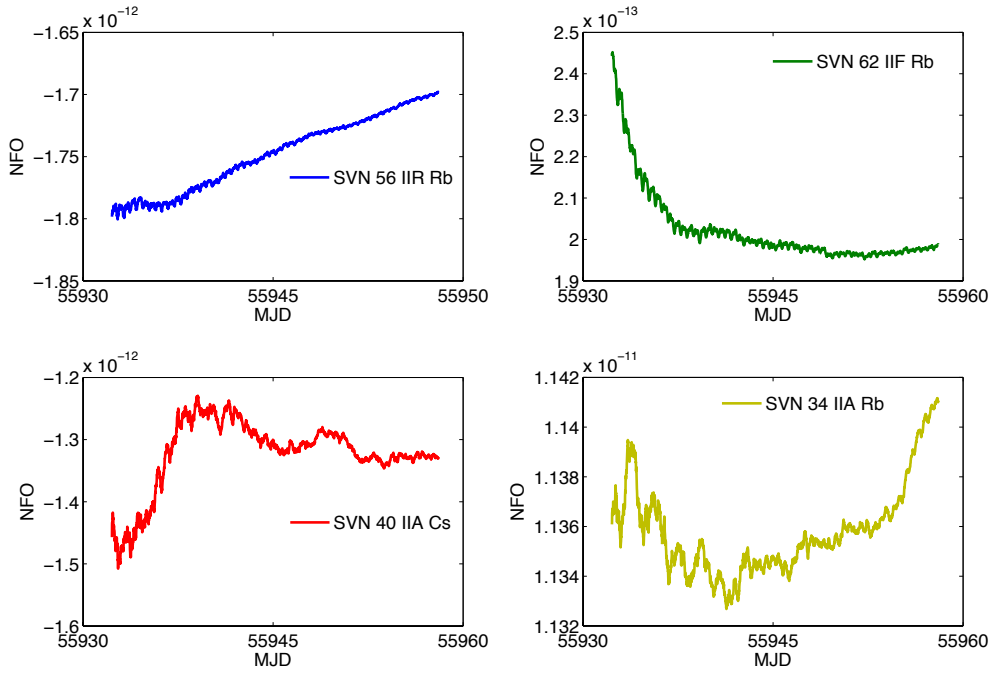

Figure 5.6: Standard CKF estimates. Normalised frequency offset.

SCKF–based estimates: Linear frequency drift

In figure 5.7, in the same way as for the FO, the LFD estimates of a selection of GPS satellite clocks are plotted against time. It is difficult to make any clear conclusion from this. But it does appear that the Rb clocks all converge to non–zero values, and the Cs clock LFD tends to zero, supporting the well–established view that there is no appreciable frequency drift in Cs clocks.

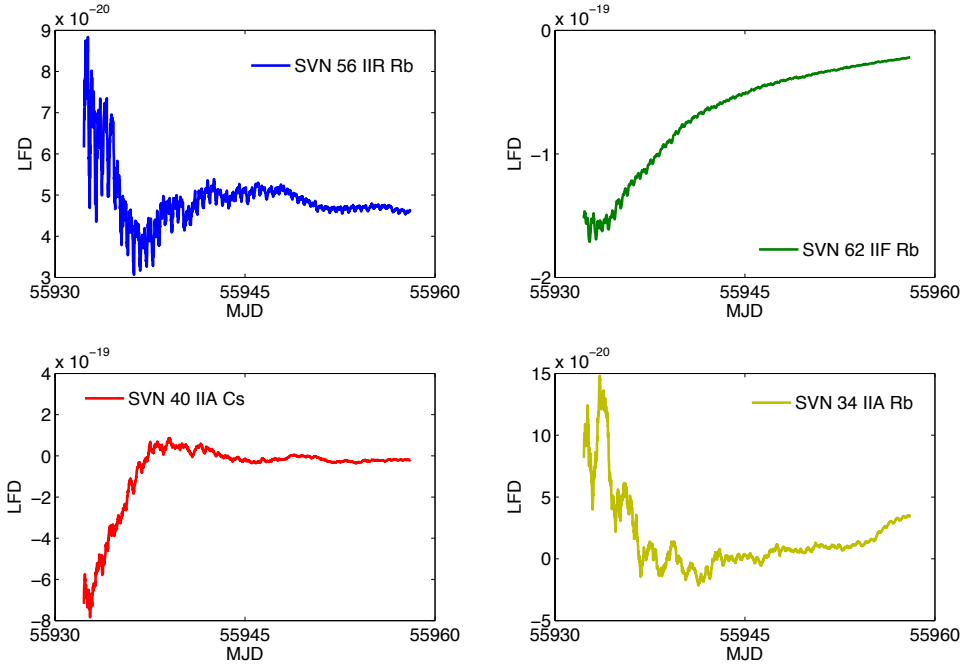

Figure 5.7: SCKF estimates: Linear frequency drift.

SCKF–based estimates: The residuals

Figure 5.8 is a plot of the residuals of the SCKF, this is the difference between actual measured value of SCTO and the Kalman filter predicted estimate of the SCTO (i.e. prior to the measurement update of the SCTO state) at a particular instance in time. The measurement sampling rate is 15 minutes. Therefore, in essence, these residuals indicates the predictability[1] of GPS satellite clocks at prediction lengths of 15 minutes. In that case, here, the SVN 62 IIF Rb is the most predictable clock, with a predictability of about 0.06 ns at 15 minutes. After this, the SVN 56 IIR Rb is predictable at the 0.25 ns level at 15 minutes, the SVN . The SVN 40 IIA Cs is the least predictable clock, with predictability at over 1 ns at 15 minutes, over an order of magnitude worse than the SVN 62 IIF Rb clocks. These results are unsurprising, and consistent with the results from the frequency stability analysis. Perhaps the most important implication of these results is that they indicate that there are no major problems in the initialisation and configuration of the SCKF for each of these clocks. Studying the SCKF residuals, and checking that the values make sense physically, is a useful method to validate the implementation of the SCKF.

[1] Predictability can be defined as an absolute measure of expected prediction error.

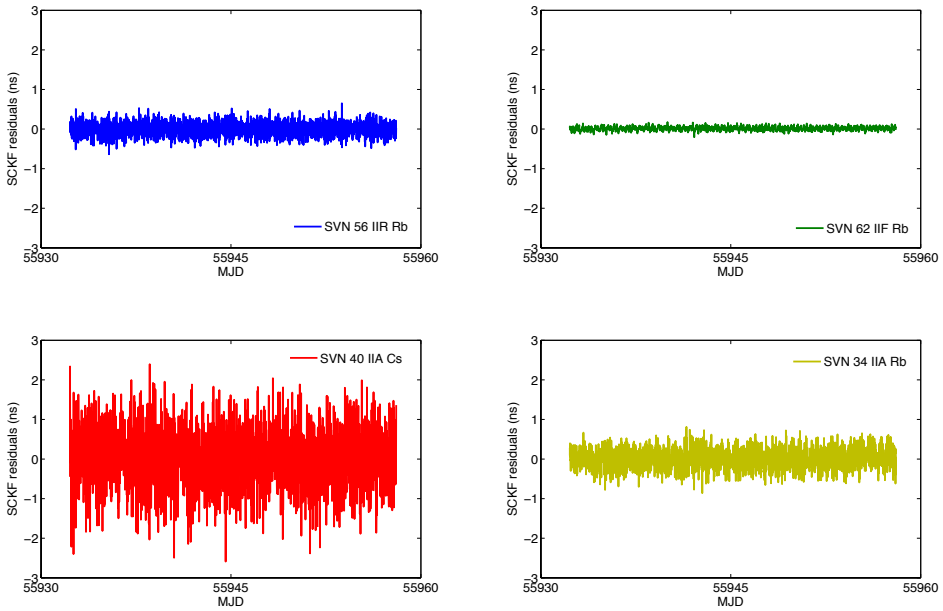

Figure 5.8: Residuals from a standard precise clock Kalman filter of a representative selection of GPS satellite clocks, during January 2012.

FFT–based spectral analysis of the SCKF residuals

With the effects of the properties of time–offset, frequency offset and linear frequency drift (deterministically and stochastically) accounted for in the SCKF, an FFT-based spectral analysis of the residuals of the SCKF can be useful in determining the exact nature of the periodic signals that the standard clock model does not account for.

In figure 5.9, the results of the FFT-based spectral analysis, for four GPS satellite clocks, are plotted. Here, there is clear evidence of the 12 hours periodic signal in all four clocks. In the SVN 56 IIR Rb and the SVN 62 IIF Rb the amplitude peaks at 6 and 4 hours are also clearly evident. There is also a spike corresponding to a 3 hours period in the SVN 56 IIR Rb.

It is not the case, in general, that the nature of the periodic signals seen in each of the clock examined in figure 5.9, are characteristics of the clock type (e.g. not all IIR Rb clocks have periodic features matching those of the SVN 56 IIR Rb clock). The fact that the nature of the periodic signals are not common across all GPS satellite clocks, or even to clocks belonging to the same category, suggests that the cause of the periodic signal seen in the GPS SCTO data are either specific to the satellite, or even specific to the satellite clock itself.

Discrete frequency steps

According to the data, there are discrete steps in the frequency of some GPS satellite clocks, that occur every now and then, in a unpredictable manner. In figure 5.10, the time–offset from IGS Time of the GPS SVN 27 IIR Rb is plotted against time, during

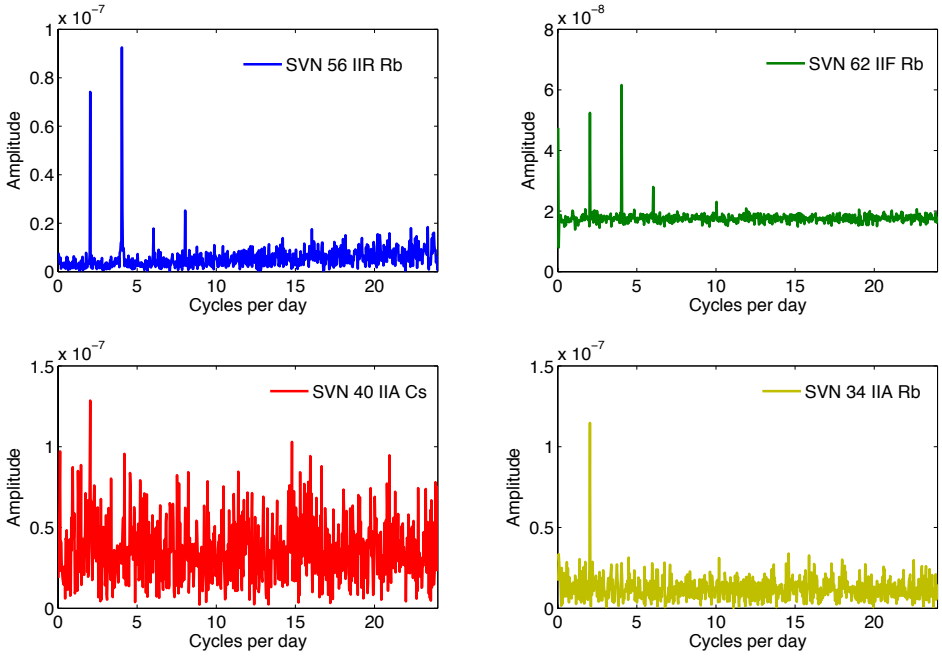

Figure 5.9: FFT-based spectral analysis of GPS satellite CKF residuals, from a representative selection of GPS satellite clocks, during January 2012. Clearly, there are periodic features in the GPS satellite clocks, which are not captured by the standard precise clock model.

January 2012. Here, there are at least four instances of a discrete frequency step for this clock. Similar frequency steps occurs in at least three other IIR/IIR-M satellite clocks during January 2012. The cause of the frequency steps is not immediately apparent. Also, at least based on this January data only, there is no reason to suspect that these frequency steps are predictable.

Missing data

In this characterisation study, satellite clocks with significant periods of missing data are excluded from the analysis. According to the rules of the SP3 format, a value of 999999.999999 μs in a satellite clock data record indicates missing data for that time instance. Thus, at step 2 of the method given in Section 5.2, it is possible to identify large periods of missing data through visualisation as shown in figures 5.11 and 5.12. During January 2012, for missing data reasons, the GPS satellite clock data from eight of the PRN slots were excluded from the analysis. At this time, each of these PRN slots corresponded to IIA satellites, with both Cs and Rb clocks.

5.3.2 GLONASS

Time–series: Satellite clock data

In figure 5.13, the pre-processed satellite clock data, as well as the detrended data, for a single GLONASS satellite clock (GN 746 M Cs), are plotted against time, during the time

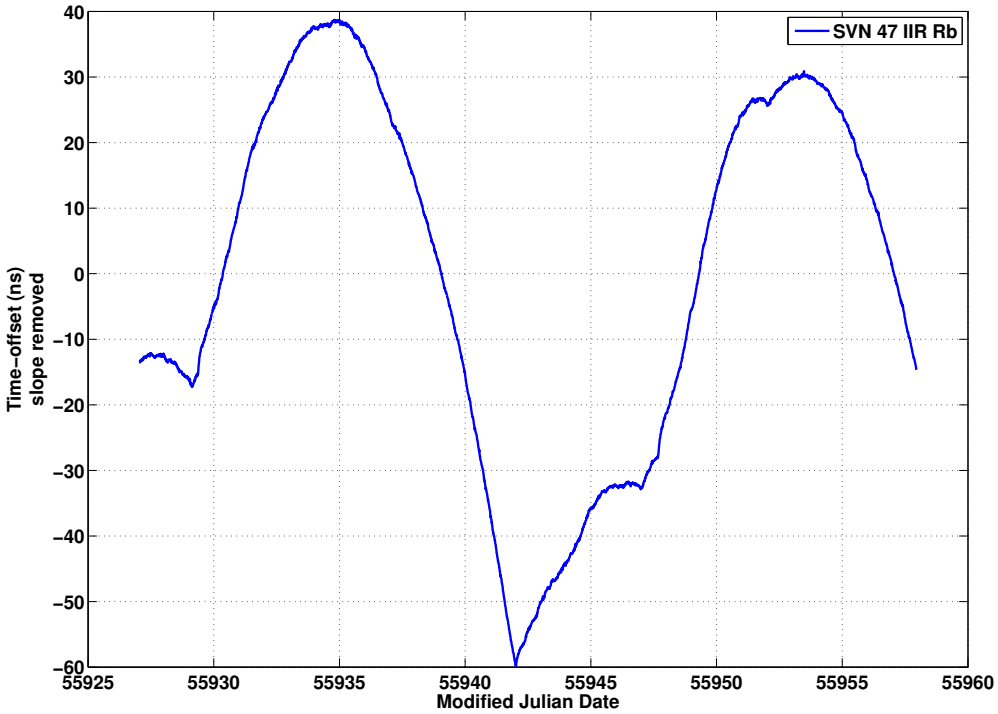

Figure 5.10: Evidence of frequency steps

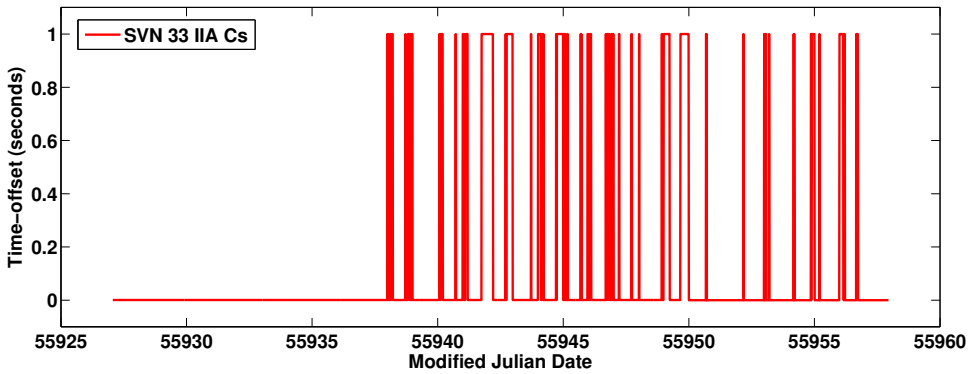

Figure 5.11: Missing data IIA Cs

period January 2012. In terms of hardware specifications, this satellite (and its onboard clocks) is representative of the entire GLONASS system. As in the GPS case, at the microseconds level, over the course of one month, the frequency offset of the GLONASS satellite clocks is purely deterministic. As with the GPS case, at the nanoseconds level, this is not the case.

Due to the way in which the ESA GLONASS SCTO estimates are produced, there are discontinuities in the SCTO estimates across day–boundaries, which are clearly seen in figure 5.13 on the bottom plot.

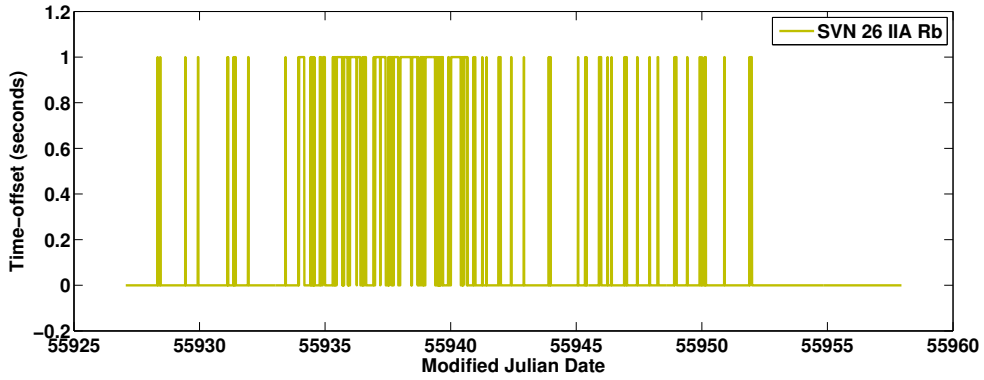

Figure 5.12: Missing data IIA Rb

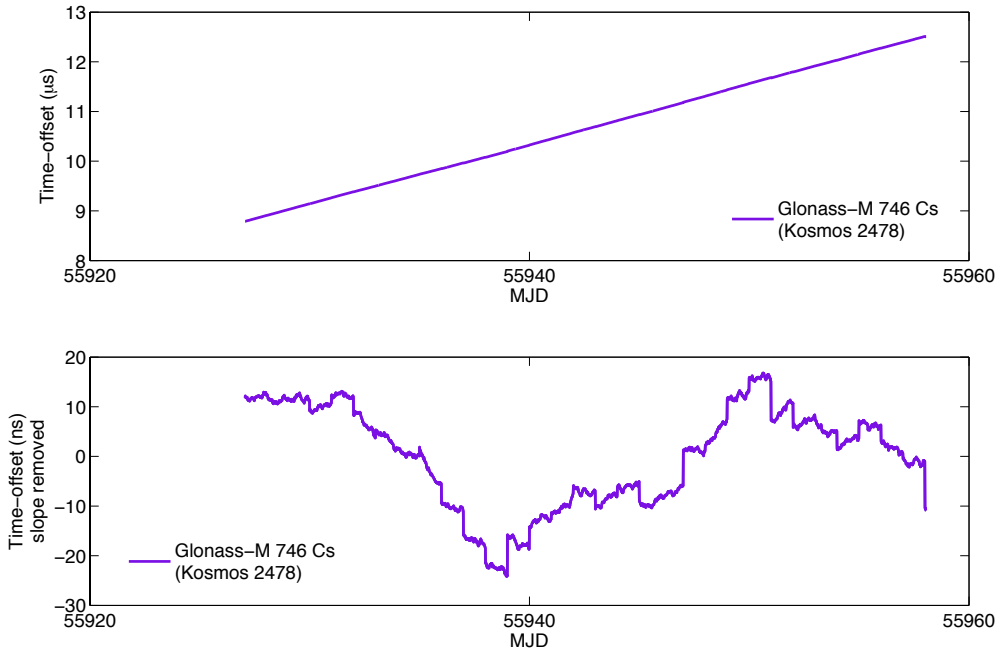

Figure 5.13: Time-series plot of the time-offset with respect to GPS system time, T_g, as realised by ESA, during January 2012 for the Cs clock onboard GLONASS 746.

Frequency stability analysis

In figure 5.14, sigma–tau curves, based on Allan deviation calculations over a range of averaging intervals, using data from twenty–three GLONASS satellite clock from January 2012, are plotted on the same set of axes to allow for direct and easy comparison. More or less, the slopes on each of these sigma—tau curves are the same at $-\frac{1}{2}$ across all averaging intervals. This implies that the underlying noise processes affecting the GLONASS satellite clock measurements is WFM noise.

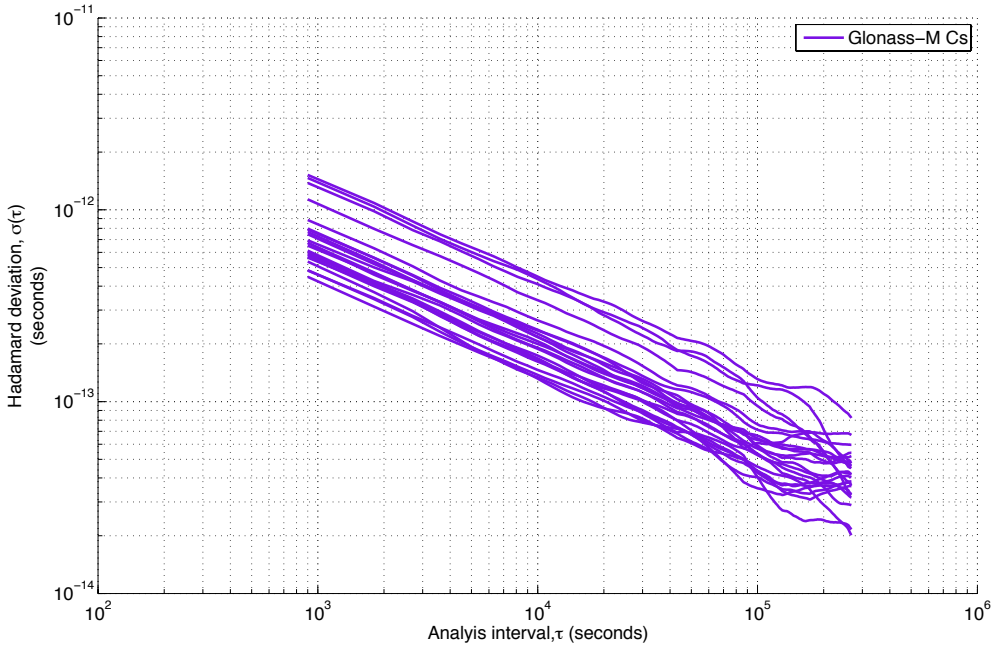

Figure 5.14: Sigma–tau (ADev–based) curves representing the frequency stability of the GLONASS satellite clocks during January 2012. Each curve represents the Allan deviation of a single GLONASS satellite clock over a range of averaging intervals from 900 s to $\approx$ 270,000 s. The data in this analysis is the ESA Final satellite clock solution for GLONASS.

These results from the frequency stability analysis of the GLONASS satellite clocks, as presented in figure 5.14, are particularly interesting when they are compared against the results of the analysis of the GPS satellite clocks, and specifically the results shown in figure 5.3. There is clear evidence of periodic signals in the GPS satellite clocks, but there is no such evidence in the GLONASS case.

Sigma–tau curves based on ADev, HDev and MDev for the clock onboard GLONASS-M are plotted on the same set of axes in figure 5.15 to enable a comparison between them. According to the MDev curve, at averaging intervals below 10,000 seconds, a slope of -1 indicates FPM noise, and at averaging intervals between 10,000 seconds and 100,000 seconds, a slope of $-\frac{1}{2}$ indicates WFM noise. At averaging intervals below 100,000 seconds, both the ADev and HDev curve indicate the dominance of WFM noise. At averaging intervals, between 100,000 s and 270,000 s, the slope on the sigma–tau curves is are almost flat suggesting that FFM noise dominates the GLONASS–M 746 clock signal in this region.

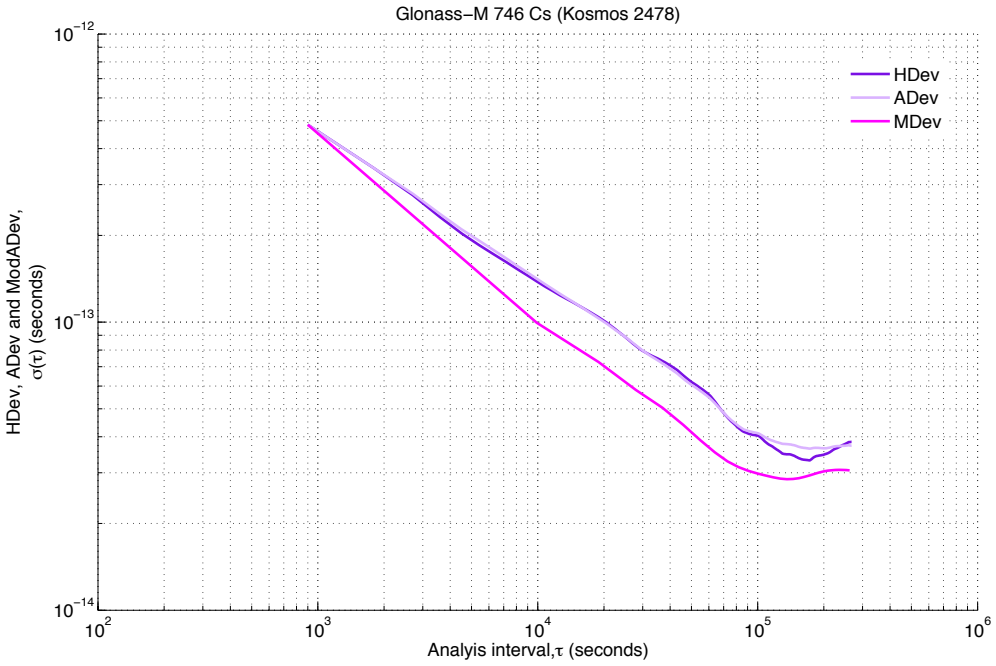

Figure 5.15: Sigma–tau curves based on ADev, HDev and MDev for GLONASS–M 746 (January 2012).

Summary statistics

Summary statistics ($\times 10^{-13}$ seconds)	For GLONASS based on ADev values at different averaging intervals (hours)				
	0.25	3	6	12	24
Mean	7.67	2.18	1.52	1.05	0.722
Median	24.4	4.46	3.01	1.62	1.54
Maximum	15.2	4.35	3.18	2.15	1.50
Minimum	4.47	1.26	0.910	0.650	0.418
Std. Deviation	3.11	0.894	0.626	0.411	0.289

Table 5.5: Summary of HDev analysis on GPS satellite clocks.

5.4 Findings

The main findings on the characterisation study are listed in this section. These are:

- At the microseconds level, the behaviours of GPS and GLONASS satellite clocks are deterministic (and thus predictable) at time periods of up to one month. At the nanoseconds level, the effect of underlying stochastic processes on the behaviours of both GPS and GLONASS satellite clocks becomes observable and significant.

- Linear frequency drift (LFD) is observable in all GPS Rb clocks. In most cases, especially in the Rb clocks onboard the newer IIR/IIR-M and IIF satellites, the LFD is stable. However, is some case the LFD varies significantly over time. In the GPS Cs clocks, and all GLONASS clocks, there is no evidence of LFD.

- There is clear evidence of periodic signals in many GPS satellite clocks. These periodic signals are present in some clocks more than others. But there is no appreciable link between these periodic signals and satellite clock type (Rb or Cs) or satellite clock age (i.e. Block). Also, there is some evidence to suggest that the period and amplitude of these periodic signal are stable over a time period of several months. In the GLONASS case, there is no evidence of any periodic signals, in any of the GLONASS clocks.

- For GPS, in a frequency stability sense, across all averaging intervals in the range 900–86400 s, the newer clocks outperform the older clocks. The newer generation of GPS satellite clocks are more predictable than the older generation clocks. At averaging intervals less than 3000 seconds, the IIF Rb clocks are better than the all other GPS clocks by an order of magnitude or more. At averaging intervals between 3000 seconds and 86400 seconds, the performance of the best IIR/IIR-M Rb clocks are comparable. At all averaging intervals, the IIA Cs clocks are about one order of magnitude less stable than the average GPS Rb clock.

- At analysis intervals below 4000 seconds, the dominant noise process in the IIR/IIR-M GPS satellite clocks is WFM noise; in the IIA and IIF clocks, either WPM noise or FPM noise, or some combination of both is dominant. At analysis intervals above 4000 seconds, there is some evidence of FFM noise in the GPS clocks. At all averaging intervals, in the range 900–86400 s, the GLONASS clocks are dominated by WFM noise, but at averaging intervals intervals over one day there is evidence of the presence FFM noise in GLONASS clock signals.

- Comparing the GPS and GLONASS satellite clocks in a frequency stability sense, the typical GPS clock is about 3–4 times more stable than the typical GLONASS clock, at all averaging intervals, see tables 5.3 and 5.4 for GPS, and table 5.5 for GLONASS.

Summary

In this chapter, we presented a discussion of the characteristics of the GNSS satellite clocks based around a review of the existing literature, as well as a detailed analysis of the GPS and GLONASS satellite clock estimates generated by the IGS—for GPS, and ESA—for GLONASS. A detailed analysis, and discussion of the in-orbit properties of GLONASS satellite clocks, based on GNSS based clock parameter estimates, is not currently found in the literature.

There are several characteristics of GNSS clocks in-orbit, which have come out of the literature and our own analysis, that are relevant for modelling, and ultimately clock

predictions based on the modelling. The GNSS clock characteristics are clock-specific, in terms of deterministic and stochastic properties both. For example, the magnitude and time-evolution of clock time-offset and frequency offset, relative to a reference timescale, are unique in all clocks. This is also true of the stochastic variations in the GNSS clocks, although to some extent, clocks belonging to the same category show similar clock noise properties, in terms of noise type and also noise magnitude.

Chapter 6

Satellite clock prediction schemes

Chapter outline

This chapter presents a performance analysis study of existing GNSS satellite clock prediction strategies, using the IGS predictions of the GPS satellite clocks as a representative case. The chapter starts with a definition of satellite clock time offset (SCTO) prediction error, which must be established, before it is possible to proceed with a quantitative analysis of any given satellite clock prediction scheme. This is followed by a definition of clock difference prediction error (CDPE); in terms of positioning applications of GNSS, it is the CDPE quantity, rather than the SCTO quantity that provides the more meaningful measure of the performance of a prediction method. In the second half of this chapter, the performance of the satellite clock prediction scheme of the IGS is analysed. The IGS predictions of the satellite clocks are used as a benchmark prediction scheme against which the performance of a new prediction method, presented in Chapter 8, is assessed.

6.1 Satellite clock time offset (SCTO) prediction error in GNSS

Here, the general approach for measuring the performance of a chosen satellite clock prediction scheme is based upon the statistical analysis of clock prediction error (CPE). Therefore, it is necessary to define carefully, what clock prediction error means.

6.1.1 Defining clock prediction error (CPE)

First, this requires that either a timescale or an individual clock to represent *true* time is defined; this is the reference timescale, T_R. Then, a data–set of clock correction values of sufficient quality, in terms of precision and accuracy, is required to represent *true* clock behaviour. Then, it is possible to define clock prediction error (CPE) as

$$E_{R,i,p,n} = (T_R - C_i)_n - (T_P - C_{i,p})_n \tag{6.1}$$

where T_R is the reference timescale, C_i is the time according to clock i at time n, $(T_P -$

$C_i)_{p,n}$ is the predicted value of the correction for clock i at time n. The difference between the true behaviour of the clock as represented by $(T_R - C_i)_n$ and $(T_P - C_i)_{p,n}$, the predicted correction is the prediction error for clock i with respect to T_R at an epoch labelled by the integer n, denoted $E_{R,i,p,n}$[1].

In equation 6.1, C_i and $C_{i,p}$ are quantities that represent time according to the same clock, labelled i. The distinction between then is that the former is an estimated quantity based on observations of clock behaviour up to and including the time during which the estimate is made, the latter is a predicted quantity—an extrapolation based on observations of past clock behaviour only. T_R and T_P are reference timescales, where T_P is a predicted reference timescale (or predicted reference clock). Their role is to enable synchronisation across all aspects of the GNSS data processing chain, and they also provide a common reference, simplifying the means by which comparisons between the clocks are made. Thus, the choice of reference timescale in itself, being common to all clocks, should have no effect on positioning performance. This is because in positioning algorithms that use GNSS measurements, the receiver clock time offset (RCTO) parameter, which is estimated or eliminated by differencing depending upon the positioning method absorbs errors that are common across all measurements used in the positioning solution, e.g. due to choice of reference timescale for representing SCTO values. And so, in positioning terms it is instead the variability of the clocks among themselves, that is the nature and the extent of the mis-synchronisation amongst the satellite clocks, that ultimately influences the quality of the end-user solution. In other words, as far as the impact of satellite clock estimation/prediction errors on positioning is concerned, the critical quantity is the differences between satellite clock pairs. The predictability of the clock differences is the ultimate metric of satellite clock performance, in positioning terms.

6.1.2 Defining clock difference prediction error (CDPE)

Therefore, at this stage, it is also necessary to define clock difference prediction error. Clock difference prediction error, $E_{ij,p,n}$, is defined as

$$E_{ij,p,n} = (C_i - C_j)_{R,n} - (C_i - C_j)_{p,n} \tag{6.2}$$

where $E_{ij,p,n}$ is the error in the prediction of clock difference for clock j with respect to clock i as reference at epoch n, $(C_i - C_j)_{p,n}$ is the predicted clock difference and $(C_i - C_j)_{R,n}$ is the clock difference derived from clock estimates based on observations.

6.1.3 Clock difference prediction error and positioning

As established in the previous section, the difference between pairs of satellite clocks—the clock differences—are the purest metric of the performance of the GNSS satellite clocks (in the context of PNT applications), not the time-offset of the individual satellite clocks with

[1] N.B. In precise time and frequency metrology, in comparing measurements (of phase or frequency) from two different clocks, it is a convention to subtract the readings of the clock being studied from the readings of the reference clock or timescale. This convention is adopted here also.

respect to a common reference timescale. How then, does clock difference prediction error, impact upon PNT error? Here, this is explored by considering a simple point positioning scenario.

Suppose at prediction length twelve hours, the typical clock difference prediction error between a pair of satellite clocks is 1 ns. Assume both clocks are comparable in performance terms, and assign each an equal contribution to prediction error, then multiplying the difference prediction error by $\frac{1}{\sqrt{2}}$, gives about 0.7 ns for each clocks. Considering this in terms of the contribution of clock difference prediction error to the User Equivalent Range Error (UERE), this is $3 \times 10^8 \times 7 \times 10^{-10} = 0.21$ cm, roughly. Say, the position dilution of precision (DOP) at the user's location is 3.0, a typical value, the we might expect an RMS error in each component of the calculated position, of about $3.0 \times 0.21 \approx 0.6$ m.

In a similar way, in Table 6.1, the expected error in each component of the calculated position of the typical GPS satellite clock (IIR/IIR–M Rb) is calculated at various prediction lengths. The clock prediction error values used in this table are based on the results of the frequency stability analysis, which are presented in Chapter 5. This simple analysis assumes that the dominant noise processes influencing the GPS SCTO signals are white (i.e. WPM or WFM) and also that that periodic signals don't exist. Both of these are not strictly true, however, in terms of the order–of–magnitude type argument being made here, these assumptions are acceptable.

Prediction length (hours)	CPE (ns)	UERE (m)	User Position Uncertainty (m)
0.25	0.288	0.086	0.260
3	0.960	0.288	0.863
6	1.75	0.526	1.57
12	1.27	0.384	1.15
24	2.05	0.61	1.84

Table 6.1: A quick–look study of the link between SCTO prediction length, CPE (or clock difference prediction error) and uncertainty in the user's computed position solution. This method of analysing the link between UERE and User Position Uncertainty using DOP values in this way is presented in Chapter 6 of Misra & Enge [2011].

So then, how good would the GPS satellite clock need to be, in terms of clock difference prediction errors, in order to meet the requirements of centimetre–level positioning? Consider the case where clock difference prediction error values were an order of magnitude less, i.e. about 0.1 ns at prediction length twelve hours. Then, by the same process introduced earlier, in this case, the expected contribution of clock prediction error to RMS error in each calculated position component would be around 6 cm. And so, for satellite clock predictions to be good enough for centimetre–level would require clock predictability at the ten of picoseconds level, around 100 picoseconds at most. Clock difference prediction errors above the nanoseconds level deny the possibility of centimetre–level positioning. But, the quality of in-orbit GPS clocks continues to improve, see chapter 5, and clocks matching, and exceeding the required level of performance have been demonstrated in the laboratory, see Chou *et al.* [2010].

6.1.4 Satellite clock predictions and the IGS

The IGS produces and disseminates a variety of satellite clock correction products, see Dow *et al.* [2009]. These products are weighted combinations of the clock solutions generated by participating analysis centres, see Kouba [2003]. Among these clock products, are the IGS ultra-rapid (IGU) products, which consist of predictions of individual satellite clocks.

The IGS ultra-rapid combinations are released four times each day at 0300, 0900, 1500 and 2100 UTC, with each file containing 48 hours of clock data; the first 24 hours is computed from observations and the second 24 hours is predicted. The 0300 IGU is referred to in this paper as the 0hr prediction file and consists of an observed component, IGU–O, from 0000 to 2345 for the previous day and a predicted component, IGU–P, from 0000 to 2345 of the current day.

In this chapter, a detailed performance analysis is presented of the IGS predictions of individual GPS satellite clocks as well as GPS satellite clock differences. The IGS predictions of the satellite clocks are widely used, and for the purposes of this discussion, the IGS predictions are classified as belonging to the high–latency, navigation message type predictions as described in Section 2.2.5. This is because the maximum prediction length provided in the IGS ultra-rapid product is twenty-four hours, and in the way that the IGS predictions are delivered, they are used at prediction lengths ranging from 3 to 9 hours.

There are other clock prediction schemes; most importantly to the average user (e.g. a mass–market portable navigation device user), those of the GNSS operational control segments of GPS, GLONASS, Beidou and soon Galileo also, but also predictions provided by several cooperating GNSS analysis centres, see figure 6.1. However, in assessing the performance of the GNSS satellite clock prediction scheme developed here, which is presented in Chapter 8, the predictions of the IGS are used as a benchmark.

6.2 The scope of the prediction scheme performance study

Parameters of study	Values
Systems considered	GPS only
Predicted quantities	SCTO; and SCTO differences between satellite clock pairs
References	IGRT; and SVN 50 IIR–M Rb
Timeframe of analysis	2012 (01 Jan – 31 Dec)
Time–resolution of analysis	15–1440 minutes (24 hours)
Data format	SP3 (15–minute sampling rate)
Data sources	IGR (as truth) and IGU (0hrs only)

Table 6.2: Scope of the GPS satellite clock prediction scheme performance analysis study. In particular, this study looks at the prediction scheme that is operated by the IGS.

The IGS predictions of the GPS satellite clocks in the IGS ultra-rapid SP3 product provide a heavily–used navigation message type, high–latency (HL) clock prediction product from

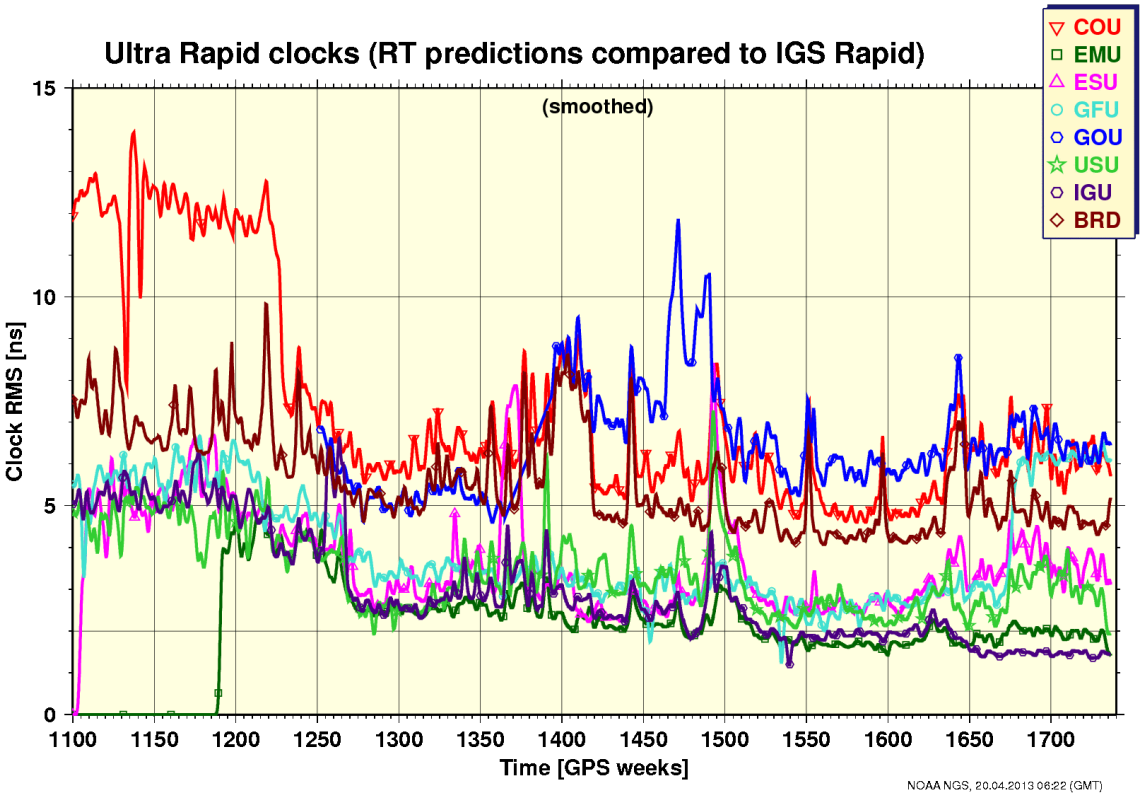

Figure 6.1: The curves show the RMS differences (ns) between individual analysis centre ultra-rapid clock predictions against the IGS rapid clock products. According to the IGS analysis centre coordinator, at http://acc.igs.org, *"the comparisons are performed on the first 6 hours (first 12 hours until week 1267) of the prediction (the second half of each IGU file), which is intended for real-time applications"*. This analysis is regularly updated, and published at http://acc.igs.org/media/Gmt_sum_ultcmp_all_clk_smooth_ALL.gif

.

a well-respected source. In this Chapter, the results of a detailed performance analysis of this IGS prediction scheme of the GPS satellite clocks are presented.

In Table 6.2, the key parameters of the prediction scheme performance analysis study are listed. Only the GPS system is considered. Currently, the IGS does not predict the GLONASS clocks. Although pre-processed data sets were prepared for each of the four—0–hr, 6–hr, 12–hr and 18–hr—IGU–P sets, only the 0–hr set is used in the analysis presented here. In terms of range of prediction lengths considered then, this is a minimum prediction length of fifteen minutes and a maximum prediction length of twenty–four hours. Of course by design, due to method by which the IGU–P are delivered, it is prediction lengths in the range three to nine hours that represent the true design performance of the IGS predictions. However, other similar prediction schemes: GPS broadcast—24 hours– and GLONASS broadcast—12 hours—are designed for use at prediction lengths up to twenty four hours. Therefore, the performance of the IGS predictions at the maximum prediction length given in the IGU-P files of twenty-four hours remains of interest.

6.3 Method

The aim of the work presented in this chapter is to quantify the performance of current GPS satellite clock prediction schemes, and to identify the factors that might be limiting their performance. For this purpose, a method was developed, which involved these steps:

1. **Data pre–processing (1),** where the satellite clock information in the IGS rapid SP3 files is fetched (from the Internet), extracted, separated (by GPS PRN) and concatenated, in the same way as the IGS SP3 final SP3 files are in step 1 of the method (Section 5.2) of the characterisation study. This process creates a time–series of IGS rapid (IGR) GPS satellite clock information. In this study, this IGS rapid clock data represents true clock behaviour.

2. There is an additional **data pre–processing (2)** step here, in which the predicted part of IGS ultra–rapid SP3 files, the IGU–P, must be extracted from the IGS ultra–rapid (IGU) files. This is necessary because the IGU product is a combination of an observed part, IGU-O, followed by the IGU-P. Each IGU file holds 48 hours of data, the first 24 hours are IGU–O, the second 24 hours are IGU–P. After the IGU-P are extracted, in the same way as in step 1, a time series of IGS predicted satellite clock data is created. Here, the aim is to study these predictions in detail. With these pre-processed sets of IGS rapid GPS satellite clock estimates and IGS ultra-rapid GPS satellite clock predictions, it is possible then to start investigating the performance of the IGS prediction scheme.

3. The **computation of individual clock prediction errors (CPE),** according to definition given in Equation 6.1. For the IGS case, this is

$$E_{igr,i,p,n} = (T_{igr} - C_i)_n - (T_{igu} - C_{i,p})_n \tag{6.3}$$

   where $E_{igr,i,p,n}$ is the prediction error, T_{igr} is the IGS rapid timescale and T_{igu} is an IGS ultra-rapid timescale.

4. The **computation of clock difference prediction errors (CDPE)**, according to the definition given in Equation 6.2. Here, this is

$$E_{ij,p,n} = (C_i - C_j)_{igr,n} - (C_i - C_j)_{p,n} \tag{6.4}$$

   where $(C_i - C_j)_{igr,n}$ is the difference between clock i and clock j, according to the IGS rapid data product, and all other terms are as defined in Equation 6.2. In principle, a complete analysis of the property of IGS GPS CDPEs should consider all possible clock difference combinations, but this would require the investigation of $31 + 30 + ... + 2 + 1 = 496$ combinations. In practise, such a study would be very difficult to implement, and for the main purpose of this study would be unnecessary. Instead, the approach taken is to choose a single GPS satellite clock as the reference clock, and to study the properties of GPS CDPEs with that clock as the reference. Thus, this approach requires the selection of an appropriate reference clock. The

reference clock should be one of the better clocks in the constellation, in terms of frequency stability. Also, the reference clock should be free, as much as possible, from data quality issues (gaps, discontinuities etc.). This is to ensure that a complete set of CDPEs can be computed[1]. Here, each computed CDPE value has an associated prediction length value, τ.

5. **Prediction length analyses,** in which the average bias and the average RMS of the GPS CDPE with respect to a chosen reference satellite clock are examined. Here, prediction lengths in the range fifteen minutes to twenty–four hours are considered. The averages are computed over the whole of 2012 using the CDPEs computed in Step 3. The average bias, b_{ij}, CDPE value for satellite clock, j, with satellite clock i as reference, at a prediction length τ, is calculated according to

$$b_{ij}(\tau) = \frac{1}{d}\sum_{k=1}^{d} E_{ij,p}(\tau) \tag{6.5}$$

where d is the total number of days for which there is a CDPE value for satellite j at prediction length τ. The average RMS CDPE value, $E_{rms,j}$, for satellite clock j, with satellite clock i as reference, at prediction length τ, is calculated according to

$$E_{rms,ij}(\tau) = \sqrt{\frac{1}{d}\sum_{k=1}^{d} E^2_{ij,p}(\tau)} \tag{6.6}$$

6.4 Results

6.4.1 Time–series: IGS GPS CPE

Figure 6.2 shows the time-series of the $E_{igr,i,p,n}$ quantities over the whole year 2012, for a chosen representative selection of the GPS satellite clocks. Looking at the four plots, it is immediately apparent that there is a common signal under each curve, this must be the influence of $T_{igr} - T_{igu}$, which is common to each. Here, the $T_{igr} - T_{igu}$ signal is biased, in the sense that, in all four cases for most of the time period considered in the analysis, the $E_{igr,i,p,n}$ quantity is negative. Also, looking at figure 6.2, it is clear the GPS CPEs are noisier in the older Block IIA Rb and Cs clocks than in the newer Block IIR and IIF Rb clocks. This is unsurprising, especially in light of the results of the GPS satellite clock characterisation study in Chapter 5.

6.4.2 The contribution of $T_{igr} - T_{igu}$ to $E_{igr,i,p,n}$

In equation 6.3, which is a special case of equation 6.1 the clock prediction error (CPE) quantity is dominated by the $T_{igr} - T_{igu}$ timescale offset signal. This is because, as

[1]Here, an alternative and more robust approach would use an ensemble average timescale based on data from all available GPS satellite clocks. In comparison to this approach, the current method less robust because the results are influenced by the behaviour of the reference clock, which can introduce biases into the analysis with all difference involving a single satellite clock being to some extent correlated. However, the implementation of an ensemble average timescale is a non–trivial exercise. Still, the development of this alternative approach is an interesting option for future work.

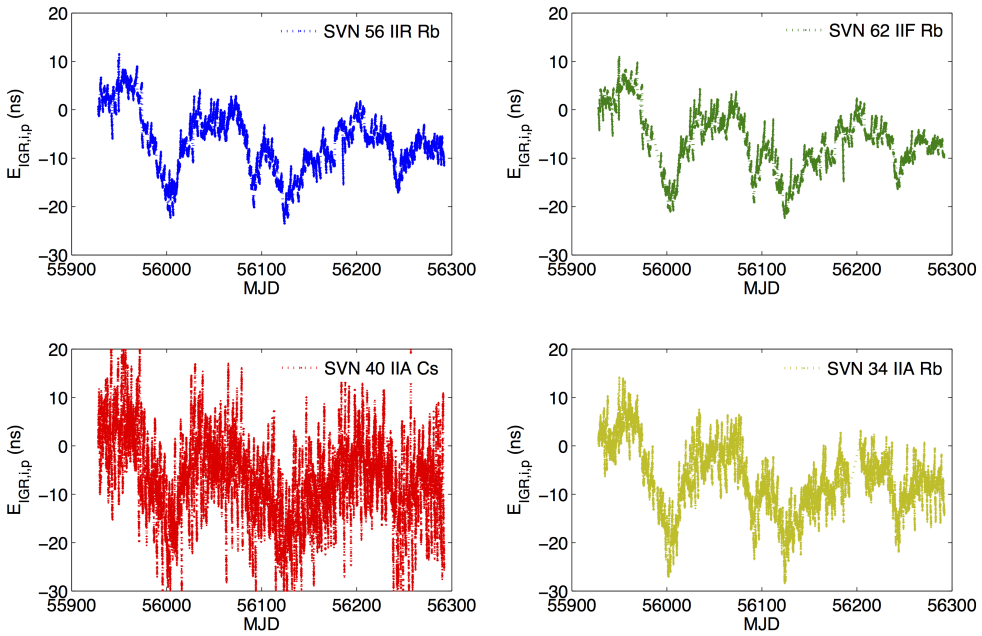

Figure 6.2: These are curves of $E_{igs,i,p}$, over the whole of 2012, for a chosen selection of GPS clocks. All curves are clearly dominated by a common underlying signal. This is the influence of the timescale offset between IGS rapid time, which closely approximates IGS system time, and IGS ultra-rapid timescales, which can be described as real-time realisation of GPS Time.

described in Senior *et al.* [2003], IGS Time is an integrated ensemble frequency scale, generated independently of GPS Time but steered to GPS Time over the long term. On the other hand, the underlying timescale of IGS ultra-rapid SCTO values GPS Time, to a good approximation. The data processing step that transforms the SCTOs from having GPS Time as reference to IGS Time as reference is not performed on the IGS ultra-rapid data set.

The effects of the $T_{igr} - T_{igu}$ timescale offset are seen in figure 6.2, where each of the curves are clearly dominated by a common underlying signal. The problem with this timescale offset signal being embedded with the GPS CPE time–series in this way is that it obscures the true performance of the IGS prediction system in predicting the behaviour of the individual satellite clocks. It is useful then to investigate the behaviour of the timescale offset signal which is common in all satellite clocks. There is a way to study this timescale offset using the full set of CPE time–series that is explained below.

The GPS satellite clocks are independent of each other and for the most part they are free–running (i.e. they operate independent of any interference from the operational control segment). By taking an (ensemble) average of the CPE time–series across all of the GPS satellite clocks for which there is data available (in this case up to a maximum number of 32 at any single time) and also calculating the scatter amongst them, by a simple standard deviation calculation, it is possible to get a picture of the average individual satellite clock prediction error over the entire collection of GPS satellite clocks. Mathematically, this process can be expressed as,

$$\begin{aligned}\frac{1}{n}\sum_{i=1}^{n} E_{igr,i,p,n} &= \frac{1}{n}\sum_{i=1}^{n}\left[(T_{igu}-C_i)_n-(T_{igu}-C_{i,p})_n\right] \\ &= \frac{1}{n}\sum_{i=1}^{n}[(T_{igr}-T_{igu})_n]-\cancel{\frac{1}{n}\sum_{i=1}^{n}(C_{i,p}-C_i)} \quad \varepsilon \sim \mathcal{N}(\mu,\sigma^2) \\ &= (T_{igr}-T_{igu})+\varepsilon\end{aligned} \tag{6.7}$$

where it is assumed here that the quantity $\frac{1}{n}\sum_{i=1}^{n}(C_i - C_{i,p})$ is a zero–mean Gaussian random variable. This zero–mean assumption may not strictly be true, but it is the working assumption here. The Gaussian assumption is a reasonable one to make because the individual $C_i - C_{i,p}$ quantities are independent of each other.

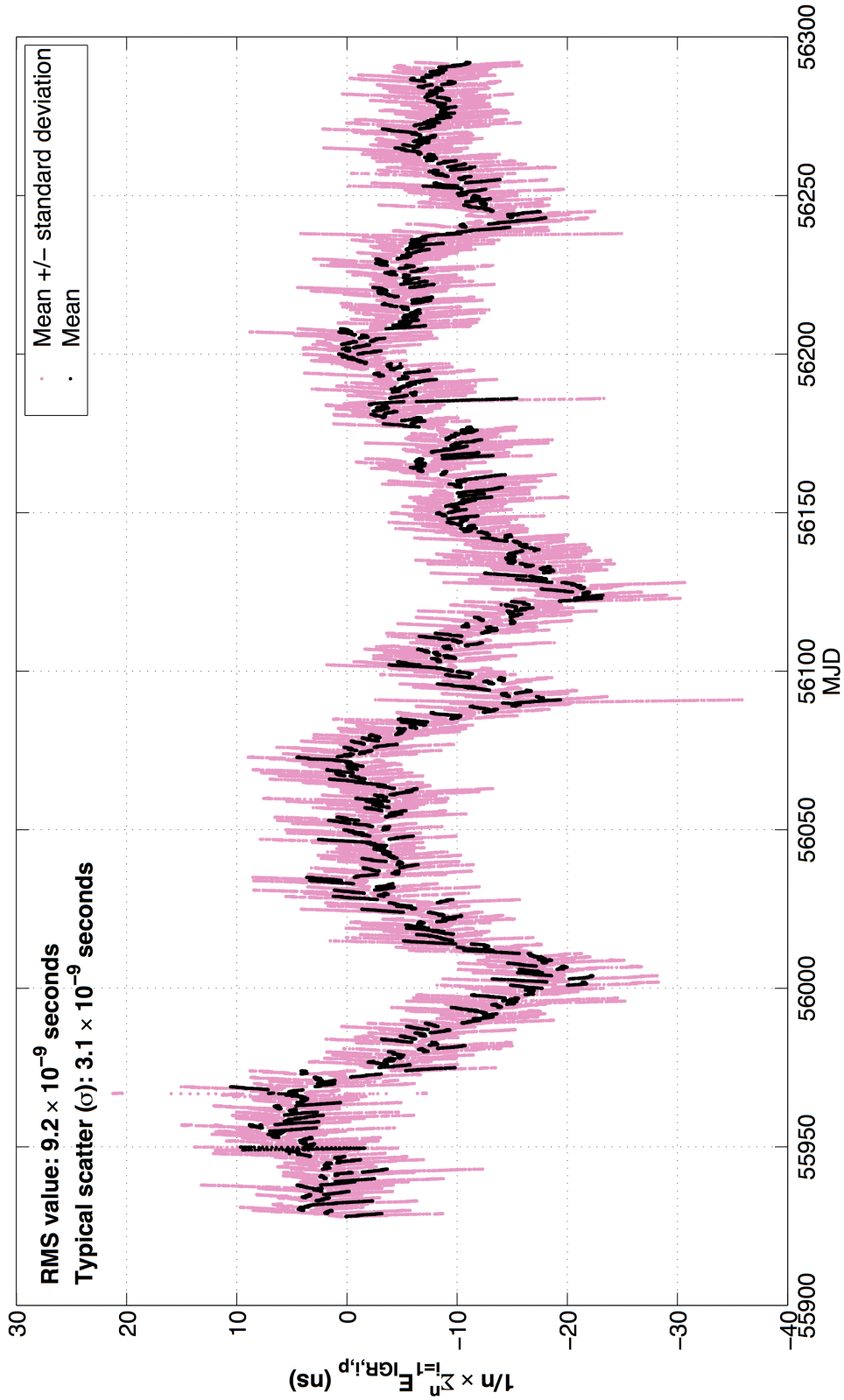

Figure 6.3: The time–series represented by the black lines is the average GPS CPE during 2012, where the average is the ensemble average taken across all of the satellite clocks for which there is data available. The pink time–series represents $\pm 1\sigma$ (standard deviation) the GPS CPE. This time–series is a representation of the $T_{igr} - T_{igu}$ timescale offset quantity over the full year 2012.

In figure 6.3, the black time–series is the average GPS satellite CPE, for the whole of 2012. Here, the average is taken across all the GPS satellite clocks for which there is data available. The pink time–series represents ±1 standard deviation from the average GPS CPE value. Here, a reasonable inference to make, is that the black time–series in 6.3 is a good representation of the offset between the IGS rapid timescale and the IGS ultra-rapid timescale. It is not systematic. It is discontinuous. It is common across all satellite clocks and can be large with a typical value of 9.2 ± 3.1 ns(1σ) over 2012.

Clearly, this timescale offset is major feature of the IGS predictions of the GPS satellite clocks, yet this feature has not been identified or studied in any of the published literature that the author is aware of. This might be because this feature does not directly influence the performance of the IGS prediction scheme in the context of PNT applications. But, it does present a challenge to the analyst who wishes to use the IGS predictions to study GPS satellite clock predictability.

Thus, the approach developed in this project (for satellite clock prediction) uses the ability to predict the difference between satellite clock pairs, i.e. the extent of the mis-synchronisation between the in–orbit clocks rather than the the ability to predict individual satellite clocks (w.r.t some reference timsecale) as the metric by which clock prediction performance is measured. In the context of predicting the behaviour of individual clocks in GNSS, the timescales are a mere convenience, a requirement for the operational side of the system, but not strictly necessary for the user requiring only a positioning solution.

6.4.3 Discontinuities at the boundary between consecutive prediction sets

For all GPS satellite clocks, there are discontinuities in the CPE time–series at the boundary between two consecutive IGS prediction sets. This can be seen in figure 6.4. Clearly, the timescale offset feature of the IGS predictions is a major source of the discontinuities in CPE time–series. But, another important contributing factor is the re–initialisation of the individual satellite clock parameters at the start of each new prediction run. Thus, it is important that the satellite clock estimator is producing accurate, unbiased estimates of the individual satellite clock parameters. The quality of predictions are highly sensitive to the quality of the initial estimates at the start of the prediction run.

In figure 6.2, the influence of the common $T_{igr} - T_{igu}$ timescale offset signal is obvious within all of the CPE time–series (looking at full year's data set). In 6.4, where a shorter time span of only three days is plotted, this common signal is not obvious in a similar way. This is evidence suggesting that the re–initialisation of the clock parameters at the start of each new prediction run contributes significantly to clock prediction error.

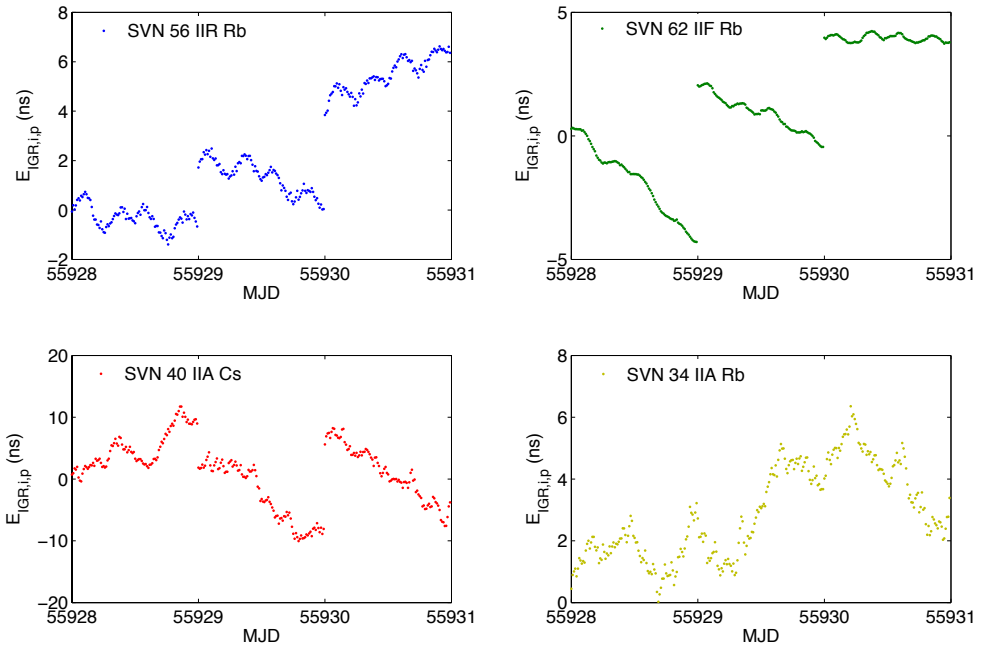

Figure 6.4: These are curves of $E_{igs,i,p}$, over three days in 2012, for a chosen selection of GPS clocks. Here, there are clear discontinuities in the CPE time–series at the boundary between two consecutive IGS prediction files in three of the four cases. Here, the exception is the SVN 34 IIA Rb clock.

6.4.4 Choosing a reference clock for CDPE computation

In this section, the processes that were undertaken to determine the reference GPS satellite clock for the clock difference prediction error analysis are explained. Here, the main requirement in the search for a suitable reference clock was to find the most stable satellite clock with a complete data set, and with no phase or frequency jumps during 2012.

At first, the full set of GPS satellite clocks were considered. This was done by looking at the detrended time-series of the GPS IGS final satellite clock data, for the entirety of 2012, as shown in figure 6.5. In this figure, the y-axes correspond to time-offset from IGS Time, but for the purpose of why these curves are present here, the magnitude on the y-axis is not relevant.

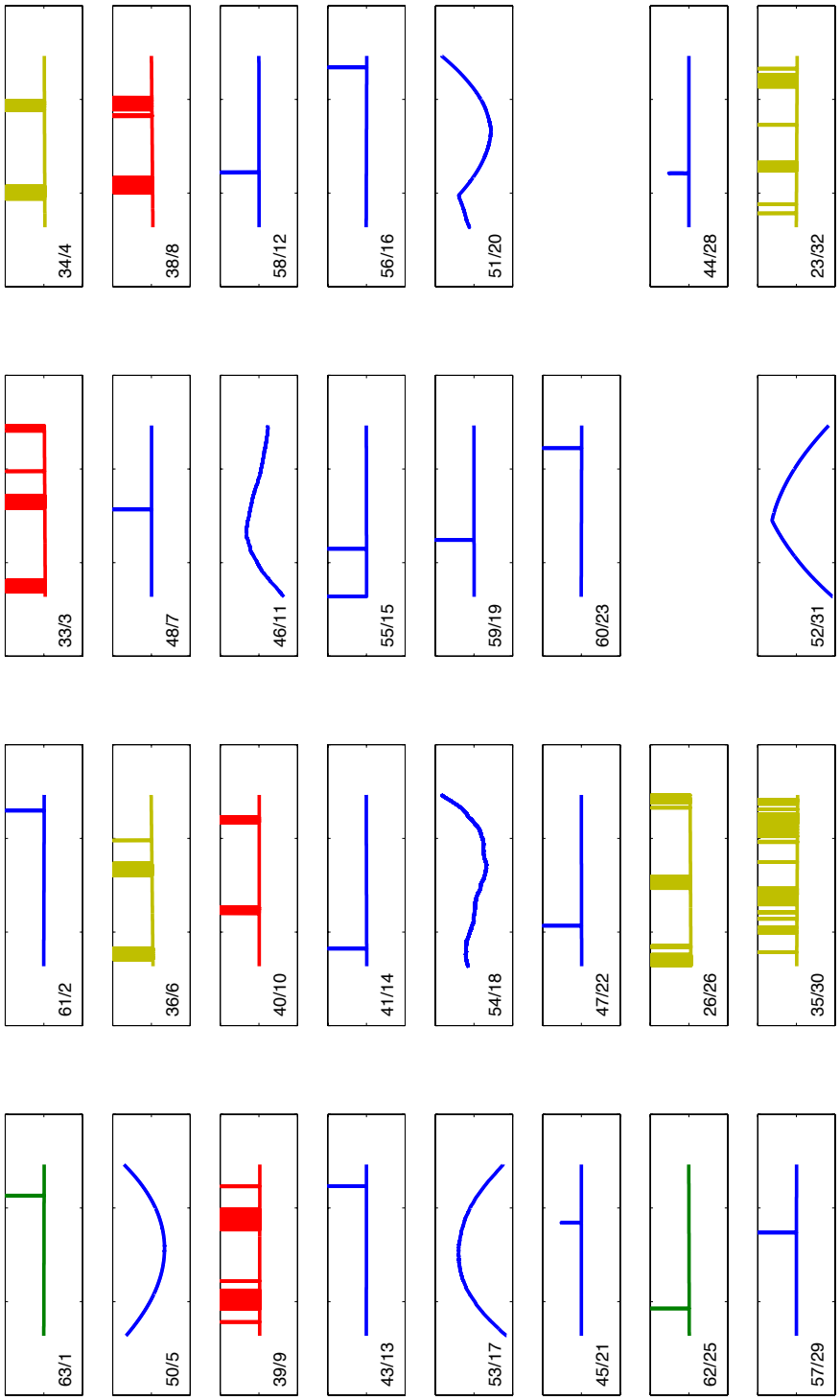

Figure 6.5: Detrended SCTO time–series for all GPS satellite clocks in 2012. Having considered the full set of clocks, the SVN 50 IIR Rb clock (left column, second from top) was chosen as the reference clock for the clock difference prediction error analysis study. KEY: Each subplot labelled with SVN/PRN information.

Looking at all the satellite clocks in this way, the GPS Block IIA Cs and Block IIA Rb clocks, of which there were nine in total, were quickly dismissed. First, in frequency stability terms, these clocks are generally much worse than the GPS Block IIR/IIR-M or the Block IIF satellite clocks. But also, as seen in figure 6.5, the data availability for these satellite clocks during 2012 is patchy[1]. Therefore, these were excluded. Beyond these, for most satellite clocks there was an almost complete set of data: 13 have one spike, 1 has 2 spikes, and here the spikes indicate missing data. There are abrupt frequency changes in data sets for two clocks: SVN 52 and SVN 51. Thus, these were excluded also.

The remaining clocks on SVN 43, SVN 50, SVN 53 and SVN 46, all IIR Rb clocks, were all suitable reference clocks. Of these clocks, the frequency stability of the SVN 50 and SVN 52 IIR Rb clocks were the best. Ultimately, the SVN 50 IIR Rb clock was chosen as the reference clock for the clock difference prediction error analysis study.

6.4.5 Prediction length analysis: GPS CDPE Biases

In figure 6.6, the GPS CDPE average bias values for twenty–nine GPS satellite clocks are plotted, at a variety of prediction lengths ranging from 15 minutes to one day ahead. In this case, the GPS SVN 50 IIR-M Rb is the reference clock. The average is taken across the whole of 2012. The average bias values are computed according to Equation 6.5 as defined in Section 6.3.

Clearly, in this time period, the IGS predictions of the GPS CDPE (with the GPS SVN 50 IIR–M Rb clock as reference) are biased. To begin with, at the shorter prediction lengths, at the 15 minutes end, the average CDPE appear unbiased, and the CDPEs are centred on zero. As the prediction length increases the CDPEs begin to show a definite bias. With the exception of the SVN 26 IIA Rb (see Table 6.3), for all the clocks represented in figure 6.6, the average CDPE biases are negative. This is an indication that the models of GPS satellite clock behaviour in the IGS GPS satellite clock prediction algorithms might not be fully accounting for, if at all, the significant frequency drifts that are observed in some of the GPS satellite clocks. The most revealing feature in figure 6.6 is the negative biases seen the GPS IIA Cs clocks. Recall from Chapter 5 that there was no real evidence to suggest the presence of linear frequency drift in the GPS Cs clocks. Thus, the implication of the negative bias of the GPS IIA Cs clocks (with SVN 50 IIR Rb as reference) is that the linear frequency drift of the GPS SVN 50 IIR Rb is not correctly accounted for in the IGS models for that clock. Here, it appears that there is a significant and positive frequency drift in the GPS SVN 50 IIR Rb clock; this is confirmed in figure 6.5 (see row 1 column 1) where the clear upward–facing parabolic shape indicates a positive frequency drift.

In figure 6.6, cyclic patterns are clearly observable in some of the IGS predictions of the GPS satellite clock differences. This is an indication that the modelling strategy used in the IGS prediction method does not fully account for the periodic signals in the GPS

[1]When enough IGS analysis centres are unable to produce clock solutions for a given satellite clock, then the IGS combination for that clock will not exist. This can occur because the satellite clock is not actively broadcasting a signal and/or because the spacecraft is performing an orbital manoeuvre, because the spacecraft is in eclipse, or because of unusual level of ionospheric activity [Senior *et al.*, 2008].

satellite clocks.

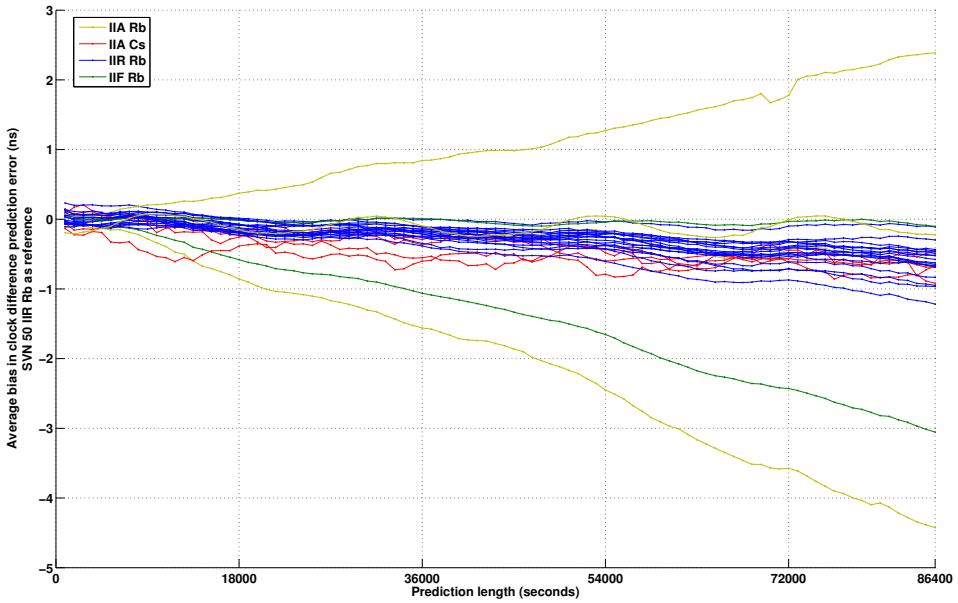

Figure 6.6: The (ensemble) average bias of the IGS GPS satellite clock difference predictions with the SVN 50 IIR Rb as reference clock, for a range of prediction lengths from fifteen minutes to twenty-four hours. Here, the IGS rapid clock differences represent truth. The average calculation uses data across the whole of 2012.

6.4.6 Summary statistics: GPS CDPE Biases

This section presents summary statistics that give an indication of the performance of the IGS prediction system in predicting the difference between satellite clock pairs with the SVN 50 IIR Rb as reference. In table 6.5, the typical values for the CDPE biases of the IGS predictions of the GPS satellite clocks in 2012 for the different categories of GPS satellite clocks are given. Here, the GPS satellite clocks are categorised according to satellite block and satellite clock type (Rb or Cs). As an example the average values for the IIR/IIR–M row is computed using the average CDPE bias for all IIR/IIR–M Rb clocks for each of the predictions lengths: 0.25 hours, 3 hours, 6 hours, 12 hours and 24 hours. The full set of statistics used to compute these average values are given in Table 6.4 in Appendix C.

PRN(SVN)	Bias ($\times 10^{-10}$ seconds) at different prediction lengths (hours)				
	0.25	3	6	12	24
Averages					
IIR/IIR–M	0.304	−0.0363	−1.64	−2.55	−6.19
IIF	0.0993	−1.29	−3.82	−6.66	−15.8
IIA	−0.327	−1.17	−2.92	−3.78	−7.07
Cs	−0.122	−1.71	−2.60	−3.75	−5.41
Rb	0.112	−0.173	−1.97	−2.99	−7.17
All	0.109	−0.450	−2.16	−3.19	−7.13

Table 6.3: The RMS prediction error of the IGS GPS satellite clock difference prediction with the SVN 50 IIR Rb as the reference clock, for a range of predictions lengths from fifteen minutes up to twenty-four hours. The IGS rapid clock differences represent truth. The RMS calculation uses data across the whole of 2012 i.e. an average RMS over 2012.

Summary statistics ($\times 10^{-10}$ seconds)	For GPS IIR/IIR–M Rb CDPE Bias Statistics different prediction lengths (hours)				
	0.25	3	6	12	24
Mean	0.304	−0.0363	−1.64	−2.55	−6.19
Median	0.335	−0.105	−1.75	−2.49	−6.00
Maximum	2.33	1.30	−0.317	−0.347	−1.11
Minimum	−1.06	−1.10	−2.84	−4.95	−12.2
Std. Deviation	0.905	0.672	0.777	1.095	2.58

Table 6.4: Summary statistics IIR/IIR–M Rb CDPE.

6.4.7 Prediction length analysis: GPS RMS CDPE

In figure 6.7, the GPS CDPE average RMS values for twenty–nine GPS satellite clocks are plotted, at a variety of prediction lengths ranging from 15 minutes to one day ahead. In this case, the GPS SVN 50 IIR-M Rb is the reference clock. The average RMS values are computed according to Equation 6.6 as defined in Section 6.3. The average RMS CDPE values provide a value for the typical predictability of the GPS CDPEs at a range of prediction lengths.

The IGS average RMS CDPEs for the GPS IIA Cs are greater at all prediction lengths than the IIA Rb, IIR/IIR–M Rb and the IIF Rb. This is expected. Although, in a frequency stability sense, the GPS IIF Rb clocks are more stable that the GPS IIR/IIR–M Rb clocks, and thus more predictable, the reference clock in this case is a IIR–M Rb, and so the predictability of the IIF Rb clock difference are limited by this.

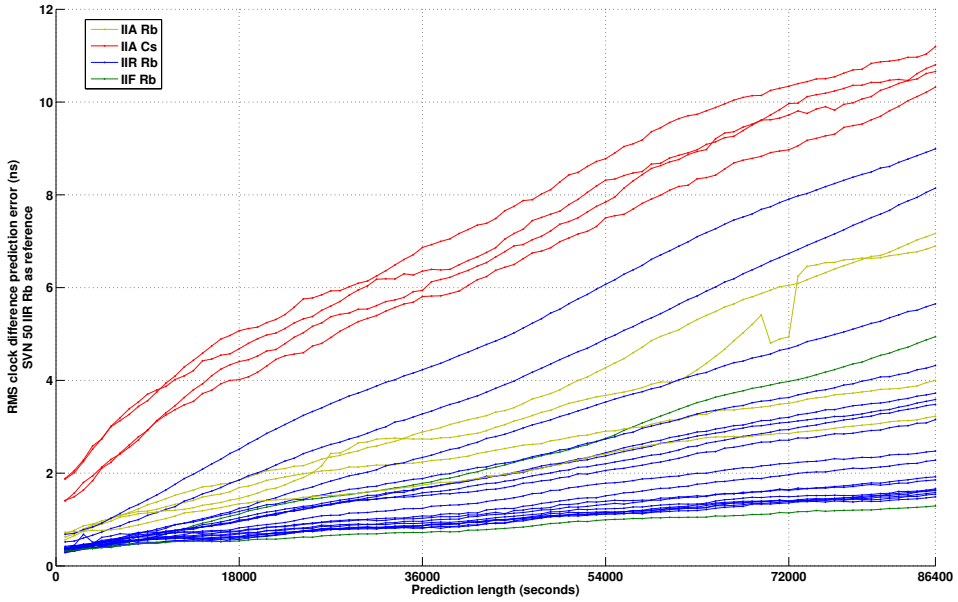

Figure 6.7: The RMS prediction error of the IGS GPS satellite clock difference predictions with the SVN 50 IIR Rb as the reference clock, for a range of predictions lengths from fifteen minutes up to twenty-four hours. The IGS rapid clock differences represent truth. The RMS calculation calculation uses data across the whole of 2012 i.e. an average RMS over 2012.

6.4.8 Summary statistics: IGS GPS RMS CDPE

This section presents summary statistics that give an indication of the performance of the IGS prediction system in predicting the difference between satellite clock pairs with the SVN 50 IIR Rb as reference. In table 6.5, the typical values for the RMS CDPE of the IGS prediction of the GPS satellite clocks in 2012 for the different categories of GPS satellite clocks are given. Here, the GPS satellite clocks are categorised according to satellite block and satellite clock type (Rb or Cs). As an example the average values for the IIR/IIR–M row is computed using the average RMS CDPE for all IIR/IIR–M Rb clocks for each of the predictions lengths: 0.25 hours, 3 hours, 6 hours, 12 hours and 24 hours. The full set of statistics used to compute these average values are given in Table C.4 in Appendix C.

PRN(SVN)	RMS ($\times 10^{-9}$ seconds) at different prediction lengths (hours)				
	0.25	3	6	12	24
Averages					
IIR/IIR–M	0.381	0.752	1.11	1.76	3.29
IIF	0.313	0.596	0.942	1.46	3.12
IIA	1.15	2.41	3.31	4.77	8.03
Cs	1.38	2.95	3.98	5.61	8.78
Rb	0.421	0.819	1.21	1.89	3.61
All	0.595	1.22	1.73	2.60	4.63

Table 6.5: Summary statistics. Typical values for the RMS CDPE IGS GPS in 2012 for the different categories of GPS satellite clocks. Here, the GPS satellite clocks are categorised according to satellite block and satellite clock type (Rb or Cs).

In table

Summary statistics ($\times 10^{-9}$ seconds)	For GPS IIR/IIR–M Rb CDPE RMS Statistics different prediction lengths (hours)				
	0.25	3	6	12	24
Mean	0.381	0.752	1.11	1.76	3.29
Median	0.365	0.691	0.879	1.32	2.38
Maximum	0.681	1.64	2.95	4.85	8.99
Minimum	0.285	0.515	0.659	0.915	1.49
Std. Deviation	0.0910	0.272	0.594	1.085	2.25

Table 6.6: Summary statistics IIR/IIR–M Rb CDPE RMS.

6.5 Findings

- There is a common signal, referred to here as the IGRT–IGUT timescale offset, which strongly influences the individual GPS satellite clock prediction errors of the IGS. In 2012, the typical (RMS) value of this IGRT–IGUT timescale offset quantity was $9.2 \pm 3.1\, ns(1\sigma)$.

- Clock difference prediction errors (CDPE) are not affected by the $T_{igr} - T_{igu}$ timescale offset quantity. The CDPE quantity is the true metric of GNSS satellite clock performance so far as GNSS positioning is concerned. The computation of clock differences requires the identification of a suitable in–orbit reference clock. In this case, for 2012, there were four suitable reference clocks. These were the clocks onboard SVN 46, SVN 50, SVN 53 and SVN 54. In this analysis SVN 50 was chosen as the reference clock because it was the best clock of the four, in frequency stability terms.

- The IGS predictions of the GPS satellite clock differences, with SVN 50 IIR Rb as reference, are biased. This is an indication of the mis–modelling of LFD in the IGS prediction method.
- Periodic signals are observable in some of the IGS predictions of the GPS satellite clock differences. This is an indication of the mis–modelling of the periodic signals in the IGS prediction method.
- At prediction lengths 0.25, 12 and 24 hours, the errors in the IGS predictions of the GPS satellite CDPE (in the IIR/IIR–M Rb case given in Table 6.6) are 32%, 38% and 60% higher the expected errors based on the results of frequency stability analysis in Chapter 5, Table 5.4. At prediction lengths 3 and 6 hours, the errors IGS predictions of the GPS satellite CDPE (IIR/IIR–M Rb) are 27% and 35% lower than the expected errors based on frequency stability analysis. This is surprising, and a likely explanation for this is the influence of the periodic signals on the HDev statistic.

6.6 Discussion

At present, with regards to the issue of SCTO predictions that meet the needs of applications requiring centimetre–level positioning accuracy, the GNSS community is, to a large extent, focussed on the challenges associated with delivery of low-latency clock predictions derived from near real-time, high-rate estimates of the SCTO based on observed satellite clock behaviour (through pseudorange and carrier phase measurements). These are the near real–time, low–latency SCTO prediction described in Section 2.2.5. Satellite clock predictions, at prediction lengths of up to twenty fours, are used by the GNSS operational control segments, as well as the IGS in their ultra-rapid product. In Section 2.2.5, these are introduced as the high–latency (HL), navigation message type SCTO predictions. These HL predictions are not good enough for centimetre level positioning accuracy, at least with the clocks in orbit today.

However, the quality of atomic-clocks in orbit continues to improve, it is not a great stretch to imagine the required quality of clock to be space-ready, clocks with the required performance are already in existence today, and have been demonstrated in the laboratory. In any case, improved techniques for space clock prediction are worth pursuing, as the vast majority of GNSS users have access to the HL predictions only. Further, the analysis of clock prediction error at a variety of prediction lengths, is in itself, perhaps the most meaningful method of characterising the performance of precise clocks, in general. Thus, improvements to existing satellite clock prediction schemes are worth pursuing.

Summary

In this chapter, a performance analysis of the IGS predictions of the GPS satellite clocks is presented, and aspects of the IGS predictions that are ultimately limiting performance are discussed. It is argued that the true metric of clock performance, in terms of PNT

accuracy at least, is the accuracy of the estimated or predicted clock differences, rather than the time-offset of the individual clocks from a reference timescale. All of this work sets the scene for Chapter 8, where a new satellite clock prediction system is presented, along with the results indicating its performance in comparison with the IGS prediction system.

Chapter 7

Enhanced modelling of relativistic time transformations in GNSS

Chapter outline

Timing applications of GNSS are typically based on the comparison of satellite clocks with ground-based clocks. This requires that the clocks being compared are synchronised—if not physically, then by means of a mathematical transformation on the actual clock measurements that are recorded. In GNSS the accuracy of the precision requirement for this synchronisation is at the level of nanoseconds, and at this level the so–called relativistic effects must be accounted for in the synchronisation procedure. In GNSS, the mathematical transformations that enable synchronisation in a manner that is consistent with relativity theory are known as the relativistic time transformations (RTT).

In GPS, the conventional approach to modelling the RTT is based on a simple model of Earth gravity that assumes that the Earth's mass is concentrated at a single point. In this chapter, an alternative approach for GPS RTT modelling is presented, but the method is applicable to GNSS RTT modelling more generally. This approach is based around the so–called precise analytical RTT, which is discussed in Chapter 2. The key feature of this alternative method is that it allows for the use of a more sophisticated model of the Earth's gravity. Previous studies into GPS RTT modelling [Kouba, 2004] looked into the impact of enhanced RTT modelling in a roundabout way, by comparing the RTT computed using predicted satellite orbits that included the effects of the J_2 term (Earth oblateness) in the satellite orbit prediction algorithms with predicted orbits that used a sequence of Keplerian–propagated orbits—an osculating Keplerian orbit—to model the real satellite trajectory. The objective in this work is to consider, in a direct way, the effects of a more rigorous model of Earth gravity on the GNSS RTT computation itself. The precise analytical RTT is precise at the 10^{-18} level, this is an approximation error of up to $\approx 10^{-13}$ s at one day if the error is systematic. The approximation errors of the conventional approach occur at the 10^{-15} level, i.e. up to $10^{-10}\frac{\text{s}}{\text{day}}$. In using a more rigorous RTT model, there is scope for meaningful improvement.

7.1 Relativistic time transformations in GNSS

In GNSS, the so–called relativistic effects on the satellite clock rates are accounted for by the relativistic time transformations (RTTs). To introduce these RTTs in the satellite clock time offset (SCTO) models, it is necessary to express the RTT as a satellite clock time relativistic correction term. This term, denoted here as Δt_{rel}, is the relativistic time transformation expressed as a satellite clock time correction term. Often it is referred to in a shorter form as the relativistic clock correction (RCC) when it is included in the GNSS measurement models.

7.1.1 The conventional GPS RTT as a correction term

In Chapter 2, the components of the GPS conventional RTT, the constant value frequency adjustment and the so–called eccentricity correction, were introduced. Here, for ease of comparison with the precise formulation of the GPS (GNSS) RTT which is given in Subsection 7.1.2, the full conventional GPS RTT is presented as a time correction term to be applied to a satellite clock time measurement, in order to recover GPS Time from that measurement. In this way, expressed in the form of a correction term, the GPS RTT can be slotted directly into an SCTO model, e.g. as the relativistic component in Equation 2.6. And so, the full conventional GPS RTT, is expressed as

$$\Delta t_{rel(c)}(t) = \Big[\frac{3GM_E}{2ac^2} + \frac{W_0}{c^2}\Big]\Delta t(t) - 2\frac{\mathbf{r}.\mathbf{v}}{c^2} \tag{7.1}$$

where the (c) part of the subscript denotes that this is, specifically, the conventional GPS RTT. Here, the reference timescale for t is GPS Time and the last term is the eccentricity correction where both $\mathbf{r}$ and $\mathbf{v}$ are time–dependent functions corresponding to satellite (ECEF) position and velocity, respectively. All other terms are defined in Subsection 2.2.4.

7.1.2 The precise GPS RTT as a correction term

To consider the effects of a more rigorous treatment of the precise GPS RTT, and its impact on GPS SCTO modelling and prediction, it is necessary first to express the precise GPS RTT in the form of a correction term. In this section, the precise GPS RTT is derived, as a correction term, from the definition of the precise GPS RTT, which is given in Subsection 2.2.4.

To begin, it makes senses to define, generally, what is meant by the GPS satellite clock RTT as a correction term. Basically, the GPS satellite clock RTT as a (time) correction term is the difference between satellite (proper) time and GPS Time,

$$\Delta t_{rel}(t) = \Delta t^s(t) - \Delta T_{gps}(t) \tag{7.2}$$

where t in this case, is time with respect to the GPS timescale, $\Delta t^s(t) = t^s(t) - t^s(t_0)$ and $\Delta T_{gps} = t - t_0$, t_0 being an initial time, where satellite time and GPS Time are (in some way) synchronised. Here, the underlying reference timescale is GPS Time.

Rearranging and integrating of the precise RTT (Equation 2.9), from t_0 to t, with t referenced to GPS Time gives

$$\Delta t^s - \Delta t = \int_{t_0}^{t} \Big[\frac{W_0}{c^2} - \frac{V}{c^2} - \frac{\Delta V}{c^2} - \frac{v^2}{2c^2}\Big] dt \tag{7.3}$$

where $V = V(\mathbf{r})$ represents the Earth's gravitational potential at $\mathbf{r}$, $v = v(\mathbf{r})$ represents the satellite's velocity at $\mathbf{r}$, $\Delta V(\mathbf{r})$ are the resultant tidal potentials due (mainly) to gravity of the Moon and the Sun, and $\mathbf{r} = \sqrt{x^2 + y^2 + z^2}$ is the satellite's position in an ECEF reference frame. Here, $\mathbf{r} = \mathbf{r}(t)$ is a time–dependent variable.

Now, using the definition of the GPS relativistic clock correction (RCC)—i.e. the GPS RTT expressed as a satellite clock time correction term—from Equation 7.2, and also noting that the $\frac{W_0}{c^2}$ is a constant, Equation 7.3 can be simplified somewhat, and expressed as

$$\Delta t_{rel(p)} = \Big[\frac{W_0}{c^2}\Big]\Delta t - \frac{1}{c^2}\int_{t_0}^{t} \Big[V + \Delta V + \frac{1}{2}v^2\Big]\, dt \tag{7.4}$$

where the (p) part of the subscript denotes that this is the full, precise GPS RTT. The basic objective of the work presented in this chapter is an in–depth investigation into the properties of the GPS RCC as expressed in Equation 7.4. The requirements for the computation of precise GPS RCC at time t_0 are: the initial conditions of the satellite position and velocity, but then also a dynamic model to describe the motion of the satellite between t_0 and t. However, the focus here is only on the influence of high–fidelity Earth gravity modelling. And for this reason, IGS SP3 Finals data files (which contain satellite orbit information alongside SCTO information) are used to determine the orbital trajectory of the satellite between t_0 and t. Here, the influence of ΔV is not studied.

7.1.3 Earth Gravity Model

The Earth gravity model used in this work is based on a spherical harmonic expansion series. In this form, the Earth's gravitational potential, $V(x, y, z)$, is expressed as

$$V(x, y, z) = \frac{GM}{r}\Big\{1 - \sum_{n=2}^{\infty}\sum_{m=0}^{n} [(\frac{a_E}{r})^n P_{nm}(\cos\theta)(J_{nm}\cos m\lambda + K_{nm}\sin m\lambda)]\Big\} \tag{7.5}$$

where a_E is the semi-major axis of the mean Earth ellipsoid, P_{nm} are the associated Legendre polynomials of degree n and order m, and because $\mathbf{r} = \sqrt{x^2 + y^2 + z^2}$, $\theta = \arctan\frac{y}{x}$ and $\lambda = \arctan\frac{\sqrt{x^2+y^2}}{z}$, the double summation of Equation 7.5, can be expressed in terms of spherical coordinates as,

$$V(x, y, z) = \frac{GM}{r} - R(\mathbf{r}, \theta, \lambda) \tag{7.6}$$

where $R(\mathbf{r}, \theta, \lambda)$ is known as the perturbing potential. And so, given position (in ECEF) as input, the Earth's gravitational potential (the geopotential) can be evaluated, if the geopotential coefficients, J_{nm} and K_{nm}, are known. Therefore, Earth gravity models are usually disseminated as ascii–formatted data files, where the data are the geopotential

coefficients. There are several publicly available geopotential models. The models vary based on complexity (i.e the resolution in terms of degree and order), and also the input data to the models [Montenbruck *et al.*, 2011]. This study uses Earth Gravity Model 2008 (EGM08) [Pavlis *et al.*, 2012], because at the time of writing, this is highest resolution Earth Gravity Model published, and uses a combination of data from the latest Earth gravity determination missions.

7.2 The scope of the GNSS RTT modelling study

Parameters of study	Values
Systems	GPS
Timeframe of analysis	January 2012
Orbit data format	SP3 (15–minute sampling rate)
Data sources	IGS Final Orbits
Earth Gravity Model	Earth Gravity Model 2008 (EGM08)
Integration arc–lengths	0.25, 3, 6, 12, 24 (hours)

Table 7.1: Scope of the GNSS RTT modelling study.

In table 7.1, the key parameters of the GNSS relativistic time transformation modelling study, which is the topic of this chapter, are listed. Here, the analysis is restricted to the GPS case only. However, the precise RTT (Equation 7.4) can be applied more generally. Certainly, the same approach can be taken for the other GNSS. In such cases, this would involve replacing instances of GPS Time in Subsection 7.1.2 with the relevant GNSS Time.

7.3 Method

The method developed for this study comprises the following steps:

1. **Data pre–processing**, which requires fetching (via the Internet) IGS final SP3 files, extracting the GPS satellite orbit (position) information, separating the information satellite by satellite (by GPS PRN), and concatenating to generate a time–series of satellite clock orbit information. Satellite clock velocity information is derived from these orbit time–series through a process of interpolation (Lagrange polynomial) and numerical differentiation. Collectively, the satellite position and velocity information, are combined into a single database. This database provides the input data for the RTT modelling study.
2. **Earth gravity modelling,** which uses the Earth Gravity Model 2008 (EGM08). In the step, the database holding the satellite and position velocity time–series is expanded to include several (seven) geopotential time–series corresponding to the positions. The difference in these geopotential time–series is the degree and order of the spherical harmonic expansion series, Equation 7.6, that is used in computing the geopotential value. Although EGM08 is complete to degree and order 2159, for this

study, the maximum resolution considered was degree and order 20. This choice is explained in Section 7.4.1.

3. Using this database of satellite orbits alongside geopotential time–series, the precise GPS RCC is computed by numerical integration (using the trapezium rule method). **Integration arc lengths of 15 minutes, 3 hours, 6 hours, 12 hours and 24 hours** are considered. For each integration length scenario, seven separate GPS RCC computations are made based on geopotential time–series that are based on **EGM08 coefficients up to degree 1, 2, 3, 4, 5, 10 and 20**. The results of these computations are compared.

The complete database that is used for the computation of the precise GPS RTT is made up of time–series of the quantities that are listed in Table 7.2.

Field	Description
Epoch	A timestamp in Modified Julian Date (MJD) format.
Clock position	ECEF position from IGS SP3 data.
Clock velocity	ECEF velocity inferred from IGS SP3 position data (by numerical differentiation).
Geopotential–1	The Earth's gravitational potential at the satellite's position based on a first–order computation, i.e. using the monopole term of EGM08 only.
Geopotential–2	The geopotential at the clock's position based on EGM08 coefficients up to degree and order 2.
Geopotential–3	EGM08 up to degree and order 3.
Geopotential–4	EGM08 up to degree and order 4.
Geopotential–5	EGM08 up to degree and order 5.
Geopotential–10	EGM08 up to degree and order 10.
Geopotential–20	EGM08 up to degree and order 20.

Table 7.2: A description of the fields of the databases that was created for the GPS precise RTT modelling study. A separate database was populated for each GPS satellite (i.e. GPS SVN), for the month of January 2012.

7.4 Results

Here, the key results of the RTT modelling study, for a single GPS satellite, during the period January 2012 are presented. Although RTT modelling for the full set of GPS satellites were considered in the analysis, the results for a single satellite are representative.

7.4.1 Earth Gravity Modelling

Using the full EGM08 (i.e. including all model coefficients up to degree and order 2000+) to determine the geopotential at a satellite clock's position, for the purposes of GPS RTT modelling is computationally (prohibitively) expensive. However, for this purpose it turns out that the full model is not necessary and a truncated version of the full EGM08 (up to degree and order 10) is sufficient. In other words, beyond degree and order 10 there

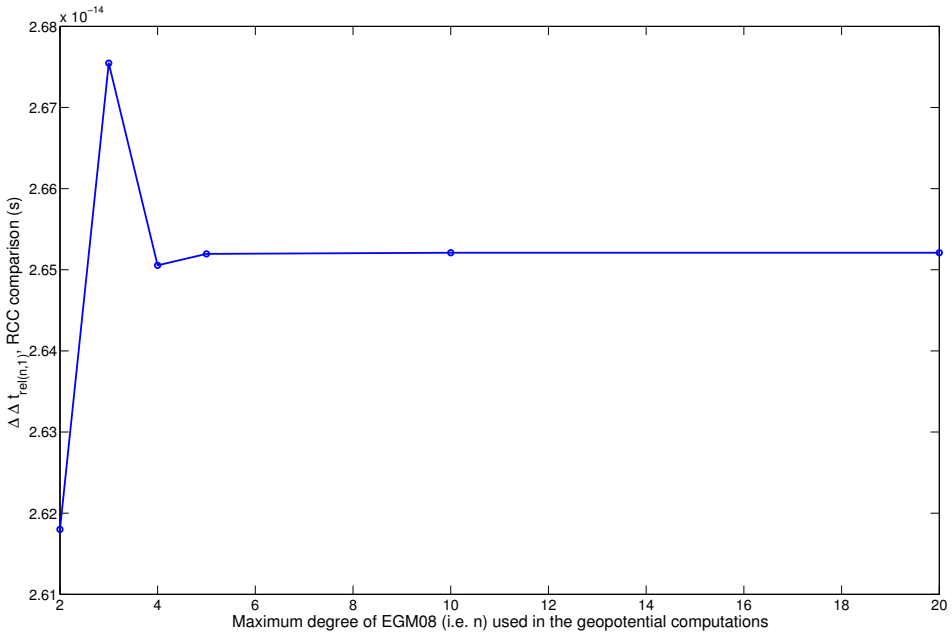

Figure 7.1: The difference between RCC computed using a point mass Earth gravity model compared against RCC computed using EGM08, where the spherical harmonic expansion is truncated at various levels, i.e. at degree 2, 3, 4, 5, 10 and 20, for GPS SVN 50. In this figure, the average value for the computed RCC across January 2012, where the integration arc–length is 15 minutes is used.

RCC comparison	$\Delta\Delta t_{rel(i,j)}$ (s)
$\mathbf{\Delta\Delta t_{rel(2,1)}}$	2.62×10^{-14}
$\mathbf{\Delta\Delta t_{rel(3,2)}}$	5.75×10^{-16}
$\mathbf{\Delta\Delta t_{rel(4,3)}}$	-2.49×10^{-16}
$\mathbf{\Delta\Delta t_{rel(5,4)}}$	1.40×10^{-17}
$\mathbf{\Delta\Delta t_{rel(10,5)}}$	1.44×10^{-18}
$\mathbf{\Delta\Delta t_{rel(20,10)}}$	4.73×10^{-22}

Table 7.3: The impact of Earth gravity model resolution on RTT modelling results. Here, the results for GPS SVN 50 are given. The integration arc–length is 15 minutes.

is no physically meaningful improvement in RTT modelling performance by using a more detailed version of EGM08. Figure 7.1 gives a useful visual indication of this. The data points of figure 7.1 are the differences between the RCC computed for GPS SVN 50 using a point mass Earth gravity model, i.e. $\frac{GM}{r}$, against RCC computed using EGM08 at a variety of resolutions, i.e. truncated at degree 2, 3, 4, 5, 10 and 20. Here, the RCC is computed at every satellite position where it is possible given the data available in the RTT study database described in Section 7.3. The difference between RCC computed using EGM coefficients up to degree and order j against RCC computed using EGM coefficients up to degree and order i is represented by the symbol $\Delta\Delta t_{rel(i,j)}$[1], and the

[1]This notation is also used in Figure 7.1.

average values for these quantities across January 2012 are given in Table 7.3. Here, the integration arc length is 15 minutes (the basic time interval of the RTT study database), which means data corresponding to two time points are used in each RCC computation.

7.4.2 RTT modelling over a variety of integration arc–lengths

A variety of other integration arc lengths: 3, 6, 12 and 24 hours were also considered in this study. The results of these longer arc–length analyses are given in Table 7.4. Due to the nature of the precise RTT, the 3 hour arc length analyses required data corresponding to 12 time points in each RCC computation, as the basic time interval of the available data is 15 minutes. For the 6 hour arc–length RTT computation, 24 time points were required; 12 hour arc–lengths required 48 time points; and for 24 hour analyses 98 time points were used.

RCC comparison	$\Delta\Delta t_{rel(i,j)}$ (s) at various integration arc lengths (hours)			
	3	6	12	24
$\mathbf{\Delta\Delta t_{rel(2,1)}}$	3.96×10^{-14}	6.45×10^{-15}	5.73×10^{-15}	6.33×10^{-15}
$\mathbf{\Delta\Delta t_{rel(3,2)}}$	1.02×10^{-16}	1.33×10^{-16}	2.20×10^{-16}	7.19×10^{-17}
$\mathbf{\Delta\Delta t_{rel(4,3)}}$	1.42×10^{-17}	1.83×10^{-17}	2.65×10^{-17}	-2.48×10^{-17}
$\mathbf{\Delta\Delta t_{rel(5,4)}}$	1.79×10^{-18}	2.62×10^{-18}	4.45×10^{-18}	1.82×10^{-18}
$\mathbf{\Delta\Delta t_{rel(10,5)}}$	3.37×10^{-19}	4.52×10^{-19}	6.15×10^{-19}	1.97×10^{-19}
$\mathbf{\Delta\Delta t_{rel(20,10)}}$	8.47×10^{-22}	8.47×10^{-22}	8.50×10^{-22}	6.70×10^{-21}

Table 7.4: The impact of Earth gravity model resolution on RTT modelling results. Here, the results for GPS SVN 50 are given. A variety of arc–lengths are considered.

7.5 Discussion

To determine the implications of the results presented in Section 7.4, in the broader context of the GNSS SCTO prediction (and estimation) work that is the underlying theme of this project, there are three factors to reconsider here. These include:

- the **precision of the analytical precise RTT as** 10^{-18}, which originates from the assumptions and approximations in the derivation of the analytical RTT. In the analytical RTT the terms below order -2 with respect to the speed–of–light quantity, c, are neglected. This means that any difference in computed RTT below the 10^{-18} level are not physically meaningful, and thus can be safely neglected. Based on the values in Tables 7.3 and 7.4, this indicates an RTT modelling strategy that uses EGM08 coefficient up to degree and order 10 at most.

- the **observed stability (HDev–based) of the in–orbit satellite clocks at the** 10^{-14} **level** in the (estimated) IGS GPS Final satellite clock combinations at intervals in the range fifteen minutes to twenty–four hours, see Chapter 5. The HDev frequency stability statistic is the standard indicator of the level of random variations seen in the GPS satellite clocks, due to clock noise. In order to independently test

the results of the RTT analysis, and to demonstrate the connection between a high–resolution Earth gravity modelling strategy, even beyond degree and order 2, requires in–orbit satellite clocks that are more stable, by about two orders of magnitude.

- the **performance level of existing prediction algorithms**, where the prediction errors that are seen at prediction lengths 15 minutes to 24 hours are at $10^{-10}/10^{-9}$ level.

The major conclusion of this RTT modelling study is that for the purposes of GNSS SCTO prediction today (or in the near future), the adoption of high–fidelity Earth gravity models in the RTT modelling strategy is not necessary. Instead, it is worth focussing efforts on the development of other aspects of in–orbit clock technology (mainly hardware), and also on development of enhanced orbit determination and prediction algorithms, which would indirectly improve RTT accuracy through higher accuracy inputs to the RCC computation.

Summary

The key motivating factor for studying RTT modelling in GNSS was to determine whether RTT mis–modelling is the cause of the periodic signals that were observed in the IGS GPS satellite clock combinations. If this was the case, then it would be worth developing modelling methods for these periodic signals based around relativistic physics. From the results of the analysis presented in this Chapter, the conclusion is that this is not the case, at least insofar as the effects of Earth gravity mis–modelling is concerned. Rather, as the RTT is a path–dependent quantity, and because the geopotential computation is satellite position dependent, it is worth focussing efforts on developing methods for improved satellite orbit prediction, which will have a knock–on effect on RTT accuracy. However, currently, it is clear that RTT modelling/mis–modelling is not a critical factor affecting the performance of GNSS SCTO prediction algorithms, and at least where the approach to geopotential modelling in RTT's are concerned, the approximation or truncation errors of the currently adopted approach are not observable in even the most precise of GPS satellite clock data products, which are the IGS Final satellite clock combinations.

Chapter 8

A new GPS satellite clock prediction system

Chapter outline

An in-depth study of the GPS and GLONASS satellite clocks, presented in Chapter 5, indicated the presence of features in many satellite clock signals that are not accounted for by the standard clock model as it is presented in Chapter 3. But, there are alternative models that can be explored, and as there are many applications (e.g. prediction of the satellite clock parameters in the GNSS navigation messages, precise point positioning (PPP)—a single–receiver technique, low–latency (or real–time) GNSS time–transfer etc.) that would benefit from interpolated or extrapolated clock values of the highest quality, it is worthwhile to do so.

In this chapter, an extension to the standard clock model (SCM) is presented. Here, this will be referred to as the extended clock model (ECM). The ECM accounts for periodic signals, present in many of the GPS satellite clocks, and deals with flicker noise processes (FPM and FFM), as seen in GPS and GLONASS satellite clocks, which are difficult to model analytically. The ECM also includes a component, known here as the reference timescale offset term, which allows for clock information of different types, or from different sources, to be combined. The KF implementation of the extended clock model forms the core component of a new GPS satellite clock prediction strategy, which uses IGS GPS satellite clock data as input. This prediction algorithm was designed in such a way that it is compatible with current IGS products—to slot into the existing framework. The prediction method that is tested here is a partial implementation of a potentially more complete prediction scheme.

In terms of content, this chapter begins with a recap of the critical factors that limit the performance of satellite clock time offset prediction strategies. The core elements of the new prediction strategy: the extended clock model, the ECM Kalman filter as estimator and predictor, and a data pre–processing method designed to address the $T_{igr} - T_{igu}$ timescale offset problem are presented. The scope of this prediction system development study is given along with the method of the study. The features of the new prediction strategy as well as the performance are investigated and the results are presented here.

8.1 A system developed around the IGS operational scheme

The prediction system developed and tested in this work was designed to fit into, and enhance, the performance of a specific operational scheme: the IGS predictions of the GPS satellite clock time offsets from IGS Time. The fundamental component of this proposed system is an extended model of satellite clock time offset (SCTO), introduced here in Section 8.3.2. This is an extended model in the sense that it it captures features that are not accounted for in the standard clock model (SCM), presented in Chapter 3. For this reason, the new prediction strategy is referred to as the extended model prediction (EMP) system.

There are elements of this new prediction system, the EMP system, that would apply generally to other IGS–like GNSS satellite clock prediction schemes, but, due to a lack of suitable data relating to these other prediction schemes this new strategy is built and tested entirely around the IGS framework. Here, an IGS–like prediction scheme refers to the strategies adopted by the various GNSS operational control segments (e.g. by GPS OC (OCS/X), GLONASS operational control etc.), but also by the various GNSS data analysis centres (e.g. ESA, JPL, GFZ, CODE etc.), see Chapter 4 for more details on the GNSS data analysis centres. These are strategies that produce high–latency satellite clock predictions, with the prediction lengths ranging from several minutes up to one day ahead. The low–latency satellite clock predictions generated as part of the IGS real-time service are a different class of prediction problem where clock values are extrapolated up to several tens of second ahead at most. Thus, these low–latency satellite clock predictions schemes are not considered here.

And so, in operating within this IGS framework, the prediction method proposed here is developed starting with an assumption that the same input data is available to both the IGS prediction method and the new method. In this way, it is possible to make a fair comparison between the predicted satellite clock values of the IGS scheme with the predicted values from the EMP method. Here, the key metric that is used to evaluate the performance of the new prediction method is prediction error ratio between the two methods.

8.2 Critical factors affecting SCTO prediction performance

In Chapters 5 and 6, the following factors were identified as limiting the performance of the IGS (and IGS–like) prediction schemes for the GPS satellite clocks. The new prediction method is designed with these factors in mind, aiming to address them where it is possible.

1. At the nanoseconds level, the influence of stochastic variations on the GPS satellite clock behaviours are significant—significant in the sense they fundamentally limit clock predictability (at $\mathcal{O}(10^{-9})$ s) over prediction lengths ranging from several minutes up to twenty–four hours. For this reason, as uncertainty in predicted clock behaviour is accumulated through time, expected clock prediction error also increases monotonically through time. Therefore, the most critical factor that determines the clock prediction accuracy is **prediction length**.

PRN (SVN)	LFD	Periodics	FFM	FPM
1 (63)	✓	✓	✓	
2 (61)	✓			
3 (33)		✓		
4 (34)		✓		✓
5 (50)	✓	✓		
6 (36)		✓		
7 (48)	✓			
8 (38)		✓	✓	
9 (39)			✓	
10 (40)		✓	✓	
11 (46)		✓		
12 (58)	✓	✓		
13 (43)	✓			
14 (41)	✓			✓
15 (55)	✓			
16 (56)	✓	✓		
17 (53)	✓	✓	✓	✓
18 (54)	✓	✓		
19 (59)	✓			
20 (51)	✓		✓	✓
21 (45)				
22 (47)	✓		✓	✓
23 (60)				
24 (—)				
25 (65)	✓	✓	✓	
26 (26)				
27 (—)	✓			
28 (44)	✓			✓
29 (57)				✓
30 (35)				
31 (52)	✓		✓	✓
32 (23)				
Total	18	13	9	8

Table 8.1: Features observed in the GPS satellite clocks during 2012, based on an analysis of the IGS final GPS satellite clock data product.

2. The contribution of the $\mathbf{T_{igr}} - \mathbf{T_{igu}}$, the offset between the IGS Rapid Timescale, which is a realisation of IGS Time, and the IGS Ultra–rapid Timescale, which a realisation of GPS Time.

3. The **re–initialisation of the time–offset and frequency offset parameters** of the individual clocks at the beginning of each prediction run.

4. **Linear frequency drift (LFD),** which is observed in most GPS Rb clocks (IIR/IIR–M and IIF). The dynamics of LFD property varies among different satellite clocks. In some clocks, LFD is relatively constant over time and in others LFD

is clearly seen to evolve through time.

5. **Periodic signals,** which are observed in many GPS satellite clocks.
6. **Complex stochastic processes,** which refers to the flicker noise processes (FPM and FFM) that are observed in many GPS satellite clocks.

Of the factors listed above, the second i.e. the $\mathbf{T_{igr}} - \mathbf{T_{igu}}$ timescale offset, applies only to the IGS prediction scheme for the GPS satellite clocks. The other factors are of general relevance and are likely to impact upon performance of any GPS (or GNSS) satellite clock prediction method. In Table 8.1, which is populated based on a quick–look analysis of the IGS Final SP3 satellite clock data presented in Chapter 5, the features observed in the individual GPS satellite clocks during 2012, are marked on a satellite–by–satellite basis. The information in this table is useful in that it indicates satellite clocks that are likely to be mis–modelled, in some way, and to a significant extent, by the standard clock model (SCM). In particular, the standard clock model does not account for the periodic signals or the influence of the flicker noise processes (FPM and FFM) that are observed in the SCTO data of a number of GPS satellite clocks.

8.3 Elements of the new prediction system

In this section, the key elements of the proposed prediction system are introduced. These include:

- the **inputs** to the prediction system and the **outputs** from the system.
- the **extended clock model**, introduced in Section 8.3.2, which can be described as a semi–analytical extension to the standard clock model, which is presented in this thesis in Section 3.3.
- a **formulation of the extended clock model (ECM) within the Kalman filter framework**, which is referred to herein as the extended clock model Kalman filter (ECKF).
- a description of how **the elements of the extended clock model Kalman filter are initialised and configured.** These are the processes that prepare the system for estimation and prediction of extended clock model parameters.
- The processes in which the state–vector and state–error covariance matrix parameters of the ECKF are re–initialised, **introducing new information into the system** as it is released are also described.

Together, all of these elements constitute the newly developed GPS satellite clock prediction system, which is referred to herein as the GPS satellite clock prediction system based on the extended clock model. Within this chapter, the prediction system is also called the extended model prediction (EMP) system, or EMP scheme, or EMP method, which are all referring to the same thing.

8.3.1 A broad overview of the EMP system

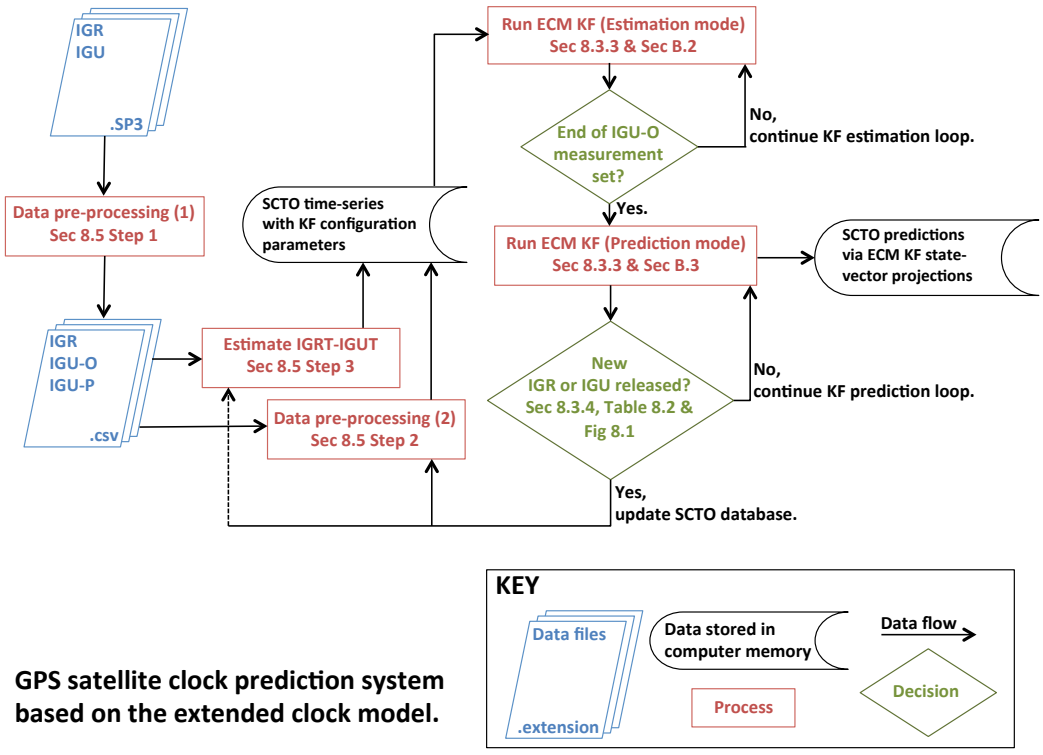

Figure 8.1: An overview of the key elements and processes that constitute the GPS satellite clock prediction system based on the extended clock model, usually referred to within this thesis as the extended model prediction (EMP) system. There are several key processes shown here that are described in greater depth in later sections within this chapter. These are explicitly referred to in the diagram.

A broad overview of the EMP system is given in figure 8.1. The inputs to the EMP system are satellite clock time offset (SCTO) estimates, which are stored in the Crustal Dynamics Data Information System (CDDIS) archive in the SP3 format; see Section 4.2 for details on the CDDIS archive and the SP3 format. This data is introduced into the EMP system through a purpose–built data file–fetching utility, which takes a start date and an end date (both in Modified Julian Date (MJD) format) as input arguments and fetches the IGS (final, rapid and ultra-rapid) SP3 data files from the Internet and stores it on a local directory. The outputs of the EMP system are SCTO predictions, with the IGS Rapid Timescale as reference. The prediction length, i.e. the time interval between the last SCTO estimate and the prediction, is configurable. However, the system is designed with prediction lengths in the range 15 minutes to twenty four hours in mind.

The EMP system 'starts up' by acquiring a suitable amount of data, e.g. up to one month of IGS Rapid (or Final) data, which is required to characterise the satellite clocks. Within the context of the EMP system, characterisation of the satellite clocks describes the processes involved in the initialisation of the extended clock model Kalman filter state–

vector and state–error covariance matrix, as well as the configuration of the clock noise parameters (the process noise covariance matrix parameters) and the measurement noise covariance matrix parameters. Here, the initialisation and configuration of the ECKF parameters is done individually, one GPS satellite clock at a time. This is the most labour–intensive part of the EMP system. But, once this is done, the EMP system is able to operate, producing SCTO estimates at a variety of prediction lengths. However, there are two types of event that interrupt the operation of the EMP system: the release of the latest IGS Rapid File, everyday, at 1700 UTC and the release of the latest IGS Ultra-rapid File, which occurs four times a day at 0300, 0900, 1500 and 2100 UTC. The introduction of this new information into the EMP system requires an update of the database of SCTO time–series that the ECKF uses in producing its SCTO estimates and predictions (as shown in figure 8.1), and it requires the ECKF to be re–operated including the newly available SCTO data. Further details on how the new data is introduced to the EMP system is given in Section 8.3.4.

8.3.2 An extension to the standard clock model

The standard clock model (SCM), as it is described in Chapter 3, is simple and effective, producing close to optimal predictions across a range of prediction lengths for some of the GPS satellite clocks. But there are features in the IGS final GPS satellite clock data product that are not accounted for in the standard clock model (see Chapter 3). These additional features are not seen in all of the GPS satellite clocks. In table 8.1, the presence—or lack—of these features in the GPS satellite clocks are summarised. Table 8.1 is populated based on the analysis that is presented in Chapter 5. The implication here is that improved predictions can be achieved by the use of an extended model. Here, the development of such an extended model, referred to herein as the extended clock model (ECM), is described. The ECM is a semi–analytical model, i.e. unlike the standard clock model the extended model is not expressed neatly as a system driven by a first–order stochastic differential equation[1]. Rather, the modelling approach is empirical, developed in response to the outcome of the SCTO data analysis studies, which are presented in Chapters 5 and 6.

There are four distinct components of the extended clock model: the standard clock model (SCM) component, the periodic signals component, the Gauss–Markov component and the $T_{igr} - T_{igu}$ timescale–offset component. Thus, the ECM can be expressed as

$$x(t) = x_s(t) + x_p(t) + x_u(t) + x_{GM}(t) \tag{8.1}$$

where $x_s(t)$ is the standard clock model component as defined in Chapter 3; $x_p(t)$ is the periodic signals components; $x_{GM}(t)$ represents the time–offset component of the Gauss–Markov process that models the flicker noise processes (FPM and FFM) and x_u represents what is referred to herein as the ultra–rapid component of the extended clock model. In this study, the ECM is used to represent IGS Rapid and IGS Ultra–rapid SCTO data. For

[1]The development of a concise mathematical formulation of the extended clock model in the language of stochastic differential equations might be an interesting topic for future work.

the IGS Rapid SCTO data, the x_u component of Equation 8.1 is zero. In the following sections, each of these components are explained, in turn.

The standard clock model component

As it is described in this thesis, the standard clock model is a first–order linear stochastic differential equation that describes the systematic time–evolution of the time–offset, fractional frequency and frequency drift parameters, as well as the noise processes associated with those parameters. In the standard clock model each of these noise processes are modelled as Gaussian noise processes with stationary increments (i.e. all increments are zero–mean Gaussian random variables, all with the same variance). In the PTFM literature, these noise processes are known as white frequency modulation (WFM) noise, random walk frequency modulation (RWFM) noise and random run frequency modulation (RRFM) noise. The development of standard model clock model is presented is some depth in Section 3.3.

The features that are observed in the GPS satellite clocks, but not accounted for in the standard clock model include the presence of periodic signals and the influence of the flicker noise processes (flicker phase modulation (FPM) and flicker frequency modulation (FFM)). In the IGS predictions of the GPS satellite clocks, the influence of $T_{igs} - T_{igu}$ timescale offset is also problematic, especially to the analyst who wishes to use the IGS SCTO data set in order to study the predictability of the GPS in–orbit clocks. Each of these additional features are accounted by the remaining components of the extended clock model.

The periodic signals component

The periodic signals component of the extended clock model, denoted $x_p(t)$, is represented as

$$x_p(t) = \sum_{i=1}^{4} [A_i \cos(\omega_i t) + B_i \sin(\omega_i t)] \tag{8.2}$$

where A_i and B_i are amplitude coefficients and ω_i is the angular velocity of i–th periodic component and is equal to $\frac{2\pi}{T}$ where T is the period in seconds. In the EMP system, it is assumed that the period of each periodic signal is known. In the GPS satellite clocks characterisation study in Chapter 5, periodic signals with period $\approx$ 3 hours, 4 hours, 6 hours and 12 hours were observed in the GPS satellite clocks, in agreement with Senior *et al.* [2008]. The results of a dynamic frequency stability analysis of the GPS satellite clocks, of which the results are shown in Section 5.3.1, indicate that the period of the periodic signals are stable over the course of several months, suggesting that the period can be modelled as (almost) constant or as a slowly varying state. Thus, for the general GPS satellite clock, the periodic signals component of the extended clock model includes fours periods, which are modelled as constant, with A_i and B_i amplitude coefficients as parameters to be estimated (or predicted).

The ultra–rapid component

In essence, the ultra–rapid component of the extended clock model, $x_u(t)$, aligns the IGS Ultra–rapid data set with the IGS rapid data set. This is necessary for two reasons:

1. the underlying reference timescale for the IGS Ultra–rapid data set is not aligned to the IGS Rapid Time (which represents "true" time in this study).
2. additionally, there is a time offset and frequency offset in each IGS ultra–rapid clock data set relative to the corresponding set of IGS rapid estimates. This is because the two data products (IGR and IGU) are produced independently of each other. Thus, to some extent, there is will be a disagreement in estimated clock behaviour between these two data sets.

In the ultra–rapid component of the extended clock model, this "mis–alignment" of the IGS Ultra–rapid clock data from the IGS Rapid clock data is expressed as

$$x_u(t) = u_0 + u_1(t - t_0) \tag{8.3}$$

where u_0 represents the initial time offset, between the IGS Rapid SCTO value and the corresponding IGS Ultra-rapid SCTO value, and u_1 represents the relative (fractional) frequency offset between the two. The basic strategy, in the EMP system, is to estimate the u_0 and u_1 parameters where there is an overlap between the IGS Rapid and the IGU-O data set.

The Gauss–Markov component

The Gauss–Markov component of the extended clock model, denoted $x_{GM}(t)$, approximates the flicker noise processes observed in the GPS satellite clocks using Gauss–Markov processes. A Gauss–Markov process is a stationary Gaussian process with an exponentially decaying autocorrelation function. In the extended clock model, the non–stationary flicker noise processes (over a finite time span) are approximated as a linear combination of several independent Gauss–Markov processes running in parallel. The development of this approach to modelling the flicker noise processes in clock measurement data sets is detailed in Davis *et al.* [2005a;b], and the same approach is taken in this work.

8.3.3 A KF implementation of the extended clock model

In this section, the implementation of the extended clock model within the Kalman filter framework is described. At this stage, the reader may find it helpful to revisit the basics of the Kalman filter method, which are given Appendix B. Also, the Kalman filter implementation of the (simpler) standard clock model is given in Section 3.5.2.

In the EMP system, the extended clock model Kalman filter (ECKF), operates in estimation and prediction mode, which are described in Appendix B. Here, the core defining elements of the ECKF: the state–vector, the state–transition matrix, the process noise covariance matrix, the measurement vector, and the measurement matrix are introduced.

The processes involved in the initialisation and configuration of these elements of the ECKF are also described.

The state vector

The state–vector of the extended clock model Kalman filter, that is set up to provide optimal (in the minimum–mean–square–error sense) estimates (and predictions) of those state–vector parameters is expressed as

$$\mathbf{x}_k = \begin{bmatrix} x_k & y_k & z_k & A_{1k} & B_{1k} & \dots & A_{4k} & B_{4k} & u_{0k} & u_{1k} & \mathbf{x}_{\mathbf{GM}k} \end{bmatrix}^T \tag{8.4}$$

where $\mathbf{x}_k$ represents the state–vector (of the extended clock model as given in Equation 8.1) at epoch k and

- x_k is the time-offset at epoch k
- y_k is the fractional frequency offset at epoch k
- z_k is the (linear) frequency drift at epoch k
- A_{ik} is the amplitude coefficient of the cosine component of the i–th periodic signal at epoch k
- B_{ik} is the amplitude coefficient of the cosine component of the i–th periodic signal at epoch k
- u_{0k} is the phase offset of the IGS ultra–rapid clock data relative to the IGS Rapid set at epoch k
- u_{1k} is the frequency offset of the IGS ultra–rapid clock data relative to the IGS Rapid set at epoch k
- $\mathbf{x}_{\mathbf{GM}k}$ represents the Gauss–Markov component of the state–vector at epoch k.

In general, for each GPS satellite clock (or clock difference), there are four periodic signals modelled. And here, the modelling of the flicker noise processes (using a linear combination of independent Gauss–Markov processes running in parallel) requires a total of eight Gauss–Markov states: four each for both FPM noise and FFM noise. Thus, in total, a total of 21 state–vector components is required, in general, for each GPS satellite clock (or clock difference).

However, the periodic signals are not observed in all GPS satellite clocks, and in all GPS satellites where periodic signals are observed, all four periods are not usually seen. Also, the influence of the flicker noise process is not seen in all of the GPS satellite clocks (or clock differences).

The state transition matrix

The state–transition matrix of the extended clock model Kalman filter is expressed as

$$\mathbf{\Phi}_k(\tau) = \mathbf{\Phi}(\tau) = \left[\begin{array}{c|c|cc|c} \mathbf{\Phi}_s & \mathbf{0}_{3\times 2n} & \mathbf{0}_{3\times 2} & & \mathbf{\Phi}_{\mathbf{GM}1[3\times m]} \\ \hline \mathbf{0}_{2n\times 3} & \mathbf{I}_{2n\times 2n} & \mathbf{0}_{2n\times 2} & & \mathbf{0}_{2n\times m} \\ \hline \mathbf{0}_{2\times 3} & \mathbf{0}_{2\times 2n} & 1 & \tau & \mathbf{0}_{2\times m} \\ & & 0 & 1 & \\ \hline \mathbf{0}_{m\times 3} & \mathbf{0}_{m\times 2n} & \mathbf{0}_{m\times 2} & & \mathbf{\Phi}_{\mathbf{GM}2[m\times m]} \end{array}\right] \tag{8.5}$$

where $\mathbf{\Phi}_k$ is the state–transition matrix at epoch k, which is constant for all k. In Equation 8.5, m is the total number of Gauss–Markov states; in the general case $m = 8$. And, n is the number of periodic signals modelled; in the general case $n = 4$. For a general GPS satellite clock, the ECKF state–transition matrix will be a 21×21 square matrix. In its representation in Equation 8.5, the ECKF state–transition matrix has been partitioned into submatrices (or blocks) as indicated by the dashed lines. Each of the diagonal block relate directly to the four components of the extended clock model (Equation 8.1). In most blocks, the subscript indicates the dimensions of that submatrix. With the exception of the top–right block, denoted $\Phi_{GM1[3\times m]}$, all other blocks are matrices of zeros. Here, each of the blocks of the ECKF state–transition matrix are described.

Φ_s	is the state–transition matrix of the standard clock model component, which is given in Equation 3.24.
$\mathbf{I}_{2n\times 2n}$	is a $2n \times 2n$ identity matrix associated with the periodic signal component of the ECKF state–vector
$\mathbf{\Phi}_{\mathbf{GM}1[3\times m]}$	is the first submatrix associated with the Gauss–Markov component of the ECKF
$\mathbf{\Phi}_{\mathbf{GM}2[m\times m]}$	is the second submatrix associated with the Gauss–Markov component of the ECKF

The elements of the Gauss–Markov submatrices are given in Davis *et al.* [2005b].

The process noise covariance matrix

The process noise covariance matrix for the ECKF is given as

$$\mathbf{Q}_k = \mathbf{Q} = \left[\begin{array}{c|c|cc|c} \mathbf{Q}_s & \mathbf{0}_{3\times 2n} & \mathbf{0}_3 & & \mathbf{Q}_{\mathbf{GM}1[3\times m]} \\ \hline \mathbf{0} & \mathbf{Q}_{2n\times 2n} & \mathbf{0} & & \mathbf{0} \\ \hline \mathbf{0}_{2\times 3} & \mathbf{0}_{2\times 2n} & q_{u_0} & 0 & \mathbf{0}_{2\times m} \\ & & 0 & q_{u_1} & \\ \hline \mathbf{0}_{m\times 3} & \mathbf{0}_{m\times 2n} & \mathbf{0}_{m\times 2} & & \mathbf{Q}_{\mathbf{GM}2[m\times m]} \end{array}\right] \tag{8.6}$$

$\mathbf{Q}_s$	is the process noise covariance matrix of the standard clock model component, which is given in Equation 3.24.
$\mathbf{Q}_{2n\times 2n}$	is a $2n \times 2n$ process noise covariance matrix associated with the periodic signal component of the ECKF state–vector, which has all non–diagonal elements equal to zero.
$\mathbf{Q}_{\mathbf{GM}1[3\times m]}$	is the first submatrix associated with the Gauss–Markov component of the ECKF, given in Davis *et al.* [2005b].
$\mathbf{Q}_{\mathbf{GM}2[m\times m]}$	is the second submatrix associated with the Gauss–Markov component of the ECKF, given in Davis *et al.* [2005b].

The measurement vector

The extended clock model Kalman filter is designed to use GPS satellite clock data from the observed–part of the IGS Ultra–rapid data product and from the IGS Rapid data product. Thus, the measurement vector is expressed as

$$\mathbf{z}_k = \begin{bmatrix} z_{rk} \\ z_{urk} \end{bmatrix} \tag{8.7}$$

where $\mathbf{z}_k$ is the measurement vector at epoch k, z_{rk} is the measurement of the SCTO (or clock difference) from the IGS Rapid product at epoch k and z_{urk} is the measurement of the SCTO (or clock difference) from the IGU-O product at epoch k.

The measurement matrix

The ECKF measurement matrix describes the relationship between the state–vector parameter and the measurements in the form of a linear transformation from state–space to measurement space. The ECKF measurement matrix is given as

$$\mathbf{H}_k = \left[\begin{array}{ccc:c:cc:c} 1 & 0 & 0 & & 0 & 0 & \\ 1 & 0 & 0 & \mathbf{H}_{p[2\times 2n]} & 1 & 0 & \mathbf{H}_{GM} \end{array}\right] \tag{8.8}$$

where $\mathbf{H}_p$ is the $2 \times 2n$ sub–matrix that corresponds to the periodic component of the extended clock model, and $\mathbf{H}_{GM}$ is the sub–matrix of the that corresponds to the Gauss–Markov component of the extended clock model.

$$\mathbf{H}_p = \begin{bmatrix} \sin(\omega_1 t) & \cos(\omega_1 t) & \dots & \sin(\omega_n t) & \cos(\omega_n t) \\ \sin(\omega_1 t) & \cos(\omega_1 t) & \dots & \sin(\omega_n t) & \cos(\omega_n t) \end{bmatrix} \tag{8.9}$$

Input data for the extended clock model Kalman filter

As input data, the proposed prediction method accepts both the IGS Rapid (IGR) satellite clock estimates and the IGS Ultra-Rapid satellite clock estimates, also known here as the observed part of the IGS Ultra-rapid file (IGU–O). IGR files (providing SCTO estimates

corresponding to the previous day) are released at 1700 hours (UTC) each day, resulting in an IGR file latency (RFL) of between 17 and 41 hours. The IGU files are released every 6 hours with a latency of 3 hours to the observed part.

Configuration of extended clock model Kalman filter

In this section, the approach used for the initialisation of the extended clock model state–vector and state–error covariance matrix parameters are described. To produce optimal predictions, the ECKF must be carefully configured for each clock (or clock pair, if predicting clock differences). Mainly, this process involves determining the magnitude of the noise parameters associated with each of the parameters of the state–vector. For the ECKF, this configuration process for the noise processes follow the same configuration method used for the standard clock model Kalman filter, which is described in Section 3.5.

Initialisation of the state–vector parameters

The initial parameters of the state–vector components should be set to realistic estimates, and the leading diagonal elements of the associated state–error covariance matrix should initially be set to values that represent the variance of those initial estimates. The non–diagonal elements should be set to zero. All of the parameters of the periodic signals component, and the Gauss–Markov components should be set to zero. For the Gauss–Markov component, the leading diagonal of the state–error covariance matrix should be set to the steady–state variance for each Gauss–Markov process included [Davis *et al.*, 2005b].

8.3.4 Introducing new information into the EMP system

In the current operational IGS prediction scheme for the GPS satellite clocks, there are five events occurring each day that make new GPS satellite clock information available, and the EMP system is designed to be able to use this information as it is released. These events, listed in table 8.2, include the publishing (on the Internet) of the IGS rapid SP3 at 1700 hours (UTC) every day and the release of the IGS ultra–rapid SP3 files. Every time one of these files are available this new satellite clock information must be introduced into the satellite clock prediction method proposed here. Essentially, this means re–initialising the Kalman filter fives time every day, with new (updated) data sets every time a new IGS data file is released.

Table 8.2 shows how prediction length and latency to the latest rapid file varies over the course of a day. This information is also presented in figure 8.2. Here, the red curve represents the prediction lengths in hours. The blue curve represents the latency to the last available clock measurement in the last published IGS GPS ultra–rapid SP3 file, referred to here as rapid file latency (RFL). There are four discrete jumps in the red curve and one discrete jump in the blue curve. These jumps correspond to the instances when new satellite clock data become available. At those times, the new data is introduced into the

prediction method, as shown in figure 8.1 the KF is re–initialised with this latest available data.

Day	Time (UTC)	Event	PL(hours)	RFL(hours)
0	1700	ig**r**xxxx0.sp3	5	41|17
0	2100	ig**u**xxxx0_**18**.sp3	9|3	21
1	0000	Day boundary	6	24
1	0300	ig**u**xxxx1_**00**.sp3	9|3	27
1	0900	ig**u**xxxx1_**06**.sp3	9|3	33
1	1500	ig**u**xxxx1_**12**.sp3	9|3	39
1	1700	ig**r**xxxx1.sp3	5	41|17
1	2100	ig**u**xxxx1_**18**.sp3	9|3	21
2	0000	Day boundary	6	24

Table 8.2: The daily publishing schedule of new GPS satellite clock information (in the IGS Rapid and IGS Ultra-rapid data products) by the IGS. Here, the prediction length (PL) column indicates the latency to the last available IGU-O estimate. The rapid file latency (RFL) indicates the latency to the last available IGS Rapid estimate.

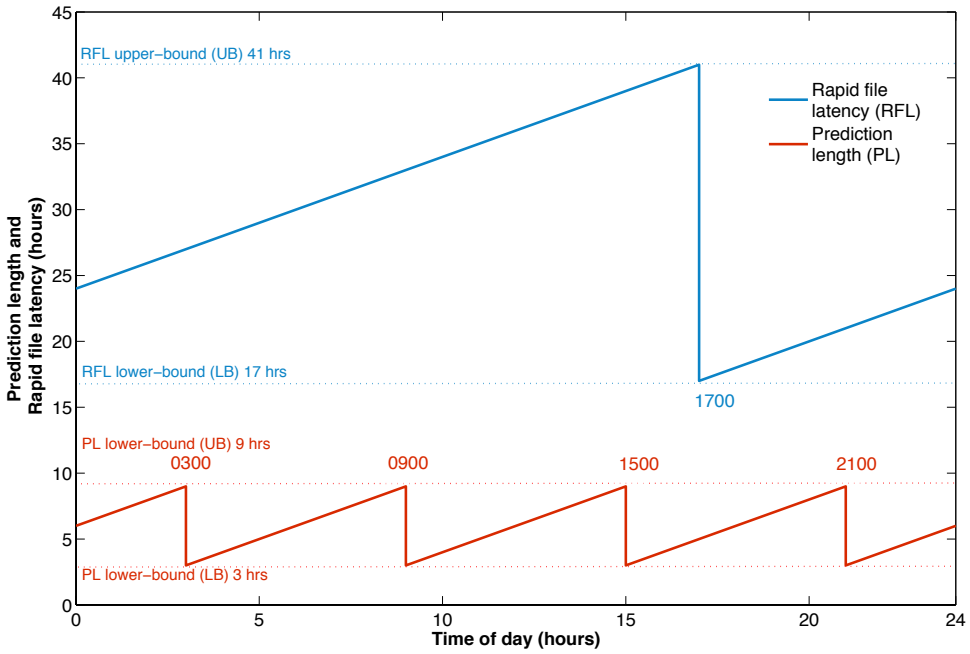

Figure 8.2: The daily publishing schedule of the IGS GPS satellite clock information. The jumps in the red and blue curve indicate the instances when a new IGS Rapid (blue) or new IGS Ultra-rapid(red) becomes available. Such an event reduces the latency to the last available estimated SCTO values, and that is shown clearly in the graph.

Note here that users of the operational IGS prediction scheme only encounter satellite clock predictions at prediction lengths 3–9 hours (as seen in figure 8.2), while users of other IGS–like prediction schemes (i.e. the navigation message satellite clock parameters) may experience prediction lengths across the 0.25–24 hours range. To reproduce the full range of prediction lengths that a user might experience, in this study, only the 0–hour

IGS ultra–rapid SP3 product is used. Further, the 0–hour product is treated as if it is released at 0000 hours and not 0300 hours. As such, the direct comparisons between the new prediction method and the IGS prediction method are only valid in the 3–9 hours range. But outside this range, the comparisons between the IGS method and the new method provides useful information about the properties of the prediction schemes that produce the navigation message clock parameters.

The implication of this is that the results presented in this Chapter represent the output of a prediction scheme that is in some ways only a partial implementation of a complete prediction scheme. Partial in the sense that, here, over the course of twenty–four hours, new satellite clock data is introduced only twice rather than five times in a complete implementation. This means that new information is introduced to the Kalman filter twice daily rather than five times per day.

8.4 Scope of the prediction system development study

Parameters of study	Values
Systems	GPS
Predicted quantities	GPS SCTO, GPS SCD
Timeframe of analysis	July 2011—February 2012
Prediction lengths	0.25–24 (hours)
Data format	SP3 (15–minute sampling rate)
Data sources	IGR (as truth) and IGU (0hrs only))

Table 8.3: Scope of the prediction system development study.

In table 8.3, the key parameters of the prediction system development study are listed. Similar to the performance analysis of the IGS predictions of the GPS satellite clocks, presented in Chapter 6, this study uses the IGS rapid GPS satellite clock solutions as the baseline to represent *true* clock behaviour. In a basic sense, the successes of the new prediction method presented here are judged purely on the results of a direct comparison with the performance of the IGS prediction method. In the version of the EMP system that is developed and tested here, one month is data (July 2011) is used for configuring the ECKF (i.e. determining the parameters of the noise processes). Then, the prediction algorithm is operated on the following six months of data (August 2011–February 2012) and the predictions of the EMP system are compared with the predictions of the IGS system.

8.5 Method

In this study, the properties of a proposed GPS satellite clock prediction strategy, referred to herein as the extended model prediction (EMP) system, are explored. The prediction strategy that is developed and tested represents a partial implementation of a potentially complete prediction system. For this partial implementation, only the the IGU–O SCTO estimates from the IGU files 18–hour and 0–hour IGU files released at 2100 and 0300

hours, respectively, are required. A complete implementation would use the full set of 0, 6, 12 and 18 hour IGU files. The reasons behind this choice are given in Section 8.4. In the following list, a step–by–step description of the clock prediction system development study is given. Note, this is not a description of the satellite clock prediction method as such. Rather, this the method associated with the study itself.

1. **Steps 1–4 of the IGS prediction scheme performance analysis,** as presented in **Chapter 6**. These steps populate a database that includes time–series of IGS Rapid satellite clock data, and IGU–P satellite clock predictions, separated on a satellite–by–satellite basis (by GPS PRN). This database also includes time–series of IGS satellite clock time offset (SCTO) prediction errors with the the IGS Rapid Timescale as reference, $E_{igr,i,p}$, and time–series of IGS GPS satellite clock difference prediction errors, $E_{ij,p}$ spanning 2012. On top of these however, a time–series of IGU–O SCTO estimates are also required in this study. The database is populated with the IGU–O satellite clock information in the same way as with the IGU–P SCTO information is collected.

2. The 18–hour IGU is released at 2100 hours each day and there is 6 hours of data overlap between the IGU–O component of this file and the IGR data set corresponding to the previous day. In this step, the 6–hour overlapping segments of IGR and IGU–O data are extracted and for each satellite clock the difference, $D_{Ri,n}$, is taken according to,

$$D_{Ri,n} = (T_{igr} - C_i)_n - (T_{igu} - C_{i,o})_n \tag{8.10}$$

   where $T_{igu} - C_{i,o}$ is the estimated (i.e. observed) value of the SCTO for clock i at time n. Over the 6–hour time segment, the average of the $D_{Ri,n}$ quantity at each epoch n is taken over all active satellite clocks to produce a single 6–hour time–series. As explained in Subsection 6.4.2, such a time–series represents a good approximation of the $T_{igr} - T_{igu}$ timescale offset. Then, the time offset and fractional frequency offset (from IGRT) of the combined $D_{Ri,n}$ time–series are estimated as parameters, using a least–squares (minimum–mean–square error) technique. These parameters are used to project the combined $D_{Ri,n}$ forward, and a time—series that corresponds to the 0–hour IGU–O data set of the following day is generated. The projected time–series is then subtracted from the 0–hour IGU–O SCTO estimates. The resulting time–series is a "corrected" IGU–O data set. **In theory, the $T_{igr} - T_{igu}$ timescale offset is accounted for in this data–preprocessing step.**

3. **Estimation and prediction of SCTO, with IGRT as reference,** using the Extended Clock Model expressed in Kalman filter form, as explained in Section 8.3.3. The pre–processed 0–hour IGU–O data along with IGR data are used as inputs to a Kalman–filter based estimator and predictor. The estimated quantities are the parameters of the Extended Clock Model (ECM). Here, to simulate a real–time process, new data is introduced to the Kalman filter twice per day: once at 1700 hours when the IGR files are released, and once at 0300 hours when 0–hour

IGU files are released. In the EMP system, only the chosen reference clock, in this case, the SVN 55 IIR–M Rb clock has to be predicted in this way. For all other clocks, the SCTO with IGRT as reference, can be recovered from the predictions of the difference between those clocks and the reference clock.

4. **Estimation and prediction of differences between satellite clock pairs, with the SVN 55 IIR–M Rb as the reference clock.** This process is similar to the previous step, the only difference is that the input data are clock differences, and because clock differences are unaffected by $T_{igr} - T_{igu}$ the 0–hour IGU–O satellite clock difference are not pre–processed as described in step 2. The EMP method always uses a reference clock.

8.6 Results

A selection of key results that give an insight into the general properties of the EMP method, specifically in relation to how the performance of the EMP method compares with the performance of the IGS SCTO prediction method, are presented in this section. These results are the product of a collaboration between the author and J. A. Davis of the National Physical Laboratory (NPL), UK. The analysis, presentation and discussion of these results in this thesis are the author's own contribution to this work.

8.6.1 Single clock against the IGS rapid timescale

Figure 8.3 shows two curves, one labelled IGU–P and the other EMP; these curves represent the RMS SCTO error (where the reference timescale is the IGS Rapid Timescale (IGRT)) of the predictions that are generated by the IGS scheme and the EMP method, respectively, and correspond to the GPS SVN 55 IIR–M Rb clock. Here, the RMS calculation uses 182 days of predictions, over a range of prediction lengths from fifteen minutes to twenty four hours, from the time period between 1 August 2011 and 29 February 2012.

In this specific case, as far as SCTO predictions using the IGRT as reference are concerned, the prediction errors from the EMP method are lower than the prediction errors of the IGS, at all prediction lengths shown, by a factor of around 5 and 10. In fact, such a result is typical for the entire constellation of GPS satellite clocks because a substantial component of the IGS prediction errors is the $T_{igr} - T_{igu}$ timescale offset signal, which is common to all IGS GPS satellite clock predictions. The exceptions are the older IIA Cs clocks, and to a lesser extent the IIA Rb clocks where the higher noise levels mask the timescale offset signal.

Due to the influence of the $T_{igr} - T_{igu}$ timescale offset, the predictability of GPS satellite clocks with IGRT as reference is not a good metric for the true performance of a satellite clock prediction method. However, in reporting the performance of their GPS satellite clock predictions, the IGS themselves use SCTO prediction error with respect to IGRT, see figure 6.1. This metric is also used in Heo *et al.* [2010] and Huang *et al.* [2013] to assess the performance of the prediction methods proposed in those studies, and for

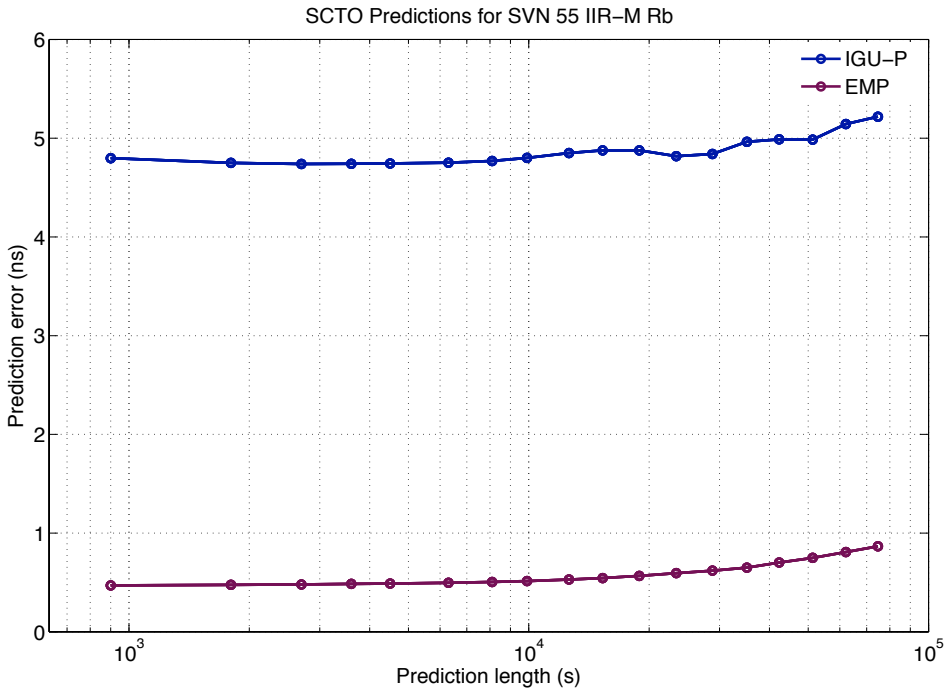

Figure 8.3: Comparison of SCTO prediction errors: the IGU–P against the results of the EMP method. The prediction errors shown here are root mean square (RMS) values, calcuated using prediction errors at a range of prediction errors lengths (15 minutes–24 hours), over 182 days (1 August 2011 to 2 February 2012).

this reason the performance of the EMP method in predicting individual GPS SCTO from IGRT are presented here also.

On the other hand, the IGS prediction of the difference in SCTO between two satellite clock pairs is not affected by timescale offset problem and therefore gives a more suitable indication the true performance of satellite clock predictor as well as the impact of predictability on positioning. Results of the EMP method in predicting the difference between satellite clock pairs are presented in the following Subsection (8.6.2).

8.6.2 Satellite clock difference predictions

Here, in studying the performance of the EMP method in predicting satellite clock differences (SCD), the GPS SVN 55 IIR–M Rb clock, is chosen as the reference clock. This is a suitable choice because this is a modern, highly predictable (relative to the other clock in the constellation) clock and for the period of this study (July 2011 to February 2012) there is a full set of IGS data (i.e. no data gaps or outliers) for this clock.

Figure 8.4 comprises two curves that represent the RMS error of the predictions of the difference between the SVN 55 and SVN 50 satellite clock pairs. Both clocks belong to the IIR/IIR–M Rb category. The blue curve, labelled IGU–P, represents prediction errors of the IGS method and the other purple curve represents errors of the EMP method. Again, the RMS is calculated using 182 days of data, from August 2011 to February 2012, and the prediction lengths considered fall into the range fifteen minutes to twenty four hours.

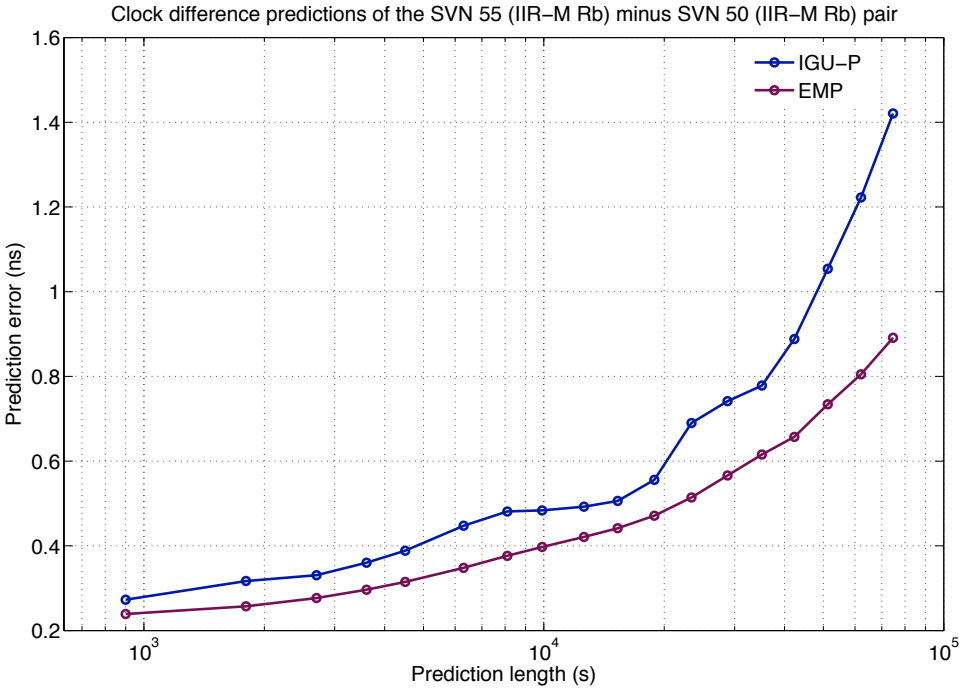

Figure 8.4: Comparison of GPS clock difference prediction errors: the IGU–P against the results of the EMP method. The prediction errors shown here are root mean square (RMS) values, calcuated using prediction errors at a range of prediction errors lengths (15 minutes–24 hours), over 182 days (1 August 2011 to 2 February 2012).

Here, in the case of this satellite clock pair, the EMP method outperforms the IGS method in that prediction errors are lower at all the prediction lengths considered. However, the difference in performance between these two methods is less than it is in the case of predictions against IGRT, which are shown in Subsection 8.6.1. Mainly, this is because of the difference between satellite clocks is not affected by the $T_{igr} - T_{igu}$ timescale offset problem.

Prediction length (days)	**IIA Cs**		
	IGU–P (ns)	**EMP (ns)**	**IGU–P:EMP**
0.25	4.70	4.27	1.10
0.5	6.52	5.94	1.10
0.75	8.87	7.87	1.13
1.0	10.30	9.35	1.10

Table 8.4: Average across the IIA Cs clocks, of the RMS errors in the prediction of the difference between satellite clock pairs, with the SVN 55 IIR–M Rb as the reference clock, at prediction lengths of 6, 12, 18 and 24 hours. Predictions of the IGS method (IGU–P) and the EMP method are used here. The prediction error ratio of the IGU–P results to the EMP results are also shown.

This result that the EMP method outperforms the IGS method in predicting the difference between satellite clock pairs, in the cases where the SVN 55 IIR/IIR–M Rb is the reference clock, is seen in all GPS satellite clock types. This is shown in figure 8.5, where the clock difference prediction errors (CDPE) of the average IIA Cs, IIA Rb and IIR/IIR–M Rb

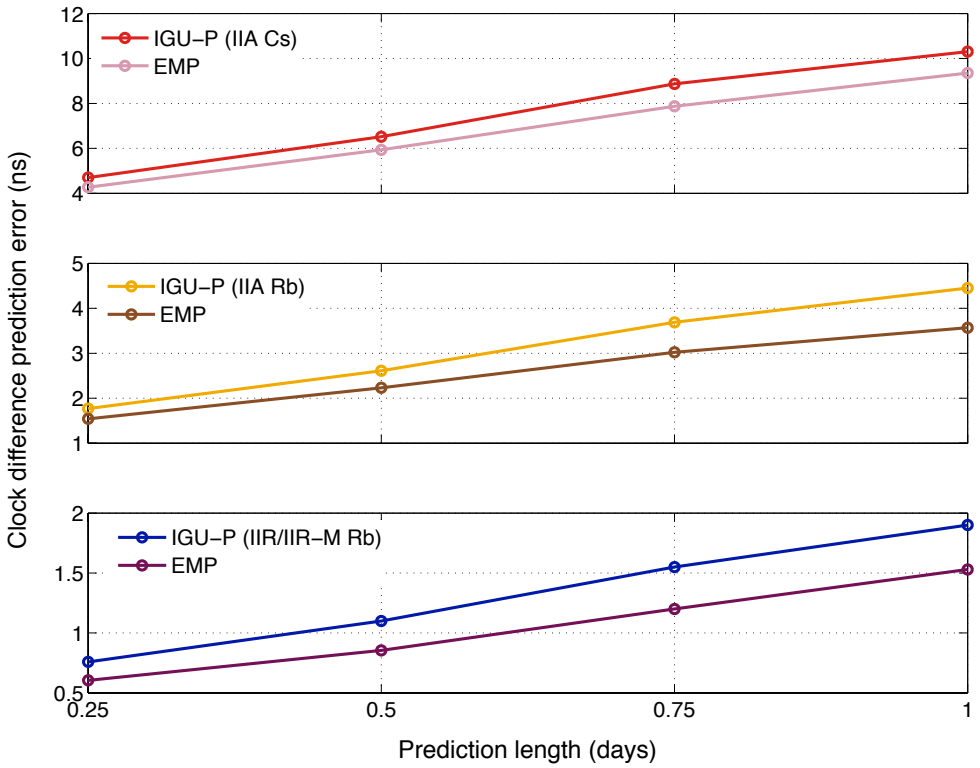

Figure 8.5: Comparison of GPS clock difference prediction errors: the IGU–P against the results of the EMP method. Here, the (ensemble) average of 4 clocks is used for the IIA Cs curves, 3 clocks for the IIA Rb curves and 12 clocks for the IIR/IIR–M Rb curves. The prediction errors shown here are root mean square (RMS) values, calcuated using prediction errors at a range of prediction lengths (15 minutes–24 hours), over 182 days (1 August 2011 to 2 February 2012).

based on the IGS method are compared with the clock difference prediction errors of the EMP method at four prediction lengths: 6, 12, 18 and 24 hours. The average IIA Cs prediction is calculated using RMS errors from four satellites: SVN 24, 33, 38, 40. In the IIA Rb case, the average clock difference prediction error was calculated using three satellite clocks: SVN 26, 34 and 36. For the IIR Rb average values, twelve satellite clocks were considered: SVN 41, 43, 45, 46, 48, 50, 51, 54, 58, 59, 69, and 61. The IIF category of satellite clocks were not considered because there was insufficient data corresponding to this time period this analysis.

Prediction length (days)	IIA Rb		
	IGU–P (ns)	EMP (ns)	IGU–P:EMP
0.25	1.77	1.54	1.15
0.5	2.61	2.23	1.17
0.75	3.69	3.02	1.22
1.0	4.45	3.57	1.25

Table 8.5: Average across the IIA Rb clocks, of the RMS errors in the prediction of the difference between satellite clock pairs, with the SVN 55 IIR–M Rb as the reference clock, at prediction lengths of 6, 12, 18 and 24 hours. Predictions of the IGS method (IGU–P) and the EMP method are used here. The prediction error ratio of the IGU–P results to the EMP results are also shown.

Prediction length (days)	IIR/IIR–M Rb		
	IGU–P (ns)	EMP (ns)	IGU–P:EMP
0.25	0.758	0.606	1.25
0.5	1.10	0.855	1.29
0.75	1.55	1.20	1.29
1.0	1.90	1.53	1.24

Table 8.6: Average across the IIR/IIR–M Rb clocks, of the RMS errors in the prediction of the difference between satellite clock pairs, with the SVN 55 IIR–M Rb as the reference clock, at prediction lengths of 6, 12, 18 and 24 hours. Predictions of the IGS method (IGU–P) and the EMP method are used here. The prediction error ratio of the IGU–P results to the EMP results are also shown.

In the case of the IIA Cs clocks, at all prediction lengths, as specified in Table 8.4, the CDPE prediction errors of the EMP method are about 10% lower than those of the IGS method. In the case of the IIA Rb clocks, the CDPE prediction errors of the EMP method are between $15-25\%$ lower than those of the IGS method, with the percentage CDPE reduction increasing with prediction length, as indicated in Table 8.5. Finally, if the IIR/IIR–M Rb case, the EMP prediction errors are between $24-29\%$ lower than than those of the IGS method, as indicated in Table 8.6. In all examined categories of satellite clock the EMP method outperforms the IGS method in the prediction of clock differences, with the SVN 55 IIR–M Rb as reference clock, in that prediction errors are lower at all prediction lengths.

8.6.3 The impact of the $T_{igr} - T_{igu}$ timescale offset modelling strategy

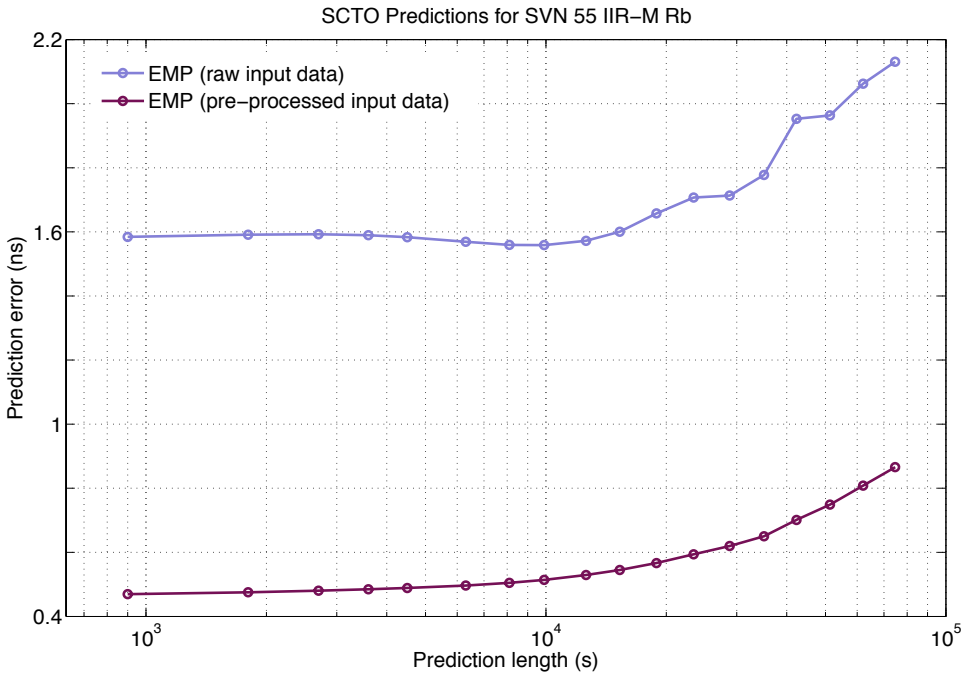

Figure 8.6: Comparison of errors in SCTO prediction of the SVN 55 IIR–M Rb clocks, between two versions of the EMP method: one using IGU–O data pre–processed according to step 2 in Section 8.5 (dark–purple) and the other using raw, unprocessed IGU–O data (light–purple) as inputs to the Kalman filter predictor. The prediction errors are RMS values computed using 182 days of data.

The effectiveness of the data pre–processing strategy described in Section 8.5 (Step 2) is examined here. The purpose of this pre–processing step is to remove the bulk of the $T_{igr} - T_{igu}$ timescale offset from the IGU–O SP3 data which the KF filter predictor receives as input data. It is this un–processed IGU–O SP3 data that is referred to as raw input data in figure 8.6. In this figure, the raw input data curve indicates prediction errors of the EMP method where raw IGU–O data is used, and the (EMP) pre–processed data curve is the same EMP curve that is also in figure 8.3. According to figure 8.6, at all prediction lengths considered here, there is a clear improvement in the SVN 55 IIR–M Rb SCTO predictions with the EMP method when the "corrected" IGU data is fed into the KF predictor. For the IIR/IIR–M Rb clocks, this is a typical result. For the IIA Rb and IIA Cs clocks, the improvement is less obvious for the same reasons as given in Subsection 8.6.1. The extent of the benefit of this pre–processing method is likely to dependent on the magnitude and variability of the $T_{igr} - T_{igu}$ signal during the prediction period. In the case of predicting the difference between the satellite clock pairs using the EMP method, no data pre–processing is required. The differencing process cancels out the $T_{igr} - T_{igu}$ signal.

8.6.4 Predicting the periodic signals

Here, the ability of the EMP method to effectively account for the periodic signals seen in the GPS satellite clocks is demonstrated. In figure 8.7, two versions of the EMP method are compared: the full EMP (purple) and the EMP minus the periodic component of the extended clock model (orange). The effectiveness of the EMP in accounting for the period signals is examined by studying the FFT–based power spectral density (PSD) periodogram of the Kalman filter residuals of the full EMP method with the PSD periodogram of residuals of the EMP minus periodic components method. Here, the residuals are RMS values computed using the KF residuals of the same 182 days of data as indicated in Subsection 8.6.1. In figure 8.7, the periodogram from the EMP minus periodic components method is overlaid on top of the periodogram corresponding to the full EMP method. Signals with period of about 3, 6 and 12 hours are clearly seen in the EMP minus periodic components method periodogram, but absent in the full EMP method periodogram. This is a good visual indication that the EMP method is effectively capturing the periodic signals present in the difference between the SVN 55 IIR–M Rb and SVN 50 IIR–M Rb satellite clock pair.

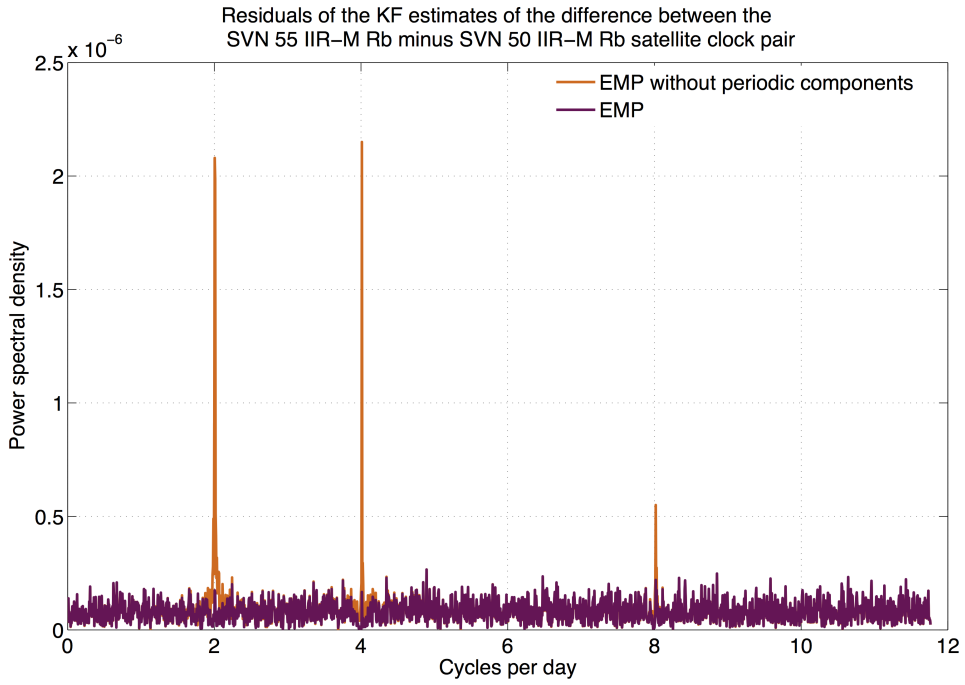

Figure 8.7: Comparing the residuals of the KF estimates of clock differences (with and without periodic components in the EMP method) in a power–spectral density periodogram. Signals with period of about 3, 6 and 12 hours are clearly seen in the EMP minus periodic components method periodogram, but absent in the full EMP method periodogram. This is a good indication that the EMP method is effectively capturing the periodic signals present in the difference between the SVN 55 IIR–M Rb and SVN 50 IIR–M Rb satellite clock pair.

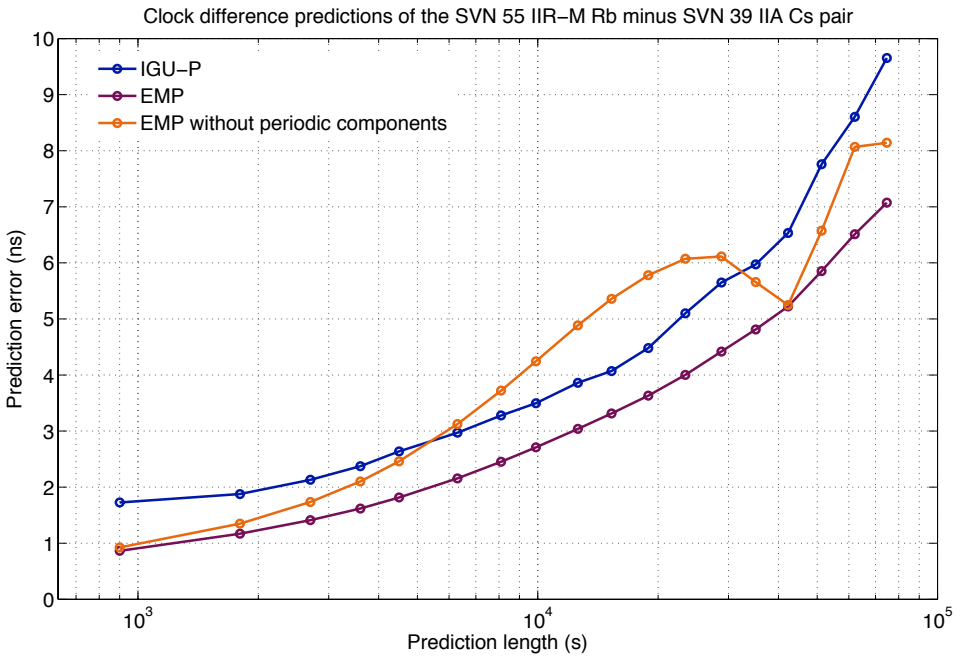

Figure 8.8: Comparing the errors in the predictions of the difference between the SVN 55 IIR–M Rb and SVN 39 II–A Cs satellite clock pair from three different prediction strategies: IGU–P, (full) EMP and EMP without periodic components.

In figure 8.8, the errors in the predictions of the difference between the SVN 55 IIR–M Rb and SVN 39 II–A Cs satellite clock pair from three different prediction strategies: IGU–P, (full) EMP and EMP without periodic components are compared. At prediction lengths 12 hours and close to 24 hours there is good agreement between the full EMP method and the EMP without periodic components. These prediction lengths are integer multiples of the periodic signals of 3, 4, 6 and 12 hours that are present in the periodic component of the extended clock model. At all other prediction lengths, the inclusion of the periodic component in the (full) EMP results in a clear improvement in prediction performance. It appears there might be some periodic behaviours in the IGU–P curve also, but to a large extent the periodic signals are well captured by the IGS predictor also. It is known that some, but not all, analysis centres that contribute to the IGU product include periodic terms in their models Ray [2000].

8.6.5 The stochastic model

In figure 8.9, the Allan deviation and Hadamard deviation statistics of the differences between the SVN 55 IIR–M Rb and SVN 50 IIR–M Rb satellite clock pair are compared with the prediction errors of the EMP method for that same pair. To produce the ADev and HDev–based sigma–tau curves shown in figure 8.9 the Allan deviation and Hadamard deviation statistics were computed over a range of analysis intervals for the SVN 55 IIR–M Rb and SVN 50 IIR Rb satellite clock pair. IGS Rapid data was used for this, and the results were plotted on a log–log scale. To generate the prediction error over prediction length curve, the prediction errors of the EMP method were used. Again, the prediction

errors are an RMS quantity with the RMS value computed using 182 days of EMP output. Here, the slope of about $-\frac{1}{2}$ on the HDev sigma–tau curve indicates that the dominant noise process is WFM. In this case, for an optimally configured predictor, a close agreement is expected between the Allan deviation (or Hadamard) deviation statistic and the prediction error to prediction length ratio quantity, denoted here as $\frac{E_p}{\tau_p}$, at all averaging intervals. This is based on the prediction error deviation equation given in Section 3.6.

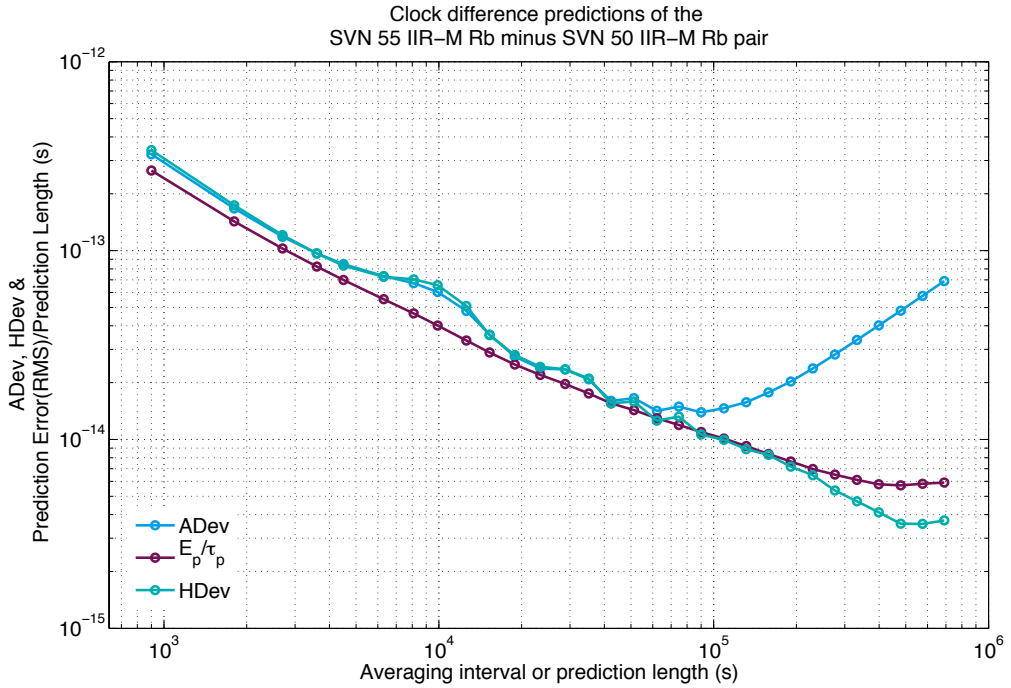

Figure 8.9: ADev, HDev and $\frac{E_p}{\tau_p}$ sigma–tau curves for the SVN 55 IIR–M Rb and SVN 50 IIR–M Rb pair. The close level of agreement between the ADev/HDev sigma–tau curves with the $\frac{E_p}{\tau_p}$ sigma–tau curves indicates that the EMP method is producing close to optimal estimates of this satellite clock pair at a range of averaging times.

In figure 8.9, at averaging intervals below 5000 seconds there is good agreement between the ADev and HDev curves, and the $\frac{E_p}{\tau_p}$ sigma–tau curve. In this range of averaging times, it appears that the ADev and HDev values exceed the $\frac{E_p}{\tau_p}$ values. Taken at face value, this would suggest that the EMP system is performing better than optimal at prediction lengths below 5000 seconds. However, as mentioned in Section 5.3.1, this result is likely to be due to the shape of ADev/HDev sigma–tau curves being affected by the presence of periodic signals.

At averaging times greater than one day, the ADev is dominated by linear frequency drift. So at longer averaging times, to evaluate the performance of the stochastic component of the extended clock model, one should compare the $\frac{E_p}{\tau_p}$ sigma–tau curve with the HDev sigma–tau curve. In this case, up to 20,000 seconds there is a good agreement between the HDev curve and the $\frac{E_p}{\tau_p}$, before the two curves separate. Based on this evidence, it can be stated that the EMP system is able to produce close to optimal predictions of the difference between the SVN 55 IIR–M Rb and SVN 50 IIR–M Rb satellite clock pair

at prediction lengths up to 20,000 seconds.

8.7 Key findings

The key findings of the GPS satellite clock prediction algorithm development study, which is presented in this chapter are listed here. These are:

- Using predictions of SCTO with IGRT as reference as a metric of performance, the EMP method considerably outperforms the IGS method. Predictions errors are typically 4 ns in the IGS case, but between 1 and 2 ns in the case of the EMP method. The bulk of this improvement originates from the handling of the $T_{igr} - T_{igu}$ timescale offset by the EMP method.
- Using predictions of the difference between satellite clock pairs with the SVN 55 IIR–M Rb as the reference clock as a metric of performance, the EMP method also outperforms the IGS method, although in this case the difference in performance between the two methods is less. For the IIR/IIR–M Rb clocks, the prediction errors using the EMP method are typically $25 - 30\%$ smaller at prediction lengths 6, 12, 18 and 24 hours.
- The improvement in the EMP method over the IGS method is greatest in the IIR/IIR–M Rb clocks.

8.8 The limitations of the EMP system

This section discusses the limitations of the the EMP system as it currently stands. Specifically, the question being considered here is: What are the key issues preventing (or discouraging) the methods that have been developed as part of the EMP system, some of which have been successfully demonstrated in this chapter, from being being absorbed into the operational IGS GPS SCTO prediction system? Here, there are several issues to consider:

- The critical quantity that determines the link between satellite clock estimation (or prediction) error and GNSS performance (for PNT applications) is the estimation (or prediction) error of the difference between satellite clock pairs. This quantity represents the extent of the mis–synchronisation of all of the satellite clocks amongst themselves. In the work presented in this chapter, a single satellite was chosen as a reference clock (SVN 55 IIR–M Rb) in order to study the properties of the EMP system in predicting the difference between satellite clock pairs. The results indicate that the methods of the EMP system produced improved predictions (compared to the IGS prediction system) of the difference between satellite clocks paired with the SVN 55 IIR–M Rb clock. But, for a meaningful improvement in GNSS PNT performance, the predictions of all satellite clock differences must be improved. The full set of GPS satellite clock difference pairs are not considered in this study, but this could be explored in future work.

- The complexity of the EMP system is a major limitation. Each GPS satellite clock (or satellite clock pair) must be configured separately, and the configuration process is manual and difficult to automate.

Summary

In this chapter, a new GPS satellite clock prediction strategy, the EMP method, is presented. The EMP method produces predictions of GPS SCTO with respect to the IGS Rapid Timescale, but also predictions of the difference between satellite clock pairs. In a wide variety of cases, the EMP method outperforms the prediction method of the IGS. The reasons for this have been attributed to several features of the EMP method: correcting for the $T_{igr} - T_{igu}$ timescale offset, accurate modelling of linear frequency drift and periodic signals in the presence of complex noise processes, and making full use of all available clock data (IGR and IGU) in the KF predictor. In the following chapter, the concluding chapter of this research thesis, the wider implications of these results in the overall GNSS context are discussed. Also, the limitations of the work are acknowledged and ideas for possible future work are presented.

Chapter 9

Conclusions and discussion

Chapter outline

The first section (9.1) of this chapter gives an overview of this thesis, and the second section (9.2) summarises the project in relation to the statement of general objectives that was given in Chapter 1. This is followed by Section 9.3 where the main findings of this research are presented in relation to the detailed objectives given in Chapter 1. In Section 9.4, the main research contributions of this work—in the view of the author—are stated. Section 9.5 is a discussion of current and planned future developments in the GNSS field, with an emphasis on the challenges associated with the satellite clock time synchronisation problem that remain pertinent in this context. Section 9.6 closes this thesis by presenting some ideas for follow–on work.

9.1 Overview of the thesis

Chapter 1 is the introduction of this thesis giving the context, motivation and objectives of the project. In Chapter 2, the essential aspects of the theory and applications of GNSS—as far as the topic of the satellite clock time offset is concerned—are presented. Chapter 3 introduces the principles of precise time and frequency metrology, which provide the set of tools that are called upon in the clock prediction method. In Chapter 4, the published literature on the topic of the satellite clock time offset in GNSS is reviewed. Also, the data sources and software tools used in the study are presented here. Chapter 5 presents the results of an in–depth characterisation of GPS and GLONASS clocks. In Chapter 6, the performance of an operational prediction scheme, the IGS predictions of the GPS satellite clock time offsets, is studied and discussed. In Chapter 7, the results of a study into the relativistic component of the model for GNSS SCTO is presented. In Chapter 8, the development of a new strategy for GPS satellite clock prediction is presented. The results of this new SCTO prediction algorithm are compared against the predictions of the IGS, and the implications of the results are discussed.

9.2 Summary in relation to the general objectives

The ultimate aim of this research was the development of a SCTO predictor, motivated principally by the link between SCTO prediction error and GNSS performance. Here, the SCTO prediction problem was broken down into four components: characterisation, modelling, estimation and prediction. The reason for this was that the SCTO prediction problem as a whole is a vast one; breaking it down in this way helps to make the problem tractable and easier to explain. Also, it requires a good understanding of each of these parts in order to build an effective SCTO predictor.

The performance of the SCTO prediction algorithm developed here was assessed by comparing the results of this algorithm with the predictions of GPS SCTO's generated by the IGS prediction scheme. In the prediction scenarios presented in this thesis, the developed prediction algorithm performs better than the IGS one, in most cases (better in the sense that RMS prediction errors are lower, over a range of prediction lengths). The performance improvement is attributed to several sources, which include the careful consideration of the linear frequency drift phenomenon (especially in the rubidium clocks) and modelling of periodic signals seen in the SCTO estimates of some but not all GPS clocks. Also, the *apparent* performance of the IGS prediction scheme—and actually all GNSS navigation–message type SCTO prediction schemes—is degraded by discrete jumps in SCTO prediction error at the boundary between two consecutive prediction sets. Here, a method is devised to account for these discrete jumps to improve prediction performance in such cases.

But, these results must be considered with care. The predictions of the IGS are the output of an operational scheme, which was set up over ten years ago [Ray, 2000]. Also, for positioning applications, it is not the absolute value of the SCTO prediction error of the clocks, individually, that affects positioning accuracy. Rather, because the effects of errors that are common across all satellites used in a position estimator tend to cancel—to a large extent, they are absorbed into the receiver clock time offset parameter—it is the extent of the *mis*-synchronisation between the satellite clocks that is of interest. And so, the performance of a GNSS SCTO prediction scheme should be judged not on the analysis of prediction errors relative to some reference timescale but rather on an analysis of prediction errors of the differences between pairs of satellite clocks.

9.3 Achievement of detailed objectives and conclusions

The detailed objectives of this project are the research tasks that were designed, at the beginning, to aid in the achievement of the general objective. In this section, the outcomes of the research in relation to each of the detailed objective are described, and the findings are summarised.

9.3.1 A characterisation of the GPS and GLONASS satellite clocks

This part of the project began with an assessment of all available GPS and GLONASS satellite clock (estimates) data[1]. Several years of data were looked at (2010 onwards), but ultimately the decision was made to work with 2012 data only. The reason for this was that the amount of data considered (i.e. one year's worth) was deemed sufficient for the purposes of justifying the findings that are presented in this thesis. For GPS, the full set of IGS SP3 Final clock products for 2012 was used. In the GLONASS case, the full set of ESA Final SP3 clock products for 2012 was used.

Method

The characterisation of the GPS satellite clock behaviours began with an analysis of the time–series of the raw (unprocessed) IGS Final SP3 clock estimates, followed by an assessment of the time–series of the same data with a linear trend removed. This was followed by time–domain stability analysis using several time–domain statistical measures for characterising clock frequency and phase variations: Allan deviation, Hadamard deviation, Modified Allan deviation and Dynamic Hadamard deviation. The results of (time–domain) stability analysis are used in the configuration of a Kalman filter estimator based on the standard clock model. The individual states of the standard clock Kalman filter: time–offset, normalised frequency offset and linear frequency drift are examined. Also, an FFT–based spectral analysis of the standard clock Kalman filter residuals is conducted for two reasons: to determine the presence of any periodic signals in the GPS satellite clocks and to probe further into the nature of the underlying noise processes.

In the case of the GLONASS satellite clocks, first, the time–series of the raw (unprocessed) and detrended (linear trend removed) ESA Final SP3 clock estimates were examined. Also, a time–domain stability analysis was performed using the ADev, HDev and MDev statistics. Based on the results coming out from these analyses, and also due to issues relating to the ESA data set, the GLONASS clocks were not studied to the same depth as was the case with the GPS clocks.

For both GPS and GLONASS, satellite clocks for which there are large quantities of missing data, or for which the data set suffers from discontinuities (due to steps in phase or frequency) are not considered in this study. In the GPS case, without exception, it was the full 2012 time–series data sets for the older GPS IIA Rb (of which there were five in orbit) and GPS IIA Cs (of which there were four in orbit) satellite clocks that contained large quantities of missing data. There were missing data points in the time–series for the other GPS IIR/IIR–M Rb and GPS IIF Rb satellite clocks, but these were limited to single epochs, and thus were easily managed by the data processing software.

[1] Although, Galileo SCTO data was available, it was limited in both quality and quantity. Beidou was not considered.

Conclusions

For the GPS case, the key conclusion of the characterisation study is that in terms of high–performance GPS SCTO modelling, each satellite clock should be considered on a clock–by–clock basis. The features relevant for modelling include linear frequency drift, periodic signals and the complexities of the underlying noise processes. In the standard clock model, these features are either accounted for in a basic way or they are not accounted for entirely. In the GLONASS case, the frequency stability analysis indicates that the behaviour of GLONASS satellite clocks is uniform across the GLONASS constellation, and as such a relatively simple modelling approach can be recommended. This model is applicable to all GLONASS clocks.

With regards to a comparison between the GPS and GLONASS clocks, in terms of predictability, the GPS clocks comprehensively outperform the GLONASS clocks, at prediction intervals in the range 900–86,400 seconds. In 2012, the GPS satellite clocks were about 3–4 times more predictable than the GLONASS satellite clocks.

9.3.2 Performance analysis of operational prediction schemes

The objective of this part of the study was to analyse, in depth, the performance of an operational GNSS SCTO prediction scheme.

Method

The IGS predictions of the GPS satellite clocks, provided in SP3 format by the IGS in the predicted part of the IGS ultra–rapid (IGU–P) files, were studied. The IGS SP3 Rapid GPS satellite clock estimates were used as a truth model. One whole year (2012), and the full constellation of (available) satellites were considered. The IGS predictions of individual GPS satellite clocks against the IGS Rapid timescale were studied. The IGS predictions of the differences between GPS satellite clocks were also considered. For the purpose of studying clock difference predictions, the active satellite clock of GPS SVN 50 (IIR Rb) was used as the reference clock. The GPS SVN 50 IIR Rb was chosen as the reference clock for this study because this was one of only four GPS satellite clocks for which there was a complete and continuous time–series of IGS satellite clock solutions. The IGS GPS satellite clock difference prediction errors (CDPEs) were compared against a theoretical performance limit indicated by frequency stability analysis.

Conclusions

Here, the GPS satellite clock prediction errors for individual clocks are strongly influenced by a common signal, which is the IGS Rapid Time (IGRT) versus IGS Ultra Time (IGUT) ($T_{igr} - T_{igu}$) timescale offset, which has a typical value of 9.2 ns across 2012. This signal is closely related to the offset between IGS Time, T_{igs}, and GPS Time, T_g. However, the IGS predictions of the difference between satellite clock pairs are not affected by this timescale offset quantity. Studying the IGS predictions of the GPS CDPEs, it seems that

the performance of the IGS prediction algorithm is degraded by the mis–modelling of the features of linear frequency drift and periodic signals, which is significant in many cases across the full set of GPS in–orbit clocks.

9.3.3 Enhanced relativistic time transformation modelling

This component of the project was an investigation into the impact of approximation errors in GNSS relativistic time transformation modelling methods in the broader context of GNSS SCTO modelling. The objective was to develop the capability to model the GNSS RTT more rigorously, which in turns means that SCTO is modelled more rigorously, using a detailed description of gravitational potential variations based on the Earth Gravity Model 2008 (EGM08) up to degree and order 20.

Method

Here, the investigation was limited to GPS satellite clocks. This enhanced RTT model requires satellite—receiver relative velocities and the Earth's gravitational potential at the satellite's position as input. For the former, IGS SP3 Final GPS satellite clock data was used, and for the latter several satellite geopotential time–series were computed (corresponding to satellite orbits from the IGS SP3 final data set) using EGM08 coefficients up to degree 1, 2, 3, 4, 5, 10 and 20. The RTT was computed separately using each geopotential time–series, over a range of integration arc–lengths (15 minutes, 3 hours, 6 hours, 12 hours and 24 hours), and these results were compared.

Conclusions

In the context of SCTO modelling for the purposes of SCTO prediction, the key finding form this component of the study was that the periodic effects observed in the GPS SCTO data sets were not caused by mis–modelling of the GPS RTT. Further, the results suggest that there is no observable (in the best available data) improvement to be expected in RTT modelling accuracy through the use of high–fidelity Earth gravity models. Rather, because the other inputs to the RTT models are the satellite orbit position and velocity, it might be that a more significant performance improvement is achieved through the use of high–fidelity orbit prediction models.

9.3.4 Performance testing of the developed SCTO prediction algorithm

In this research, a new GPS satellite clock time offset prediction method was developed. In many aspects (i.e. in terms of the inputs to the algorithm, the way in this prediction scheme was imagined to operate, etc.), this new SCTO prediction method was based around the IGS predictions of the GPS SCTOs. The fundamental component of this new prediction algorithm is an extended model of the SCTO, and for this reason this method is referred to as the extended model prediction method (EMP). The outputs of the EMP method were compared against the outputs of the IGS prediction scheme. The predicted

quantities compared include individual SCTO prediction errors, and also the prediction errors of the difference between satellite clock pairs. Using the prediction of SCTO with IGS Rapid Time as the reference timescale as a metric of performance, the EMP method outperforms the IGS method considerably. In this case, prediction errors are typically 4 ns in the IGS case, but between 1–2 ns in the EMP case. Most of this improvement arises from the ability of the EMP method to account for the $T_{igr} - T_{igu}$ timescale offset, which it manages by making use of both IGS Rapid and IGS Ultra-rapid SCTO data in the prediction model. In the case of CDPEs, in most cases the EMP method outperforms the IGS method by between 10% to 30% with the magnitude of the perform improvement dependent upon clock type.

9.4 Research contributions

During the course of this project, the following original work was conducted:

- An in–depth, clock–by–clock characterisation of the in–orbit behaviour of GPS and GLONASS satellite clocks. There is no such prior study of the GLONASS satellite clocks published in the literature, perhaps, because the data to conduct such an analysis has only become available in recent years[1]. As such, the report on the characteristics of GLONASS satellite clocks presented in Chapter 5 of this thesis goes some way towards addressing this issue. In a frequency stability sense, the GPS satellite clocks were found to be 3–4 times more stable than the GLONASS clocks, but periodic signals and linear frequency drift observed in the GPS satellite clocks are not seen in any of the GLONASS satellite clocks.

- A performance analysis of the IGS GPS satellite clock prediction scheme, the results of which are presented in Chapter 6. This component of the work is relevant (and original) in the context of prior studies into GNSS SCTO prediction methods because it identifies the key factors that are limiting the performance of the IGS predictions of the GPS satellite clocks. This is important because each of these prior studies uses the outputs of the IGS prediction scheme as a benchmark against which a newly developed prediction method is tested[2]. The major factor—which these other studies do not address—that limits the apparent quality of the IGS predictions is the $T_{igr} - T_{igu}$ offset. Besides this, the presence of periodic signals and linear frequency drift, in the GPS satellite clocks are also shown to be important features that the IGS prediction methods do not fully account for.

- This project looked into relativistic time transformation (RTT) (mis)modelling as a potential physical explanation for the periodic features observed in the GPS satellite clock data. The results from this study indicate that RTT mis–modelling is not the source of the periodic signals observed in the GPS satellite clock data. Nevertheless,

[1] The ESA GLONASS satellite clock estimates—this project's source for GLONASS satellite clock data—has only been published since March 2010 [Springer, 2010].

[2] This study also adopts the same approach.

these results are informative in the broader context of SCTO models in GNSS, of which the relativistic correction is a significant component. The results validate the conventional approach to RTT modelling in GNSS that relies upon a point mass Earth gravity model in the RTT computation.

- The development, demonstration, testing and analysis of a prediction algorithm that goes some way to addressing the limitations of the IGS prediction scheme for the GPS satellite clocks.

- The development of a substantial software tool–set, which might be considered an early prototype of a fully–operational GNSS satellite clock prediction software that would output SCTO predictions and make them available to users. All of the processes described in this thesis including data–fetching, data storage and management as well as all of the experiments and data analysis were conducted within this software. This software was developed in this way, from the ground up, because pre–existing software did not meet the requirements of this project. This software code base now offers a good platform for any future research in this area of GNSS satellite clock prediction to build upon.

- There are a number of classification schemes introduced in this thesis that develop the set of concepts that represent the fundamental principles of satellite clocks in GNSS. It was necessary to create these classifications to communicate, to the reader, the scope and implication of the work presented here. Examples of this include: the classification of satellite clock prediction schemes (to clarify the distinction between the so called real-time, or near real-time, low-latency clock prediction and the navigation–message style, high–latency GNSS satellite clock prediction schemes); the breakdown of the SCTS problem into the components of characterisation, modelling, estimation and prediction; standard clock model vs. extended clock model; standard clock model KF vs. extended clock model KF prediction methods.

9.5 Developments in GNSS and related technologies

This section discusses areas of on–going development in the field of GNSS (and related technologies e.g. space–ready atomic clocks) that are relevant in the context of the algorithms and methods that relate to the problem of satellite clock time synchronisation (SCTS) in GNSS, as it is described in Section 1.1. In concluding this thesis it is worth reconsidering the broader context of the project in this way, because it is within this context that the motivations for follow–on work based around the outcomes of this research might arise.

Multi–constellation GNSS

Multi–constellation GNSS is a broad term for a sub–field within GNSS that captures everything from politics and economics to the science and technology challenges associated with

the operation and exploitation of multiple, independent and fully operational GNSS's. In one sense, it might be considered that multi–constellation GNSS as a technology (loosely, the ability to compute a PNT solution using a combination of measurements from two or more (independent) GNSS's) arrived in 2011, when GLONASS became fully operational with a (nominally) full constellation of 24 in–orbit satellites. This meant that receivers (with the capabilities to do so) could compute a PNT solution based on some combination of GPS and GLONASS measurements. This is significant because GNSS performance is degraded in certain challenging environments where signals may be blocked (by buildings, tree cover, the terrain etc.). The ability to receive and process measurements from multiple constellations mitigates this, providing improved availability with a higher number of satellites in view. Beidou and Galileo are continuing to develop towards full–operational capacity, but this is still a few years away. It is estimated that Beidou will provide full global coverage in 2020, and Galileo in 2016. Other notable developments within multi–constellation GNSS include the first PNT solution from a commercial Beidou receiver, and the first position–fix from the four Galileo IOV satellites. Although these are encouraging developments, multi–constellation GNSS is still far from mature, and there are still many technical challenges associated with interoperability and compatibility of these systems.

Where does the issue of clock modelling and time synchronisation come into this? Well, imagine the following scenario: a GPS receiver is located within an urban canyon, where only two GPS satellites and only two GLONASS satellites are in view. Now although this exact scenario is an unlikely one, some of the challenges associated with GPS/GLONASS interoperability can be explained using this example. Imagine then, that the receiver is GPS and GLONASS enabled, which means that it can track and measure pseudoranges to GPS and GLONASS satellites. In this scenario, the receiver is only able to compute a PNT solution if it is able to use all available GPS and GLONASS measurements. One problem that arises when attempting to combine these measurements in a PNT algorithm relates to the underlying reference timescales. Implicitly, all time–varying parameters associated with the GPS system are time–tagged in GPS Time. In the GLONASS case, all time–varying parameters are implicitly associated to GLONASS Time. This suggests that there is an inter–system timescale offset that must be accounted for in some way, in order for GPS and GLONASS measurements to be correctly accounted for in any combined GPS/GLONASS position determination algorithm. Yes, there are various other issues (such as the inter–frequency biases among the GLONASS measurements) besides the inter–system timescale offset that create problems in combining GPS and GLONASS measurements, but understanding and accounting for the behaviour of the GPS/GLONASS timescale offset is certainly an important one in this context.

GNSS modernisation

GNSS modernisation refers to the processes whereby the components of a GNSS: space segment, operational control segment and user segment are gradually updated over time. As far as the work in this thesis is concerned, it is the updates to the satellite clock prediction systems that are used by the operational control segments that are relevant. This

includes the complete modernisation programme of the GPS operation control segment (hardware, software and algorithms), which is to be known as the GPS next–generation operational control system (OCX). It is certain that new methods associated with GPS SCTO estimation and prediction will be introduced as part of this GPS OCX roll–out programme. Alongside this, there are on–going developments in the Galileo and Beidou SCTO estimation and prediction systems, which are due to become fully–operational in 2020 and 2016, respectively.

The continuing development of precise clock technologies

Clock (precise time–keeping) technologies in general continue to advance. Alongside this, motivated by the on–going modernisation of the GNSS's and various other space missions requiring precise time–keeping (i.e. GRACE, SBAS, TWSTFT etc.), the field of space–ready precise timekeeping technologies also continues to be the focus of major research and development (R&D) efforts.

Some examples that might indicate the candidate technologies on which these R&D efforts will be focussed include: the deployment of passive hydrogen masers in orbit as part of the payload on the GIOVE–B spacecraft [Droz *et al.*, 2006], the development work on space–ready mercury–ion (Hg^+) atomic clocks by NASA's Jet Propulsion Laboratory for the purposes of deep–space navigation [Prestage & Weaver, 2007], and there is the long–running (but still active) European project, the Atomic Clock Ensemble in Space (ACES) experiment, which has seen the development of a variety of space–ready clock technologies for the purpose of conducting fundamental science experiments in Earth–orbit on the International Space Station [Bize *et al.*, 2005].

An exciting recent development within the laboratory setting is the demonstration of a pair of optical atomic clocks based on individually trapped aluminium ions (Al^+) with frequency stabilities reported at 8.7×10^{-18} and 2.3×10^{-17}, respectively [Chou *et al.*, 2010]. The frequency stability of this pair of clocks is good enough that relativistic time dilation effects due to relative motion (between the pair of clocks) of less than ten metres per second are observable in the clock measurements. Using this pair of clocks, it is possible to detect gravitational time dilation resulting from a height difference of less than one metre on the Earth's surface. Comparing them to the in–orbit GPS satellite clocks, this pair of clocks are about three orders of magnitude more stable. If such frequency stability is ever achieved in a space–ready atomic clock this would significantly impact upon the way in which GNSS are operated, by potentially removing (or at least strongly mitigating) the nuisance effects of satellite clock behaviours (as a significant source of error) from the overall GNSS data processing chain.

In the context of precise clock technologies being deployed commercially, there has been encouraging development work relating to the integration of low–power, chip–scale atomic clocks (CSACs) into mobile devices such as GNSS receivers [Ucar *et al.*, 2013]. This technology have the potential to improve the PNT performance of GNSS receivers in GNSS–challenged environments.

Other topics

There are other areas of research and development, within the GNSS domain, which are closely associated with satellite clock prediction and estimation in some way, but which were not studied in great depth within the course of this project. It would be interesting to explore how some of the ideas developed and demonstrated within this project might be applied within these areas. These include:

- **receiver clock time offset (RCTO) modelling and prediction** and its influence of GNSS performance. Traditionally, in GNSS data processing for PNT, the RCTO is treated as a parameter to be estimated. This is because the receiver clock is usually driven by a quartz oscillator with relatively poor frequency stability at the intervals beyond a few seconds. But, (low–power) chip–scale atomic clocks have now been demonstrated in GNSS receivers [Ucar *et al.*, 2013]. A question that arises naturally from this: is PNT possible with an algorithm that models, rather than estimates, the RCTO? This would have the effect of increasing GNSS availability by reducing the minimum number of required satellites for a PNT solution, from 4 to 3, which would be useful in GNSS–challenged environments. Some early work in exploring this question is presented in Weinbach & Schön [2011].

- **enhanced long–term SCTO prediction and its influence of the performance of self–assisted GNSS.** In difficult signal reception areas, GNSS–enabled devices can struggle to acquire the the full set of broadcast navigation message parameters (i.e. the parameters associated with the satellite position and the satellite clock time offset) required in order to determine a position fix. As an example, in the GPS case, this requires that the receiver must maintain continuous tracking of a satellite for up to thirty seconds in order to acquire the latest navigation message parameters for that satellite, if it has not already done so. Self–assisted GNSS describes a technique whereby the GNSS broadcast navigation message parameters are predicted, independently, within the GNSS–enabled device itself, for a period of up to several days ahead. In challenging environments for GNSS, where network assistance is also not available, self–assisted GNSS can drastically reduce the time–to–first–fix (TTFF) for a GNSS receiver (i.e. the time between when the GNSS receiver first starts tracking (or attempting to track) satellites when the receiver is able to determine its first set of position coordinates). As far as the self–assisted GNSS problem is concerned, it appears there is a significant body of work into the orbit prediction (and orbit determination) aspect of the problem Sepännen *et al.* [2012]; Stacey & Ziebart [2011]; van Diggelen [2009], but work on the satellite clock prediction aspect of this problem appears limited. Some early work on the topic of long–term satellite clock time offset prediction in the context of self–assisted GNSS for TTFF reduction is presented in Martikainen *et al.* [2012].

9.6 Further work

In this section, ideas for follow–on work to further develop and validate the research in this thesis are presented. These are:

- A (validation) study exploring the impact of using outputs from an EMP–like SCTO prediction system in the applications domains (e.g. in standard GPS (or other GNSS) point positioning, in GPS precise point positioning, in meteorology etc.). GNSS performance and satellite clock performance are intrinsically connected. As such, there are a wide variety of application scenarios that might be studied, each with good justification. The challenges associated with conducting such a study include: choosing the application domain, development of a data processing software that (at the very least) would enable the EMP SCTO prediction system to interface with the application–specific data processing, and the design of experiments that would highlight the specific effects of using ideas from the developed prediction method against conventional SCTO prediction methods.

- Further development work on the clock characterisation and prediction software that was used to generate most of the results within this thesis. Here, a priority would be to explore how methods from statistical inference and machine learning might be applied to automate the processes of initialisation and configuration of the relevant satellite clock Kalman filter parameters. Particularly, it would be interesting to develop an adaptive method for determining the Kalman filter process noise covariance matrix. In the methods used in this thesis, Kalman filter initialisation and configuration are the most time–consuming parts of the overall SCTO prediction method.

- A study investigating the potential application of the ideas presented in this thesis to both the Galileo and Beidou constellations. This thesis does not consider the in–orbit characteristics of Galileo or Beidou satellite clocks in great depth. This is because these clocks were not studied in this project as the required satellite clock data sets for these systems were not available.

- The SCTO prediction strategy developed in this project and presented in Chapter 8 of this thesis was designed in such a way that it could operate within the framework of an operational, widely–used and well–regarded SCTO prediction system: the IGS prediction system for the GPS satellite clocks. At this stage, it would be interesting to engage directly with the IGS, considering whether the methods developed could actually be incorporated into the IGS operational framework and the challenges associated with this. As a first step in this task (of engaging directly with the IGS), a poster entitled "*A performance analysis of the IGS predictions of the GPS satellite clocks*" will be presented on 26 June 2014 at the IGS Workshop 2014: Celebrating 20 years of service (1994–2014), which is being hosted by the California Institute of Technology (Caltech) in Pasadena, California, USA. This poster is

broadly based around the methods and results of the IGS satellite clock prediction system performance analysis study that is the topic of Chapter 6 of this thesis.

Appendix A

The power law noise processes

A random or stochastic process is a time-varying phenomenon, continuous or discrete, that is represented at each instance in time by a random variable, $X(t)$, whose probability density function, $f_X(t)$, may or may not be known. In precise time and frequency metrology (PTFM), these are usually referred as noise processes. The power-law noise processes are stochastic processes whose frequency and phase noise power spectral densities vary as a power of the Fourier[1] frequency. Power, in this case, is usually denoted by the symbols α or β, and both α and β are restricted to the domain of the integers. Here, α corresponds to a power-law description of frequency noise, and similarly β corresponds to a power-law description of phase noise.

The power-law noise processes are usually expressed in the form [Riley, 2008]

$$S_y(f) \propto f^{\alpha} \tag{A.1}$$

where $S_y(f)$ is the power spectral density of the frequency fluctuations, or alternatively as

$$S_x(f) = \frac{S_y(f)}{(2\pi f)^2} \propto f^{\beta} \tag{A.2}$$

where $S_x(f)$ is the power spectral density of the phase variations and $\beta = \alpha - 2$.

Power–law noise processes in the time domain

Power–law noise processes can also be expressed in the time domain, in terms of the characteristics of Allan variance type statistics, i.e. $\sigma_y^2(\tau)$, for that power–law noise sequence over a range of analysis intervals, τ. In this form, power–law noise processes can be expressed as

$$\sigma_y^2(\tau) = g_\gamma \tau^{\gamma} \tag{A.3}$$

[1] Here, the Fourier frequency refers to the independent variable in the FFT–based power spectral density periodograms that are produced as the result of a (Fourier) frequency domain analysis of a time–series of (normalised) frequency measurements.

or if modified Allan variance type statistics are used, then

$$mod\sigma_y^2(\tau) = g'_{\gamma'}\tau^{\gamma'} \tag{A.4}$$

where $\sigma_y^2(\tau)$ and $mod\sigma_y^2(\tau)$ represent the values of the Allan (or similar i.e Hadamard) variance and modified Allan variance (or similar) variance, τ is the averaging interval, and g_γ and $g'_{\gamma'}$ are positive, real–valued quantities (independent of τ) that scale the component of the power–law noise process that is dependent on τ.

Oscillator noise as a linear combination of power–law noise processes

In particular, there are five power-law noise processes, with α ranging from -2 to 2 which are observed in the precise clock measurements. These are white phase modulation (WPM) noise ($\alpha = 2$), flicker phase modulation (FPM) noise ($\alpha = 1$), white frequency modulation (WFM) noise ($\alpha = 0$), flicker frequency modulation (FFM) noise ($\alpha = -1$) and random walk frequency modulation noise (RWFM) noise ($\alpha = -2$).

Noise type	α	β	γ	γ'
WPM	2	0	-2	-3
FPM	1	-1	~ -2	-2
WFM	0	-2	-1	-1
FFM	-1	-3	0	0
RWFM	-2	-4	1	1

Table A.1: The five power-law noise processes which are commonly observed in clock measurements. Here, the α, β, γ and γ' values correspond to the powers associated with these individual power–law clock noise components represented in the (Fourier) frequency domain using the power spectral densities of the frequency (α) and phase (β) variations, or in the time domain using Allan variance (γ) or Modified Allan variance (γ') type statistics.

In table A.1, the α and β values of the five common power–law clock noise processes are listed. In general, the power spectral density of a clock's noise is well described as a linear combination of these five power–law noise processes, such that

$$S_y(f) = \sum_{\alpha=-2}^{+2} h_\alpha f^\alpha \tag{A.5}$$

where the h_α are positive, real–valued, scalar quantities that indicate the influence of the corresponding power–law noise process on the overall clock noise. The power spectral density description of clock noise is a frequency domain representation of clock noise. For a general time domain representation Allan variance or modified Allan variance statistic and their power–law relationships with analysis (or averaging) intervals can be used. The γ and γ' values of the third and fourth columns of table A.1 represent the values of the powers in the power–law relationships of the five–power law noise processes between the

Allan variance, $\sigma_y^2(\tau)$ and the analysis interval, τ

$$\sigma_y^2(\tau) = \sum_{\gamma=-2}^{+1} g_\gamma \tau \tag{A.6}$$

and between the modified Allan variance, $mod\sigma_y^2(\tau)$, and the analysis interval, τ

$$mod\sigma_y^2(\tau) = \sum_{\gamma'=-3}^{+1} g'_{\gamma'} \tau^{\gamma'} \tag{A.7}$$

respectively. Again, the coefficients, g_γ in equation A.6 and $g'_{\gamma'}$ in equation A.7 are positive, real–valued, scalar quantities that indicate the influence of the corresponding power–law noise process on the overall clock noise. They are related to the h_α coefficients in equation A.5. The relationships between (Fourier) frequency domain representation of the power law noise and the time domain representation can be can derived using inverse Fourier transforms; these are outlined explicitly in Stein [1985].

White Phase Modulation (WPM) Noise

White Phase Modulation (WPM) noise is a constant–mean, constant–variance random process affecting the clock time-offset (or phase offset) quantity as it is described in section 3.3.2. This means that a discrete WPM noise sequence can be represented as a sequence of independent random variables with identical Gaussian probability density functions, which are usually denoted $\mathcal{N}(\mu, \sigma^2)$.

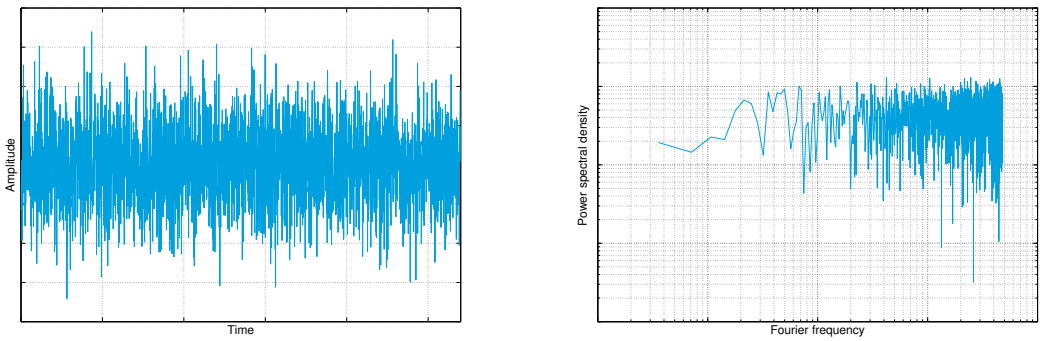

(a) A realisation of a WPM noise process as it would appear in a set of time–offset (phase offset) data.

(b) FFT–based power spectral density periodogram of WPM noise as it would appear in a set of of time–offset data. Each major tick on the axes represent a single unit on a log–log scale.

Figure A.1: A (discrete) realisation of a WPM noise process as it would appear within a set of time–offset data, along with an FFT–based power spectral density periodogram for that realised noise process. Here, the initial value for the realised WPM noise process is 0 at time $t = 0$.

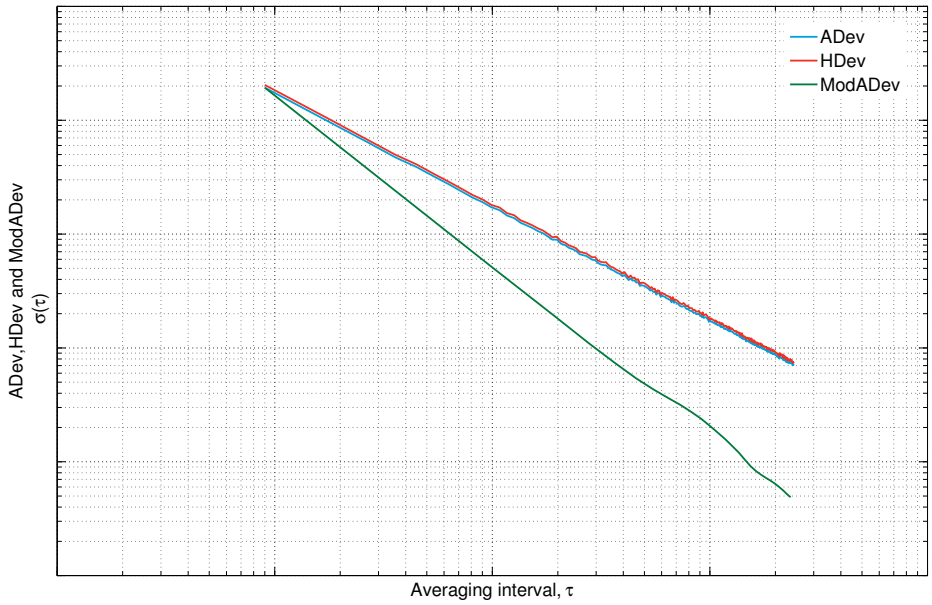

Figure A.2: Stability analysis of a sample realisation of a WPM noise process. Each major tick on the axes represent a single unit on a log–log scale.

A realisation of a WPM noise process

Within this thesis, there are methods that rely upon the comparison of simulated noise processes with noise processes that are observed in clock (time–offset) data. The results of these comparisons are used in the configuration of the Kalman filter process noise covariance matrices, as described in Section 3.5.2. The realisation (or simulation) of a WPM noise process (or a white noise processing general) is a relatively straight–forward, but does require a good random number generating function. In this project, the inbuilt MATLAB random number generating function **randn**, which returns a scalar value from the standard normal distribution, i.e. $\mathcal{N}(\mu = 0, \sigma^2 = 1)$, was used.

Here, in figure A.1a, the result of a single realisation of a WPM noise process, as it would appear within a time–offset data set is shown. The data from this simulation of a WPM noise sequence is transformed into the (Fourier) frequency domain, and the energy of the WFM noise sequence over a range of (Fourier) frequencies are investigated. The results of this are given in the form of a power spectral density (PSD) periodogram in figure A.1b. In this figure, overall, the slope of the PSD curve is flat (i.e. $\beta = 0$) on a log–log plot, which indicates that this simulated sequence is a good representation of a WPM noise process. In a time–domain stability analysis of the generated WPM sequence, shown in figure A.2, the slope of the ADev and HDev–based sigma–tau curves are -1 (i.e. $\gamma = -2$) and the slope of the MDev–based sigma–tau curve is $-\frac{3}{2}$ (i.e. $\gamma' = -3$), on a log–log plot. This is further evidence that the simulated sequence represents a good representation of a WPM noise process.

Oscillator frequency noise

In many cases, the fractional frequency deviation, i.e. the quantity that represents random fluctuations in the frequency of a clock's oscillator, can be adequately described as a combination of a white noise process and a random walk process. In this context, the white noise process is usually referred to as White Frequency Modulation (WFM) noise and the random walk process is referred to as random walk frequency modulation (RWFM) noise.

White Frequency (WFM) Modulation Noise

Mathematically, a WFM noise process can be expressed as a zero mean white noise sequence affecting a sequence of fractional frequency measurements, such that

$$\mu_{\epsilon_k} = E[\epsilon_k] = 0 \tag{A.8}$$

and

$$\sigma^2_{\epsilon_k} = E[(\epsilon_k - \mu_{\epsilon_k})^2] = E[\epsilon_k^2] \tag{A.9}$$

where ϵ_k is the random variable associated with the k-th element of the WFM noise sequence, μ_{ϵ_k} is the expected value of ϵ_k at epoch k and $\sigma^2_{\epsilon_k}$ is the variance of ϵ_k.

A realisation of a WFM noise process

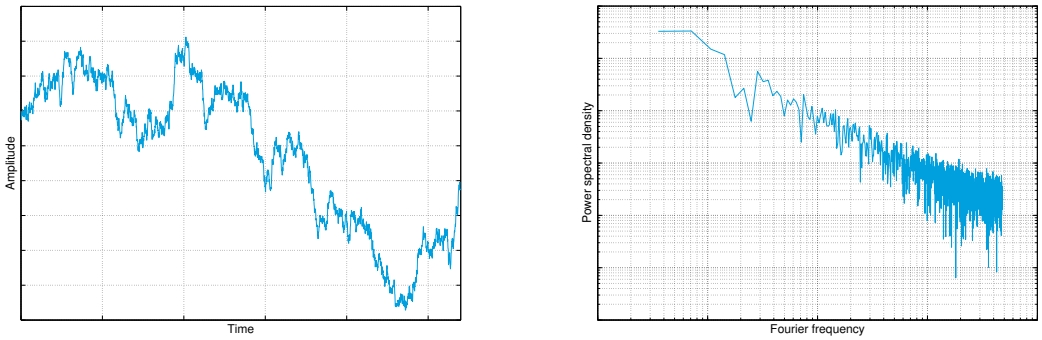

(a) A realisation of WFM noise as it would appear in a set of in time–offset (phase) data.

(b) FFT–based amplitude spectra of WFM noise realised as it would appear within a set of phase data. Each major tick on the axes represent a single unit on a log–log scale.

Figure A.3: A (discrete) realisation of a WFM noise process as it would appear with a set of time–offset data, along with an FFT–based power spectral density periodogram for that realised noise process. Here, the initial value for the realised WFM noise process is 0 at time $t = 0$.

The influence of a WFM noise sequence as it would appear in a time–series data set of a clock's time–offset is demonstrated by the shape of the noisy curve in figure A.3a. In a time–offsets data set, WFM noise appear as a random walk (in the time–offset quantity). The example of WFM noise process shown here is a realisation of a random walk (in the

time–offset) process as a zero–mean, Gaussian process, with stationary increments. The variance grows according to $w\tau$, where w is a scalar constant. The results of FFT–based power spectral density periodogram for the WFM noise sequence is plotted in figure A.3b. Overall, the slope on the power spectral density curves falls within the -3 to $-\frac{3}{2}$ range, and the slopes on the the sigma–tau curves in figure A.4 are $-\frac{1}{2}$ for the most part indicating that the realised WFM noise data set approximates WFM noise reasonably well, in agree with the power–law indices listed in table A.1.

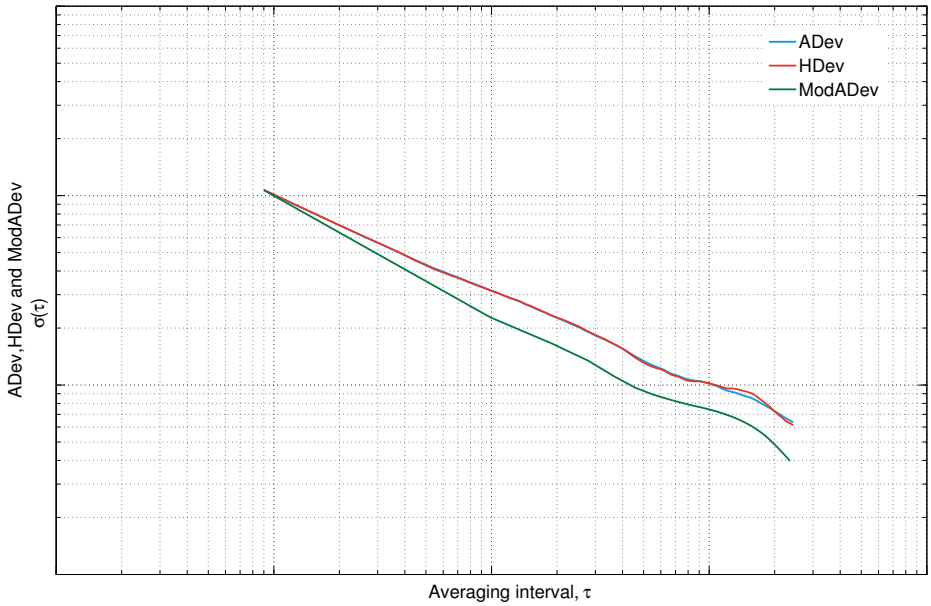

Figure A.4: Stability analysis of a sample realisation of a WFM noise process. The major ticks on the axes represent units on a log–log scale.

The sigma–tau curves in figure A.4 are not $-\frac{1}{2}$ at all averaging intervals, with some "flattening" of the sigma–tau curves at longer intervals. This may be a caused by the random number generating function (which is not truly random, but rather pseudo–random) that is fundamental here in simulating the WFM noise process.

Random Walk Frequency Modulation (RWFM) Noise

Oscillator frequency noise can also be influenced by noise associated with the frequency drift of that oscillator. In such cases, a random walk noise process (on the frequency) can be used to represent the influence of frequency drift variations on the fractional frequency. In this case, the random walk process is referred to as Random Walk Frequency Modulation (RWFM) Noise. Mathematically, a discrete RWFM sequence is represented by

$$\zeta_k = \zeta_{k-1} + \xi_{k-1} \tag{A.10}$$

where ζ_k is the value of the random variable ζ at epoch k, ξ_k is the value of a zero–mean normally distributed random variable at epoch k with variance equal to a constant multiple of the time increment $\tau = t_k - t_{k-1}$ (i.e. it is a stationary increment) such that

$$\sigma_\xi^2 = w\tau \tag{A.11}$$

where w is a positive constant.

A realisation of an RWFM noise process

In figure A.5a, an instance of an RWFM noise process as it would appear in a time–series datas set of a clock's time offset's are shown.

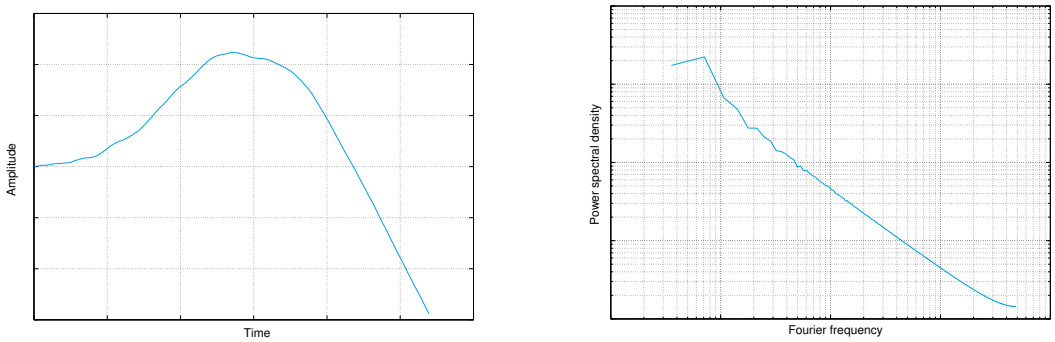

(a) A realisation of a RWFM noise process as it might appear in a time–offset data set.

(b) FFT–based power spectral density periodogram of a simulation of a RWFM noise process. The major ticks on the axes represent units on a log–log scale.

Figure A.5: A (discrete) realisation of a RWFM noise process as it would appear with a set of time–offset data, along with an FFT–based power spectral density periodogram for that realised noise process. Here, the initial value for the realised RWFM noise process is 0 at time $t = 0$.

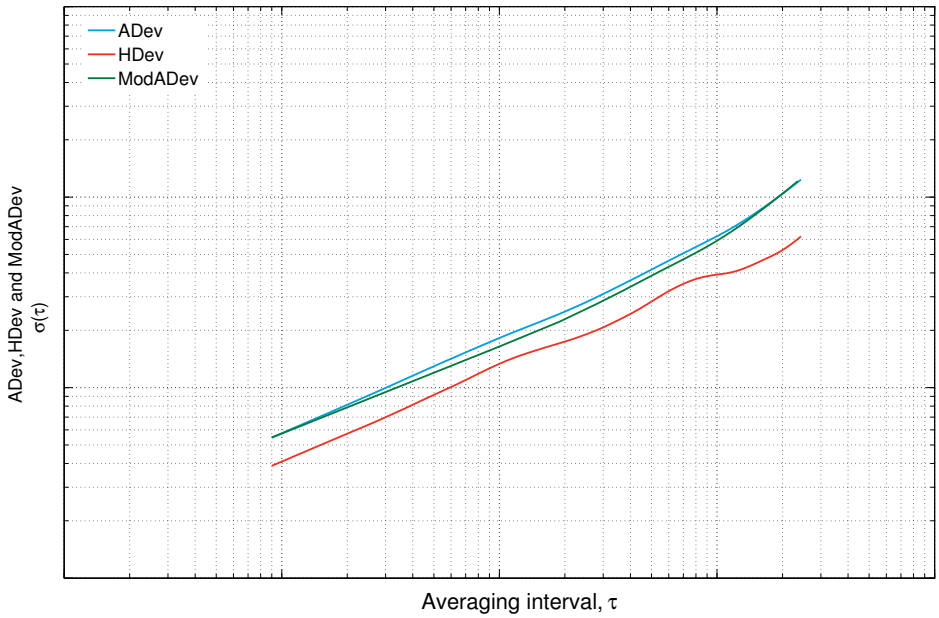

Figure A.6: Stability analysis of a sample realisation of a WFM noise process. Each major tick on the axes represent a single unit on a log–log scale.

The results of FFT–based power spectral density periodogram for the RWFM noise sequence is plotted in figure A.5b. The slopes on the the sigma–tau curves in figure A.6 are all $+\frac{1}{2}$ (corresponding to $\gamma = 1$, $\gamma' = 1$) that the realised RWFM noise data set is a good approximation of a RWFM noise process.

Clock noise in the standard clock model

Clock noise as a linear combination of the WFM and RWFM noise processes shown here along with random run frequency modulation noise (RRFM) noise can be simulated in the standard clock model Kalman filter. This process is described in Section 3.5.

The flicker noise processes

The flicker noise processes, flicker phase modulation (FPM) noise and flicker frequency modulation (FFM) noise, are the noise processes corresponding to $\alpha = 1$ and $\alpha = -1$, respectively. In this work, these flicker noise processes are modelled using a combination of Gauss–Markov processes, i.e. as the sum process of several independent stationary Markov processes running in parallel. The development of this approach is described in Davis *et al.* [2005b], where it was used to model the flicker frequency modulation noise that was dominant in NPL's hydrogen masers.

Appendix B

The discrete Kalman Filter

In this appendix, the Kalman filter method is introduced with a short and general presentation. The principal components of the Kalman filter technique are described. The Kalman filter can be operated in an estimation mode or in a prediction mode. In estimation mode, the KF algorithm is operated to output optimal estimates of the state–vector parameters. In prediction mode, the KF is operated without the use of measurements—and in this case the state error covariance matrix provides an indication of the quality of the predicted state–vector parameters. The procedure for KF operation in either estimation or prediction mode is shown. For those readers interested in a more in–depth study of the Kalman filter technique, a good place to start would be Kalman [1960]. An introductory, but highly accessible treatment of the KF method is given in Brown & Hwang [2012]—in presenting the Kalman filter equations here, the aim is to follow closely the notation conventions of this book. In preparing this appendix, Groves [2013] was also used and is recommended, particularly to those readers interested in the practicalities of implementing the KF method.

B.1 The Kalman filter

The Kalman filter method requires a process model and a measurement model. The process model encapsulates all assumptions and prior knowledge of both the deterministic and stochastic properties of the system dynamics. The process model is used to optimally estimate the state–vector, before the arrival of the latest measurement.

$$\mathbf{x}_{k+1} = \mathbf{\Phi}_k \mathbf{x}_k + \mathbf{w}_k \tag{B.1}$$

The measurement model describes a linear relationship between the measured quantities (through which the process is observed) and the state–vector.

$$\mathbf{z}_k = \mathbf{H}_k \mathbf{x}_k + \mathbf{v}_k \tag{B.2}$$

where:

$\mathbf{x}_k$	(m × 1) state–vector at time t_k
$\mathbf{\Phi}_k$	(m × m) matrix relating the state vector at time t_k to an estimate of the state vector at time t_{k+1}
$\mathbf{w}_k$	(m × 1) vector of white, Gaussian random variables that describe noise processes influencing the state vector
$\mathbf{z}_k$	(n × 1) vector of measurements at time t_k
$\mathbf{H}_k$	(n × m) vector relating the measurements to the state vector at time t_k
$\mathbf{v}_k$	(n × 1) vector of white, Gaussian random variables representing noise in the measurements

It is a strict requirement of the Kalman filter technique that the (sequence of) vectors of random variables $\mathbf{w}_k$ and $\mathbf{v}_k$ are independent, white and Gaussian, (from one epoch to next) such that the following conditions are satisfied:

$$E\left[\ \mathbf{w}_k\mathbf{w}_i^T\ \right] = \begin{cases} \mathbf{Q}_k, & i = k \\ 0, & i \neq k \end{cases} \tag{B.3}$$

$$E\left[\ \mathbf{v}_k\mathbf{v}_i^T\ \right] = \begin{cases} \mathbf{R}_k, & i = k \\ 0, & i \neq k \end{cases} \tag{B.4}$$

$$E\left[\ \mathbf{w}_k\mathbf{v}_i^T\ \right] = 0, \forall\ k \text{ and } i \tag{B.5}$$

In general, the KF model components $\mathbf{\Phi}$, $\mathbf{Q}$, $\mathbf{H}$ and $\mathbf{R}$, are time-dependent, but in many applications these are determined using historical data, and held constant. Once these components have been determined, we start with an initial estimate of the state of the process at time t_k. This initial estimate may be obtained by any reasonable means—but should be based on all knowledge of the process prior to t_k. This is then known as the *a priori* estimate of the state, $\hat{\mathbf{x}}_k^-$, where the $\hat{}$ symbol denotes an estimated quantity and the superscript $^-$ denotes an estimate prior to a state–vector update using the measurement at time t_k. The estimation error, the quantity being minimised is defined then as

$$\mathbf{e}_k^- = \mathbf{x}_k - \hat{\mathbf{x}}_k^- \tag{B.6}$$

where $\mathbf{x}_k$ is the true value of the state at epoch k and the state error covariance matrix is

$$\mathbf{P}_k^- = E\left[\ \mathbf{e}_k^-\mathbf{e}_k^{-T}\ \right] = E\left[\ (\mathbf{x}_k - \hat{\mathbf{x}}_k^-)(\mathbf{x}_k - \hat{\mathbf{x}}_k^-)^T\ \right] \tag{B.7}$$

The next step, once this prior estimate $\hat{\mathbf{x}}_k^-$ is obtained, is to use the measurement $\mathbf{z}_k$ to improve that estimate. This is done according to

$$\hat{\mathbf{x}}_k = \hat{\mathbf{x}}_k^- + \mathbf{K}_k(\mathbf{z}_k - \mathbf{H}_k\hat{\mathbf{x}}_k^-) \tag{B.8}$$

where $\mathbf{K}_k$ is a blending factor that combines that state–vector estimates with the measurement. In the special case where $\mathbf{K}_k$ minimises the mean–square estimation error, i.e. minimises the individual terms along the major diagonal of $\mathbf{P}_k$, then $\mathbf{K}_k$ is known as the Kalman gain which takes the form

$$\mathbf{K}_k = \mathbf{P}_k^- \mathbf{H}_k^T (\mathbf{H}_k \mathbf{P}_k^- \mathbf{H}_k^T + \mathbf{R}_k)^{-1} \tag{B.9}$$

B.2 Estimator

In estimation mode, the Kalman filter is a recursive loop. The initial inputs to this recursive loop are prior estimates of the state–vector, $\hat{\mathbf{x}}_0^-$, and the state error covariance matrix, $\mathbf{P}_0^-$. Here, the 0 subscript denotes that these are the initial prior estimates, i.e. $k = 0$. With these inputs, the estimation mode Kalman filter loop (as given in page 147 of Brown & Hwang [2012]) comprises the following steps:

1. **Kalman gain computation**, as described in Equation B.9.
2. **Update of state–vector estimate with measurement $\mathbf{z}_k$**, according to Equation B.8, where K_k is the Kalman gain.
3. **Error covariance matrix update for updated state–vector estimate**, which in done according to

$$\mathbf{P}_k = (\mathbf{I} - \mathbf{K}_k \mathbf{H}_k) \mathbf{P}_k^- \tag{B.10}$$

4. **Predict one step ahead**, according to

$$\hat{\mathbf{x}}_{k+1}^- = \mathbf{\Phi}_k \hat{\mathbf{x}}_k \tag{B.11}$$

$$\mathbf{P}_{k+1}^- = \mathbf{\Phi}_k \mathbf{P}_k \mathbf{\Phi}_k^T + \mathbf{Q}_k \tag{B.12}$$

5. Measurement z_{k+1} is collected. **Increment k by one** such that $\hat{\mathbf{x}}_{k+1}^-$, $\mathbf{P}_{k+1}^-$ and $\mathbf{z}_{k+1}$ are $\hat{\mathbf{x}}_k^-$, $\mathbf{P}_k^-$ and $\mathbf{z}_k$, respectively. **Return to step 1.**

B.3 Predictor

The Kalman filter recursive loop, presented in Section B.2, includes a one–step prediction; this is step 4. Prediction in this way is allowed because the elements of $\mathbf{w}_k$, in the process model (Equation B.1) are assumed to be white noise processes. With this same argument, it is possible to project N steps ahead of the current measurement. In this way, the Kalman filter is used as an N–step predictor. The equations for predicting N steps ahead are simple variations of Step 4 in Section B.2.

$$\hat{\mathbf{x}}_{k+N|k} = \mathbf{\Phi}_{k+N,k} \hat{\mathbf{x}}_{k|k} \tag{B.13}$$

$$\mathbf{P}_{k+N|k} = \mathbf{\Phi}_{k+N,k}\mathbf{P}_{k|k}\mathbf{\Phi}_{k+N|k}^{T} + \mathbf{Q}_{k+N,k} \tag{B.14}$$

where

- $\hat{\mathbf{x}}_{k|k}$ state–vector estimate updated *given* measurements up to time t_k
- $\hat{\mathbf{x}}_{k+N|k}$ prediction of state–vector for time t_{k+N} *given* measurements up to time t_k
- $\mathbf{\Phi}_{k+N,k}$ state transition matrix from step k to $k+N$
- $\mathbf{P}_{k|k}$ error covariance matrix corresponding to $\hat{\mathbf{x}}_{k|k}$ (updated *given* measurements up to t_k)
- $\mathbf{P}_{k+N|k}$ prediction of error covariance matrix corresponding to $\hat{\mathbf{x}}_{k+N|k}$ for time t_{k+N} *given* measurements up to time t_k
- $\mathbf{Q}_{k+N,k}$ covariance resulting from the accumulation of the $\mathbf{w}_k$ white noise inputs from step k to step $k+N$

Appendix C

Individual satellite clock statistics

In this appendix, statistics from the frequency stability analysis study (Chapter 5), and from the IGS prediction algorithm performance analysis study (Chapter 6), for each clock that was studied, are given here.

C.1 GPS individual clock statistics

PRN(SVN)	HDev ($\times 10^{-14}$) at different averaging intervals (hours)				
	0.25	3	6	12	24
1 (63)	3.79	2.72	1.24	0.636	0.501
2 (61)	20.9	3.30	2.07	1.47	0.951
4 (34)	26.8	9.45	9.05	4.31	3.40
5 (50)	22.1	4.13	2.91	1.27	0.908
7 (48)	21.9	3.10	2.37	1.79	1.73
8 (38)	94.3	32.4	29.5	12.9	9.06
10 (40)	77.6	24.3	20.3	12.6	6.77
11 (46)	25.5	5.32	6.08	2.11	2.51
12 (58)	24.1	5.98	4.07	1.01	0.668
13 (43)	38.9	5.47	3.16	1.56	1.75
14 (41)	22.1	3.83	2.17	1.55	1.18
16 (56)	21.8	6.69	4.40	0.953	0.649
17 (53)	27.7	5.70	2.81	1.94	2.36
18 (54)	26.9	3.91	2.95	1.11	0.741
19 (59)	22.0	3.81	2.18	1.34	0.974
20 (51)	35.8	4.67	2.46	1.69	1.36
21 (45)	38.7	4.88	3.08	1.54	0.911
22 (47)	23.5	4.25	3.10	3.00	4.12
23 (60)	20.3	2.92	1.98	1.10	0.738
25 (65)	3.38	3.85	2.42	0.592	0.317
27 (37)	98.4	72.2	86.3	14.4	8.63
28 (44)	25.7	3.97	3.77	4.66	5.62
29 (57)	24.7	5.38	2.86	2.30	2.85
31 (52)	21.0	3.73	3.17	1.89	1.91

Table C.1: Statistics arising from the frequency stability analysis (HDev) of the GPS satellite clocks at several analysis intervals.

C.2 GLONASS individual clock statistics

PRN(SVN)	ADev ($\times 10^{-13}$) at different averaging intervals (hours)				
	0.25	3	6	12	24
1 (730)	6.01	1.62	1.18	0.865	0.588
2 (728)	5.88	1.60	1.15	0.800	0.571
3 (744)	4.47	1.26	0.910	0.650	0.480
4 (742)	4.84	1.42	1.02	0.730	0.504
5 (734)	5.83	1.58	1.07	0.721	0.473
6 (733)	7.65	2.16	1.48	0.986	0.707
7 (745)	5.35	1.34	0.924	0.694	0.418
8 (729)	11.3	3.25	2.23	1.48	1.06
9 (736)	5.66	1.65	1.15	0.778	0.516
10 (717)	8.85	2.58	1.84	1.21	0.862
11 (723)	7.44	2.10	1.52	1.01	0.687
12 (737)	7.89	2.29	1.63	1.16	0.805
13 (721)	6.96	2.06	1.38	0.964	0.634
14 (715)	13.8	3.94	2.68	1.85	1.24
16 (738)	6.71	1.84	1.29	9.43	0.678
17 (746)	4.84	1.35	0.961	0.661	0.424
18 (724)	14.7	4.13	2.80	1.86	1.28
19 (720)	5.69	1.59	1.06	0.707	0.495
20 (719)	15.2	4.35	3.18	2.15	1.50
21 (725)	6.10	1.81	1.28	0.882	0.619
22 (731)	7.97	2.29	1.58	1.04	0.650
23 (732)	6.68	1.97	1.36	0.969	0.695
24 (735)	6.53	1.93	1.37	0.943	0.713

Table C.2: Statistics arising from the frequency stability analysis (ADev–based) of the GLONASS satellite clocks at several analysis intervals.

C.3 GPS CDPE Bias clock–by–clock statistics

PRN(SVN)	Bias ($\times 10^{-10}$ seconds) at different prediction lengths (hours)				
	0.25	3	6	12	24
1 (63)	−0.0394	−2.62	−7.08	−12.7	−30.6
2 (61)	1.34	0.0839	−0.0609	−0.188	−5.76
3 (33)	0.0773	−0.0637	−1.01	−2.67	−4.66
4 (34)	−0.0613	−0.00646	−1.99	−2.35	−6.54
6 (34)	−1.19	−3.91	−10.4	−17.8	−44.3
7 (48)	0.600	0.607	−0.500	−0.347	−1.11
8 (38)	−0.540	−1.28	−4.04	−7.20	−6.69
9 (39)	−1.32	−5.51	−4.86	−4.77	−9.18
10 (40)	1.47	−1.00	−3.30	−3.03	−6.90
11 (46)	−0.124	0.230	−1.70	−2.42	−6.49
12 (58)	2.33	1.30	−0.317	−1.29	−4.61
13 (43)	1.39	0.197	−1.02	−2.51	−6.84
14 (41)	0.416	−0.150	−2.23	−3.53	−8.33
15 (55)	0.587	0.225	−1.75	−3.53	−9.48
16 (56)	−0.632	−0.936	−1.75	−2.00	−2.97
17 (53)	−0.628	−0.0602	−2.46	−4.31	−9.65
18 (54)	−0.717	−0.353	−2.43	−2.80	−6.24
19 (59)	−0.235	−0.866	−1.93	−2.71	−5.23
20 (51)	−1.06	−0.475	−2.30	−2.66	−5.17
21 (45)	−0.293	−1.10	−2.30	−3.20	−6.80
22 (47)	−0.463	−0.614	−2.14	−1.97	−4.56
23 (60)	0.982	0.236	−1.55	−2.46	−6.69
25 (65)	0.592	0.0394	−0.552	−0.632	−1.02
26 (26)	0.739	2.21	4.31	9.88	23.9
28 (44)	1.19	0.936	−0.660	−1.55	−4.92
29 (57)	0.536	−0.201	−0.948	−1.80	−4.35
31 (52)	0.254	−0.471	−2.84	−4.95	−12.2
32 (23)	−1.94	7.17	−2.07	−2.23	−2.25

Table C.3: Summary. IGS GPS CDPE Bias 2012.

C.4 GPS CDPE RMS clock–by–clock statistics

PRN(SVN)	RMS ($\times 10^{-9}$ seconds) at different prediction lengths (hours)				
	0.25	3	6	12	24
1 (63)	0.302	0.688	1.31	2.13	4.94
2 (61)	0.344	0.616	0.759	1.11	1.92
3 (33)	1.41	3.30	4.66	6.66	10.7
4 (34)	0.696	1.28	1.88	2.49	4.00
6 (34)	0.624	1.45	2.08	3.31	7.17
7 (48)	0.334	0.692	0.915	1.42	2.48
8 (38)	1.88	3.94	5.31	7.49	11.2
9 (39)	1.87	3.87	5.02	6.86	10.8
10 (40)	1.40	3.25	4.45	6.37	10.3
11 (46)	0.370	0.742	1.13	1.79	3.48
12 (58)	0.395	0.633	0.674	0.915	1.49
13 (43)	0.362	0.618	0.843	1.22	2.28
14 (41)	0.318	0.725	1.19	1.94	3.59
15 (55)	0.285	0.531	0.659	0.929	1.63
16 (56)	0.397	0.581	0.721	0.991	1.55
17 (53)	0.377	0.812	1.33	2.19	4.32
18 (54)	0.321	0.587	0.705	0.989	1.58
19 (59)	0.339	0.602	0.772	1.04	1.66
20 (51)	0.422	0.748	1.10	1.65	3.15
21 (45)	0.374	0.738	0.843	1.16	1.85
22 (47)	0.518	1.22	2.18	3.83	8.14
23 (60)	0.298	0.515	7.03	1.00	1.64
25 (65)	0.563	1.19	1.68	2.99	6.90
26 (26)	0.563	1.19	1.68	2.99	6.90
28 (44)	0.681	1.64	2.95	4.85	8.99
29 (57)	0.362	0.691	1.11	1.93	3.72
31 (52)	0.368	0.842	1.47	2.79	5.65
32 (23)	0.724	1.02	1.42	1.94	3.23

Table C.4: Summary. RMS CDPE IGS GPS 2012.

References

Allan, D. & Weiss, M. (1980). Accurate time and frequency transfer during common-view to a GPS satellite. In *Proceedings of the 34th Annual Frequency Control Symposium*.

Allan, D.W. (1987). Time and frequency (time-domain) characterisation, estimation and prediction of precision clocks and oscillators. *IEEE Transactions on Ultrasonics, Ferroelectrics and Frequecy Control*, **UFFC-34**.

Allan, D.W. & Barnes, J.A. (1981). A modified Allan variance with increased oscillator characterisation ability. In *Proceedings of the 35th Frequency Control Symposium*, 470–474.

Altimimi, Z., Collilieux, X. & Métivier, L. (2011). ITRF2008: an improved solution of the international terrestrial reference frame. *Journal of Geodesy*, **85**, 457–473.

Altimimi, Z., Collilieux, X. & Métivier, L. (2013). Preliminary analysis in preparation for the ITRF2013. In *Proceedings of the EGU General Assembly*, vol. 15 of *Geophysical Research Abstracts*.

Arias, E.F., Panfilo, G. & Petit, G. (2011). Status of UTC/TAI. In *Proceedings of the 30th URSI general assembly and scientific symposium*.

Ashby, N. (2008). Relativity in the Global Positioning System. *Living Reviews in Relativity*, **6**.

Ashby, N. & Spilker Jr., J.J. (1996). *Global Positioning System: Theory and Applications*, vol. 1 of *Progress in Astronautics and Aeronautics*, chap. Introduction to relativistic effects on the Global Positioning System. American Institute of Aeronautics and Astronautics, 163rd edn.

Audoin, C. & Guinot, G. (2001). *The measurement of time: time, frequency and the atomic clock*. Cambridge University Press.

Bar-Sever, Y.E. (1996). A new model for GPS yaw attitude. *Journal of Geodesy*, **70**, 714–723.

Baugh, R.A. (1971). Frequency modulation analysis with the Hadamard variance. In *Proceedings of the 25th Frequecy Control Symposium*, 222–225.

Bernier, L. (2005). Predictability of a hydrogen maser timescale. In *Proceedings of the 19th European Frequecy and Time Forum*.

Beutler, G., Kouba, J. & Springer, T. (1995). Combining the orbits of the IGS analysis centers. *Bulletin Géodésique*, **69**, 100–222.

BIPM (1969). Resolution 1 of the 13th Conferénce Générale des Poids et Mesures (CGPM). Metrologia.

Bisnath, S. & Gao, Y. (2009). Precise Point Positioning: A powerful technique with a promising future.

Bize, S., Laurent, P., Abgrall, M., Marion, H., Maksimovic, I., Cacciapuoti, L., Grünert, J., Vian, C., dos Santos, F.P., Rosenbusch, P., Lemonde, P., Santarelli, G., Wolf, P., Clarion, A., Luiten, A., Tobar, M. & Salomon, C. (2005). Cold atom clocks and applications. *Journal of Physics B: Atomic, Molecular and Optical Physics*, **38**.

Brown, R.G. & Hwang, P.Y.C. (2012). *Introduction to random signals and applied Kalman filtering: with MATLAB excercises*. John Wiley & Sons, Inc., 4th edn.

Brown Jr., K. (1991). The theory of the GPS composite clock. Tech. rep., IBM.

Cacciapuoti, L. & Salomon, C. (2009). Space clocks and fundamental tests: The ACES experiment. *The European Physical Journal Special Topics*, **172**, 57–68.

REFERENCES

Caissy, M., Weber, G., Argotis, L., Wübbena, G. & Hernandes-Pajares, M. (2011). The IGS real-time pilot project - the development of real-time IGS correction products for precise point positioning. In *Proccedings of the 13th EGU General Assembly*, vol. 13.

Chaffee, J.W. (1987). Relating the Allan variance to the diffusion coefficients of a linear stochastic differential equation for precision oscillators. *IEEE Transactions on Ultrasonics, Ferroelectrics and Frequency Control*, **UFFC-34**.

Chou, C.W., Hume, D.B., Rosenband, T. & Wineland, D.J. (2010). Optical clocks and relativity. *Science*, **329**, 1630–1633.

Conley, R., Consentino, R., Hegarty, C., de Haag, M.U. & van Dyke, K. (2006). *Understanding GPS Principles and Applications*, chap. Performance of stand-alone GPS, 301–378. Artech House, Norwoord, MA, 2nd edn.

Dach, R., Schaer, S. & Meindl, M. (2012). Comparison of GPS/GLONASS clock solutions. IGS Workshop on GNSS Biases.

Davis, J., Greenhall, C.A. & Stacey, P.W. (2005a). A Kalman filter clock algorithm for use in the presence of flicker frequency modulation noise. *Metrologia*.

Davis, J.A. (2011). Use of Kalman filters in time and frequency analysis. Tutorial at the 25th European Frequency and Time Forum.

Davis, J.A., Greenhall, C.A. & Boudjemaa, R. (2005b). The development of a Kalman filter clock predictor. In *Proceedings of the 19th European Frequecy and Time Forum*.

Department of Defense, United States of America (2008). *Global Positioning System: Standard Positoning Service Performance Standard*. 4th edn.

Dow, J.M., Neilan, R.E. & Rizos, C. (2009). The International GNSS Service in a changing landscape of Global Navigation Satellite Systems. *Journal of Geodesy*, **83**, 191–198.

Droz, F., Mosset, P., Barmaverain, G., Rochat, P., Wang, Q., Belloni, M., Mattioni, L., Schmidt, U., Pike, T., Emma, F. & Waller, P. (2006). The on–board Galileo clocks: Rubidium standard and passive hydrogen maser–Current status and performance. In *Proceeedings of the 20th European Frequency and Time Forum*.

Galileo ICD (2006). *Galileo Open Service: Signal In Space Interface Control Document*. European Space Agency.

Galleani, L. (2008). A tutorial on the two-state model of the atomic clock noise. *Metrologia*, **45**.

Galleani, L. & Tavella, P. (2009). The Dynamic Allan Variance. *IEEE Transactions on Ultrasonics, Ferroelectrics and Frequency Control*, **56**.

Galleani, L. & Tavella, P. (2010). Time and the Kalman filter. *IEEE Control Systems Magazine*.

Galleani, L., Sacerdote, L., Tavella, P. & Zucca, C. (2003). A mathematical model for atomic clock error. *Metrologia*, **40**, S257–S264.

Ge, M., Chen, J. & Douša, J. (2012). A computationally efficient approach for estimating high-rate satellite clock corrections in realtime. *GPS Solutions*, **16**, 9–17.

GLONASS ICD (1998). *GLONASS Interface Control Document*.

Greenhall, C.A. & Riley, W.J. (2003). Uncertainty of stability variances based on finitde differences. In *Proceedings of the 35th Annual Precise Time and Time Interval (PTTI) Meeting*.

Griffiths, J. (2013). Status of IGS core products. 2013 AGU Fall Meeting.

Griggs, E., Kursinski, E.R. & Akos, D. (2013). An investigation of GNSS atomic clock behaviour at short time intervals. *GPS Solutions*.

Groves, P. (2013). *Principles of GNSS, Inertial and Multisensor Integrated Navigation Systems*. Artech House, 2nd edn.

Gurtner, W. & Estey, L. (2007). *RINEX: The Receiver Independent Exchange Format Version 2.11*. IGS/RTCM working group.

Gurtner, W. & Estey, L. (2009). *RINEX: The Receiver Independent Exchange Format. Version*

3.01.

Harris, R.B. & Mach, R.G. (2007). The GPSTk: an open source GPS toolkit. *GPS Solutions*, **11**.

Hauschild, A. & Montenbruck, O. (2009). Kalman-filter-based GPS satellite clock estimation for near real-time positioning. *GPS Solutions*, **13**.

Hauschild, A., Montebruck, O. & Steigenberger, P. (2013). Short-term analysis of GNSS clocks. *GPS Solutions*, **17**, 295–307.

Heng, L., Gao, G.X., Walter, T. & Enge, P. (2011). Statistical characterisation of GLONASS broadcast ephemeris errors. In *Proceedings of ION GNSS 2011*.

Heo, Y.J., Cho, J. & Heo, M.B. (2010). Improving prediction accuracy of GPS satellite clocks with periodic variation behaviour. *Measurement Science and Techology*, **21**.

Hernández-Pajares, M., Juan, J.M., Sanz, J. & Oŕus, R. (2007). Second-order ionospheric term in GPS: Implementation and impact on geodetic estimates. *Journal of Geophysical Research*, **112**.

Hesselbarth, A. & Wanniger, L. (2008). Short-term stability of GNSS satellite clocks and its effects on precise point positioning. In *Proceedings of ION GNSS 2008*, 1855–1863.

Hilla, S. (2010). *The Extended Standard Product 3 Orbit Format (SP3-c)*. National Geodetic Survey.

Hofmann-Wellenhof, B., Lichtenegger, H. & Wasle, E. (2008). *GNSS—Global navigation satellite systems: GPS, GLONASS, Galileo and more*. SpringerWienNewYork.

Huang, G. & Zhang, Q. (2012). Real-time estimation of satellite clock offset using adaptively robust Kalman filter with classified adaptive factors. *GPS Solutions*, **16**, 531–539.

Huang, G.W., Zhang, Q. & Xu, G.C. (2013). Real-time clock offset prediction with an improved model. *GPS Solutions*.

Hutsell, S.T. (1995). Relating the Hadamard variance to MCS Kalman Filter Clock Estimation. In *Proceedings of the 14th annual precise time and time interval applications and planning meeting*, 291–301.

IEEE (2009). IEEE Standard Definitions of Physical Quantities for Fundamental Frequency and Time Metrology—Random Instabilities.

IS-GPS-200E (2010). *Interface specification IS-GPS-200 Revision E*. Global Positioning System Wing (GPSW): Systems Engineering and Integration.

Kalman, R.E. (1960). A new approach to linear filtering and prediction problems. *Trans. ASME - J. Basic Eng.*, **82**, 35–45.

Kouba, J. (2002). Relativistic time transformations in GPS. *GPS Solutions*, **5**, 1–9.

Kouba, J. (2003). *A guide to using the International GNSS Service (IGS) products*.

Kouba, J. (2004). Improved relativistic time transformations in GPS. *GPS Solutions*, **8**, 170–180.

Kouba, J. & Springer, T. (2001). New IGS station and satellite clock combination. *GPS Solutions*, **4**, 31–36.

Kruse, L.P., Sierk, B., Springer, T. & Cocard, M. (1999). GPS-Meteorology: Impact of predicted orbits on precipitable water estimates. *Geophysical Research Letters*, **26**, 2045–2048.

Larson, K.M., Ashby, N., Hackman, C. & Bertiger, W. (2007). An assessment of relativistic effects for low Earth orbiters: the GRACE satellites. *Metrologia*, **44**, 484–490.

Leandro, R., Landau, H., Mitschke, M., Glocker, M. & Deking, A. (2011). RTX Positioning: The next-generation of cm–accurate real-time GNSS positioning. In *Proceedings of ION GNSS 2011*, 1460–1475.

Lepek, A. (1997). Clock prediction and charcterisation. *Metrologia*, **34**.

Mallette, L.A., White, J. & Mirage, R. (2008). An introduction to satellite based atomic frequency standards. *Aerospace Conference, 2008 IEEE*.

REFERENCES

Martikainen, S., Picke, R. & Ali-Löytty, S. (2012). Outlier–robust estimation of GPS satellite clock offsets. In *Proceedings of the 2012 International Conference on Localisation and GNSS (ICL-GNSS)*.

McCarthy, D.D. & Seidelmann, P.K. (2009). *Time - From Earth rotation to atomic physics*. Wiley-VCH.

Misra, P. & Enge, P. (2011). *Global Positioning System: Signals, measurements and performance*. Ganga-Jamuna Press, revised second edition edn.

Montenbruck, O. & Gill, E. (2000). *Satellite Orbits*. Springer.

Montenbruck, O., Gill, E. & Kroes, R. (2005). Rapid orbit determination of LEO satellites using IGS clock and ephemeris products. *GPS Solutions*, **9**, 226–235.

Montenbruck, O., Hugentobler, U., Dach, R., Steigenberger, P. & Hauschild, A. (2011). Apparent clock variations of the Block IIF-1 (SVN62) GPS satellite. *GPS Solutions*.

Øksendal, B. (2013). *Stochastic differential equations: An introduction with applications*. Springer, sixth edn.

Panfilo, G., Harmegnies, A. & Tisserand, L. (2012). A new prediction algorithm for the generation of International Atomic Time. *Metrologia*, **49**.

Pascual-Sanchéz, J. (2007). Introducing relativity in global navigation satellite systems. *Annalen der Physik*, **16**, 258–273.

Pavlis, N.K., Holmes, S.A., Kenyon, S.C. & Factor, J.K. (2012). The development and evaluation of the Earth Gravitational Model (EGM2008). *Journal of Geophysical Research*, **117**.

Percival, D. (2004). Modeling of clock behaviour. International Workshop on Galileo Time, Modeling and characterisation of atomic clocks, Torino, Italy.

Petit, G. & Wolf, P. (1997). Computation of the relativistic rate shift of a frequency standard. *IEEE Transactions on Instrumentation and Measurement*, **46**.

Petit, G., Arias, F., Harmegnies, A., Jiang, Z., Konaté, H., Lewandowski, W., Panfilo, G. & Tisserand, J. (2012). UTCr: a rapid realisation of UTC. In *Proceedings of the 26th European Frequency and Time Forum*.

Petit, G. & Luzum, B. (eds) (2010). IERS Conventions. IERS Technical Note No. 36, International Earth Rotation Service (IERS).

Prestage, J.D. & Weaver, G.L. (2007). Atomic clocks and oscillators for deep-space navigation and radio science. *Proceedings of the IEEE*, **95**.

Rawicz, H.C., Epstein, M.A. & Rajan, J.A. (1993). The time keeping system for GPS Block IIR. In *Proceedings of the 24th Annual Precise Time and Time Interval (PTTI) Applications and Planning Meeting*, ITT Aerospace.

Ray, J. (2000). [IGSMAIL-2962]: USNO ultra-rapid clock predictions. http://acc.igs.org.

Ray, J. & Griffiths, J. (2008). Status of IGS ultra-rapid products for real-time application. AGU Fall meeting.

Ray, J. & Gurtner, W. (2010). *RINEX: Extensions to handle clock information*. International GNSS Service, 3rd edn.

Ray, J. & Senior, K. (2003). IGS/BIPM pilot project GPS carrier phase time/frequency transfer and timescale formation. *Metrologia*, **40**, S270–S288.

Revnivykh, S. (2011). GLONASS—Status and progress. CGSIC Meeting.

Riley, W.J. (2008). Handbook of frequency stability analysis. Tech. rep., NIST.

Rizos, C., Jansen, V., Roberts, C. & Grinter, T. (2012). Precise point positioning: Is the era of differential GNSS positioning drawing to an end? FIG Working Week 2012.

Rocken, C., Mervart, L., Johnson, J., Lukes, Z., Springer, T., Iwabuchi, T., Cummins, S., Toor, P., Arciuch, M. & Shi, X. (2011). A new real-time global GPS and GLONASS precise point positioning correction service: Apex. In *Proceedings of ION GNSS 2011*, 1825–1838.

REFERENCES

Schmid, R., Steigenberger, P., Gendt, G., Ge, M. & Rothacher, M. (2007). Generation of a consistent absolute phase center correction model for GPS receiver and satellite antennas. *Journal of Geodesy*, **81**, 781–798.

Schmid, R., Collilieux, X., Dilssner, F., Dach, R. & Schmitz, M. (June 2010). Updated phase center corrections for satellite and receiver antennas. IGS Workshop 2010.

Senior, K., Koppang, P. & Ray, J. (2003). Developing an IGS time scale. *IEEE Transactions on Ultrasonics, Ferroelectrics and Frequecy Control*, **50**.

Senior, K., Ray, J.R. & Beard, R.L. (2008). Characterisation of periodic variations in the GPS satellite clocks. *GPS Solutions*, **12**, 211–225.

Sepännen, M., Ala-Luhtala, J., Piché, R., Martikainen, S. & Ali-Löytty, S. (2012). Autonomous prediction of GPS and Glonass satellite orbits. *Navigation*.

Sesia, I. & Tavella, P. (2008). Estimating the Allan variance in the presence of long periods of missing data and outliers. *Metrologia*, **45**.

Springer, T. (2010). [IGSMAIL-6107]: ESA/ESOC Ultra-Rapid and Rapid GNSS Solutions. http://acc.igs.org.

Springer, T.A. & Hugentobler, U. (2001). IGS Ultra Rapid Products for (Near-) Real-Time Applications. *Phys. Chem. Earth (A)*, **26**, 623–628.

Stacey, P. & Ziebart, M. (2011). Long-term extended ephemeris prediction for mobile devices. In *Proceedings of the 24th International Technical Meeting of the Satellite Division of the Institute of Navigation*.

Stein, S.R. (1985). *Frequency and time—their measurement and characterisation*, vol. 2, 191–416. Academic Press, New York.

Stein, S.R. (1988). Kalman filter analysis for real time applications of clocks and oscillators. In *Proceedings of the 42nd Annual Frequency Control Symposium*.

Sullivan, D., Allan, D., Howe, D. & Walls, F., eds. (1990). *NIST Techinal Note 1337 - Characterisation of clocks and oscillators*. United States Department of Commerce, National Institute of Standards and Technology.

Ucar, A., Bardak, B., Paparo, C., Berry, R. & Kale, I. (2013). A chip scale atomic clock driven receiver for multi–constellation GNSS. *The Journal of Navigation*, 449–464.

Urschl, C., Beutler, G., Gurtner, W., Hugentobler, U. & Schaer, S. (2007). Contribution of SLR tracking data to GNSS orbit determination. *Advances in Space Research*, 1515–1523.

van Diggelen, F. (2009). *A-GPS: Assisted GPS, GNSS and SBAS*. Artech House.

Waller, P., Gonzalez, F., Binda, S., Sesia, I., Hidalgo, I., Tobias, G. & Tavella, P. (2010). The in-orbit performances of GIOVE clocks. *IEEE Transactions on Ultrasonics, Ferroelectrics and Frequency Control*, **57**, 738–745.

Weinbach, U. & Schön, S. (2011). GNSS receiver clock modelling when using high-precision oscillators and its impact on PPP. *Advances in space research*, **47**, 229–238.

Whibberley, P.B., Davis, J.A. & Shemar, S.L. (2011). Local representations of UTC is national laboratories. *Metrologia*, **48**, S154.

Zhang, V., Parker, T.E. & Weiss, M. (2007). Long–term stability of remote clock comparisons with IGS clock products. In *Proceedings of the 29th Annual Precise Time and Time Interval (PTTI) Meeting*.

Zhang, X., Li, X. & Guo, F. (2010). Satellite clock estimation at 1 Hz for realtime kinematic PPP applications. *GPS Solutions*, **15**, 315–324.

Zumberge, J.F. & Bertiger, W.I. (1996). *Global Positioning System: Theory and applications*, vol. 1, chap. Ephemeris and clock navigation message accuracy. Progess in Astronautics and Aeronautics.

Zumberge, J.F., Heflin, M.B., Jefferson, D., Watkins, M.M. & Webb, F.H. (1997). Precise point positioning for the efficient and robust analysis of GPS data from large networks. *Journal of Geophysical Research*, **102**, 5005–5017.